Systems analysis of robustness in cellular networks

Von der Fakultät Maschinenbau der Universität Stuttgart
zur Erlangung der Würde eines
Doktors der Ingenieurwissenschaften (Dr.-Ing.)
genehmigte Abhandlung

vorgelegt von

Jörg Stelling

aus Hildesheim

Hauptberichter:	Prof. Dr. E. D. Gilles
Mitberichter:	Prof. Dr. F. J. Doyle III
Tag der mündlichen Prüfung :	2. Juni 2004

Institut für Systemdynamik und Regelungstechnik
der Universität Stuttgart
2004

Forschungsberichte aus dem Max-Planck-Institut
für Dynamik komplexer technischer Systeme

Band 8

Jörg Stelling

Systems analysis of robustness in cellular networks

D 93 (Diss. Universität Stuttgart)

Shaker Verlag
Aachen 2004

Bibliographic information published by Die Deutsche Bibliothek
Die Deutsche Bibliothek lists this publication in the Deutsche Nationalbibliografie; detailed bibliographic data is available in the internet at http://dnb.ddb.de.

Zugl.: Stuttgart, Univ., Diss., 2004

Printed in Germany.

ISBN 3-8322-3164-1
ISSN 1439-4804

Shaker Verlag GmbH • P.O. BOX 101818 • D-52018 Aachen
Phone: 0049/2407/9596-0 • Telefax: 0049/2407/9596-9
Internet: www.shaker.de • eMail: info@shaker.de

ACKNOWLEDGMENTS

This work evolved during the time I spent at the Systems Dynamics and Control Engineering group (ISR) at the University of Stuttgart and at the Max Planck Institute for Dynamics of Complex Technical Systems in Magdeburg.

First and foremost, I want to thank my supervisor and director at both institutions, Prof. Ernst Dieter Gilles who offered me these possibilities, always encouraged me in pursuing my research interests in great freedom, and enabled me to gather invaluable experience in many other aspects of science.

I am deeply grateful to Prof. Francis Doyle (University of California, Santa Barbara) for our exciting collaboration on circadian rhythms, many fruitful discussions, and his acceptance to referee this thesis.

For supporting central parts of this work through a fellowship, I gratefully acknowledge the Peter and Traudl Engelhorn Foundation and its director Prof. Herwig Brunner.

Many aspects of this thesis involved collaborations with different groups that provided expertise and shared data regarding the biological systems and the theoretical methods. I am particularly indebted to Prof. Wolfgang Seufert (University of Stuttgart), Prof. Stefan Schuster (University of Jena), and Dr. Uwe Sauer (ETH Zürich).

I want to express my thanks to all my current and former colleagues at the ISR and the MPI. They supported this work directly and indirectly by an excellent working atmosphere and their cooperativeness. In particular, I greatly enjoyed (and still do) working with Steffen Klamt and Martin Ginkel on structural network analysis.

A very special thank belongs to Christine, who – among many other things – contributed to make the final version of this thesis (more) readable.

Finally, as this list will necessarily be incomplete, I want to acknowledge the constant support by many other people I have been associated with during the past years.

CONTENTS

1. INTRODUCTION

1.1 Motivation

Under real-life conditions, biological systems from single cells to entire organisms have to cope with a constantly varying environment, be it changing conditions of nutrient availability, or noisy external signals that have to be processed. Moreover, their internal properties are also subject to uncertainty, since they can, for instance, be changed by mutations. Evolution, therefore, most probably implied strongly favored robustness, that is, a system's ability to maintain (key) functional characteristics despite potentially harmful external or internal perturbations. A now widely accepted notion is that many (or most) cellular sub-systems are robust [136]. Examples for this capacity can already be found in such simple organisms as the bacterium *Escherichia coli*, which displays perfect adaptation in its search for nutrients (chemotaxis) [4], and also a high resistance towards gene deletions. The inactivation of any single gene out of approximately 90% of all genes does not affect viability when the organism is cultivated under (idealized) laboratory conditions.

Robustness has long been recognized as an important property of biological systems, for instance described as 'canalization' (towards a specific outcome despite uncertain starting conditions) in developmental biology. However, the understanding of how robustness is accomplished at the cellular or molecular level is still limited [102]. A major reason for this fact is that robustness is intimately linked to the apparent complexity of cellular systems as several lines of evidence suggest [30, 151]. In principle, complex systems may either show a behavior or a design difficult to understand [275]. However, the behavior of biological systems is in most cases relatively simple. Even genome-wide regulation of gene expression during the yeast and human cell cycle can be reconstructed by using a few fundamental expression patterns [113, 114]. The comparison of, for instance, the number of metabolic and regulatory genes shows that complexity in biology arises mainly from abundant control circuits, that is, from the system's design: "In a nutshell, the system complexity is built in to provide for simple behavior." [151]. In analogy to evidence from highly evolved engineered systems, the main purpose of cellular control systems seems to be to guarantee reliable performance of vital functions under conditions of uncertainty [45]. Understanding the design principles ensuring robustness, hence, requires the analysis of degrees of complexity, which can not be achieved by intuition alone.

The emergent field of systems biology is directed towards a quantitative, system-level understanding in biology. Systems biology relies on an interdisciplinary approach combining concepts from biology, information sciences and systems engineering [137]. In this area of

research, theory-based approaches, especially mathematical modeling of complex biological systems, play a central role. Developing virtual representations of cells and organisms finally enables one to perform computer experiments similar to experiments with real biological systems. Mathematical modeling requires and entails a precise representation of the knowledge on the system, and of hypotheses for unknown mechanisms. It allows one to apply formal methods of analysis. Mainly these two characteristics are expected to lead to a deepened understanding of the biological systems under consideration [67, 88].

Mathematical modeling consequently played a central role in the recent re-discovery of robustness as an important property of cellular systems. Barkai and Leibler [11], by using a simplified biochemical network model, were the first to suggest that the ability of the bacterial chemotaxis system to adapt to constant stimuli is a robust property of the network, and not a result of fine-tuning of biochemical parameters. This proposition was later confirmed by detailed theoretical and experimental analysis [4]. Other systems, for which robustness was demonstrated based on mathematical models include, for instance, protein kinase cascades acting as switches in intracellular signaling [73, 116], the reduced cell cycle regulation of *Xenopus* eggs [19, 180], and complex networks controlling the development in *Drosophila melanogaster* [61, 171, 272]. Relatively few studies, such as an investigation of the phage λ gene regulatory circuit [160], addressed this topic exclusively through experimentation.

The exact causes for robustness, however, in most instances have yet to be determined. Specifically, how network structure and functionality are related is a largely open question. One obvious factor contributing to robustness is regulation. For the case of adaptation in chemotaxis, robustness could be explained by the fact that the regulatory network structurally corresponds to the biochemical implementation of an integral feedback control [284]. It is, however, unclear and difficult to understand, how complex, composite mechanisms ensure robustness [202]. Regulation, especially in complex systems, additionally, always implies a trade-off between robustness and fragility [45]. Understanding the design principles of cellular networks, which evolved to (optimally) cope with this constraint, represents a major, but largely unresolved challenge.

The approach followed in this work is to uncover the principles underlying robustness, and the consequences of robustness for a system-wide understanding by analysing robustness in cellular networks from three different angles. The first part deals with the interplay between network structure, function and cellular regulation in larger systems in order to evaluate, for instance, to what extent regulation supports potential alternative routes to enhance robustness. As in many cases it is not evident how additional complexity could improve a system's performance, the second direction of research focuses on the contribution of individual regulatory loops in simultaneously achieving robustness and precision of cellular control. The third part deals with the question whether robustness represents an obstacle for system identification, because largely invariant behavior provides only scarce information on the internal structure of a system. All three problems will be addressed by model-based analysis of different, representative biological examples.

1.2 Outline

Systems analysis of robustness in cellular networks first requires a definition of the term ”robustness” as well as the specification of suitable quantitative measures for this property. Chapter 2 is devoted to this purpose. It also reviews the current understanding on the mechanisms contributing to robustness in living cells, with a particular emphasis on open questions and conceptual approaches in the field.

Investigations into the relationship between network structure, function, and regulation with respect to robustness will be performed for two biological examples, which represent two extreme positions in the spectrum of dynamic properties of cellular functional entities. Metabolism is mainly characterized by a requirement for homeostasis, whereas signal generation and processing in general involve more complex dynamics. Hence, different forms of control should prevail owing to their different sensitivities [107]. From the point of view of systems analysis, metabolic networks are amenable to structural analysis without significant loss of description accuracy. Since this approach is also suitable for the analysis of large-scale networks, it will be applied to the fairly complex, yet well-studied central metabolism of the bacterium *Escherichia coli* (chapter 3).

Genetic oscillators generate an important class of intracellular signals. They may show complex dynamics and have emerged as model systems for studies in systems biology. Especially those systems establishing intracellular clockworks show desirable features such as moderate size and a well-established knowledge of the biological mechanisms. Relatively low-dimensional parameter spaces of the associated mathematical models makes them suitable for systematic dynamic analysis. In chapter 4, comparative analysis of two published models of the oscillator underlying circadian rhythms in the fruit fly is performed to study, to what extent structural features of the system, such as individual control loops, contribute to the observed robustness and precision of the clock.

As noted above, robustness of cellular systems may hinder the identification of internal working principles from the observable behavior. It may facilitate mathematical modeling, because exact values of kinetic parameters do not have to be known. However, it is unclear, which consequences robustness has for the construction of valid and predictive mathematical models based on experimental data. Mathematical modeling and model analysis of a complex control module in the yeast cell cycle will be used to address this problem (chapter 5).

Matching mathematical analysis with biological reality requires the analysis of specific biological examples, and, thus, of specific forms of robustness and its generation. Ultimately, however, systems biology approaches should allow for the uncovering of cellular design principles that are valid in a more general sense. In the summary (chapter 6), an emphasis is therefore laid on the comparison across the biological systems studied and the analytical methods employed to approach this aim.

2. SYSTEMS ANALYSIS OF ROBUSTNESS

2.1 Robustness: Definition and measures

The notion of robustness has recently received considerable interest in diverse fields for which the existence of complex networks is characteristic. Examples include the internet, social networks, and biology [249]. Not surprisingly, the term ”robustness” has been associated with different, sometimes conflicting interpretations. Here, starting from a broad definition, which encompasses a common denominator of the understanding of robustness, the aim is to obtain an operational definition that proves suitable for analyzing the properties of cellular networks.

In general, robustness means the persistence of a system’s characteristic behavior under perturbation or conditions of uncertainty. Robustness is, hence, defined for a specific system, which, however, may have arbitrary structural and behavorial features. The concept is closely related to stability in dynamical systems theory, but usually employed with respect to a broader class of phenomena [30, 137] (for a contrary, but rarely encountered point of view see e.g. [160]). In engineering, the task of determining a system’s robustness is often accomplished by transformation into a suitable stability problem. However, compared to stability theory in systems dynamics, no elaborate theory of robustness exists yet. In principle, thus, apart from these two differences, robustness and stability refer to identical concepts; they will be used as synonyms in this work (but see also [125]). It has to be noted that robustness (such as stability) encompasses a relative, not an absolute, property of a system. No system can maintain stability for all its functions when encountering any kind of perturbation. Any operational definition of robustness, and systems analysis thereof, thus, requires two additional specifications. Namely, it has to be explicitly clarified, (1) which characteristic behavior or function remains unchanged, and (2) for which type of disturbances or uncertainties this invariance property holds.

For relatively simple systems, the characteristic behavior can often be captured by definition of a dynamical regime. Investigations of oscillators may thus focus on the persistence of a regular periodic solution. As can be seen from this example, robustness in general refers to a qualitative property, and does not preclude quantitative changes (in period or amplitude of the oscillations) to occur [11]. For engineered or biological systems, one often understands by characteristic behavior the ”desired system characteristics” [30] to be maintained. A typical task in control engineering is to achieve robust stability or robust performance (i.e.. guaranteed tracking) in the face of plant uncertainty captured by describing the plant as belonging to a (structured or unstructured) set, for every member of which the characteristic has to hold [51]. Here, robustness directly connects to functionality. In technical as well as in living systems,

it makes sense to protect key functions by design, or as a result of evolution. Especially in biology, however, function can, in many cases, not easily be assigned to a particular subsystem of a cell or organism [180]. In bacterial chemotaxis, for instance, maintaining the ability to adapt to changing nutrient concentrations, whereas adaptation times are allowed to fluctuate, is intuitively understandable. As a counter-example, signal transduction relies upon sensitive detection, amplification and decoding of input signals. It would not be sensible to react identically irrespective of the signals received. Identification of key inputs and outputs for specific subsystems, however, may not be evident from the complex overall network structure, and cellular signaling requires both robustness and precision [79]. The claim of higher-order behavior or entire modules to be robust and, hence, imply functional advantage, therefore requires careful justification.

Similar considerations apply for the specification of perturbations. Cellular systems face three broad classes of uncertainties: (1) externally induced perturbations owing to variable environments, (2) internal perturbations arising from changes in the structure of the system, such as mutations affecting kinetic properties of proteins, or leading to the lack of components, and (3) intrinsic noise as a consequence of the low copy number of many cellular components. The first two classes of disturbance can be dealt with in a deterministic framework. External perturbations may directly influence the solutions of a dynamical system; resistance to these influences equals the notion of stability in dynamic systems theory. Perturbations affecting the structure of the systems itself, but which do not result in qualitatively different dynamics, reveal structural stability of a system [125]. These two types of perturbations can, hence, be mapped on changes in inputs and system parameters, respectively.

Stochastic effects resulting from the random character of biochemical reactions in principle require an explicit inclusion of noise in robustness analysis [202]. In gene expression, for instance, intrinsic noise considerably contributes to overall variation, with potential amplification and propagation by regulatory dynamics [63, 254]. Theoretical and experimental studies, however, demonstrated that stochastic noise in gene expression can efficiently be suppressed by regulation, especially when employing autoregulation via negative feedback [15, 254]. Moreover, deterministic behavior is not necessarily linked to high molecule numbers. A phenomenon called stochastic focusing has the potential to enhance the reliability of cellular control through noise. This principle bears similarity to the repression of output noise by signal noise in standard nonlinear control [191]. In particular, noise has been demonstrated not to dramatically change the behavior of a complex intracellular oscillator that will be analyzed herein [95]. This work will exclusively be concerned with deterministic analysis of cellular networks, but limitations of this approach can not be excluded. However, for the example systems investigated, they do not seem to impose severe restrictions on the generality of results.

In this framework, measurements of robustness will mainly rely on assessing the influence of changes in system parameters onto the observed behavior [219]. Parameters in this context encompass kinetic constants as well as information on interactions, initial concentrations, and

time-varying entities such as inputs. Also structural information (existence of links or components) can by these means be encoded in the form of system parameters. A model of a biochemical network then serves as a mapping from parameter space to behavior space [180]. Different measures of robustness based on parametric studies have been employed so far. Early in the 1970s, Savageau introduced parameter sensitivities, which quantify the change of a system's state in response to a change in parameters into the realm of biology [218]. This measure, however, usually does not directly reflect robustness, since it has to be connected (via a derived feature) to the quality of a behavior, or a specific functionality. Other approaches use the size of parameter space, in which the desired behavior occurs as a measure of robustness. Examples include the bandwidth of compliant single parameter values obtained, for instance, through bifurcation analysis [165], the optimum margin of stability [180], or criteria inspired by biology such as mutation load [233], and mutational expansion [171]. In contrast to parameter sensitivities, however, for practical reasons, these measures enable analysis only in low dimensions of parameter space. Interactions between many parameters may yield complex synergistic or antagonistic outcomes. For this reason, the methods are limited in assessing the effect of multidimensional uncertainty in complex systems [165].

Furthermore, all measures discussed so far describe local (with respect to a specific point in parameter space) properties of a system. For revealing general design principles of networks, however, one needs to examine global characteristics, that is, the type of behavior a network may show independent of a specific parameterization. In principle, two ways for avoiding, or at least diminishing this shortcoming exist: First, rigorous methods such as the structured singular value developed in robust control theory [293] guarantee a valid answer. The methods are, however, limited by the efforts required to apply them to highly nonlinear biological systems of reasonable complexity. For this reason, presumably, only smaller biological subsystems were subjected to a very simplified version of this analysis up to now [165]. Monte Carlo methods, secondly, randomly sample the parameter space, and in combination with local analysis can provide for an estimate of global properties. Random search can not guarantee general robustness of a system, but for complex systems, it seems to be most suitable to obtain evidence for (or against) global robustness.

It has to be noted that the type of analysis proposed here is distinct from a Monte-Carlo approach often used for studying robustness of biological networks. There, identical behavior of a system for a large population of randomly generated parameter vectors is interpreted as an indicator of robustness [11, 61, 272]. Identical behavior, however, does not necessarily entrain invariance of behavior in case of perturbations, as it is characteristic for robustness. In principle, a high number of very small regions in parameter space yielding the same qualitative dynamics could be captured by the randomly generated sets of parameters. Then, even smaller perturbations in the nominal parameters would cause the system to leave the corresponding region in the behavior space. Random search, hence, can only account for global robustness properties when combined with local evaluation of sensitivities.

The analysis of robustness, thus, has to be based on detailed specification of the behavorial regimes, the types of disturbances, and the measures for robustness considered. The following section will refine these general principles for the case of cellular networks by discussing specific forms of robustness in biological systems, their (broader) functional role and emergence.

2.2 Robustness in complex systems

To understand the functional role of robustness in biological systems in more detail, three points deserve attention: the phenomenology of robustness, the means by which it is achieved, and the evolution of robustness. As noted above, robust systems show relative insensitivity to alterations of the systems' parameters, and the ability to adapt to varying environments. Moreover, a high degree of robustness is present when "graceful degradation" occurs. This phenomenon refers to an ordered degradation of functionality after large perturbation in contrast to immediate catastrophic failure. Apoptosis (programmed cell death) in case of unrecoverable damage is a prominent example of this feature [136, 137].

Biological systems, however, also show extremely contrary, highly sensitive characteristics under circumstances, for instance, when small changes in single key regulatory proteins lead to complete deregulation of cell growth in cancer. Theoretical approaches are desired in order to explain such counter-intuitive behavior on the basis of general characteristics of complex systems. They could allow for conclusions on the existence and features of potential design principles and, thus, provide a framework for understanding robustness in complex cellular networks.

A general concept for explaining the existence and characteristics of extremely robust systems termed "Highly Optimized Tolerance" (HOT) was recently suggested by J. Doyle and co-workers. It relies on the central idea that robustness - in technical as well as in biological systems - has to be regarded as a limited and conserved resource. This quantity (tolerance) requires careful distribution, adapted to the function a system is intended to perform, and the associated uncertainties. High optimization refers to a strategy of simultaneously achieving high performance and error-tolerance by a high degree of internal structure. The management and overall conservation of robustness lead to a "robust yet fragile" behavior of such systems, namely a high robustness ("barriers to cascading failures") in the face of anticipated or usually encountered disturbances, but hypersensitivity towards unexpected perturbations or design flaws. Hence, it means a highly structured sensitivity [28, 29].

Highly optimized tolerance accounts for two important characteristics that distinguish sophisticated engineered and biological systems from complex physical systems: their structural complexity and the notion of function [103]. It furthermore emphasizes a necessary connection between complexity and robustness. Making certain functions of a system more insensitive towards disturbances, for instance, may require additional control loops. This, in turn, leads to higher complexity and to new potential sources of fragility [30]. Finally, highly optimized

tolerance does not require global optimization of a system or its deterministic development, but may be established either through purpose-driven, but in practice iterative design or as an outcome of evolutionary processes [29, 294].

Highly optimized tolerance encompasses a theoretical framework for linking characteristics of the behavior of robust systems to their inherently complex structure, and the development of the latter. It encompasses robustness as a guiding principle for explanation of cellular complexity, which, in turn, implies the possibility of deriving cellular design principles through robustness analysis, when taking the trade-offs captured by HOT into account. Moreover, similarities between engineered and biological systems could enable one to base the search for such principles on well-known mechanisms used to confer robustness to technical systems. For this purpose, however, two points deserve critical consideration: the extent of similarity between the two classes of systems, and the assumptions underlying the concept of highly optimized tolerance.

Evidence for the general validity of the theory up to now stems either from the study of highly simplified (lattice percolation) models [28, 29, 294], or from analogies between various aspects of living and technical systems [30, 45]. Direct applicability to biology, for example, by uncovering predicted design principles, remains to be shown. Concerning potential differences, especially the fact that natural evolution acts on populations of cells or organisms, and that its outcome depends on e.g. the population size needs to be taken into account. For instance, the existence of apoptosis in unicellular organisms such as yeast can only be explained by a competitive advantage for the group (i.e. the clone), not for the individual cell providing the suicide mechanism [80]. In this respect, however, several pieces of evidence support the general scheme of the HOT framework. First, in model-based scenarios of evolution of gene networks in changing environments, in which robust behavior was required, simple expression pattern and temporally stable, highly organized structures were favored [20, 21]. In experimental studies, independently evolved strains of *E. coli*, secondly, showed convergent patterns of development towards higher fitness [39]. Finally, evolutionary arguments indicate that robustness may in fact not impose barriers to evolution, but instead enhance 'evolvability'. Robustness enables genotypic variability (flexibility) without immediate functional consequences, which shortens the path for further development to (favorable) phenotypes [134, 160].

The concept of highly optimized tolerance takes an extreme position in it assumptions on the strategies and goals for handling the trade-off between performance and reliability. In particular, it implies a high-risk strategy in that all marginal performance benefits are captured, at the expense of the risk of high losses upon unexpected perturbations. A different strategy could consist in trading small losses in average performance against drastical reduction of the risk and size of catastrophes. Such a risk-aware variant of the HOT concept was recently proposed as "constrained optimization with limited deviations" (COLD). Using identical models as for the HOT scenario, it was shown that this regime can enhance robustness (in terms of utility), while showing similar overall system behavior [184].

To summarize, theoretical concepts relying on connections between robustness, complexity and overall design principles capture important robustness characteristics of man-made as well as of living systems. At present, how the implicit trade-offs described by the theories is handled in real-world systems requires studying more complex, realistic examples. Also, the concepts' applicability for detailed analysis of functional and design principles operational in cellular systems remains to be determined. The theories, however, strongly support the existence of general design principles for achieving robustness. Additionally, they provide guidelines for the analysis of such principles, namely, as a first approximation to employ engineering principles for extrapolation to biology. The following section therefore focuses on basis mechanisms conferring robustness to technical systems and their relevance for understanding cellular networks.

2.3 Mechanisms conferring robustness

In engineering complex technical systems, design for protection against deleterious disturbances mainly employs four ingredients. These encompass (1) back-up systems (redundancy and diversity), (2) disturbance rejection through feedback control, (3) structuring of complex systems into semi-autonomous functional units (modularity), and (4) their reliable coordination via establishment of hierarchies and protocols. Examples for all of these features exist in biology as well [45, 136]. Their potential contributions for conferring robustness to cellular networks – and for the analysis thereof – are discussed in this section.

2.3.1 Redundancy

The simplest strategy to protect against failure of a specific component is to provide for alternative ways to carry out the function the component performs. At the cellular level, this back-up strategy can appear in two principal forms. Either two or more duplicate genes play identical physiological roles, or groups of different genes constitute alternative pathways for achieving the required functionality. Both mechanism are also referred to as 'genetic buffering' in the biological literature [102]. In contrast to redundant systems in engineering, however, completely identical genes that do not diverge in functionality or regulation would not survive during natural evolution [146]. Instead, structurally different entities perform similar functions owing to functional overlap, which lead to the suggestion to use 'degeneracy' as a more appropriate term for this phenomenon than redundancy [54].

The question, whether characteristics of individual components or network characteristics contribute most to genetic buffering is highly debated. Analysis of a limited set of duplicate genes in yeast discovered no significant correlation between sequence similarity and the effect of mutations on phenotype and gene expression [273]. Based on evolutionary arguments, a study on robustness of metabolic networks in humans and mice reached a similar conclusion. Here, the gene evolution rate, which serves as a negative indicator of mutational effects, showed

no difference between structurally related and unrelated genes, whereas the pattern of network connections did so [135]. A recent analysis of deletions in all yeast genes, however, unraveled statistically significant connections between duplicate genes and functionality. This finding is compatible with a view of network structures making a dominant contribution in providing robustness through redundancy, but indicates that the issue remains open [99].

Closer investigation of robustness in cellular networks as a consequence of redundant pathways, thus, offers one approach to the uncovering of design principles unclarified at present. In this respect, the previous studies cited above suffer from the fact that direct links between robustness and gene or pathway function were not established. They relied on indirect evidence such as sequence similarity or topological proximity owing to unspecified interactions. Abstract graph-theoretical reasoning on interaction networks, for instance, leads to the conclusion that robustness is a feature only of specific classes of redundant networks [2], into which cellular networks do not *per se* have to fall.

2.3.2 Feedback control

Control circuits undoubtedly play a decisive role in maintaining cellular functions in the face of internal or external uncertainties [45]. Intimately linked to this fact, they account for most of the cellular complexity. Understanding cellular design principles requires deeper inspection of cellular regulation [87], which, however, meets difficulties owing to the highly integrated character of these circuits. This section, therefore, will focus on general contributions of control to robustness in biochemical systems, and on methods for the analysis of these contributions in cellular networks of increasing complexity.

Most importantly, feedback loops can account for robustness in cellular network function. In brief, by using the output of a function to be controlled in order to determine appropriate input signals, feedback enables a system to adjust the output by monitoring it. In general, negative feedback is employed in reducing the difference between actual output and a given set-point, thereby dampening noise and rejecting perturbations. The role of positive feedback (or autocatalysis) in conferring robustness to biological systems is less obvious, since it may cause instabilities. For this reason, the design of technical systems tries to avoid positive feedback. In biology, however, decisions for example in development need to be derived from noisy and graded input signals and have to be maintained. Enhanced sensitivity through positive feedback also speeds up stress responses. Depending on which cellular functionalities require protection from perturbations, hence, both forms of feedback and combinations thereof can contribute to robustly achieve a desired behavior [79].

It is essential to note that the role of feedback is ambiguous with respect to robustness. Feedback, in general, also introduces fragilities to the system. Such fragilities include the possibility of self-sustaining and cascading failures as a consequence of positive feedback. Uncontrolled tumor growth illustrates this danger. A high gain in negative feedback, in principle, leads to

faster control but fragilities enter in potentially inaccurate transient responses, namely because time-varying perturbations can be amplified [45]. As already shown in the context of the general definition of robustness, the degree to which a control circuit contributes to a system's robustness in comparison to an unregulated system, thus, depends on the circuit design, the control objective, and the type of perturbations affecting the system.

Design of artificial gene circuits on the basis of mathematical models is one promising approach for analyzing simplified cellular functions in detail [106]. Engineered genetic circuits in model organisms provided direct means for testing the predicted features of regulatory schemes of low complexity *in vivo*. In particular, it was shown that a simple feedback loop relying on negative auto-regulation of a transcription factor stabilizes steady-state gene expression levels despite the inherent noise in gene expression. Importantly, autoregulation proved advantageous over unregulated transcription for a range of biologically plausible parameters. Not surprisingly, this effect was enhanced by high gain of the feedback loop [15]. Experimental work thus confirmed predictions already made in a classical theoretical study of stability in gene regulation [220]; inferiority of positive autoregulation with respect to steady-state stability remains to be determined experimentally [106].

Combined experimental and theoretical approaches were also employed to study systems mimicking bistable switches that could be involved in cellular decision-making. Two genes mutually repressing each other's expression (double-negative feedback) proved sufficient to construct a reliable irreversible switch [84]. A certain robustness was furthermore demonstrated for autocatalytic gene activation in combination with cooperative activator-DNA interactions - a simpler system mimicking a bistable switch [16]. In this case, however, experimentally determined stochastic transitions between the two stable steady states [16] indicate a very constrained robustness of the system when subject to realistic perturbations. Similar observations were made for an oscillatory circuit, which was engineered by coupling three transcriptional repressors [62].

These examples illustrate current limitations of the approach using simple artificial gene regulatory circuits: under real-life conditions with intracellular noise and uncertain components, more complex circuits are required. One possibility for achieving higher robustness consists in combining multiple levels of regulation, for instance, controlled transcription, translation, post-translational modification and degradation [267]. Investigating the robustness of cellular control circuits, moreover, has to account for the fact that in many cases where highly precise and reliable behavior is indispensable for overall cellular functionality, multiple intertwined feedback loops operate [74]. Structural properties such as robustness can not be elucidated by simple addition of component properties. Genetic circuit engineering thus has a particular strength in testing theoretical predictions, which, however, requires more realistic descriptions of biological regulation and their thorough analysis.

Instead of building up regulatory circuits from simple elements to approach cellular complexity, an other approach tries to extract the core control logic out of realistic models of bio-

logical systems. In particular, delineating an equivalence between biological regulatory circuits and technical controllers, for which theoretical foundations are well-established, proved successful. Several regulatory networks, including the chemotaxis network in *E. coli* were shown to establish an integral feedback scheme [60, 158, 284]. As integral feedback is necessary and sufficient for robust steady-state control, robustness of phenomena such as perfect adaptation or homeostasis are readily explained by the equivalence [45]. Difficulties arising in this type of analysis result from two factors: the process of extracting basic control schemes from complex network schemes, and limitations in current control theory. The latter constraint is more fundamental, because a well-established body of general theory for complex non-linear control is lacking.

For this reason, among others, direct investigation of mathematical models for cellular regulatory circuits has become a prominent method for analyzing robustness. As discussed in section 2.1, however, a critical issue in this approach lies in properly deducing robustness of a particular control structure from numerical simulations. Uncovering design principles conferring robustness through intertwined feedback control furthermore requires an analysis of the role that individual control loops play. Experimental evidence supports the assertion that different instances of feedback possess individual roles and significance in cellular regulation [79]. As suggested recently in the context of model validation [180], comparative analysis of robustness of different models incorporating different aspects of the real control structure could help to clarify these roles. In contrast to recent studies such as those for a simplified model of a circadian clockwork [244], therefore a general link between control structure and robustness properties has to be established. Up to now, the approach primarily proved successful in pointing to missing links in current understanding. Analysis indicated that even the well-studied control scheme of the bacteriophage λ does not entirely explain the observed robustness [10].

Whereas for simpler feedback control circuits, thus, experimentally and theoretically founded analyses of robustness properties exist, the understanding of complex intertwined regulatory networks is still limited. The bottom-up concept of engineering gene circuits has to rely on an understanding of complex composite circuits, and its comparison to biological reality. A reduction of cellular control networks to basic technical control schemes is currently confined to the elucidation of design principles underlying the robustness of particular functionalities. Systematic comparison of differences in robustness properties based on biologically realistic mathematical models, however, could provide a way to elucidate working principles of specific example networks in a first step towards elaborating cellular design principles.

2.3.3 Modularity

Focusing on the internal structure of cellular systems, one central, increasingly accepted notion is that these systems are composed of 'functional units' or 'modules'. Modules can be understood as semi-autonomous entities that show dense internal functional connections, but

looser connections with their environment [90, 148]. An example for a modular structuring of metabolic networks is shown in Fig. 2.1. An enzymatic reaction in glycolysis belongs accordingly to the functional unit ”glycolysis”. This in turn can be regarded as part of the larger unit ”catabolism”. Hence, modularity of cellular systems is closely connected to the concept of hierarchical structures that will be considered in the following section.

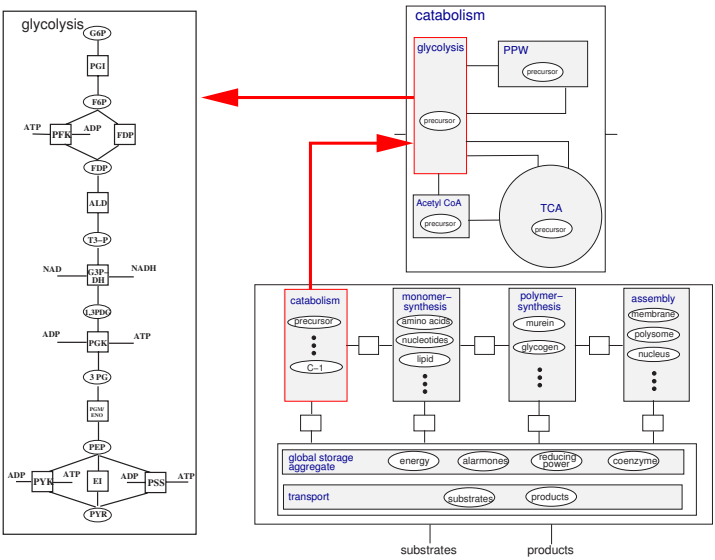

Fig. 2.1: Modular structures in metabolic networks. The scheme refers to the decomposition of cellular metabolism into smaller modules. Arrows indicate containment relations. Glycolysis (left) is considered to be a functional unit that constitutes one part of catabolism, which again is connected to other higher-order modules of the metabolic network. Abbreviations are ’PPW’ for pentose phosphate pathway and ’TCA’ for tricarboxylic acid cycle.

With respect to robustness, modularity leads to a benefit for overall functionality of complex systems. Encapsulation of simpler functions can reduce the risk of catastrophic failure by preventing the spread of damage in one module throughout the network [2, 103]. As a consequence of modularity, among other criteria, biological systems seem to be more closely related to synthetic, engineered systems than to physical systems [45, 103, 151]. Therefore, a promising way to come to a system-level understanding of cells is to identify common features in the large-scale organization of complex networks in both domains, and to extend successful theoretical concepts established for the analysis and synthesis of complex technical systems to biological systems [87]. For this purpose, however, two critical issues have to be clarified, namely to prove the existence of modularity in cellular systems, and to establish methods for the unanimous identification of modules [151]. Both problems are intimately linked.

Several lines of functional experimental evidence suggest that cellular networks are organized in a modular fashion. A large-scale analysis of yeast mutants provided important support for modularity. It focused on synthetic lethality, which captures the phenomenon of cells carrying individual deletions in two genes the cells being viable, whereas the combination of both mutations is lethal. Analysis revealed synthetic lethality predominantly of genes acting in the same (intrinsic) or functionally similar (extrinsic) pathways. The results have to be interpreted with caution owing to caveats in experiment design, but they are completely in accordance with features of a modular system [102]. Moreover, some complex functional units such as translation or controlled proteolysis could be reconstituted *in vitro*, which underlines their (limited) autonomy [103].

One class of approaches for identification and demarcation of functional modules also relies on experimental data. Concerning the first task, it supports the existence of modules, although it may be biased due to the explicit search for them. Network topology, that is, the pattern of network connections, was analyzed in several studies. Irrespective of whether metabolic networks spanned by components and reactions [126, 203], protein-protein interaction networks [168,208], or gene regulatory networks [168] were considered, separable clusters were always found. Topological network analysis also showed that transcriptional regulation networks in *E. coli* [177, 235] and yeast [153] are composed of recurrent 'network motifs' or simple building blocks that can perform functions such as feedback control. Moreover, a recent study of a large compendium of yeast gene expression profiles came to similar conclusions based on functional data [61]. Importantly, when the modular structures obtained were compared to current classifications of metabolic or regulatory pathways, large overlaps between them, as well as discrepancies were revealed [61, 203, 208].

Other approaches for demarcation of modules rely on a conceptual identification of modules [132, 148]. For this demarcation, for instance, a preliminary set of three biologically motivated criteria was introduced [148, 248]. To be (relatively) self-contained, the modules have (i) to perform a common physiological task such as to represent a linear pathway for amino acid synthesis, (ii) to be controlled at the genetic level by common regulators (i.e. identical transcription factors or the organization in one operon for prokaryotic systems), and (iii) to possess a common information processing (signal transduction) network. The essential feature of this approach is the combination of classical concepts in the analysis of metabolic systems with a signal-oriented perspective to cellular regulation. Distinct to this approach, several authors addressed the question of demarcation in a more quantitative, flux-oriented way regarding either metabolic pathways [212, 223, 227] or intracellular signal processing networks [131, 229].

Strong evidence from experimental investigations, hence, exists to sustain the assertion that cellular networks are structured into functional units having their own identity and limited autonomy. Moreover, different criteria for identification of modules show considerable overlap. However, these module boundaries are partially not consistent with biological intuition. This may be explained by more flexible concepts of modularity, which allow, for instance, for one

component to occur in more than one module [103], or to consider a non-unique representation of module boundaries owing to dynamic processes [9]. Clearly, further systematic theoretical investigations on larger modular systems such as in [262] will be necessary to come to a more stringent formulation of criteria for demarcation. However, the substantial agreement between the results obtained from different decomposition methods suggests to regard units identified by these approaches as reasonable approximations to real cellular modules.

Modularity in biochemical networks entails two important consequences for the analysis of robustness in such networks. First, it lets one refer to general concepts linking modularity and robustness that were established for different domains, for instance, in the realm of man-made systems. There, especially graph-theoretical analysis suggested that certain network structures involving modularity should be robust to random perturbations [2] (see also chapter 3.2). Recently, these predictions were claimed to be valid for cellular networks, especially metabolic networks, accordingly [126, 203]. These assertions, however, remain to be validated (or falsified) by comparing the predictions to experimental observations. In particular, it is unclear, in how far high-level abstractions based on interaction patterns only are able to capture network functionality. A simple example for this potential problem is provided by a study on protein interaction networks [168]. There, the authors argue that the observed suppression of direct links between central hubs in the network enhances robustness by avoiding cross-talk between different modules and, thus, localizing effects of potential damage. If, however, cross-talk was vital for coordination of cellular functions, the pure topological argument implying equal importance of all interactions would not hold. Analysis of network structures, thus, has to take into account the interplay between different cellular networks and their potential dynamics, when necessary [188, 235]. Furthermore, judgment on the power of theoretical concepts must rely on comparison with experimental observations, which is lacking so far.

The notion of a living cell being composed of subunits of limited autonomy, second, simplifies modeling and abstraction of general properties [45]. For the mathematical modeling of cellular systems, the modular structure raises the possibility to independently develop mathematical models for each of the functional units. Hence, submodels as entities in the ”model world” correspond to functional units in the ”real world”. These submodels can later be connected to obtain a description at the system-level [148, 248]. Consequently, the analysis of robustness can proceed from the detailed investigation of individual modules to their interplay and its consequence for overall systems performance. Modularity of cellular systems, hence, provides one with testable hypotheses derived from top-down studies as well as with opportunities for a more detailed bottom-up approach. Both approaches should finally converge.

2.3.4 Hierarchies and protocols

Protocols encompass the set of rules aiming at an efficient management of relationships between the parts (i.e. modules) that constitute a system. They include, for instance, the organizational structures for embedding modules, and the interfaces between modules that allow for system function [45]. Protocols, hence, are of primary importance for an understanding of how information in complex systems such as in living cells is integrated [103]. As already discussed in the previous section, analysis of robustness at the system level has to include these aspects, which have only received few attention so far. The purpose of this section is to give an outline of predominant protocols in biology, and of their potential implications for system robustness.

In general, an efficient means for coordination in complex systems is to organize a system hierarchically, namely to establish different layers of integration [174]. This architecture, in particular, helps to reduce the costs of information transmission [100]. In cellular systems, different facets of hierarchical organization can be distinguished. At a very abstract level, a cell can be divided into two general subnetworks, a regulatory network and a metabolic network [148] as shown in Fig. 2.2. These networks possess very different characteristics: The metabolic network is mainly occupied with substance transformation, e.g. to provide metabolites and cellular structures. In many cases it involves fast biochemical reactions. The regulatory network's main task is information processing, e.g. for the adjustment of enzyme concentrations to the requirements of variable internal and external conditions. This network involves the use of genetic information. Compared to information flow, mass flow only plays a subordinate role in the regulatory network. In this sense, the regulatory network is superimposed onto the metabolic network, fulfilling functions analogous to a controller in a technical process.

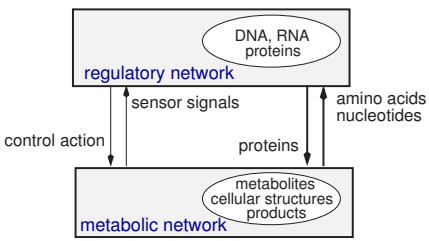

Fig. 2.2: Regulatory network and metabolic network: Cellular components constituting the networks and the major connections between them implying signal exchange (left) and substance flow (right).

The interaction between both networks is necessarily bound to substance exchange due to the requirements for precursors and proteins. However, the main connections consist in directed signal flow, i.e. sensor signals (e.g. generation of second messengers) and control action (e.g. adjustment of enzyme concentrations). For a system-wide understanding and description of cellular function, these relations between metabolism and regulation imply that analysis will

have to integrate both organizational levels. Moreover, it is important to note that for the communications within the levels, standard protocols exist, which include, for instance, exchange of energy and reduction equivalents through general currencies for the metabolic network, and gene expression, covalent modifications or common mechanisms of controlled degradation for the regulatory network [45].

Cellular regulation is established by especially complex gene and protein networks. In cell cycle regulation of bacteria, for instance, genome-wide analysis of gene expression clearly demonstrated a hierarchical control architecture [150]. A closer look at the hierarchical structure of cellular regulation may thus help to deal with this kind of complexity. As shown in Fig. 2.3 for transcriptional regulation in budding yeast, the system's possible behavior on a lower level is constrained by regulation at higher levels. For example, the presence of RNA-Polymerase offers a wide variety of different gene expression patterns, but the actual gene expression is adjusted by combinatorial control involving associated factors and specific transcription factors. Transcription is thus affected by layers above the influence of gene-specific regulators, which enables the cell to establish global to local layers of regulation by controlling the availability of more and more specific components associated with a general transcriptional machinery [112]. Similar control structures can be found as a common theme in translation [216] and in intracellular proteolysis [133].

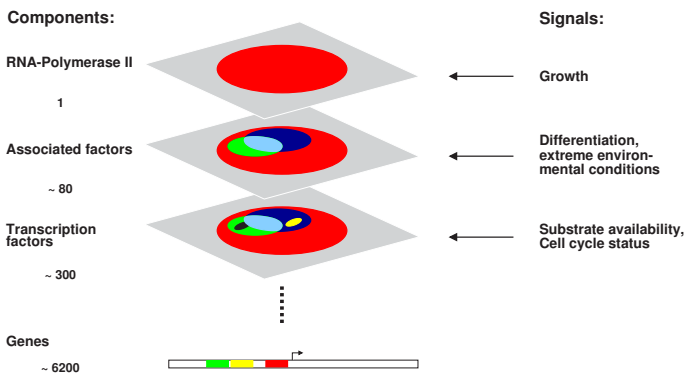

Fig. 2.3: Hierarchical structure of the regulatory network: Example of transcriptional regulation in budding yeast. Specificity of regulation increases from global regulation to single gene expression (top to bottom), whereby the components involved (left) become more specific as well as the internal or external signals (right) processed. Shaded areas at each regulatory level indicate the respective behavior in a system-theoretical sense [276, 277] allowed by the combination of all regulatory interactions including higher levels of control.

Several lines of evidence suggest that hierarchical structures confer robustness to cellular systems. One major proposition, already encountered in the context of modularity, is that sep-

aration of functions, and their integration at higher levels, reduces the average damage owing to arbitrary deletions of links in the network. Topological studies showing hierarchical modularity in metabolic networks argue along these lines [203]. Analysis of dynamical networks with overall structures similar to those of cellular networks demonstrated a superior systems performance and controllability when feedback control specifically operates on higher levels of integration [274]. Moreover, it is intuitively clear that well-designed hierarchies and protocols contribute to the robustness of complex systems, for instance, by constraining the effects of local de-regulation, or by providing common standards for robust coordination of cellular functions [45]. For cellular networks, however, the major challenge consists in elucidating the links between different levels of organization [188]. In particular, it is unclear, how trade-offs between, for example, robustness and efficiency are handled by means of protocols and hierarchies. For this purpose, cellular networks will have to be analyzed across different levels of integration in order to uncover the operating principles underlying functional integration. Apart from the very general investigations cited above, detailed studies of these aspects of robustness have not yet been carried out for specific biological examples.

2.4 Conclusions

The view that biological systems are highly resistant to perturbations is largely undisputed. Beyond this basic notion, however, no generally accepted approach to the analysis of robustness in cellular systems exists. In any instance, however, it has to be taken into account that robustness refers to the maintenance of specific functionalities of a system that is subjected to specific perturbations. In the model world, the analysis of parameter sensitivities offers a method to capture this link, especially when it is designed so as to investigate structural features of a system, and not only one particular instance of its behavior.

The current knowledge about robustness in biological systems, and the cellular design principles underlying it, shows a large bias. At very high levels of abstraction, concepts such as highly optimized tolerance elaborate general features, namely the trade-off between efficiency and robustness, and necessary connections between robustness and complexity. Large-scale topological analysis of cellular networks gives clues on structural features of cellular networks that could confer robustness to cellular function. Both high-level approaches, however, currently suffer from the fact that beyond analogies with engineered systems, their central hypotheses remain to be evaluated by analysis of specific biological examples that connects mathematical modelling and experimental observations.

At the other end of the spectrum, studies of robustness in small systems proved successful. However, they have to be extended to more complex systems to enable one to infer general design principles from specific biological examples. In this respect, further investigations should be guided by, and specifically address current hypotheses on which mechanisms could contribute to robustness in biology. In particular, the relative importance of redundancy of compo-

nents vs. pathways, the role of individual feedback circuits, the modular organization of cellular networks, and the integration of cellular functionality across hierarchies are of predominant interest. The robustness analysis of selected metabolic and regulatory networks to be described in the following chapters will therefore focus on these aspects.

3. METABOLIC NETWORKS: STRUCTURAL ANALYSIS

3.1 Introduction

Structural analysis of complex networks in diverse fields such as the World Wide Web, scientific citations or cellular metabolism recently attracted considerable attention for one major reason: As network function is always affected by structure, topological analysis can yield insight into network function and behavior [249]. Current theoretical approaches have different strengths and shortcomings in providing an integrated, predictive description of cellular networks. Specifically, dynamic mathematical modeling of large-scale networks meets difficulties as mechanistic detail and kinetic parameters are rarely available. In contrast, structure-oriented analyses only require network topology, which is well-known in many cases.

Previous approaches of structural analysis of metabolic networks have focused on the development of the theoretical foundations for this type of analysis in conjunction with a systematic concept of metabolic pathways [223, 227, 228], and on specific aspects of the functionality of metabolic networks. Such specific aspects include the identification of individual (extreme) operation modes in networks of moderate size [226], theoretical yield determination [57,226,227] and the analysis of shifts in flux patterns due to external or internal changes [58, 59, 222]. Structure-oriented analysis of metabolic networks has generated important results on the prediction of essential genes [58] and the ability of topology-based methods to be used for such predictions in principle [57]. System-wide, global properties of metabolic networks, however, have only been investigated with respect to the optimality of bacterial growth performance [57, 58], and, recently, by showing pathway redundancy in different systems [190, 200].

Although some studies on robustness in metabolism exist [59, 126], so far the relationship between metabolic network structure, functionality, robustness and cellular regulation has not been investigated systematically. Such an analysis may, for instance, allow for important insight into the design principles of metabolic regulation and their role in making the system robust towards disturbances. As regulation implies the realization of various behaviors on the background of the metabolic network structure, it should itself be adapted to, and thus affected by, the structure. Enzymes that always have to operate together in any potential steady state of the metabolic system, are, hence, expected to be coded for by co-expressed genes [40]. Here, for studying the connections between network functionality, robustness and gene regulation on the

basis of network structure alone, among other network characteristics, the non-decomposable pathways able to operate coherently at steady state (elementary flux modes) were determined and analyzed. The central metabolism of the well-studied bacterium *Escherichia coli* served as a model system.

3.2 Principles of structural network analysis

At a very abstract level, cellular metabolism can be thought of as a complex network in which substances (nodes) are linked to each other via reactions (links). For analysis of these networks, two major approaches can be distinguished: In the narrower field of systems biology, most analysis methods rely on network stoichiometry, reaction reversibilities and potentially other constraints such as maximal pathway capacities. Applications of graph theoretical methods on metabolism only use the scheme of network connections as a starting point [126]. The underlying principles of both approaches will be briefly described in this section.

3.2.1 Stoichiometric approach

Metabolism usually involves fast reactions and high turnover of substances when compared to regulatory events. Therefore, analysis of metabolic networks is often based on the approximation that on longer time scales metabolite concentrations and reaction rates are constant (quasi steady-state assumption). With the stoichiometry of the network represented in a stoichiometric matrix $\mathbf{S}$ (dimension: $q \times m$, q: number of reactions, m: number of metabolites), the quasi steady-state assumption leads to the fundamental metabolite balancing relation

$$\frac{d\mathbf{c}(t)}{dt} = \mathbf{S} \cdot \mathbf{r} = \mathbf{0} \,. \tag{3.1}$$

Here, $\mathbf{c}(t)$ denotes the time-dependent vector of metabolite concentrations and $\mathbf{r}$ the vector of net reaction rates representing a flux distribution in the network, respectively. Dilution of metabolites due to cell growth is neglected.

In general, an infinite number of flux distributions comply to the system of linear equations given by (3.1). However, all possible solutions are contained in a vector space called the null space. Its analysis in turn allows one to investigate the complete space of admissible network functionalities based on the network topology [108]. Previously established analysis methods in the field can be differentiated into three major approaches: elementary-mode analysis [228], extreme pathway analysis [224], and flux balance analysis (FBA) in a narrower sense, as it has been introduced in [264]. They all employ mathematical methods from convex analysis [210].

Elementary-mode analysis and extreme pathway analysis follow very similar concepts, namely to decompose the metabolic network into meaningful smaller units or pathways. Elementary flux modes $\mathbf{e}_i$ can be defined as the smallest sub-networks enabling the metabolic system to operate in steady state [226]. They are subject to the non-decomposability condition

saying that there must not be any steady-state flux vector $\mathbf{r}$ that has zero components wherever any $\mathbf{e}_i$ does and at least one additional zero component. This condition also implies genetic independence of elementary modes, because the set of enzymes (genes) in one mode can not be the subset of enzymes in any other mode [108, 226]. Such as any steady-state flux distribution, elementary flux modes have to fulfill the metabolic balancing equation (3.1). Moreover, elementary modes have to be thermodynamically feasible, i.e. all irreversible reactions must proceed into the right direction.

For example, in a hypothetical network (Fig. 3.1), five elementary modes exist, which cannot further be decomposed. In each elementary mode, the enzymes are weighted by the relative fluxes they carry. By linear combination of elementary modes, all thermodynamically and stoichiometrically feasible flux distributions can be obtained, i.e.

$$\mathbf{r} = \sum_i \lambda_i \cdot \mathbf{e}_i \quad \text{for all} \quad \lambda_i \geq 0 \tag{3.2}$$

with the non-negative scaling factors λ_i. Up to these scaling factors for each mode, the set of elementary modes is unique for a given network structure [227]. Hence, it enables to investigate the space of all physiological states that are meaningful for the cell in the long-term perspective.

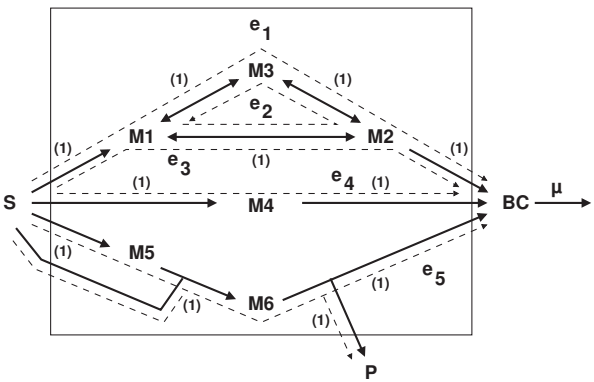

Fig. 3.1: Example network. Reactions (solid arrows, 1:1 stoichiometry for substrates and products) convert substrate S into a biomass component BC and a secreted by-product P via internal metabolites M1-M6. Cellular growth rate μ is approximated by the production of BC. The hypothetical network comprises five elementary flux modes e_i (dashed arrows, relative flux in braces). The modes e_1, e_3 and e_4 give the same BC:S yield of 1:1, while e_5 gives a yield of 1:2. In this network, extreme pathways and elementary flux modes are identical.

Extreme pathways differ from elementary modes in that their computation requires a slightly different model formulation. External sources and sinks such as extracellular substrates are connected to the network by exchange fluxes (which may be reversible or irreversible), while all

internal reactions must be irreversible. If necessary, reversible internal reactions have to be split up into forward and backward reactions. Elementary modes can be non-negative linear combinations of other elementary modes. This situation does not occur for extreme pathways, which may result in a smaller set of pathways compared to elementary modes if some exchange fluxes are reversible [223], otherwise both sets coincide [139]. The compactness of the set of extreme pathways has been argued to be an advantage of this concept. However, as shown in [139], this smaller set size compared to elementary modes may lead to incomplete results e.g. for analysis of network flexibility. For metabolic models approaching the whole-cell level, moreover, such reversible exchange fluxes are hardly conceivable and are not employed in earlier models [58, 190, 200]. As for the hypothetical network in Fig. 3.1, for practical applications, therefore extreme pathways and elementary modes will be identical.

Elementary-mode analysis as well as extreme pathway analysis compute and use a set of several (or many) independent pathways uniquely describing the entire flux space. Flux balance analysis (FBA), in contrast, determines a single flux solution through linear optimization [58]. For this purpose, in most cases it is assumed that cells adjust metabolic fluxes in such a way that optimal growth rates are achieved. However, one uncertainty associated with this approach arises from the fact that the objectives according to which e.g. cellular regulation works optimally – its underlying logic – are essentially unknown. Moreover, the optimal solution obtained by FBA is included in the set of elementary modes as long as no additional constraints have to be obeyed [226], but it is only valid for a specific situation, and not necessarily unique. This is obvious, for example, in the network shown in Fig. 3.1, where three elementary modes ($\mathbf{e}_1, \mathbf{e}_3, \mathbf{e}_4$) lead to the same, maximal growth yield. Further shortcomings of this method for the type of study to be carried out here result from FBA's focus on a specific behavior. Sub-optimal flux distributions for a given situation can not be determined by FBA. As a consequence, FBA is hardly able to handle functional features linked to network flexibility such as robustness. Without additional constraints, for example the incorporation of additional knowledge on cellular control circuits (an approach termed "regulatory FBA" [42, 43]), FBA will also be unable to cope with metabolic regulation.

Taken together, elementary-mode analysis provides the most promising method for assessing robustness and its underlying mechanisms in metabolic networks. For the reasons given above, results obtained by this method will be the same as for analysis of extreme pathways. Flux balance analysis, however, characterizes a different – albeit presumably limited – approach. It will be employed for comparison to elementary-mode analysis.

3.2.2 Graph-theoretical approach

The graph-theoretical approach to capturing structure and function of complex networks in quantitative terms entirely differs from the methods presented so far. It only uses the pattern of network connections to derive structural parameters, which are supposed to characterize net-

work function and dynamics [249]. From the reaction scheme, graph representation including nodes (metabolites) and links (reactions) are derived. Two metabolites are considered to be connected when they are involved in the same reaction. e.g. one as substrate and the other as product. For analysis of this graph, the connectivity k of a node, i.e. the number of links it is attached to, is of primary interest.

The distribution of probabilities $p(k)$ for a node to have a defined connectivity k allows to classify networks according to their overall topology. In statistically homogeneous networks (random graphs, Fig. 3.2a), the connectivity follows a Poisson distribution with most nodes having a connectivity close to the average connectivity $\langle k \rangle$. Accordingly, the chance of detecting a highly connected node decays with

$$P(k) \approx e^{-k} \quad \text{for} \quad k \gg \langle k \rangle \,. \tag{3.3}$$

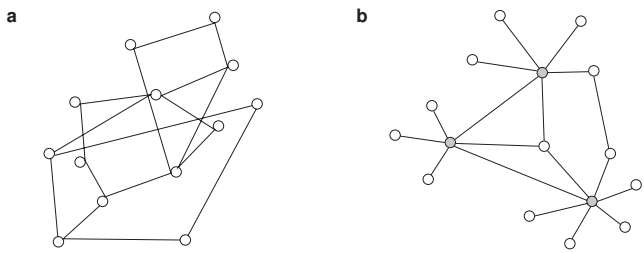

Fig. 3.2: Classes of network graphs. a, Representative structure of a random graph. **b,** Scale-free network, in which the overall topology is dominated by some highly connected nodes (gray).

Unlike random networks, scale-free networks are characterized by few dominating hubs with high connectivity, around which nodes with lower connectivity are clustered (Fig. 3.2b). Their extreme heterogeneity is reflected by a probability distribution of connectivities without accentuated peak. For large k, its decay follows a power law with parameter γ (the slope of a linear regression in a double logarithmic plot):

$$P(k) \approx k^{-\gamma} \quad \text{for} \quad k \gg \langle k \rangle \,. \tag{3.4}$$

As graph-theoretical analysis of genome-scale metabolic networks pointed out, these networks have scale-free character. The overall topology as well as the major hubs of these networks such as ATP, a general energy current for many reactions, are well conserved among species [72, 126]. More importantly, the network topology has been shown to be robust against random removal of nodes; only when central hubs are deleted, system fragmentation occurs. In particular, the network diameter D, defined as the average minimal path length between any two nodes (substances), turned out to be relatively invariant upon random removal of nodes in metabolic networks. This has been suggested to reflect network robustness, since an increasing

diameter would indicate network disintegration [126, 143]. This prediction, however, awaits correlation with real-world behavior especially since random mutations in cellular networks correspond more to the removal of links (reactions), than deletion of nodes. For robustness analysis of *E. coli* metabolism, the graph-theoretical approach will therefore be evaluated in parallel with methods relying on stoichiometric network analysis.

3.3 Model of *Escherichia coli* central metabolism

Elementary-mode analysis has mainly been applied to biochemical networks of moderate complexity [48, 211, 226, 227]. To explore the utility of the approach for a system of realistic complexity, the central metabolism of the bacterium *Escherichia coli* was chosen as an example. The central carbon catabolism, in particular, provides a plethora of alternative routes for generating essential precursor molecules, energy (ATP) and reduction (NAD(P)H) equivalents. Focusing on this part of metabolism seemed best suited to analyze network robustness, which may result from pathway redundancy. In analogy to other network analyses [58, 187], hence, central carbon metabolism was modeled in - partially extended - detail (Fig. 3.3). In the anabolic part of the model, lumping predominantly linear pathways into single assembly reactions served to reduce model complexity. The following paragraphs will give a concise overview of the model structure; details can be found in appendix A, Tab. A.1-A.2.

In brief, the model contains pathways for the uptake of representative substrates feeding into different parts of catabolism, namely the PTS system and the hexokinase transporter for glucose, as well as single uptake pathways for glycerol, succinate and acetate. The following major catabolic pathways were included and mostly captured at the single-reaction level:

(1) Glycolysis and gluconeogenesis: major pathways for conversion of glucose-6-phosphate to pyruvate (and vice-versa for gluconeogenesis), for fueling the cell with C_6 and C_3 building blocks, and for the generation of ATP through substrate-level phosphorylation;

(2) Pentose phosphate pathway (PPW): interconversion of carbohydrates and production of NADPH as reduction equivalent mainly used for biosynthetic purposes (oxidative branch) and fueling with precursors such as erythrose-4-phosphate (non-oxidative branch);

(3) TCA cycle: general pathway for the final oxidation of fueling compounds, provides electrons for oxidative phosphorylation by the respiratory chain as well as precursors for biosynthesis;

(4) Glyoxylate bypass: shunt to the TCA cycle, which by avoiding decarboxylation reactions, allows for synthesis of succinate from acetate;

(5) Anaplerotic reactions: linker reactions between the TCA cycle and glycolysis for replenishing pools of intermediates;

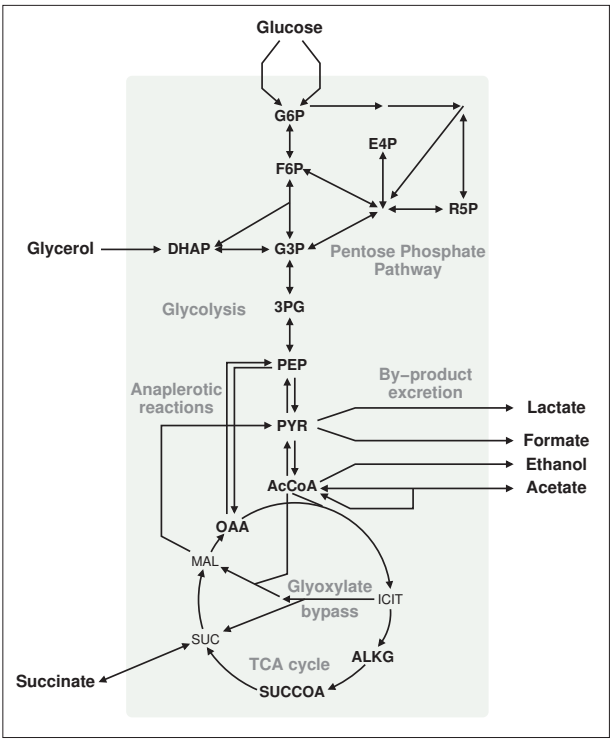

Fig. 3.3: Overview of *E. coli* central catabolism. Shaded areas indicate the intracellular space. Only major nodes and the twelve precursor metabolites (bold face) identified in [183] are named explicitely (G6P, glucose-6-phosphate; F6P, fructose-6-phosphate; R5P, ribose-5-phosphate; E4P, erythrose-4-phosphate; DHAP, dihydroxy-acetone-phosphate; G3P, glyceraldehyde-3-phosphate; 3PG, 3-phosphoglycerate; PEP, phosphoenol-pyruvate; PYR, pyruvate; AcCoA, acetyl-coenzyme-A; ICIT, iso-citrate; ALKG, α-ketoglutarate; SUCCOA, succinyl-coenzyme A; SUC, succinate; MAL, malate; OAA, oxalo-acetate). The combination of the readily interconvertible metabolites DHAP and G3P constitutes the pool precursor "Triose phosphate" according to [183]. Reactions were partially combined. Reversibility of a pathway does not necessarily indicate reversibility of all reactions, but may rely on pairs of counter-acting, irreversible reactions.

(6) Energy / reduction equivalents: ATP supply by oxidative phosphorylation, surplus ATP production for cellular maintenance, and interconversion of NADH and NADPH (transhydrogenation);

(7) By-product excretion: formation of lactate, formate, ethanol, acetate and succinate, which are released into the medium.

Previous networks [58] were extended by - among others - the anaplerotic reactions via malic enzyme and pyruvate oxidase as well as by parallel pathways for initial acetate metabolism. Some parts of the catabolic network of *E. coli*, which are mainly activated for anaerobic growth such as the Entner-Doudoroff pathway or the uptake of external electron acceptors were omitted in order to obtain a model of manageable complexity.

Anabolism comprises the part of metabolism, which is mainly responsible for the conversion of precursor metabolites into building blocks of macromolecules. To finally enable one to describe biomass synthesis, the pathways for building blocks for all relevant cellular macromolecules were included in the model. In particular, synthesis of all amino acids, of nucleotides for RNA and DNA, of fatty acids, and of sugars and lipopolysaccharides for cell wall assembly were captured. Most of these biosynthetic pathways are linear such that they could be lumped into one single pseudo-reaction each. Branch points in, for instance, amino acid interconversion, required a more detailed description.

For polymer synthesis from monomers, again, the fact that polymer compositions in *E. coli* are relatively constant under varying growth conditions [183,264] was exploited to set up overall reactions for these pathways. The growth rate is approximated by the production rate of macromolecular cellular constituents like DNA and protein. It is modeled as one reaction converting a fixed ratio of precursors into biomass. The implicit assumption of a fixed macromolecular composition of the cell, however, constitutes a simplification, since it is known that parameters such as the protein content or the type of storage compound varies with growth conditions. To assess the effect of this variability on model predictions, two alternative, experimentally determined average patterns of macromolecular composition (Tab 3.1) were considered. Unless stated otherwise, in the following the first scenario will be used as the standard parameter set.

Tab. 3.1: Two alternative scenarios for overall macromolecular biomass composition. Data for the standard scenario 1 were adapted from [264]. The second macromolecular composition from [183] does not amount to 100% since the soluble pool of building blocks as well as inorganic ions are not captured by the stoichiometric model used herein.

Macromolecule	Percentage of dry weight	
	Scenario 1	Scenario 2
Protein	64.0	55.0
DNA	18.5	20.5
RNA	3.0	3.1
Lipid	10.0	9.1
Lipopolysaccharide	1.5	3.4
Peptidoglycan	1.5	2.5
Glycogen	1.5	2.5

Altogether, the network contains 89 substances and 110 reactions, of which 68 reactions can be attributed to single gene products or to multi-enzyme complexes co-operating in a single reaction. The stoichiometric model thereby allows a concise description of the central metabolism in *E. coli* from substrates to biomass and, simultaneously, the analysis of major parts of the metabolic network at the single-reaction or single-gene level.

3.4 Structural network analysis

In this section, structural network analysis for the *E. coli* central metabolism will first consider the calculation of elementary flux modes and interpretation of the overall number of modes in terms of network flexibility (section 3.4.1). Next, the method was evaluated for prediction of mutant phenotypes to assess the validity of the approach to describe the *in vivo* situation (section 3.4.2). Closer studies on robustness in the metabolic network using different methods of structural network analysis follow (section 3.4.3), which will finally be connected to an investigation into the role of cellular regulation, namely of metabolic control by gene regulation (section 3.4.4).

3.4.1 Elementary-mode determination and network flexibility

Pathway analysis in metabolic networks is a combinatorial problem. With increasing numbers of metabolites and reactions, the number of alternative, overlapping routes increases more than linearly [138]. Computation of elementary modes (or extreme pathways) in complex networks such as the *E. coli* model studied here, therefore requires efficient software tools. For this purpose, the ”FluxAnalyzer” [140], a program with graphical user interface for the analysis of metabolic networks based on Matlab (Mathworks, Inc.) was used and further developed. In particular, the software contains a core algorithm for determination of elementary modes described previously [227]. This algorithm was optimized with respect to computation speed and memory requirement by additional pre-processing steps as well as by a modified implementation of the comparison of preliminary flux patterns, the most time-consuming step in the iterative procedure [138, 140].

Elementary modes were determined for the network model described above for the simultaneous uptake of the four substrates glucose, glycerol, succinate and acetate. Selecting subsets of modes allows for detailed analysis of e.g. different substrate uptake regimes. For instance, to analyze growth on glucose alone, all modes have to be selected, in which either the PTS system or hexokinase are active, and all the uptake systems for the other substrates display zero flux. Tab. 3.2 gives an overview of the number of elementary flux modes for different specifications. Here, the number of modes simultaneously meeting a set of conditions $C_1, \ldots, C_n$, is denoted by $N(C_1, \ldots, C_n)$. These conditions include, for example, the situation where cells can grow, which is abbreviated by μ. Excess energy production in the form of ATP (ATP), the sub-

strate metabolized (S_k for the k-th substrate) and oxygen uptake (O_2) are specified accordingly. The operator '$\neq$' indicates that certain fluxes must not occur. The total number of modes for single-substrate uptake includes one futile cycle without substrate consumption.

Tab. 3.2: Number and distribution of elementary flux modes. Abbreviations of substrates are: Glc, glucose; Gly, glycerol; Suc, succinate, Ac, acetate. The notation for selecting sets of elementary modes is explained in the main text.

		Single substrate uptake:					Simultaneous
Selection		Glc	Ac	Gly	Suc	Total	utilization
-	N	27,099	598	11,332	4,249	43,279	507,633
Growth only	$N(\mu, \neq ATP)$	73.1%	58.7%	78.6%	76.3%	74.6%	90.2%
ATP only	$N(\neq\mu, ATP)$	3.2%	5.0%	2.4%	2.4%	3.0%	0.6%
Growth and ATP	$N(\mu, ATP)$	6.6%	2.0%	5.1%	4.2%	5.9%	4.0%
No growth / ATP	$N(\neq\mu, \neq ATP)$	17.1%	34.3%	13.9%	17.1%	16.5%	4.3%
Aerobic growth	$N(\mu, O_2)$	73.1%	60.7%	83.6%	80.5%	76.4%	93.4%
Anaerobic growth	$N(\mu, \neq O_2)$	6.6%	0.0%	0.0%	0.0%	4.1%	1.7%

The total number of elementary modes for the given conditions is here used as a quantitative measure of the degrees of freedom [108], that is, of network flexibility or redundancy. As the comparison of the absolute numbers of pathways shows, although all substrate regimes comprise the same number of reactions and metabolites, they differ by two orders of magnitude. When considering only single-substrate regimes, glucose, for example, can be utilized in approximately 45 times more different ways than acetate, which corresponds to biological intuition. Simultaneous utilization of all substrates enhances the number of alternative pathways by a factor of ten. Compared to other studies in the field [190, 200], which obtained no more than approximately 20.000 functional units (extreme pathways), the complex model of *E. coli* central metabolism analyzed here shows considerably higher structural flexibility. This also reflects the structural information inherent to the elementary modes, which makes them valuable tools for the analysis of network functionality.

Within the six sets of elementary modes compiled in Tab. 3.2, a majority for each regime supports growth, i.e. could sustain the organism's viability by alternative routes in cases when disturbances in specific reactions occur. The possibility to use different carbon and energy sources enhances this ability. The fact that anaerobic growth is comparably under-represented presumably results from the specific formulation of the network model as discussed in section 3.3. However, these data provide an example of how flux mode number directly relates network structure to function. An empty set implies that no steady-state flux distribution fulfilling the stoichiometric and thermodynamic constraints described, and complying with the specifications exists, hence predicting an inviable phenotype. For instance, as observed *in vivo*, anaerobic utilization of any of the four substrates but glucose is impossible without additional terminal

electron acceptors. As a prerequisite for the analysis of network robustness to be carried out, this property will be exploited to assess the quality of predictions obtained by elementary-mode analysis, in particular concerning mutant phenotypes.

3.4.2 Predicting mutant phenotype

Based on the set of elementary modes determined for wild type, the ability to grow or not of mutants carrying deletions in single genes was investigated. For this purpose, the number of flux modes for a mutant Δi utilizing substrate S_k is determined by (additionally) selecting for those flux modes that do not require the reaction catalyzed by the product of gene i. The number of flux modes N showing a positive growth rate μ for this mutant is denoted by $N(\mu, \Delta i)$. Theoretical predictions were then compared to experimental data on mutant phenotypes, which have been compiled in appendix A, Tab. A.3.

Here, 90 different combinations of single-gene deletion and carbon source were investigated. The relative number of flux modes for these mutant strains allows a correct prediction of the experimentally determined growth phenotype in the overwhelming majority of cases (Fig. 3.4a).

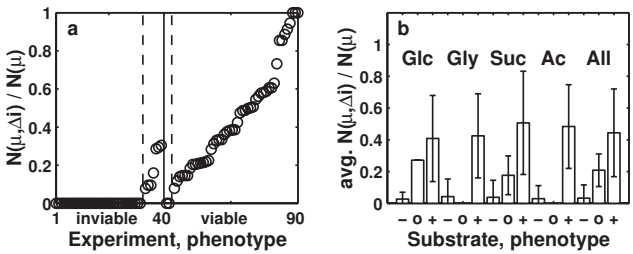

Fig. 3.4: Metabolic network topology and phenotype. a, Relative number of elementary modes enabling deletion mutants Δi of *E. coli* to grow for 90 different combinations of mutation and carbon source. The solid line separates experimentally determined inviability from viability. Dashed lines delimit the situations with erroneous predictions. **b,** Averaged ratios of flux mode numbers separated by three classes of mutant phenotype (+: viable, o: ambiguous results, -: inviable) and the carbon sources used in growth experiments (glucose, glycerol, succinate, acetate and all four substrates).

Most situations with an empty (non-empty) set of flux modes correspond to inviable (viable) mutants. Altogether 90% of the predictions (81 out of 90 cases) were correct. Incorrect predictions were obtained in 9 cases, which are summarized in Tab. 3.3. Among these, two false negatives, i.e. the prediction of viability whereas *in vivo* cells can not grow, are linked to the gene for phosphogluco-isomerase (*pgi*), which inter-converts fructose-6-phosphate and glucose-6-phosphate. This can be accounted for by the model structure that requires glucose-

Tab. 3.3: Incorrect predictions of mutant phenotype. Cases, in which mutants were predicted to be viable, whereas *in vivo* they are not (false positives) are separated from cases of incorrect assignment of viability by the analysis (false negatives).

	Gene	Substrate(s)	*in vivo* situation
False positives:	*pfkA*	Glc	
	fba	Glc	inhibition of stable RNA synthesis [241]
	tpiA	Glc	potential formation of toxic methylglyoxal [78]
	ppc	Gly	
	sucAB	Suc, Ac	
	mdh	Ac	severely impaired growth [41]
False negatives:	*pgi*	Gly, Suc	substitutable precursor glucose-6-phosphate [27]

6-phosphate for growth and, hence, its production via gluconeogenesis when the cell utilizes substrates other than glucose, whereas *in vivo* this precursor is substitutable [27]. Erroneous positive predictions are partly explained by side-effects caused by the respective mutations, which can not be captured by the model. They may also be caused by insufficient pathway capacities (kinetic constraints) *in vivo*, i.e. the inability to install the flux ratios that would be required for balancing the network.

As can be noted in Fig. 3.4a, the share of elementary flux modes operational in a specific mutant may vary to a large degree. To assess the influence of this variation on prediction quality, mean values and standard deviations of the number of elementary modes were determined separately for the four substrates and for the growth phenotype (Fig. 3.4b). A statistically significant classification of growth behavior ($p < 10^{-5}$ for all substrates) results from the analysis. Taken together, it seems, hence, justified to regard the relative number of elementary modes as a reliable indicator of network function. In this respect, however, the flux-balance approach is complimentary to the analysis of elementary modes, since by both methods similarly good predictions of *E. coli* mutant phenotypes were obtained [58].

3.4.3 Analysis of network robustness

For the metabolic network of *E. coli*, the structure-function relationship with respect to network robustness might be addressed by elementary-mode analysis as well as by using a graph-theoretical approach. In both cases, robustness is defined operationally as insensitivity of network function, i.e. the ability to sustain bacterial growth, despite internal disturbances like mutations [11]. The view of an ”optimal” architecture of metabolic control that serves to provide robustness, for instance, forms the core of the successful cybernetic modeling approach [144]. Here,in particular the effects of deletions of single genes coding for metabolic enzymes were investigated, since for these disturbances predictions correspond well to the behavior *in vivo*.

Analyzing the effect of changes in, for example, kinetic parameters is not possible using the structural analysis, which does not incorporate reaction dynamics. However, the gene deletions investigated here would represent an extreme case of parameter perturbations, such that results obtained by structural analysis provide a framework for more detailed analysis.

The number of elementary modes qualitatively indicates whether a mutant is viable or not, but it does not necessarily describe, to what extent a mutation affects growth quantitatively. Therefore, additionally the maximal biomass yield Y^{max} for each combination of mutant and substrate was calculated as a quantitative measure of network performance. Maximal biomass yield Y^{max} for a given substrate was defined as the optimum of

$$Y_{i,X/S_k} = \frac{e_i^{\mu}}{e_i^{S_k}} \tag{3.5}$$

The superscripts to e specify single reaction rates - here, growth and substrate uptake - in elementary flux mode i selected for utilization of the k-th substrate S_k.

The effect of random mutations on bacterial growth was assessed by determining number and biomass yield of flux modes after deletion of each single reaction for the four (exclusively used) substrates glucose, acetate, glycerol, or succinate, respectively. The maximal biomass yield depending on the share of operational modes in the mutants is summarized in Fig. 3.5a. Central metabolism of *E. coli* behaves highly robust, since mutants with significantly reduced metabolic flexibility show a growth yield similar to wild type. Only when the number of elementary modes is severely cut down by a mutation, functionality is affected. On average, approximately 10% of the modes will be sufficient to enable nearly wild type growth capability.

Robustness relies, at least in part, on pathway redundancy. Analysis of the set of elementary modes in wild type reveals the existence of multiple, alternative pathways with identical biomass yield (Fig. 3.5b). No pronounced decrease of the share of elementary modes towards higher yields can be detected, which explains the finding of relative insensitivity of growth when a single gene is deleted. Taken together, however, elementary-mode analysis points to a co-existence of robustness (against most types of genetic perturbations) and fragility (regarding few, specific gene deletions), as already shown for cellular regulation [45, 248, 272].

A plausible hypothesis concerning the connection between network flexibility and robustness is that the degrees of freedom of a network could be used to predict its sensitivity towards disturbances. Therefore, next, the question whether the number of elementary modes N directly relates to network robustness was investigated. As a measure for robustness, the maximal growth yield for each mutant as already shown in Fig. 3.5a was used. Counting the number of cases for which $Y^{max}(\Delta i) > 0$ gave the number of viable single-gene mutants for each substrate regime, i.e. a measure of the probability to tolerate deletion mutations.

For different single-substrate uptake regimes, the organism's resistance to arbitrary gene deletions correlates well ($r^2 = 0.93$) with N for the corresponding wild type (Fig. 3.5c). Similar results are obtained when considering the cases when more then one substrate can be utilized.

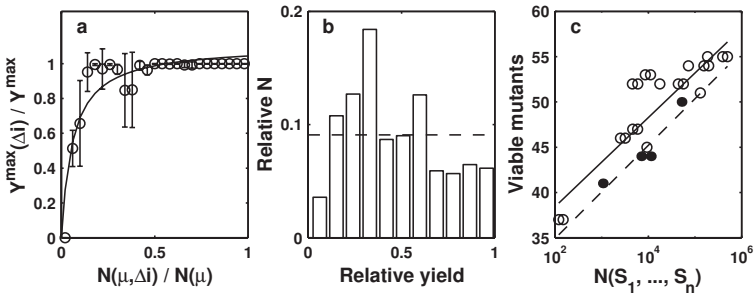

Fig. 3.5: Robustness analysis using elementary flux modes. a, Dependency of the mutants' maximal growth yield $Y^{max}(\Delta i)$ on the share of elementary modes operational in the mutants. Data were binned to reduce noise. The regression curve was obtained by fitting $y = k_1 \cdot x/(k_2 + x)$ with $k_1 = 1.11$ and $k_2 = 0.06$. **b,** Distribution of growth-supporting elementary modes, i.e.share of elementary modes in wild type having a specific relative growth yield compared to wild type utilizing the respective substrate. For comparison, an equal distribution (−−) has been included. **c,** Effect of arbitrary gene deletions on viability for single substrate uptake (•) and for simultaneous uptake of multiple substrates (○) assessed by relating the number of viable mutants to the total number of elementary flux modes in the respective wild type. Linear regressions for single substrates and for all data points shown in the panel are indicated by −−and —, respectively.

Here, in general, the number of viable mutants is higher than for single-substrate regimes showing a comparable number of elementary modes. Most likely, this represents the effect of higher degrees of independence of metabolic pathways for the multi-substrate case. The ability to utilize different carbon sources simultaneously could, thus, also be advantageous for the organism when the type of robustness discussed here is considered. In general, these data show that to a certain extent the number of elementary modes provides an estimate for fault-tolerance of metabolic networks.

Graph-theoretical methods are widely used to analyze complex networks [17, 126, 249] and could provide important clues on the robustness of metabolic networks. In particular, invariance of the network diameter D towards random disturbances in the network structure has been suggested to reflect network robustness, i.e. absence of network disintegration [126]. In a first step, graph-theoretical parameters of the network studied herein, and of the elementary modes as specific sub-networks were checked for consistency with topological characteristics of large-scale metabolic networks. Analysis of network connectivity was performed as described in [126].

The network studied here is scale-free, i.e. the probability $P(k)$ for a substance to participate in k reactions decays according to $P(k) \approx k^{-\gamma}$ (Fig. 3.6a). The corresponding exponents $\gamma_{in} = 1.5$ and $\gamma_{out} = 1.3$ for incoming and outgoing links, respectively, were obtained by least square

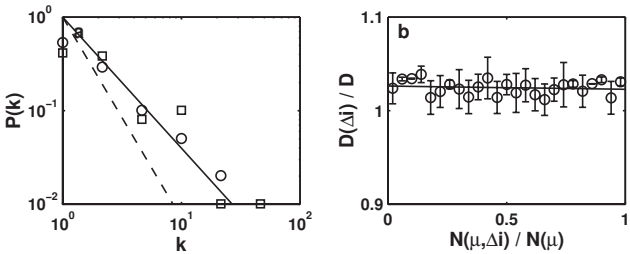

Fig. 3.6: Graph-theoretical analysis. a, The distribution of network connectivities $P(k)$ is shown separately for incoming (○) and outgoing (□) links. Data were binned to reduce noise. Linear regressions for the *E. coli* network with $\gamma = 1.4$ (—) and for $\gamma = 2.15$ reported in [126] (−−) are included. **b,** Average mutant network diameters $D(\Delta i)$ relative to the network diameter of wild type D as a function of the (relative) number of growth-supporting elementary modes in the mutants considered (—: linear regression).

fit to the binned data. The regression of the probability distribution for the average $\gamma = 1.4$ is shown in the panel. Compared to a previous analysis of the genome-scale *E. coli* metabolic network [126] (dashed line, $\gamma = 2.15$), the characteristic slope is smaller due to the focus on the highly interconnected central metabolism. Less connected metabolites in the periphery of the metabolic network have been under-represented in this selection, whereas for energy and and reduction equivalents often also occurring in peripheral pathways, the connectivity numbers are lower than in the genome-scale networks.

The diameter of the entire network ($D = 2.9$) as well as the average network diameter of elementary modes ($D = 2.9 \pm 1.1$) correspond well to the values of $D = 3 - 3.5$ previously reported [17, 126]. However, for the network studied here, a constant diameter does not necessarily imply identical functionality (Fig. 3.6b). If the diameter reflected network functionality, for a decreasing number of elementary modes as a reliable indicator of mutant viability, the diameter should increase significantly. In contrast, only a slight increase can be detected, which proves to be statistically insignificant. For all mutants considered, the diameter turned out to be slightly higher than for wild type, but this is uncorrelated to the *in vivo* growth behavior of the specific deletion strains.

Robustness and fragility, hence, are not predicted by a pure graph-theoretical measure of network topology. In contrast to elementary modes, for instance, the network diameter does not reflect specific characteristics of metabolism such as molar yields. Moreover, metabolic networks are not simple graphs as suggested by this direction of research, but hyper-graphs, in which one edge (reaction) may link more than two nodes (substances). For the specific requirements of analysis of structural robustness in metabolic networks, thus, the approach based on elementary flux modes could be validated for the network studied, whereas the graph-theoretical approach proved to be less suitable.

3.4.4 Robustness and genetic control

Elementary-mode analysis of the *E. coli* metabolic network underlines the network's robustness when drastic perturbations such as the complete inactivation of a specific gene for a metabolic enzyme occur. During a bacterium's average life, however, it seems more likely that the majority of perturbations will be caused by short-term fluctuations in the environmental conditions, for instance variations in nutrient availability or the exposure to toxic compounds. A suitable strategy to cope with these challenges would be to provide certain aspects of the flexibility encoded in the metabolic network structure by cellular regulation. The cell could adjust transcript levels and / or protein levels such that they not only enable optimal flux distributions for a specific situation [57], but also allow for fast re-adjustment of fluxes in case of different conditions. A basal expression of enzymes likely to be required to reject common disturbance - and their down-regulation by, for example, allosteric control in situations where these enzymes are not needed - would be in accordance with such a concept of metabolic regulation. This, in turn, leads to the question whether the steady–state results of the intrisically dynamic regulation in complex metabolic networks could be predicted by elementary-mode analysis.

A direct, quantitative correlation between metabolic fluxes and transcriptome or proteome patterns has not been observed [186, 187, 253]. However, the existence of a more indirect link seems likely. To assess the degree to which cellular regulation accounts for metabolic robustness, the basic assumption employed herein is that optimization during biological evolution can be characterized by the two objectives of flexibility - associated with robustness - and efficiency [11, 108]. This is, for example, supported by evidence from the evolution of energy transduction [195]. Comparison of predictions based on structural network analysis with *in vivo* data on cellular regulation should allow for conclusions on the relative importance of the two objectives.

Flexibility means the ability of cellular systems to adapt to a wide range of environmental conditions, i.e. to realize a maximal bandwidth of thermodynamically feasible flux distributions, hence of elementary flux modes. Efficiency, as the second objective, could be defined as the fulfillment of cellular demands with an optimal outcome such as maximal cell growth [57, 58], using a minimum of constitutive elements (i.e. genes and proteins) [108]. Since these two criteria impose contradictory challenges, optimal cellular regulation needs to find a trade-off. The analysis will therefore rely on a parameter characterizing flexibility and efficiency derived from metabolic network structure, for which the term "control-effective flux" is introduced.

Control-effective fluxes are determined directly from the set of elementary modes, and do not require optimization. The analysis begins by assigning an efficiency to each elementary mode. These efficiencies ε_i relate the output of the i-th mode (growth or ATP production for cellular maintenance requirements) to the investment required to establish the mode, i.e. to produce the enzymes. This investment is approximated by the sum of all (absolute) fluxes, since for comparable metabolite concentrations, the flux through an enzymatic reaction scales

linearly with enzyme concentration. With flux modes normalized by the total substrate uptake, efficiencies $\varepsilon_i(S_k, \Omega)$ for the targets for yield optimization - growth and ATP generation - are defined as

$$\varepsilon_i(S_k, \mu) = \frac{e_i^{\mu}}{\sum_l |e_i^l|} \quad \text{and} \quad \varepsilon_i(S_k, ATP) = \frac{e_i^{ATP}}{\sum_l |e_i^l|} \quad . \tag{3.6}$$

The calculation of efficiencies and control-effective fluxes will be illustrated using the hypothetical network shown in Fig. 3.1. In this network, ATP is not generated, and, hence, only the growth rate has to be considered. It is assumed to be identical to the production rate of the biomass component BC. Tab. 3.4 gives the absolute fluxes for each reaction in each elementary mode of the example network required for these calculations. They can easily be derived from the graphical representation. For all reactions in the fifth mode, fluxes have to be normalized by the two units of substrate consumed. According to (3.6), the efficiency of $\mathbf{e}_1$ then, for instance, is obtained by dividing the growth rate e_1^{μ}, which equals the rate of production of BC via the reaction M2 →BC, by the total flux in the mode, i.e. it is 1/4. The other efficiencies are determined accordingly. For the example network, thus, elementary mode $\mathbf{e}_4$ would be favored over $\mathbf{e}_1$ and $\mathbf{e}_3$ involving more enzymatic steps for obtaining the same growth yield.

Tab. 3.4: Determination of control-effective fluxes. All data refer to the hypothetical network shown in Fig. 3.1. Absolute fluxes are normalized by the total substrate uptake in each mode, which in the case of the fifth mode amounts to two units of substrate per unit of biomass produced.

Reaction l	Elementary mode					Control-effective fluxes
	$\mathbf{e}_1$	$\mathbf{e}_2$	$\mathbf{e}_3$	$\mathbf{e}_4$	$\mathbf{e}_5$	$\frac{17}{12} \cdot \nu_1(S)$
	Absolute flux l in mode i $\lvert e_i^l \rvert$					
S →M1	1	0	1	0	0	7/12
M1 →M2	0	1	1	0	0	1/3
M1 →M3	1	1	0	0	0	1/4
M3 →M2	1	0	0	0	0	1/4
M2 →BC	1	0	1	0	0	7/12
S →M4	0	0	0	1	0	1/2
M4 →BC	0	0	0	1	0	1/2
S →M5	0	0	0	0	1/2	1/6
M5 →M6	0	0	0	0	1/2	1/6
M6 →BC	0	0	0	0	1/2	1/6
$\sum_l \lvert e_i^l \rvert$	4	2	3	2	3/2	
	Growth rate e_i^{μ}					
	1	0	1	1	1	
	Efficiency $\varepsilon_i(S, \mu)$					
	1/4	0	1/3	1/2	1/3	$\sum_i \varepsilon_i(S, \mu) = 17/12$

Subsequently, control-effective fluxes ν_l are determined for a specific reaction l as the (normalized) average flux through this reaction in all elementary modes, whereby for each mode the actual flux is weighted by the mode's efficiency. In other words, control-effective fluxes $\nu_l(S_k)$ are obtained by averaged weighting of the product of reaction-specific fluxes and mode-specific efficiencies over the inventory of elementary modes using the substrate under consideration:

$$\nu_l(S_k) = \frac{1}{Y^{max}_{X/S_k}} \cdot \frac{\sum_i \varepsilon_i(S_k, \mu) \cdot |e^l_i|}{\sum_i \varepsilon_i(S_k, \mu)} + \frac{1}{Y^{max}_{A/S_k}} \cdot \frac{\sum_i \varepsilon_i(S_k, ATP) \cdot |e^l_i|}{\sum_i \varepsilon_i(S_k, ATP)} \quad . \tag{3.7}$$

Here, Y^{max}_{X/S_k} and Y^{max}_{A/S_k} denote optimal yields for biomass production and for ATP generation for cellular maintenance, respectively (experimentally determined yield parameters can, however, easily be incorporated into the approach). Due to the normalization of modes, the effect of system input (substrate utilization) is implied in (3.7). As the case of the hypothetical network shows (Tab. 3.4), reactions participating only in an inefficient mode with respect to biomass production ($\mathbf{e}_5$) will be weighted less than e.g. the most efficient mode ($\mathbf{e}_4$). Reactions S $\rightarrow$M1 and M2 $\rightarrow$BC, however, are assigned even more importance, which reflects the incorporation of flexibility as the second objective into the determination of control-effective fluxes.

In general, control-effective fluxes represent the importance of each reaction for efficient and flexible operation of the entire network. In contrast to flux-balance analysis (FBA) used to predict (optimal) flux distributions, this approach directly takes network flexibility into account because optimal and sub-optimal modes are considered. There exists, however, not such a strict separation between these two methods, but rather a continuum. By selection of sub-sets of elementary flux modes, for which the control-effective fluxes are calculated, the logic behind FBA can be approached; in the limit, only the most efficient flux modes would be considered.

Cellular control on longer time scales is predominantly achieved by genetic regulation. With control-effective fluxes relying on steady-state flux patterns, the control-effective fluxes should correlate with mRNA levels. Theoretical transcript ratios $\Theta(S1, S2)$ for growth on two alternative substrates $S1$ and $S2$ were therefore calculated as ratios of control-effective fluxes

$$\Theta_l(S_1, S_2) = \frac{\nu_l(S_1)}{\nu_l(S_2)} \, . \tag{3.8}$$

These theoretical predictions were compared to previously published cDNA-microarray data for *E. coli* growing exponentially on glucose, glycerol and acetate [186, 187]. The relevant experimental data can be found in Tab. A.3

The structure-derived prediction of the differential expression of 50 genes for acetate vs. glucose shows good agreement with experiment (Fig. 3.7a). The majority of predictions deviates from the measured values only by a factor of two or less. However, several theoretically derived transcript ratios differ from the corresponding experimental data to a higher degree. To elucidate, to which extent these differences could be attributed to random noise, or to systematic effects, a test for systematic errors was subsequently performed. It relied on comparing the distribution of residuals - the deviations between theoretical and measured values - to the normal distribution that would be expected if the differences were completely random [35].

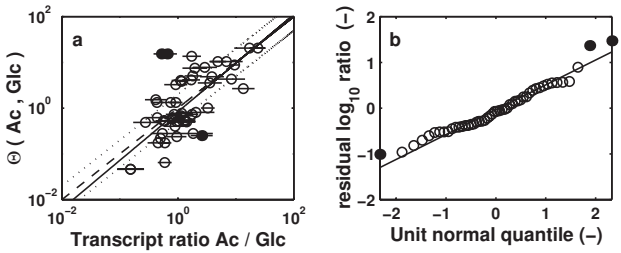

Fig. 3.7: Prediction of gene expression patterns (I). a, Calculated ratios between gene expression levels during exponential growth on acetate vs. growth on glucose (•= outliers, see panel **b**) based on all elementary modes versus experimentally determined transcript ratios reported in [186]. Lines indicate 95% confidence intervals for experimental data (horizontal lines), linear regression (—), perfect match (−−) and two-fold deviation from perfect match (· · ·). **b,** Distribution of residuals with outliers (•) identified by the deviation from the normal distribution. The straight line corresponds to the expected normal distribution when mean value and standard deviation of the residuals are considered.

This test leads to identification of three presumable outliers (Fig. 3.7b). Two overestimated transcript ratios are linked to genes involved in acetate metabolism (*pta*, *ackA*) and, hence, expected to be up-regulated on acetate. This counter-intuitive finding has also been discussed in [187]. It can be explained by the functionally related gene *acs*, which provides a parallel pathway for conversion of acetate to the central metabolite acetyl coenzyme A. Experimental observations [186] and the theoretical prediction agree in up-regulation of *acs* transcription when the cells use acetate as sole substrate.

The transcript ratio of *aspA* encoding for aspartase was underestimated by the control-effective flux method. The sets of elementary modes using or not involving this gene were therefore studied in more detail. Elementary mode analysis suggests that aspartase is required for an effective conversion of excess NADPH generated by the TCA cycle to NADH (Fig. 3.8), since, for growth on acetate, transhdyrogenase and apartase occur mutually exclusively in the elementary modes. This reaction cycle has also been detected earlier by analysis of a smaller sub-system of the metabolic network [226].

Residual analysis thus sustained or generated hypotheses amenable to further experimental investigation. Removal of the three outliers from a total of 50 data sets leads to a high correlation between prediction and experiment ($r^2 = 0.60$) with a linear regression close to perfect match. For a judgment on the quality of the predictions, also the variability in microarray studies of gene expression has to be taken into account. For instance, average expression ratios from independent experimental studies of *E. coli* growing on acetate vs. glucose [186, 187] correlate with $r^2 = 0.84$ (not shown).

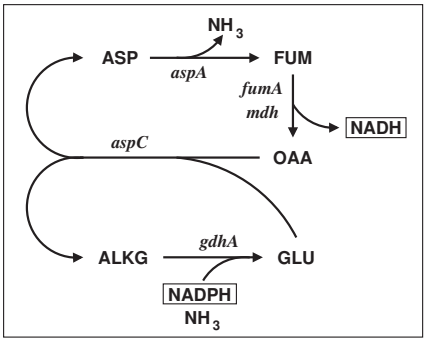

Fig. 3.8: Transhydrogenation via aspartase. Transhydrogenase and aspartase play a mutually exclusive role in growth-supporting elementary modes for acetate. Aspartase may thus be required for an effective transhydrogenase activity (i.e. the conversion of excess NADPH generated by the TCA cycle to NADH) via the reaction cycle shown here, which corresponds to an elementary mode found earlier [226]. Metabolites are: ASP, aspartate; FUM, fumarate; OAA, oxaloacetate; GLU, glutamate; ALKG, α-ketoglutarate. The cycle involves aspartase (*aspA*), fumarase (*fumA*), malate dehydrogenase (*mdh*), glutamate-synthase (*gdhA*) and aspartate-synthase (*aspC*).

The extent to which network flexibility or robustness is supported by the pattern of gene regulation was assessed by varying the set of elementary modes underlying the calculation of control-effective fluxes. As mentioned above, in an extreme case, which corresponds to the approach followed by FBA or regulatory FBA [42], only the two flux modes with optimal ATP and biomass yield were considered. A reasonable prediction quality for derivation of gene expression from optimal fluxes alone would imply a strong influence of the objective of efficiency on cellular regulation. It would result in extreme patterns of gene regulation tending to switch genes 'on' and 'off' in a binary fashion. However, as shown in (Fig. 3.9a), these predicted transcript ratios $\Theta^{opt.}(Ac, Glc)$ displayed a weak correlation with experimental data. Only 28 data points appear in the plot since many fluxes are zero and, hence, yield zero or undefined predictions.

A systematic investigation into this issue was performed by calculating the number of successfully predicted gene expression ratios and the number of outliers for varying mode optimality (Fig. 3.9b). Here, elementary flux modes were ordered according to their efficiency, and an increasing fraction of sub-optimal modes was included in the analysis. These data indicate that for a reliable prediction of the gene expression patterns observed *in vivo*, a significant fraction of potential pathways, i.e. of network flexibility, has to be taken into account. Neglecting flexibility may explain why FBA - even when supplied with information on regulatory circuits - only provides qualitative predictions for a subset of genes [42].

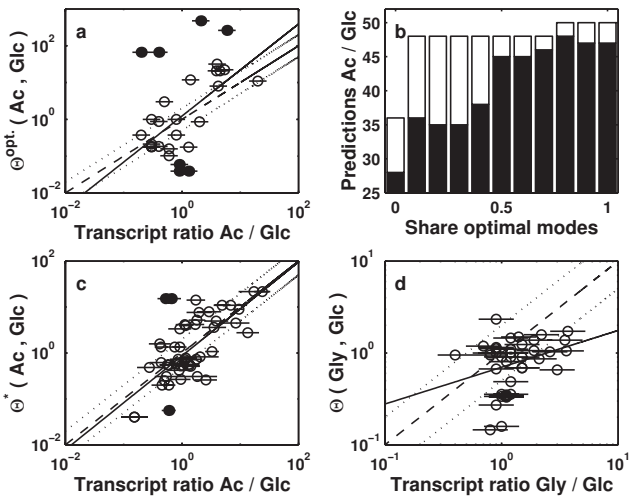

Fig. 3.9: Prediction of gene expression patterns (II). a, Predicted transcript ratios for acetate vs. glucose based on the two elementary modes with highest biomass and ATP yield. For setup of the panel, see Fig. 3.7. **b,** Prediction quality as a function of the share of elementary modes used for calculation of control-effective fluxes. Modes were ordered descendingly with respect to growth and ATP yield. Filled bars indicate the number of successfully predicted transcript ratios, open bars denote the (additional) number of outliers identified. **c,** Transcript patterns obtained by assuming an average biomass composition as reported in [183]. **d,** Gene expression ratios for glycerol vs. glucose based on experimental data from [187].

For testing the validity of the structure-based predictions of cellular regulation, three additional cases were considered. First, as already mentioned in section 3.3, the assumptions on cellular growth constitute a critical part of the stoichiometric model. Therefore, elementary flux modes were calculated and analyzed assuming a different scenario for biomass composition (Tab. 3.1). However, neither the number of elementary modes nor the predictions on mutant phenotype (not shown), nor the theoretical values for transcript ratios (Fig. 3.9c; $r^2 = 0.58$) were significantly influenced by this kind of modification. The overall metabolic network structure, hence, seems to dominate the results of the structural analysis, whereas they are insensitive towards moderate variations in specific stoichiometric coefficients.

Secondly, in view of the fact that experimental errors are large compared to the effects of changes in the medium, the predictions for the comparison of growth on glycerol with growth on glucose also agree reasonably well with experiment (Fig. 3.9d). Finally, prediction quality was poor when for elementary-mode analysis a simultaneous uptake of all substrates was enabled (not shown).

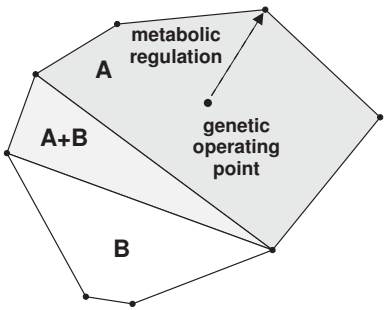

Fig. 3.10: Hierarchical control of metabolism. The cross-section of the flux cone that contains all admissible flux distributions (edges correspond to elementary flux modes) is sub-divided into regions involving the uptake of substrate 'A', of substrate 'B', or of both ("A+B'). With 'A' and 'B' present in the medium, but 'A' being the preferred substrate, it is suggested that a 'genetic operating point' will be established in the center of the 'A' region. Metabolic regulation serves to optimize flux efficiency as illustrated by the arrow pointing to one (optimal) edge.

The combination of these findings points to a multi-level, hierarchical organization of metabolic regulation [248] that is illustrated in Fig. 3.10. Transcriptional regulation for growth on a specific substrate seems to rely on selection of this substrate regime by the cell, for instance by catabolite repression. According to the substrate regime, gene expression levels are adjusted to provide a general set-up for metabolic efficiency and flexibility, which leads to a certain robustness of network function towards perturbations. At a lower level, short-term regulation of fluxes for a specific situation, such as for one defined substrate concentration, can then be achieved, for instance, by allosteric control of metabolic enzymes [57]. By providing the optimal framework for lower levels of regulation, control of genes directly related to metabolic function could thus serve as an intermediate layer of control between the top-level selection of the substrate regime and the bottom-level fine-tuning of fluxes.

Finally, the question of whether robustness through redundancy mainly relies upon duplicate genes, or on alternative pathways (see chapter 2.3.1) was addressed. It is known, that often isoenzymes, that is, enzymes able to carry out identical reactions, are differentially regulated. A large deviation between the gene expression patterns of isoenzymes could point to a minor role for duplicate genes in conferring robustness, because it is unlikely that considerable functional substitution would be achievable.

For this purpose, the isoforms of glycolytic (*gapA*, *pfkA*, *pykA*) and TCA cycle (*acnA*) enzymes, which under conditions of exponential growth contribute little to total enzymatic activity, were included in the comparison of predicted and theoretical transcript ratios (Fig. 3.11). In agreement with previous experimental studies [46, 215], the respective genes *epd*, *pfkB*, *pykA* and *acnB* turned out to be unregulated with respect to growth on acetate and glucose. Importantly, two of the transcripts for isoenzymes of genes that according to elementary-mode

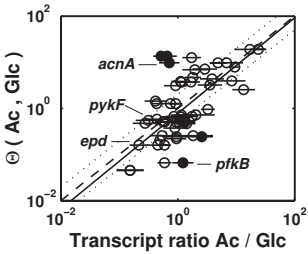

Fig. 3.11: Gene expression patterns and isoenzymes. In comparison to Fig. 3.7, data points for the previously not considered genes encoding for minor isoenzymes of pyruvate kinase (pykF), phosphofructokinase (pfkB), aconitase (acnA) and glyceraldehyde-3-phosphate dehydrogenase (epd) were included.

analysis were predicted to be differentially regulated, here were identified as outliers. Neither theoretical, nor experimental analysis of gene regulation for isoenzymes thus especially supports the assertion that cellular regulation is designed such as to provide robustness through closely related duplicate genes.

3.5 Conclusions

Elementary-mode analysis decomposes complex metabolic networks into simpler units performing a coherent function. The integrative analysis of elementary modes presented here can be used to reconstruct key aspects of cellular behavior from metabolic network topology, namely to reliably classify mutant phenotypes, to analyze network robustness, and to quantitatively predict functional features of genetic regulation. Including additional knowledge, for example, of newly annotated genes is straightforward [227].

For the model of *E. coli* central metabolism using identical network structures, elementary-mode analysis and extreme-pathway analysis yield equivalent sets of functional entities and, thus, identical results. Whereas these approaches characterize the spectrum of different, potential functionalities of the metabolic system, FBA focuses on a single flux distribution. FBA fails whenever network flexibility - for instance in the analysis of pathway redundancy or in quantitative prediction of gene expression - has to be taken into account. Similarly, the graph-theoretical approach proved unsuitable for assessing network robustness.

In subsequent studies, it will be intriguing to apply the analysis developed here to organisms other than *E. coli* and to further validate it with upcoming transcriptome and mutant data. More generally, the results lead to the conclusion that robustness of metabolic networks is primarily linked to pathway redundancy. Moreover, comparison of alternative theoretical models to experimental data strongly suggests that hierarchical genetic control supports this robustness by

finding a trade-off between network efficiency and flexibility. In this context, differential regulation of isoenzymes points to a minor role of redundant duplicate genes for robustness of the metabolic network. Structural analysis of cellular networks, as a complementary approach to the development of dynamic mathematical models, can thus contribute to elucidate fundamental design principles of living cells.

4. GENETIC OSCILLATORS: DYNAMIC ANALYSIS

4.1 Introduction

Complex dynamics in biological systems are most evident when considering rhythmic phenomena such as oscillations in metabolism, intracellular calcium signaling or cardiac rhythms at the organ level. Their interesting dynamic properties in combination with the essential role of many of the underlying oscillators in establishing cell or organ functionality made these systems prominent model systems for experimental and theoretical studies [94]. In general, feedback processes and cooperativity are two important mechanisms leading to nonlinearities in biological systems. They can force the systems to display instabilities which ultimately lead to sustained oscillations instead of simply reaching a steady state. Since the ground-breaking theoretical work of Goodwin in 1965 [96], it is clear that even a single gene may be sufficient to establish a genetic oscillator, provided that its gene product negatively regulates its own expression.

Genetic oscillators responsible for circadian rhythms represent the obvious manifestations of this principle in a relevant biological example. Circadian clocks provide endogenously controlled oscillations at the cellular level with a period of approximately 24 hours, which allow the organism to adapt to the day-night rhythms imposed by the environment. In contrast to other genetic oscillators, for instance, when compared to those underlying cell cycle regulation, circadian clocks are characterized by their simplicity. The network consists of a handful of components and their interactions. Furthermore, it is highly conserved between species such as the fungus *Neurospora*, the fruit fly *Drosophila melanogaster*, and humans [287]. This situation favorable to theoretical approaches elicited the development of a variety of different mathematical models for circadian oscillators, especially for the experimentally best investigated organism *Drosophila* [92, 155, 157, 221, 243, 244, 260, 261].

Model-based analyses of the *Drosophila* network pointed out its remarkable robustness in the presence of molecular noise [12, 95, 261]. Stochastic analysis showed that different models display model-specific robustness and fragility properties [292]. For several models, also a rejection of parametric perturbances was observed. However, these investigations were confined to analyzing the effect of parameter changes at one point in parameter space [243, 244], or to establish bifurcation diagrams for selected model parameters [156]. For the field of circadian

oscillators, moreover, few studies exist on the contribution of individual model parts such as single control loops on robustness [244, 260]. In a more systematic approach, Morohashi and colleagues recently focused on the comparative analysis of robustness in models of *Xenopus oocyte* cell cycle regulation by parameter variation and determination of characteristic features of the oscillatory region with the aim of assessing model - more specifically, parameter set - plausibility [180]. However, none of the above mentioned studies relied on determination of parameter sensitivities, which could, for example, provide a quantitative picture of how individual parameters contribute to model robustness - or fragility.

Taken together, at present a systematic investigation of the relationship between parameter sensitivity, model structure and behavior for circadian oscillators is lacking. The present work aims at addressing this topic by employing tools from systems engineering to perform a comparative analysis of global robustness and fragility properties of two published mathematical models for circadian clocks. After a brief introduction into the molecular biology of circadian clocks (4.2), the two related mathematical models describing this system in *Drosophila* will be presented (4.3). Their analysis will rely on the determination of parameter sensitivities, the methodological basis for which is outlined in (4.4). The discussion of the results obtained by comparative model evaluation will emphasize their biological implications (4.5).

4.2 Molecular biology of circadian clocks

The evolutionary conserved period generator displays a complex architecture, in which delayed negative feedback loops play a prominent role. Although the picture is not yet complete, it is clear that in *Drosophila*, the regulatory network consists of at least two negative auto-regulatory feedback loops controlling the expression of timeless (*tim*) and period (*per*) interlocked with a positive feedback loop established via the clock (*clk*) and *cyc* genes [101, 189, 278]. Complex formation, regulated translocation and degradation of several of these gene products, which are additionally controlled (and delayed) by protein phosphorylation, add further levels of complexity to the system [189]. The core interactions establishing the regulatory network in the fruit fly are depicted in Fig. 4.1.

As long as PER and TIM protein levels are low, from the early part of the (subjective) day until the beginning of evening, the transcription factors CLK and CYC (cycle, which is not shown in the scheme, because, contrary to its name, its concentration remains constant) coordinately activate per and tim gene expression. PER and TIM protein, however, accumulate in the cytoplasm only after a time delay of approximately 6 hours. The time required for transcription and translation alone can not account for this delay. It has been shown that both proteins are phosphorylated at multiple sites [56]. For the case of PER, one kinase responsible for this phosphorylation, and thereby rendering the protein instable, has been identified as double-time (DBT) [199]. In a similar manner, TIM is modified post-translationally by the kinase encoded by the *shaggy* gene [167]. Recent studies indicate that components of the ubiquitin-dependent

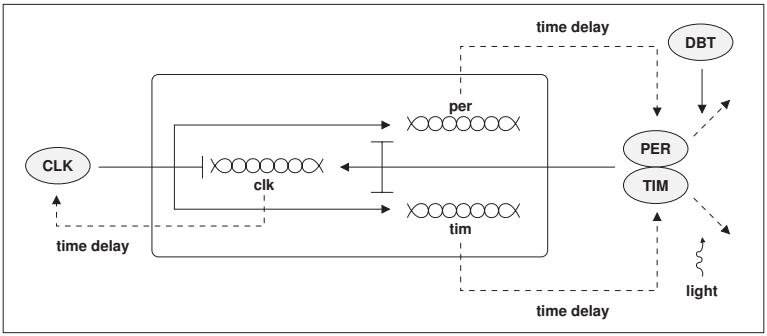

Fig. 4.1: Molecular interactions governing circadian rhythms in *Drosophila*. The network scheme connects protein products (shaded ellipses, names in upper case) and genes (double helices, names in lower case) by regulatory interactions (solid lines, arrows indicate positive influences, whereas bar heads mean repression) and substance flows (dashed lines). The inner box comprises all processes occurring in the nucleus, whereas the rest of the system is localized to the cytoplasm. The figure was adapted from [101, 189].

protein degradation pathway, a general cellular machinery for controlled proteolysis, are involved in the control of PER and TIM levels [98].

PER and TIM proteins accumulated in the cytoplasm are able to form heterodimeric complexes and, as such, enter the nucleus. The exact control of this process, for instance, additional requirements regarding phosphorylation of components or the role of DBT in it, await further clarification [189]. In the nucleus, the PER-TIM-complex represses the expression of its own genes, presumably by displacing the CLK-CYC transcriptional activator from the promoters. Concomitantly, progressive repression of per and tim leads to reduced levels of the inhibitory nuclear PER-TIM complex (in the night and early morning) such that a new cycle may start by re-initiating gene expression. At the same time, the PER-TIM complex acts as a positive regulator for clk, namely by relieving the auto-regulated repression of this gene. Recently, the products of the vri and $pdp1$ genes were shown to be involved in this second feedback loop. Both genes are activated by the product of clk, and act as transcriptional repressors and activators competing for the clk promoter, respectively [47]. As a consequence of this second feedback loop, oscillations in CLK protein are in antiphase to those of PER and TIM, and regulation of the limiting factor CLK, hence, additionally contributes to driving the next cycle [104, 287].

In the absence of external cues, these interactions establish autonomous sustained oscillations. External signals, in addition, have to have the ability to reset the clock in order to synchronize internal and external time (entrainment). The most important entrainment concerns matching of the circadian clock to the day-night cycle. This is achieved by light-dependent induction of TIM degradation relying on additional factors. In constant darkness, however, cir-

cadian rhythms exhibit extraordinary stability with deviations of period lengths in the order of minutes [104, 287].

The network architectures of the circadian clock in the fly and in mammals are characterized by identical elements at the level of feedback loops and their interconnections. Gene orthologues were found for flies and mammals. Important variations, however, exist that point to an independent evolutionary development of the circadian clocks [287]. Orthologues in different organisms possess different genetic and biochemical roles. For instance, the homologues of clk ($CLOCK$) and cyc ($BMAL1$) switched functions in mammals, and the homologue of gene coding for a photoreceptor in *Drosophila* fulfils the role of tim in higher eukaryotes [189]. In different clocks, the relative roles of trancriptional control and post-translational regulation also seem to vary [47]. Owing to the conservation of the key structural elements of circadian clock in eukaryotes, however, the genetically tractable fruit fly is the prominent model organism for studying circadian rhythms.

Beside many open questions concerning mechanistic detail of circadian clockworks, the core structure of the network seems to have been elucidated. However, the contribution of individual regulatory interactions or control loops to the precision and stability of the systems still remains largely unclarified. For instance, by verbal reasoning, it has been argued that the positive control loop enhances the robustness [104], whereas model-based analysis has been unable to detect a significant degeneration when the positive feedback loop is removed [244]. The second feedback loop, hence, may not play a prominent role in conferring robustness to the clock, but instead serve to generate antiphase outputs, or allow for integration of multiple inputs [47]. Moreover, it is unclear, and has not been addressed yet, which additional purpose a two-branched compared to a single negative feedback loop could serve. The two branches are not simply redundant and their existence may, thus, not easily be explained by enhancement of robustness.

4.3 Mathematical models

Many published mathematical models for circadian rhythms in *Drosophila* contain explicit time delays, which leads to systems of time-delay differential equations [157, 221, 243, 244, 260]. This modeling approach fosters models of reduced complexity. It, however, abstracts from biological reality. Furthermore, as time-delay differential equations are not easily amenable to analysis of parameter sensitivities, this group of models was not further considered. Two models for circadian clocks aiming at a more realistic, yet still concise representation were selected. Both models rely upon negative auto-regulatory feedback for generating the oscillations. A less complex model comprises only one branch [93] (single-feedback model) and the other model includes two distinct branches of the control system for *per* and *tim* [155] (dual-feedback model). Owing to the models' analogous structural set-up, this choice enabled direct model comparison.

4.3.1 Single-feedback model

The single-feedback model as the first molecular model of the circadian clock in *Drosophila* was proposed by Goldbeter in 1995 [92]. Its structure is depicted in Fig. 4.2.

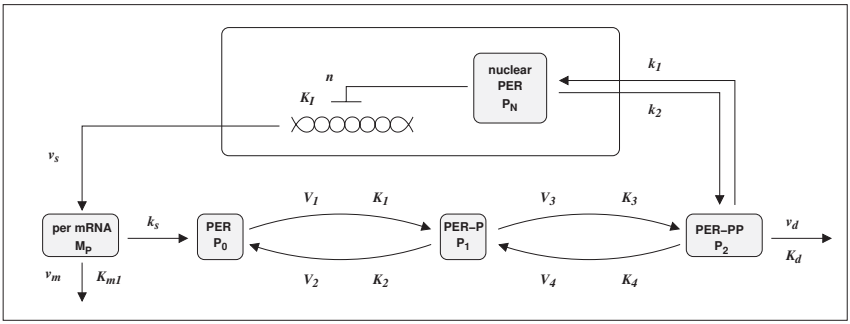

Fig. 4.2: Structure of the single-feedback model. The scheme was adapted from [92]. Description and variable names of system-theoretic states are shown in gray boxes. Single and double phosphorylation are indicated by '-P' and '-PP', respectively. Kinetic parameters (in italics) were positioned adjacent to the biochemical reactions they are associated with in the model.

In an attempt to capture the biological knowledge available at that time, the model (only) describes the negative control loop via PER. In brief, expression of *per* mRNA is assumed to be repressed by nuclear PER protein (P_N) in a cooperative fashion (see model equations compiled in Tab. B.1, Appendix B). Transcribed *per* mRNA (M_P) serves as a template for translation yielding unphosphorylated PER protein (P_0) and is subject to degradation. A cascade of two coupled phosphorylation / dephosphorylation cycles - which is responsible for the required time delay - leads to the formation of single-phosphorylated PER (P_1) and double-phosphorylated PER (P_2), respectively. Whereas the other forms of the protein were modeled to be stable, P_2 is proteolytically degraded. It can also be translocated from the cytoplasm to the nucleus via a reversible transport reaction, where the double-phosphorylated PER exerts its function as a transcriptional repressor. Altogether, the single-feedback model comprises five state variables and 18 kinetic parameters (Tab. 4.1, see also Fig. 4.2).

One aim of the present study is to analyze the role of regulatory mechanisms in providing robustness of the circadian clock, for example, to compare the importance of post-translational protein modification and control of gene expression in this respect. Clearly, this requires an analysis above the level of individual model parameters. Parameters were therefore grouped according to their functional role, that is, the biochemical processes they are associated with. Altogether, seven different functional classes were established (Tab. 4.1): transcription / translation (T), intracellular transport (TR), gene regulation (GR), phosphorylation (P), dephosphorylation (DP), and two classes of degradation parameters, namely those representing common cellular processes (DG) and those specific for the (components of the) circadian clock (DL).

Tab. 4.1: Parameters of the single-feedback model. Parameter functions are classified into the following categories: M = maximal reaction rate, R1 = 1st order rate constant, MM = Michaelis-Menten affinity constant, C = dimensionless coefficient. For description of the biochemical reactions individual parameters are associated with, cellular compartments are abbreviated by 'Cp' for cytoplasm and 'Nu' for nucleus. Parameter values for the reference model were taken from [92]. Entries in the columns for parameter status with respect to control hierarchy and to functional grouping refer to the categories described in the text.

Nr.	Name	Category	Biochemical process	Reference value	Functional group	Global/ Local
1	v_s	M	transcription	0.76 $\mu M/h$	T	G
2	v_m	M	mRNA degradation	0.65 $\mu M/h$	DG	G
3	k_s	R1	translation	0.38 h^{-1}	T	G
4	v_d	M	protein degradation	0.76 $\mu M/h$	DG	G
5	k_1	R1	transport Cp →Nu	1.90 h^{-1}	TR	M
6	k_2	R1	transport Nu →Cp	1.30 h^{-1}	TR	M
7	K_I	MM	auto-inhibition gene expression	1.00 μM	GR	L
8	K_m	MM	mRNA degradation	0.50 μM	DL	M
9	K_d	MM	protein degradation	0.20 μM	DL	M
10	K_1	MM	phosphorylation I	2.00 μM	P	L
11	K_2	MM	dephosphorylation I	2.00 μM	DP	L
12	K_3	MM	phosphorylation II	2.00 μM	P	L
13	K_4	MM	dephosphorylation II	2.00 μM	DP	L
14	V_1	M	phosphorylation I	3.20 $\mu M/h$	P	L
15	V_2	M	dephosphorylation I	1.58 $\mu M/h$	DP	L
16	V_3	M	phosphorylation II	5.00 $\mu M/h$	P	L
17	V_4	M	dephosphorylation II	2.50 $\mu M/h$	DP	L
18	n	C	transcriptional repression (Hill coefficient)	4	GR	L

The latter two groups point to a further classification that can be made at a higher level. Kinetic parameters can be attributed to global cellular properties, that is, those features of cellular regulation, that affect many regulatory processes besides the circadian clockwork. Examples include maximal transcription / translation rates determined by the properties of the cell's transcriptional and translational apparatus, respectively, and not by characteristics of an individual gene or mRNA. Similar arguments hold for maximal rates of mRNA degradation and of ubiquitin-dependent proteolysis. At the other end of the spectrum, many parameters in the model reflect purely local functionality, for instance, repression of specific *per* gene expression. This parameter status with respect to hierarchical control, however, does not always allow a unique grouping. Therefore, three classes were introduced: global (G), local (L) and mixed (M) functionality.

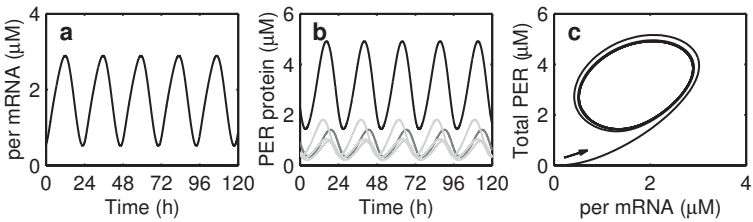

Fig. 4.3: Dynamic behavior: Limit cycle oscillations. The reference parameter set compiled in Tab. 4.1 was used for numerical integration of the model equations. **a,** time course of per mRNA during sustained oscillations. **b,** corresponding total concentration of all species of the PER protein (black), double-phosphorylated PER in the nucleus (dark gray), and the protein species in the cytoplasm (light gray). **c,** phase plane plot for protein vs. mRNA concentration showing the evolution towards a limit cycle when starting from arbitrary initial concentrations. The arrow indicates the direction of time.

The model's dynamic behavior describing an autonomous oscillator is shown in Fig. 4.3. For the set of parameter values used in this simulation, starting from arbitrary initial conditions, the system evolves towards a limit cycle, that is, sustained regular oscillations with a period length of approximately 24 hours. Note that concentration units do not necessarily reflect intracellular conditions [92]. When parameter values are changed to appropriate values, the model generates a second type of behavior, namely excitable steady state for all components. Besides this restriction to two behavioral regimes, the single-feedback model also does not account for the effect of light on circadian rhythms (since TIM was not modeled) [94]. However, this simple molecular model reflects the core of the circadian oscillator in *Drosophila* and, for this reason, it continues to be used to study the robustness of the system [12, 95].

4.3.2 Dual-feedback model

Owing to the above mentioned limitations of the simple model, and to the discovery of tim as the other major clock gene, Leloup and Goldbeter presented an extended model incorporating both feedback loops via per and tim [155]. Fig. 4.4 schematically represents the model structure in analogy to that of the single-feedback model (Fig. 4.2).

Compared to the smaller model, this model contains a symmetric copy of the original PER feedback loop for TIM. Note that by the choice of the standard parameter set given in [155], this symmetry between the two branches is also retained (Tab. 4.2). Major differences in the models occur regarding the nature of the transcriptional repressor. Here, the double-phosphorylated forms of PER and TIM are assumed to form a heterodimeric complex, which shuttles between cytoplasm and nucleus. In contrast to the single-feedback model, the complex undergoes proteolytic degradation in both compartments. Moreover, a general, unspecific degradation reaction affecting each component has been introduced (described by k_d, not shown). Altogether,

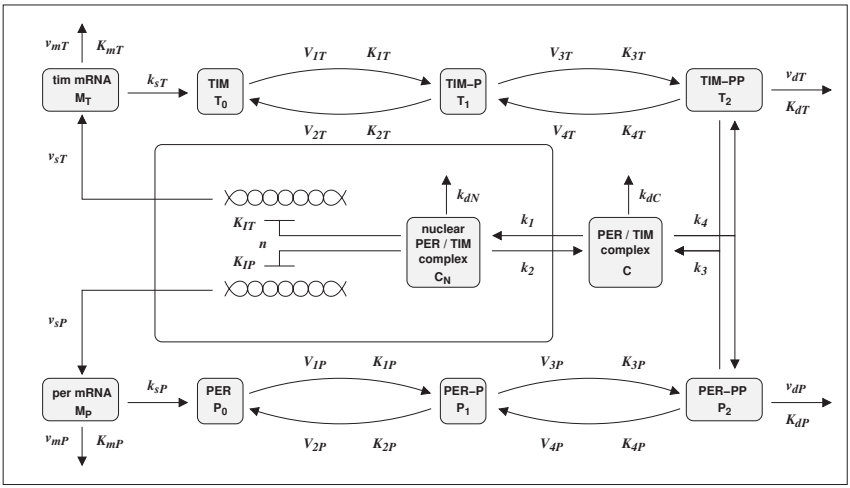

Fig. 4.4: Structure of the dual-feedback model. The scheme was adapted from [155] according to the same structuring principles as in Fig. 4.2.

this more realistic representation of the core circadian clock in *Drosophila* leads to a mathematical model of moderate size, which comprises 10 state variables and 38 parameters (for the model equations see Tab. B.3, Appendix B).

Interestingly, the higher degree of complexity of the dual-feedback model also generates a richer dynamic behavior. Under conditions of constant darkness, in addition to steady state and

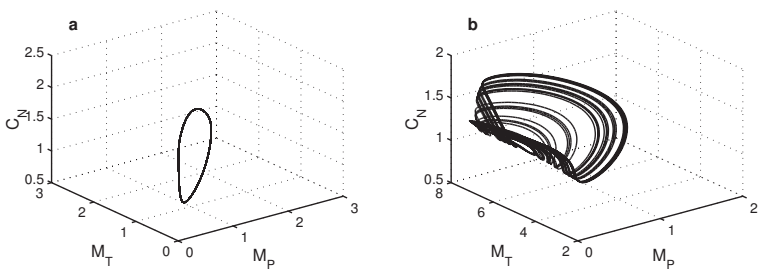

Fig. 4.5: Dynamic behavior: Regular oscillations and chaos. a, Limit cycle generated by the model in the phase plane spanned by *per* mRNA concentration (M_P), *tim* mRNA concentration (M_T) and the nuclear concentration of the PER/TIM complex (C_N), when setting all parameter values to the reference values compiled in Tab. 4.2. **b,** Strange attractor corresponding to chaotic oscillations obtained for $v_{mT} = 0.28\ nM/h$ and $v_{dT} = 4.8\ nM/h$; all other parameter values are identical to **a** [156].

Tab. 4.2: Parameters of the dual-feedback model. Here, 'Nu' refers to nuclear and 'Cp' to cytoplasmic reactions. Other abbreviations are explained in the legend to Tab. 4.1, p. 50. Parameter category 'R2' refers to the rate constant for bi-molecular reactions. The parameter set from [155, 156] was used as reference.

Nr.	Name Name	Cate-gory	Biochemical process	Reference value	Functional group	Global/ Local
1	v_{sP}	M	PER transcription	1.00 nM/h	T	G
2	v_{sT}	M	TIM transcription	1.00 nM/h	T	G
3	v_{mP}	M	PER mRNA degradation	0.70 nM/h	DG	G
4	v_{mT}	M	TIM mRNA degradation	0.70 nM/h	DG	G
5	v_{dP}	M	PER protein degradation	2.00 nM/h	DG	G
6	v_{dT}	M	TIM protein degradation	2.00 nM/h	DG	G
7	k_{sP}	R1	PER translation	0.90 h^{-1}	T	G
8	k_{sT}	R1	TIM translation	0.90 h^{-1}	T	G
9	k_1	R1	transport Cp $\rightarrow$Nu	0.60 h^{-1}	TR	M
10	k_2	R1	transport Nu $\rightarrow$Cp	0.20 h^{-1}	TR	M
11	k_3	R2	PER-TIM association	1.20 $nM^{-1}h^{-1}$	TR	M
12	k_4	R1	complex dissociation	0.60 h^{-1}	TR	M
13	K_{mP}	MM	PER mRNA degradation	0.20 nM	DL	M
14	K_{mT}	MM	TIM mRNA degradation	0.20 nM	DL	M
15	K_{IP}	MM	PER auto-inhibition gene expr.	1.00 nM	GR	L
16	K_{IT}	MM	TIM auto-inhibition gene expr.	1.00 nM	GR	L
17	K_{dP}	MM	PER protein degradation	0.20 nM	DL	M
18	K_{dT}	MM	TIM protein degradation	0.20 nM	DL	M
19	K_{1P}	MM	PER phosphorylation I	2.00 nM	P	L
20	K_{1T}	MM	TIM phosphorylation I	2.00 nM	P	L
21	K_{2P}	MM	PER dephosphorylation I	2.00 nM	DP	L
22	K_{2T}	MM	TIM dephosphorylation I	2.00 nM	DP	L
23	K_{3P}	MM	PER phosphorylation II	2.00 nM	P	L
24	K_{3T}	MM	TIM phosphorylation II	2.00 nM	P	L
25	K_{4P}	MM	PER dephosphorylation II	2.00 nM	DP	L
26	K_{4T}	MM	TIM dephosphorylation II	2.00 nM	DP	L
27	V_{1P}	M	PER phosphorylation I	8.00 nM/h	P	L
28	V_{1T}	M	TIM phosphorylation I	8.00 nM/h	P	L
29	V_{2P}	M	PER dephosphorylation I	1.00 nM/h	DP	L
30	V_{2T}	M	TIM dephosphorylation I	1.00 nM/h	DP	L
31	V_{3P}	M	PER phosphorylation II	8.00 nM/h	P	L
32	V_{3T}	M	TIM phosphorylation II	8.00 nM/h	P	L
33	V_{4P}	M	PER dephosphorylation II	1.00 nM/h	DP	L
34	V_{4T}	M	TIM dephosphorylation II	1.00 nM/h	DP	L
35	k_d	R1	unspecific degradation	0.01 h^{-1}	DG	M
36	k_{dC}	R1	degradation complex, Cp	0.01 h^{-1}	DG	M
37	k_{dN}	R1	degradation complex, Nu	0.01 h^{-1}	DG	M
38	n	C	transcriptional repression	4	GR	L

regular oscillations, chaotic behavior occurs in certain regions of parameter space (Fig. 4.5). Although physiological implications of these chaotic oscillations are unclear, at least in the model, autonomous chaos constitutes a rather robust phenomenon, as it is not confined to single points (but smaller regions) in parameter space [156]. For other parameter combinations, the model can also show birhythmicity, that is, the co-existence of two limit cycles or of a limit cycle and a steady state; which of the behaviors is realized largely depends on the initial conditions [156]. Regarding the robustness of the physiological function of the circadian clock, adding a second branch of negative feedback might thus lead to instabilities. Hence, decision on the (positive) contribution of additional control circuits to system robustness does not seem to be possible *a priori* , but requires systematic investigation of sensitivities and model comparison.

4.4 Principles of parameter sensitivity analysis

Sensitivity analysis deals with the question, how variations in model output can be (qualitatively or quantitatively) attributed to variations in model components such as parameters, inputs, or others [217]. To gain insight into the structure-function relationship for the models of the circadian clock, the deterministic models' robustness towards internal perturbations, namely variations in parameter values (as opposed to assessing the effect of stochastic noise) will be studied. The aim of this section is to outline the theoretical basis of this approach and its implications regarding computational aspects and interpretation of results.

4.4.1 State and feature sensitivities

In a general form, the mathematical models considered here are formulated as systems of ordinary differential equations (ODEs). Each set of model equations has the form $\mathbf{M}(\mathbf{x}, \mathbf{u}, \mathbf{p}, t)$ depending on the state variables $\mathbf{x}$ (corresponding to the vector of concentrations $\mathbf{c}$ described by the model), the inputs $\mathbf{u}$, the model parameters $\mathbf{p}$ and time t. More precisely,

$$\mathbf{M}(\mathbf{x}(t), \mathbf{u}(t), \mathbf{p}, t) \;=\; \dot{\mathbf{x}} - \mathbf{f}(\mathbf{x}(t), \mathbf{u}(t), \mathbf{p}, t) \;=\; \mathbf{0} \tag{4.1}$$

with the time variable $t \geq t_0$, the functional for the right hand sides $\mathbf{f}(\mathbf{x}(t), \mathbf{u}(t), \mathbf{p}, t)$, and the initial conditions $\mathbf{x}(t_0) = \mathbf{x}_0$.

State sensitivities, that is, the quantitative description of how changes in parameter values locally influence model states, are defined as the partial derivatives of $\mathbf{x}$ with respect to $\mathbf{p}$ (first-order local sensitivities):

$$\mathbf{S}(t) = \frac{\partial \mathbf{x}(t)}{\partial \mathbf{p}} \,. \tag{4.2}$$

The information obtained by this analysis is only locally valid, because it is a linear estimator confined to a given point in parameter space. Furthermore, in the general case, local parameter sensitivities have a double time dependence: they depend on the time at which parameters are perturbed and on the time point, for which the sensitivities are defined. As a sensitivity measure

that can efficiently be determined computationally, it is, however, often used for the explorative investigation of model properties in parameter space [259].

Several methods exist for numerical calculation of local parameter sensitivities. The so-called indirect (or brute-force) method simply relies upon computation of the state trajectories when, one at a time, parameters are slightly (usually by 1%) varied around their nominal values. Via this finite-difference approximation, the elements of the sensitivity matrix are determined for all n_S states and n_P parameters according to

$$S_{i,j}(t) \approx \frac{x_i(p_j + \Delta p_j, t) - x_i(p_j, t)}{\Delta p_j} \quad \forall \quad i = 1 \ldots n_S\,,\; j = 1 \ldots n_P\,. \tag{4.3}$$

This method, however, may be associated with inaccuracies; results should therefore be compared to those originating from other methods [259].

The direct method starts from the system equations (4.1) and, by simple differentiation, arrives at the variation equation

$$\frac{d}{dt}\left.\frac{\partial \mathbf{x}}{\partial \mathbf{p}}\right|_{\mathbf{p},t_i} = \mathbf{J}_x \cdot \left.\frac{\partial \mathbf{x}}{\partial \mathbf{p}}\right|_{\mathbf{p},t_i} + \mathbf{J}_p\,, \tag{4.4}$$

whereby the Jacobians $\mathbf{J}_x$ for the states and $\mathbf{J}_p$ for the parameters are given by

$$\mathbf{J}_x = \left.\frac{\partial\, \mathbf{f}(\mathbf{x}, \mathbf{u}, \mathbf{p}, t)}{\partial \mathbf{x}}\right|_{\mathbf{p},t_i} \quad \text{and} \quad \mathbf{J}_p = \left.\frac{\partial\, \mathbf{f}(\mathbf{x}, \mathbf{u}, \mathbf{p}, t)}{\partial \mathbf{p}}\right|_{\mathbf{p},t_i}\,. \tag{4.5}$$

These differential equations and the initial conditions of zero for all sensitivities allow one to directly solve the augmented system of ODEs containing the original system equations plus the sensitivity differential equations to obtain the complete sensitivity matrix in one simulation run. Again, it has to be underlined that the sensitivities are time dependent and local with respect to parameter space.

The interpretation of parameter sensitivity information in terms of the questions addressed in this study, however, requires additional definitions. For instance, raw sensitivities from (4.2) do not enable one to directly compare the parameter-specific effects of perturbations. Model parameters usually differ in orders of magnitude of the parameter values, and also in physical meaning (units). One possibility to circumvent this problem is to analyze the normalized local sensitivity matrix $\mathbf{S}'(t)$ [259], the elements of which are

$$S'_{i,j}(t) = \frac{p_j}{x_i(t)} \frac{\partial x_i(t)}{\partial p_j}\,. \tag{4.6}$$

Each element of this $n_S \times n_P$ matrix provides a linear estimate of the relative change in the state variable x_i owing to a relative change in the model parameter p_j and, hence, allows for comparison of model parameters.

Furthermore, it is desirable to calculate a single indicator that reflects how much changes in single model parameters affect the overall model behavior. Such an indicator σ_j (hereafter

referred to as overall state sensitivity) for parameter p_j can be derived by integration over (discrete) time and over the state variables using

$$\sigma_j = \frac{1}{n_S}\, p_j \left(\sum_{k=2}^{n_T} \sum_{i=1}^{n_S} \left[\frac{1}{x_i} \frac{\partial x_i(t_k, t_1)}{\partial p_j} \right]^2 \right)^{1/2} \tag{4.7}$$

Here, t_1 denotes a fixed time of perturbation of the system, the effect of which is tracked for subsequent time points $t_2 \ldots t_{n_T}$. The number of time steps and number of state variables are n_T and n_S, respectively. Normalization by the number of state variable accounts for differences in model size. The exponent $1/2$ in eq. 4.7 was introduced solely to facilitate computations; it does not influence the results of forthcoming analyses.

Apart from state sensitivities, feature sensitivities describe the dependency of other characteristics of model behavior on model parameters [259]. Period sensitivities and amplitude sensitivities are the most important of these measures for oscillators. Period length τ and amplitude A represent time-independent model characteristics and, hence, so do the corresponding sensitivities σ_j^P and σ_j^A. These partially normalized sensitivities are defined by

$$\sigma_j^P = p_j \frac{\partial \tau}{\partial p_j} \quad \text{and} \quad \sigma_j^A = p_j \frac{\partial A}{\partial p_j}\,. \tag{4.8}$$

Again, as for state sensitivities, several methods exist for calculation of period sensitivities. An approximation using the local state sensitivities has been proposed [55]:

$$\sigma_j^P \approx \frac{\frac{\partial x_i(t_2)}{\partial p_j(t_1)} - \frac{\partial x_i(t_2+\tau)}{\partial p_j(t_1)}}{\frac{dx_i(t_2)}{dt}}\,. \tag{4.9}$$

However, due to numerical instabilities associated with implementation of equation (4.9), for the study of circadian clock models, normalized period sensitivities were calculated through the indirect method, i.e.

$$\sigma_j^P \approx p_j \, \frac{\tau(p_j + \Delta p_j) - \tau(p_j)}{\Delta p_j}\,. \tag{4.10}$$

The determination of the feature (period τ or amplitude A) for the original and the perturbed parameter set and the finite-difference approximation shown above were used for computation of period and amplitude sensitivities in an equivalent manner.

4.4.2 Computational approach

For a global investigation of model properties, it would be highly desirable to systematically determine parameter sensitivities in large regions of parameter space. Owing to the high dimensionality of this space, however, combinatorial explosion of possible combinations of individual parameter values impedes the direct approach of determining these model properties even for a limited number of discrete values per parameter. For instance, discretizing the interval for each parameter of the single-feedback model into only 10 grid points would require a total of

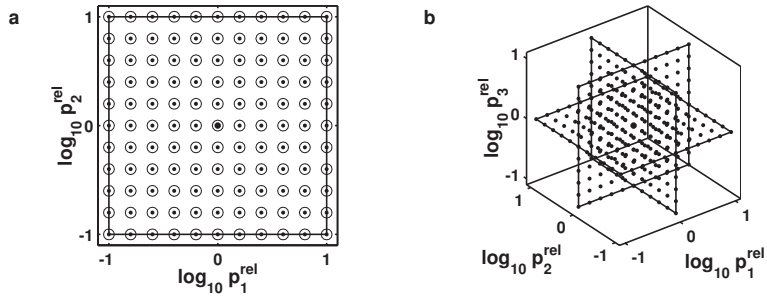

Fig. 4.6: Systematic approach to evaluation of model properties. a, Illustration of systematic evaluation of parameter sensitivities in a quadratic section (lines) of the two-dimensional plane spanned by parameters p_1 and p_2 around the reference point (large dot). Small dots indicate discrete points at which analysis is performed to obtain sensitivities valid for the local neighborhoods (circles). **b,** Extension of the approach to three dimensions in parameter space.

$18^{10} = 3.6 \cdot 10^{12}$ evaluations. Instead, two complementary methods were used: scanning the parameter space on two-dimensional planes and random generation of parameter sets.

The systematic approach relying on two-dimensional sections of parameter space is depicted in Fig. 4.6. Whereas all other parameters retain their reference values, two parameters are varied within a limited interval, such that a regular, quadratic grid develops. In general, intervals were chosen equal in logarithmic space to obtain equal fold variations. Relative parameter values p_j^{rel} were usually varied between 10^{-1} and 10^{+1} times the reference parameter value p_j^{ref}. Computation of parameter sensitivities then characterized the neighborhood of each grid point, which, when extended to higher dimensions, leads to a systematic coverage of parameter space (Fig. 4.6b). Depending on the number of model parameters n_P, $\frac{n_P(n_P-1)}{2}$ planes - e.g. 703 plane sections of 21×21 grid resolution for the dual-feedback model - had to be analyzed. However, as the figure also shows, only certain directions of parameter variations can be included by this approach. In complimentary analyses, therefore, parameter sets were generated randomly (following a normal distribution within the given intervals). Results obtained by two-dimensional scanning and by analysis of random parameter vectors, respectively, will be compared in the next section.

Each of the so defined points in parameter space was analyzed with respect to behavorial parameters (oscillatory regime, period, amplitude), state and feature sensitivities (via the direct or the indirect method for computation of parameter sensitivities, see section 4.4)). This distinction of methods was made to ensure accurate computation of period sensitivities. Consistency of state sensitivities obtained by the two methods was checked for selected cases (data not shown).

All calculations relied upon numerical integration of model and sensitivity equations using Matlab (Mathworks, Inc.). Integration was performed on a compact time interval of 100h (approximately four times the reference period length) after discarding initial transients in the state variables. Parameters were varied by 1% in each direction for the indirect method and the mean value was further employed. Altogether, this construction of the study resulted in the generation of several million data points for each model, the major analysis results of which will be presented in the following section.

4.5 Systems analysis

Systems analysis of the two models aimed at elucidating global functional properties to relate them to structural features. Employing the computational methods outlined above, both models will first be analyzed separately in sections 4.5.1 and 4.5.2. Model comparison will be the subject of section 4.5.3.

4.5.1 Single-feedback model

For a first characterization of the mathematical model comprising a single feedback branch, its behavior was analyzed with respect to the size of the domains in parameter space, in which it is able to generate regular oscillations. An example of the model behavior is shown in Fig. 4.7.

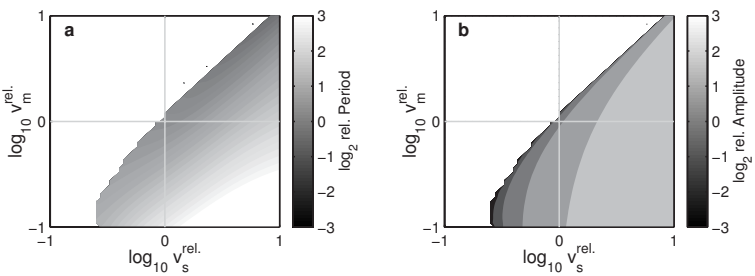

Fig. 4.7: Oscillatory behavior of the 5-state model in the $\mathbf{v_s} \times \mathbf{v_m}$ plane. a, Relative period compared to the $\approx$ 24h period at the reference point. Grey lines indicate the parameters' reference values. In the white region, the system shows steady-state behavior. **b,** relative amplitude of oscillations for per mRNA (M_P). Computations were performed on a regular 51 $\times$ 51 grid.

Here, the parameters v_s and v_m describing maximal transcription and mRNA degradation rate, respectively, were varied according to the principles outlined in the previous section. Obviously, the model behaves robust in the sense that the circadian clock oscillates in a wide range of parameter values, although the two parameters chosen belong to the most sensitive ones (see next paragraph). The shape of the oscillatory region points to the (intuitively foreseeable)

requirement for a certain minimal net mRNA production rate for oscillations to occur. Furthermore, Fig. 4.7 illustrates that robustness of the system, when parameter values are adjusted in a larger interval, is not absolute. For specific parameter combinations, periods attain lengths of >100h; the amplitude of oscillations similarly shows considerable variability.

Similar observations were made regarding overall state sensitivities for this example section in parameter space (Fig. 4.8). For each parameter, as well as concerning all model parameters, these sensitivities vary by several orders of magnitude. Oscillatory regions and those corresponding to steady state model behavior do not show pronounced differences. In general, however, this representation hardly allows for assessing the relative sensitivity of model parameters.

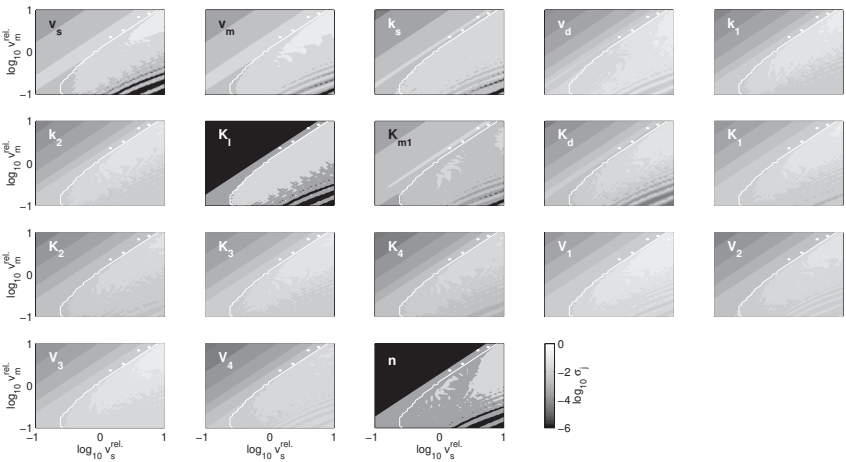

Fig. 4.8: Overall state sensitivities ($\log_{10}\ \sigma_j$) in the $\mathbf{v_s} \times \mathbf{v_m}$ plane. Sensitivities normalized by the maximal value are encoded by gray-levels (see color scale at the bottom) in one panel per model parameter. The white line separates the oscillatory region from steady state behavior.

For each point in parameter space analyzed, parameters were therefore rank-ordered according to their overall state sensitivities. This transformation for highly non-linear data simply means assigning rank 1 to the largest value of a variable, rank 2 to the second largest, and so on up to the parameter with lowest sensitivity [109]. Rank-ordered sensitivities are shown in Fig. 4.9. For the individual model parameters, their rank with respect to sensitivities appears relatively uniform. Furthermore, clearer distinctions between the parameters become visible. Predominantly dark colors for v_s, v_m and others indicate the parameters' important role in providing sources of fragility for the system. In contrast, the degree of cooperativity for transcriptional repression (n), in general, appears to be relatively insensitive, which corresponds to previously published results of robustness analysis [95].

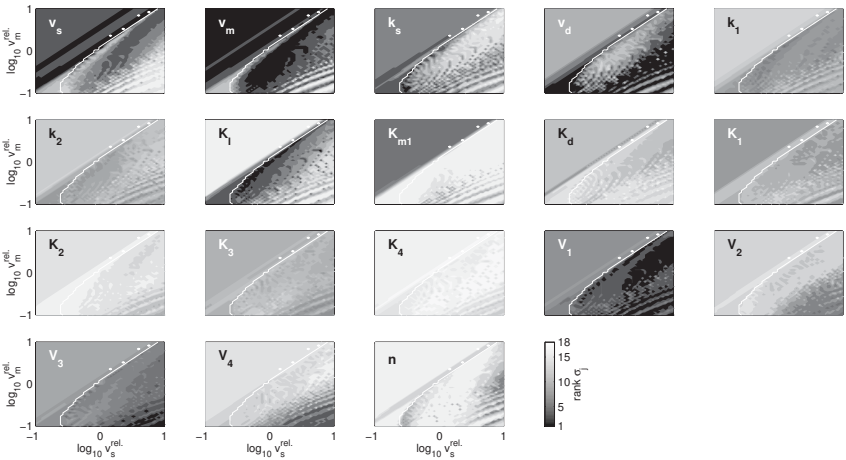

Fig. 4.9: Rank order of parameter sensitivities in the $\mathbf{v_s} \times \mathbf{v_m}$ plane. Data were obtained by ranking the parameter sensitivities shown in Fig. 4.8 for each grid point.

As described in section 4.4.2, two-dimensional sensitivity analysis (on coarser grids of 11×11 points) was subsequently performed for all possible parameter combinations in the 5-state model. Specifically, 153 sections in parameter space were investigated, amounting to a total of $1.8 \cdot 10^4$ parameter sets. To elucidate global sensitivity properties of the single-feedback model, rank-ordered sensitivities were averaged over all points analyzed (Fig. 4.10). These global indicators of robustness and fragility associated with the model parameters point to a certain conservation of robustness properties, because most parameters show a relatively low variation regarding their rank. This invariance is largely independent of the operating regime of the system, namely oscillation or steady state (see below). For instance, the existence of broadly two groups of parameters, namely those with higher sensitivity (low rank) and those with lower sensitivity (high rank) becomes obvious.

Furthermore, it is important to note that functionally related groups of parameters exhibit similar properties. Parameters associated with processes of transcription / translation, transport and protein phosphorylation belong to the first group, whereas the other parameters fall into the second group. The constant for inhibition of gene expression (K_I) constitutes an exception, because its high standard deviation prevents unambiguous classification. However, owing to the large samples, when assayed for the pair-wise significance of differences in the average ranks, more than 90% of the combinations passed the Wilcoxon rank sum test ($\alpha = 5\%$, not shown).

Finally, overall state sensitivities for the single-feedback model were also analyzed by generating random parameter sets in order to address two issues. First, the comparison with sen-

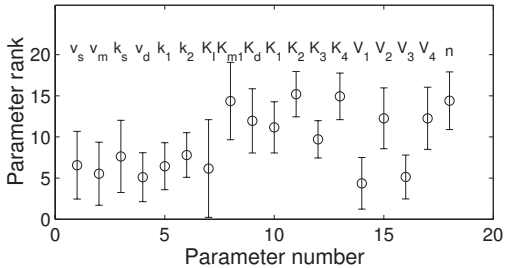

Fig. 4.10: Global sensitivity analysis according to parameter ranking (single-feedback model). Average rank of overall state sensitivities determined by $\pm 1\%$ variation of parameter values, employing the indirect method. Data are based on all 153 possible two-dimensional analyses in parameter space.

sitivity data from the two-dimensional scanning of parameter space should disclose whether variations in only two parameters at a time will bias the analysis results. A good correlation between the results would, secondly, enable one to investigate global model properties in a computationally less expensive manner than by the systematic approach.

For different conditions, parameter sets were generated randomly within given minimal and maximal parameter values. Each parameter was allowed to be varied independently and the probability distributions of all individual deviations from the reference parameter values followed normal distributions. Fig. 4.11 shows selected analysis results for a sampling size of $n = 500$. In general, however, average values rapidly converged within approximately 100-200 iterations to the data presented in the figure.

Sensitivity analysis by random parameter variation was first performed using parameter constraint conditions identical to those applied for the systematic analysis (ten-fold variation in each direction, Fig. 4.11a-c). In this large domain in parameter space, only a few of the randomly parameterized models generate oscillations, most show steady state. Average parameter ranks as well as corresponding standard deviations correlate very well with the results from the systematic scanning method.

For further analysis, a reduced domain (two-fold variation, Fig. 4.11d-f) was considered, which leads to a higher presence of oscillatory regimes. It hardly influences the average relative position of parameters. As would be expected, the rank variances in this more local approach are, however, reduced. Intriguingly, conducting the analysis in the vicinity of a considerably different reference point [95] (see Tab. B.2, Appendix B and Fig. 4.11g-i) leads to the same observations. In all three cases, a regression coefficient of $r > 0.94$ was obtained for the linear correlation between the average parameter ranks.

One can, hence, conclude that random search offers the possibility of rapidly assessing global properties of the 5-state model, and that it is unlikely that the systematic method intro-

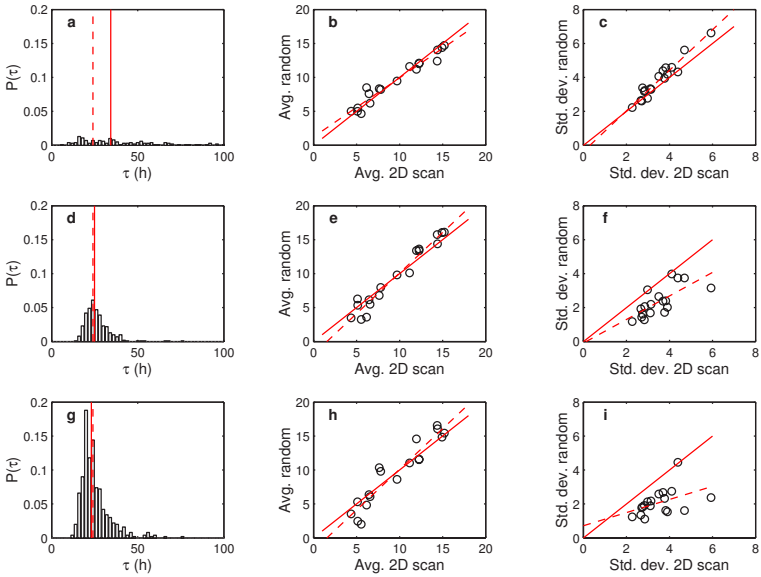

Fig. 4.11: Comparison of systematic and random sampling method. Three different conditions were considered: random generation of parameter vectors around the standard parameter set in the interval $0.1\,p_j^{ref.} \ldots 10\,p_j^{ref.}$ (**a-c**), in the interval $0.5\,p_j^{ref.} \ldots 2\,p_j^{ref.}$ (**d-f**), and using the same interval, around a modified reference parameter set reported in [95] (see Tab. B.2, Appendix B) (**g-i**). **a,d,g,** Probability distribution of period lengths, that is, the probability $P(\tau)$ to encounter a regime having period τ. Vertical lines mark the mean value (solid) and the 24h period length (dashed). **b,e,h,** Correlation between average parameter ranks obtained by systematic scanning of two-dimensional planes in parameter space (cf. Fig. 4.10a) and by random sampling. The solid line corresponds to perfect match, whereas the dashed line was obtained by linear regression. **c,f,i,** Correlation of standard deviations of parameter ranks in analogy to (**b,e,h**). Details on computations are given in the main text.

duced significant biases regarding these properties. These results also underline the relative conservation of robust and fragile model parts being a characteristic feature of the single-feedback model for circadian rhythms. Analysis of the more complex dual-feedback model along the same lines should allow one to elucidate whether this is a more general phenomenon or not.

4.5.2 Dual-feedback model

As mentioned above, the dual-feedback model for the circadian clock in *Drosophila* can exhibit more complex dynamic behavior than the simpler model. Chaos and birhyhmicity, for instance,

may occur in certain regions of parameter space. In analogy to the 5-state model, the 10-state model of the circadian clock was therefore first inspected regarding the model behavior in the vicinity of the reference parameter values. An example for such a systematic two-dimensional simulation study is shown in Fig. 4.12. Here, a section of parameter space spanned by the parameters for maximal mRNA production rate in *per* (v_{sP}) and *tim* (v_{sT}) gene expression, respectively, was analyzed.

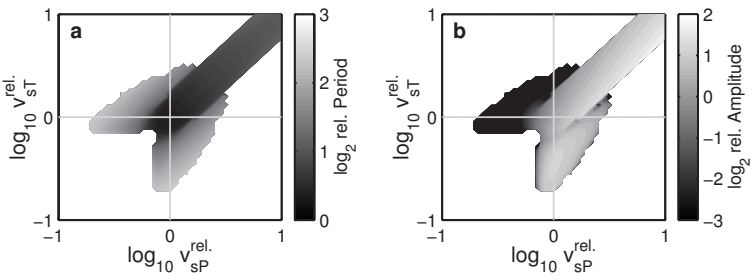

Fig. 4.12: Oscillatory behavior of the 10-state model in the $v_{sP} \times v_{sT}$ plane. a, Relative period and **b,** relative amplitude (per mRNA M_P) of sustained, regular oscillations .

Either regular oscillations, or simple steady state solutions (white regions) are generated by the model in this parameter plane. The figure indicates that, compared to the single-feedback model, the reference parameter set is located more distant from the border of the oscillatory region. This region is not necessarily larger and variations in period and amplitude are not smaller than for the less complex model. Hence, it does not indicate enhanced systems robustness. The region's shape reflects the symmetric character of the model structure (and of the chosen parameter values), because it is symmetric to the diagonal. Torsion of the model, for instance by changing PER-associated and corresponding TIM-associated parameters in different directions, abrogates the functioning as rhythm generator. Indeed, it can be shown by singular-value decomposition of the sensitivity matrix, that the most important direction for parametric disturbances implies symmetry-breaking (F. Doyle, personal communication).

For assessing global model robustness properties, again, the systematic approach was applied to calculate parameter sensitivities for variations in all possible combinations of two model parameters. Owing to the number of 38 model parameters, altogether 703 parameter planes needed to be investigated by applying a coarse grid of 11 × 11 data points. For illustration of the finally obtained rank-ordered overall state sensitivities, however, a higher resolution of 51 × 51 nodes was used (Fig. 4.13).

Three observations reminiscent to those resulting from the corresponding analysis of the single-feedback model can be made. Average ranks of many model parameters, that is, the general appearance of a panel with respect to its darkness, seem relatively uniform. Moreover, there exists no sharp division between parameter sensitivities in oscillatory and steady-state

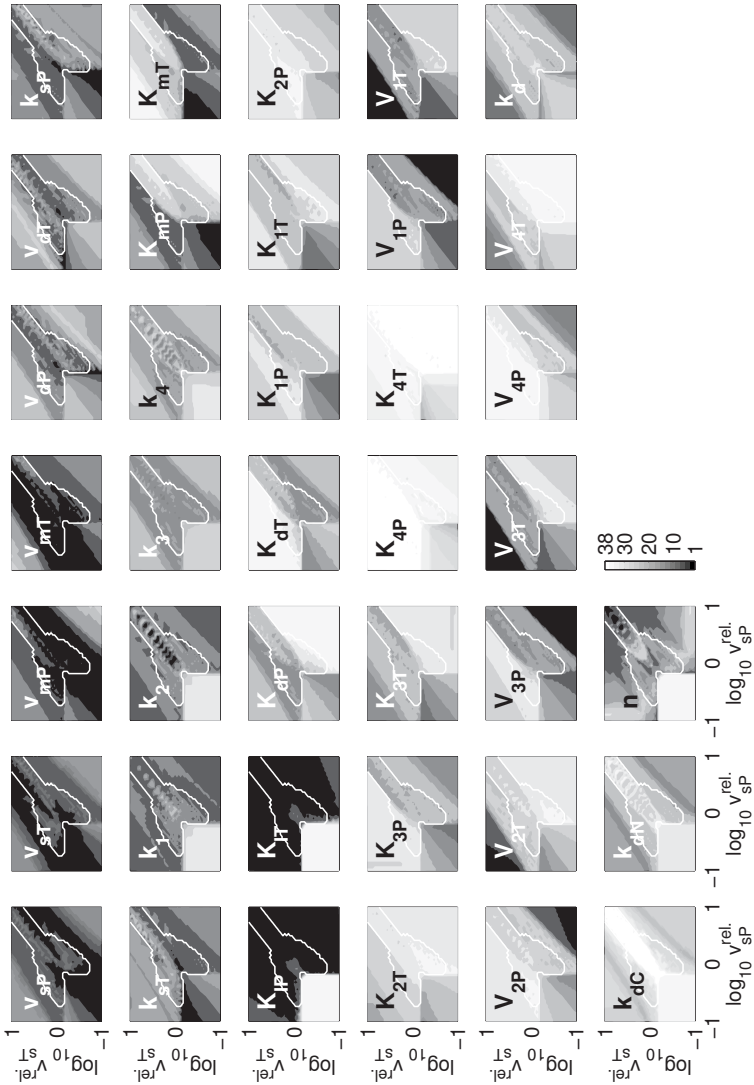

Fig. 4.13: Rank order of parameter sensitivities in the $v_{sP} \times v_{sT}$ plane (10-state model) in analogy to Fig. 4.9 (5-state model).

regions, which is suggestive of a certain conservation of robustness and fragility properties independent of the system's operating regime. And finally, parameters such as v_{sP} and v_{sT}, which reflect properties of the cellular regulatory system as a whole, appear to be more important sources of fragilities for the circadian clock as described by the dual-feedback model than local characteristics such as kinetic parameters for PER and TIM protein phosphorylation and dephosphorylation.

Systematic analysis of parameter sensitivities in all two-dimensional planes corroborates these findings (Fig. 4.14). Model parameters show a significant conservation regarding their relative position according to parameter sensitivity even if the system operates in very different dynamic regimes such as steady state, regular oscillations, or chaos. The invariance in parameter position for the 10-state model is more pronounced than for the 5-state model (compare to Fig. 4.10). This is particularly evident for the highly sensitive global parameters associated with transcription and translation (parameter numbers 1-8). Higher insensitivity and also variability is observed for local parameters. More specifically, control of gene expression for *per* and *tim* (parameters 15-16 and 38) turns out to be a source of fragility in the 10-state model, a position that in the 5-state model was connected to protein phosphorylation. As for the single-feedback model, independent sensitivity analysis by random generation of parameter vectors agreed very well with the results from systematic investigation of parameter space (data not shown).

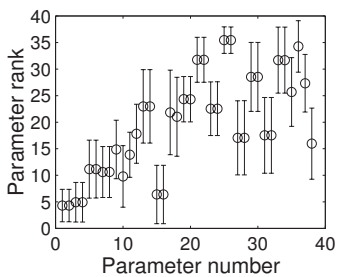

Fig. 4.14: Global sensitivity analysis according to parameter ranking (dual-feedback model). Rank according to indirect determination of overall state sensitivities averaged over all 703 two-dimensional sections in parameter space.

Parameter sensitivity analysis indicates that for both models of the circadian clock investigated herein, a similar degree of conservation of robustness and fragility exists. At a first glance, this also concerns the distinction of sensitive and less sensitive model parts according to functionally related groups of parameters. To analyze this issue in more detail, and to directly connect it to the physiological function of the system, namely to generate stable circadian rhythms, it seems sensible to directly compare the two models.

4.5.3 Model comparison: Biological implications

For a comparison of the two models for the circadian clock relying on transcriptional feedback, it is important to note that the dual-feedback model provides an additional regulatory circuit that is not redundant in a narrow sense. Splitting up the negative feedback into two interconnected branches might enhance robustness of the circuit, especially when taking into account the assertion of a direct link between complexity and robustness of cellular control systems. Higher complexity, however, involves more sources of fragility, for instance, owing to the higher number of components involved. Relative robustness of the models, hence, can not simply be deduced from the circuit structures, but requires detailed analysis.

For this purpose, local properties of the two models in the neighborhood of the reference parameter sets were investigated. For instance, all state sensitivities from two-dimensional analysis were compiled, and their probability distributions were analyzed. The mean values of the respective distributions pointed to a higher robustness of the 10-state model (data not shown). This observation was made either for all operation modes of the system, or for regular oscillations only. Interestingly, this is caused by a high probability to encounter less sensitive parameters, whereas highly sensitive parts of the models do not differ significantly. Robustness of the oscillators described by the models was directly assessed through determination of period and amplitude sensitivities. Results obtained by random sampling of parameter vectors are summarized in Fig. 4.15.

In general, overall state sensitivities σ_j and period sensitivities σ_j^P are correlated to a certain degree, which lets one expect to find (similar) differences in model robustness. Note that feature sensitivities were determined via the indirect method, and had to rely upon numerical detection of period lengths. This explains, for instance, high period sensitivities that presumably are artifacts. When comparing the probability distribution functions for period and state sensitivities, again, the dual-feedback model according to both criteria shows higher robustness than the single-feedback model. In contrast to the overall state sensitivities, this higher stability additionally relies upon a shift in the distribution towards lower sensitivities. This is suggestive of a robust design of the control circuit regarding its physiological function.

Analysis of robustness as a property of the structure of the regulatory circuits, in principle, has to rely upon investigation of the entire parameter space. Local analysis as performed above does not suffice to elucidate structural properties. Moreover, closer analysis of the types of perturbations the systems may tolerate best was intended. Since true global analysis is computationally infeasible, subsequent studies were designed such as to diminish the effects of specific locations in parameter space. For this purpose, starting from the published parameter sets, new reference parameter sets p^k were generated that enabled autonomous oscillations in the physiological range ($23h\tau \leq 25h$). For each of the parametrized models ($n = 37$ for single-feedback and $n = 41$ for dual-feedback), the effect of local normally distributed random perturbations was analyzed (200 simulations). As a measure of oscillator precision, the normalized period

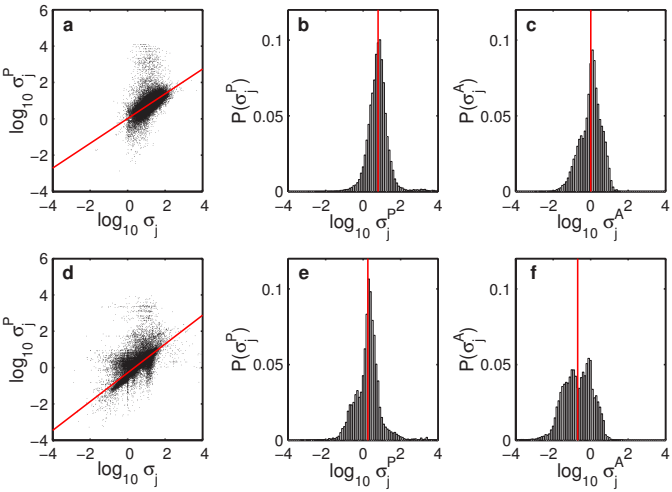

Fig. 4.15: Local comparison of model robustness with respect to oscillator function. Identical plots are provided for the single-feedback model (**a-c**) and the dual-feedback model (**d-f**). Data from random sampling of parameter and feature sensitivities - simulations presented in Fig. 4.11**a-f** and equivalent computations for the more complex model - were analyzed ($n = 6.984$ and $n = 11.932$, respectively). **a,d,** Period sensitivities σ_j^P plotted against relative parameter sensitivities σ_j with linear regression (line). **b,e,** Probability distribution of period sensitivities; the horizontal line corresponds to the average value. **c,f,** Probability distribution of amplitude sensitivities σ_j^A with mean value.

deviation $\Delta\tau_l^k$ of the locally perturbed system p_l^k was defined by:

$$\Delta\tau_l^k = \left| \frac{\tau(p^k) - \tau(p_l^k)}{\tau(p^k)} \right| . \tag{4.11}$$

Accordingly, $\Delta\tau_l^k = 10^{-2}$ means a 1% change in period length relative to the reference value. For each of the perturbation modes described below, simulation results ($n \geq 6,000$) for all reference parameter sets were pooled, and the (cumulative) frequencies of encountering a given or higher oscillator precision were calculated.

Both mathematical models were subject to this analysis under two regimes of random parameter variations, namely single-parametric disturbances and vectorial perturbations. The first regime mimicks the effect of local disturbances in the control circuits, and involves identical distributions of absolute parameter variations for both models. The assumption underlying the second regime is that each function of the circuit may be mutated independently. As the number of parameters is higher for the dual-feedback model than for the single-feedback model, it also implies higher absolute parameter variation for the more complex model.

The results of global robustness analysis summarized in Fig. 4.16 show that comparison of the single- and dual-feedback models with respect to robustness requires more differentiated judgements than those suggested by local analysis alone. An additional branch of feedback apparently proves to be advantageous for the system in terms of buffering it against perturbations in single components or underlying biochemical reactions (Fig. 4.16a). Enhanced robustness primarily concerns the robustness of the precision of circadian rhythms. This finding is in agreement with the physiological importance and experimental observations of extreme fine-tuning of the circadian clock.

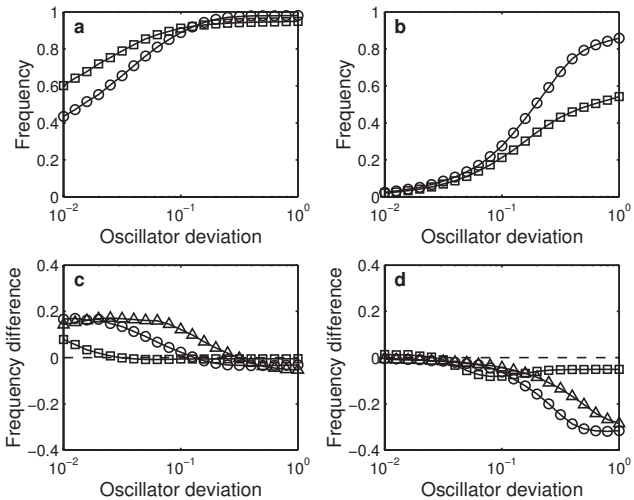

Fig. 4.16: Comparison of oscillator precision. a, Frequencies of obtaining a circadian clock with a given or higher precision (lower deviation of period length) averaged over all reference parameter sets after perturbation of single model parameters in the range of $0.5p^k \ldots 2p^k$ for the single-feedback model (circles) and the dual-feedback model (squares). **b,** Same as **a** for vectorial perturbations, that is, the cases in which all parameters were perturbed simultaneously but independently in the given range. **c,** Differences between probability distributions resulting from single-parametric disturbances for the dual-feedback model vs. the single-feedback model. Different perturbation strenghts were applied, namely in the ranges of $0.9p^k \ldots 1.1p^k$ (squares), $0.5p^k \ldots 2p^k$ (circles) and $0.1p^k \ldots 10p^k$ (triangles). In all cases, the data presented were obtained by substracting probabilities for the 5-state model from those calculated for the 10-state model. **d,** Effect of perturbation strenght on relative oscillator precision in analogy to **c** for multi-parametric variation.

For robustness with respect to generation of stable oscillations *per se*, however, the dual-feedback structure of the more complex model shows higher fragility than the structure involv-

ing only a single branch of feedback. This fact is illustrated by the lower probability of retaining imprecise oscillations after single-parametric perturbations as well as the large differences in the occurence of any type of oscillations when the models were subjected to vectorial perturbations to the reference parameter values (Fig. 4.16b). In an additional series of analyses, the effects caused by different absolute strengths of perturbations were examined by adjusting the ranges of allowed parameter variations. As shown in Fig. 4.16c-d, the phenomenon of higher robustness of precision for the dual-feedback model, but increased overall fragility was observed for all cases examined. Importantly, larger differences in model behavior were consistently revealed for disturbances of higher impact. Model behavior was barely distinguishable for slight modifications of parameter values.

All analyses of this type covered a larger region in parameter space, subject to the condition that the models in their reference parametrizations reflected the physiological behavior of circadian clocks. Comparing the two models, it can, thus, be concluded that the two-pronged negative feedback structure as realized in biology confers robust precision to the circadian clock under conditions when variations in only single (or few) parameters occur. The design, however, leads to increased fragiliy with respect to generation of unphysiological rhythms, and, in general, for simultaneous disturbances in multiple parameters.

To elucidate the 'control logic' behind the two mathematical models, and to identify potential reasons for the observed differences in model robustness and fragility properties, the role of functionally related model parameters was analyzed. For this purpose, parameters were classified either according to the type of biochemical processes they describe, or according to their position in the control hierarchy, that is, their association with local or global processes. Grouped sensitivities obtained from systematic two-dimensional analysis of paramater space around the previously published parameter values are shown in Fig. 4.17. The abbreviations used were explained in section 4.5.1.

When first regarding functional groups (panels a,b), the dominant role of parts of the model concerned with transcription / translation (T), global degradation (DG) and, partially, transport (TR) in sensitivity towards parameter variations becomes evident. A clearer separation of robust and fragile model parts exists for the dual-feedback model, which means a concentration of fragilities in few points. Moreover, as already recognized by separate model analysis, fragilities in the 5-state model reside in phosphorylation (P), whereas in the 10-state model specific gene regulation (GR) fulfills a corresponding role.

At the more abstract level of parameter status with respect to functional hierarchy, distinctions between the two models for the circadian clock in *Drosophila* become even more evident (panels c,d). In the single-feedback model, although these grouped parameter ranks have relatively high variability, fragile parts of the model display the tendency to be associated with parameters classified as being global. The dual-feedback model clearly shows this difference. In other words, the additional branch of negative feedback incorporated in the more complex model contributes to an even higher degree to separation of robustness and fragilities. This is

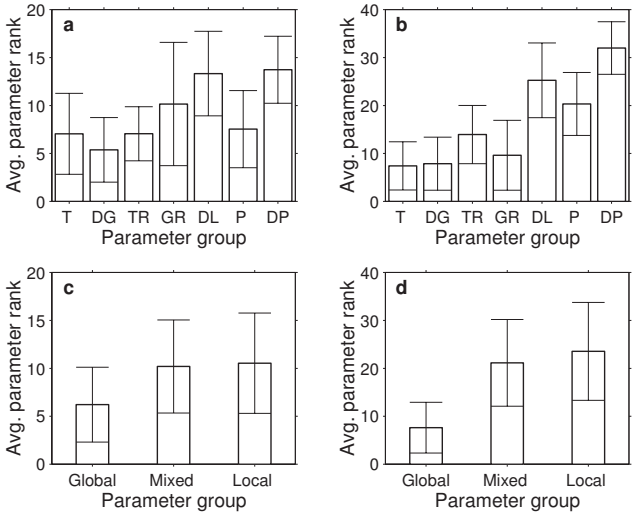

Fig. 4.17: Classification of functionally related parameter groups. Average parameter ranks were determined for parameter groups defined in Tabs. 4.1 and 4.2 by using systematically collected data sets for all two-dimensional sections in parameter space of the 5-state model (**a,c**) and the 10-state model (**b,d**). Functional categories (**a,b**) and classification according to control hierarchy (**c,d**) constituted the criteria for grouping. Analysis was performed based on overall state sensitivities (open bars).

consistent with the more extreme robustness properties of this model when subjected to parametric disturbances. In particular, highly sensitive parameters described globally controlled processes like general transcription, translation or proteolysis. Interpreted in biological terms, these results are suggestive of a design principle of cellular regulation, in which robustness of specific (local) functions is achieved by delegation of fragilities to global control circuits.

To further investigate this possibility, overall state sensitivities for the two models were grouped according to the same functional criteria as used above and compared to each other (Fig. 4.18). This analysis reveals that, also in absolute terms, the second branch of negative feedback contributes to making the interior of the regulatory module constituting the circadian clock less sensitive to disturbances in parameter values. This concerns, in particular, post-translational modifications of PER and TIM proteins, and also to a certain extent protein-specific degradation parameters. Gene regulation constitutes an exception from this scheme, but in this case smaller variability is indicative of a more focused role of these processes in the 10-state model. This, in turn, could lead to enhanced controllability of the module.

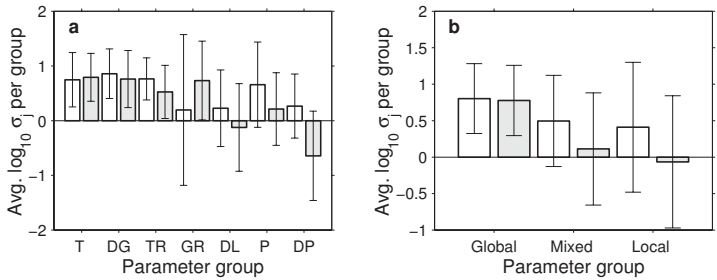

Fig. 4.18: Comparison of absolute influence of functionally related parameters. Overall state sensitivities were grouped in analogy to parameter ranks shown in Fig. 4.17. Here, open bars represent average values for the 5-state model. Filled bars refer to the 10-state model.

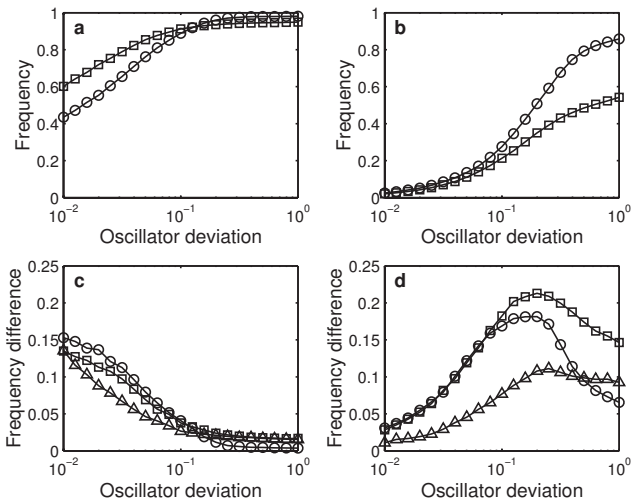

Fig. 4.19: Robustness through hierarchical control. a, Effect of stabilization of the system by hierarchical control under conditions of perturbations in single parameters (**a**) or vectorial perturbations (**b**) in analogy to Fig.4.16c (range of perturbations: $0.5p^k \ldots 2p^k$), but employing 1% variability of global parameters compared to all other model parameters. Differences between the cumulative probability distributions for the single-feedback model (circles) and dual-feedback model (squares) with and without hierarchical control are shown. As a control, local parameters were stabilized for the dual-feedback model (triangles).

Sensitivity towards disturbances in parameters associated with global cellular functions, however, is not affected by differences in model structure. The concept of export of fragilities to global control, hence, should be interpreted in relative terms. It means a concentration of sensitivities of the control circuits in those parts, for which global regulatory networks are able to provide well controlled-inputs to the particular regulatory sub-network by a locally improved design that reduces the impact of perturbations in the 'local' parts of the model. As for the example of gene regulation mentioned above, such a hierarchical control scheme could contribute to enhance the controllability and, hence, the robustness of the cellular system as a whole.

The plausibility of this hypothesis was, finally, tested by comparison of model robustness when reduced variability of global parameters was assumed (Fig. 4.19). Analysis relied on the set of models parametrized such as to show nearly physiological behavior. It was carried out as described for the global comparison of model robustness, but differed in the fact that global - or for control purposes local - model parameters were allowed only to vary in a small range compared to all other model parameters (1% relative variability). The general effect of thereby simulated hierarchical control is an increase of robustness for both models. Interestingly, the dual-feedback model shows a considerably higher enhancement of robustness compared to the simpler model for multi-parametric perturbations, that is, its most important points of fragility. In agreement with the results obtained from sensitivity analysis, stabilization of local parameters leads to a less pronounced effect despite the higher number of local versus global model parameters. Hierarchical control modes can, thus, substantially further enhance the precision of the circadian clock when incorporating the dual-feedback loop, while also reducing the probability of the most severe failures of the system.

4.6 Conclusions

Systematic analysis of parametric sensitivity of two models based on negative transcriptional feedback for the circadian clock in *Drosophila* revealed that robustness and fragility of the network are largely determined by its structure, not by the actual operational regime. Concerning differences between a simple model incorporating one branch of negative feedback and a more complex model with two branches, according to all criteria applied, the dual-feedback model showed higher robustness, especially with respect to its physiological role of an autonomous oscillator.

In particular, the ordered sensitivity of model parameters as well as group-averaged absolute sensitivities reveal that 'global' parameters are the most important, remarkably conserved points of fragility. Adding a second control loop to the system does not change these fragilities in absolute terms, but leads to enhanced robustness of model parts associated with only local functionality and, hence, more focused control of the system by externally provided signals such as those originating from the general transcriptional apparatus. This observation was made irrespective of the particular method of analysis (determination of state sensitivities vs.

application of direct perturbations to the system) and of the way in which the parameter space was investigated (two-dimensional planes vs. random search).

Based on these results, a design principle of cellular regulation, namely to 'export' a specialized control circuit's points of fragility to global, well-controlled regulatory systems like general transcription can be suggested. In future studies, it will be intriguing to test the method presented herein using more complex models of oscillatory genetic circuits, for instance involving (interlocked) positive and negative feedback loops [243, 261]. Including other regulatory networks could also serve to gain deeper insight into the relations between (hierarchical) control structures of cellular regulation and the key properties of robustness and fragility.

5. ROBUSTNESS VS. IDENTIFIABILITY OF REGULATORY MODULES

5.1 Introduction

For a long time, cellular regulatory networks have been seen as overwhelmingly complex, highly interacting assemblies of genes and their products. Only recently, it has been suggested, that the architecture of these networks is in fact modular. Different tasks are fulfilled by specialized quasi-autonomous subsystems (modules), which perform functions analogous to controllers in technical processes [151, 248]. In this context, one way to achieve fault tolerance for a biological system is to evolve robust regulatory modules. Robustness is supposed to be an essential feature of, for instance, control of cellular proliferation and of development, as there robust control is closely linked to the organism's survival.

This aspect of biological regulation has been examined by mathematical modeling, for example, of the segment polarity network and of developmental regulatory circuits in *Drosophila* [171, 272]. The models displayed the qualitative behavior observed *in vivo* and robustness of this behavior. As for the models of circadian oscillators analyzed in the previous chapter, these features turned out to be properties of the model structure, and only to a very limited degree of the parameter values. If this finding would hold true in general, it would have important implications for the understanding of cellular systems as a whole. The key characteristics of modularity and robustness could greatly facilitate the mathematical modeling of larger regulatory networks [137].

However, for a quantitative understanding at the system level, finding the right model structures for small networks and then combining them will prove insufficient. Also the quantitative aspects of cellular regulation have to be described in an appropriate way. Unless the quantitative behavior is captured, a tight coupling of model and experiment, and the purpose-driven manipulation of the system will be impossible. For the development of mathematical models, this task implies identifying the model parameters as well as the structure. Identification of model parameters can be complicated, as robustness and identifiability are contradictory system characteristics. The input-output behavior of a robust module is almost invariant and, thus, could provide little information on the internal working principles. The quantitative (internal) behavior of robust systems nevertheless varies if perturbed. In control engineering, for instance, the principles of dual (adaptive) control rely on controlling the process as well as possible, while

injecting probing perturbations in order to improve the information on the system and, thereby, future control action [69, 70]. In biology, systematic directed perturbations at the genetic level were applied to elucidate control structures for (smaller) example systems such as the galactose system in yeast, or by genome-scale generation of deletion mutants. There, as in most current biological studies, however, only qualitative or semi-quantitative effects of the perturbations were measured [119]. The most eminent difficulties in development of quantitative mathematical models are therefore thought to arise from the combination of robustness and today's prevailing qualitative biological knowledge [105]. Under these circumstances, the correct determination of internal parameters can be impeded, especially if robustness depends on the cooperation of multiple, redundant pathways in order to achieve the control objectives [103].

As a more differentiated view on (cellular) systems, Doyle and co-workers recently introduced the theory of highly optimized tolerance (HOT), which was discussed in chapter 2.2. In brief, the concept points out the combination of generally robust input-output behavior, but extreme sensitivity or fragility in the case of selective disturbances [29, 209]. As a consequence, regulatory modules obeying these principles could be more easily captured in quantitative terms. Theoretical concepts on robustness are thus directly linked with the development of acceptable mathematical descriptions in cell biology.

This section, hence aims at both a preliminary distinction of the competing theories, and at assessing to what extent quantitative mathematical modeling is possible given the current status of biological knowledge. These issues can only be dealt with by studying specific biological examples. Here, a complex regulatory system heavily relying on redundancy of sub-systems - the control of mitotic events in cell cycle regulation of the budding yeast *Saccharomyces cerevisiae* - will be analyzed. For this purpose, a mathematical model able to describe the system under consideration in sufficient quantitative accuracy first needed to be established. Extending the pioneering work of Tyson and colleagues [32] in this field, mathematical modeling aims at providing a more detailed picture of the regulatory processes, both by regarding an enlarged network and by using parameter estimation to adjust the model to experimental data. A differentiated study of model robustness and model identifiability by means of sensitivity analysis and determination of parameter estimation accuracy will then be performed.

5.2 Cell cycle regulation in budding yeast

Owing to its genetic accessibility, the budding yeast *Saccharomyces cerevisiae* is widely used as an eukaryotic model organism. This is especially true for the biology of cell cycle regulation, for which this yeast belongs to the best understood biological systems. As the control of cell proliferation is also one of the most highly conserved intracellular regulatory networks, considerable homologies to higher eukaryotes exist. The general regulatory scheme as well as the molecular mechanisms to be described in the following can therefore be regarded as a blueprint of eukaryotic cell cycle regulation. However, larger differences between yeast and mammals

exist in the coordination of growth and cell cycle progression [38] that would require more specific consideration if one was interested in this particular aspect of the field.

5.2.1 The general picture

In every eukaryotic cell, passage through the cell cycle is a tightly controlled process. Cell cycle regulation, the control system, is essential for the coordination of cell growth and division. The complexity of this task can be estimated from the fact that in budding yeast the transcription of approximately 800 out of 6,300 genes is cell-cycle regulated [246].

At the physiological level, the cell division cycle is characterized by a fixed sequence of cell cycle phases (Fig. 5.1). Cells starting the cycle in G1 phase have to accumulate sufficient cellular material to reach a critical size for all subsequent processes to begin. Once this aim is accomplished, a checkpoint called 'START' (or 'restriction point' in higher eukaryotes) enables DNA replication in S ('synthesis') phase. In parallel, bud formation is induced. During S phase, surveillance mechanisms ensure that DNA is replicated completely, and only once.

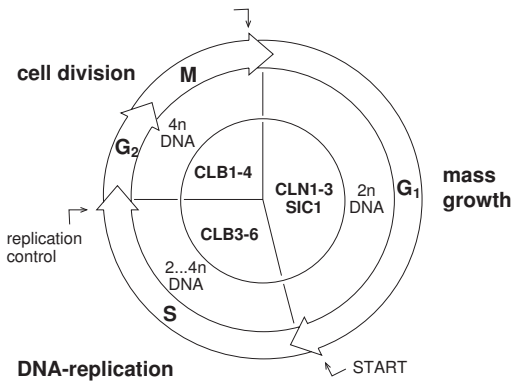

Fig. 5.1: Cell cycle regulation in budding yeast. The scheme shows the main cellular tasks in specific cell cycle phases (outermost ring), the DNA content of the cell (middle) and the dominant cell cycle regulators (center). Arrowheads indicate checkpoints.

The next important cell cycle phase is mitosis (M), during which chromosomes have to be aligned and attached to the spindle apparatus in metaphase, before in anaphase sister chromatides are separated. Finally, telophase encompasses the processes for distribution of DNA to mother and daughter cell, which are then separated by cytokinesis. Each of these steps is controlled by checkpoints, for instance, sensing correct positioning of the mitotic spindle, the macromolecular assembly that generates the mechanical forces necessary for chromosome movement and positioning.

At the molecular level, cyclin dependent kinases (CDKs), their activators called cyclins, and their inhibitors (CKIs) form the core of the regulatory network. The yeast *Saccharomyces cerevisiae* possesses one catalytically active CDK (Cdc28). It associates with nine different cyclins, leading to activation of the kinase. A characteristic feature of these cyclins is their periodic accumulation and destruction during the cell cycle (Fig. 5.2). Although, in principle, periodic CDK activation alone could establish a minimal cell cycle regulation, strong evidence suggests that in all eukaryotes, cyclins additionally function to target the activated CDKs to stage-specific substrates [176].

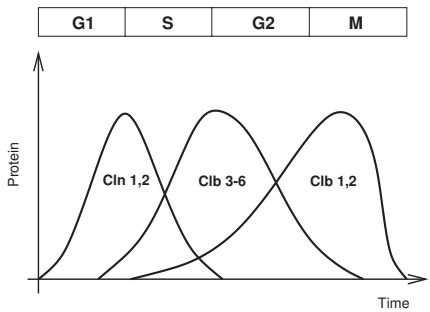

Fig. 5.2: Sequence of CDK activities. Phase-specific activities of cyclin-dependent kinase are given qualitatively in terms of the time courses of cyclin concentrations. For corresponding cell cycle phases see top bar.

In yeast, entry into S phase is induced by the G1 cyclins Cln1-3. The S phase cyclins Clb5-6 are responsible for controlling the processes of DNA replication and for initiating mitosis. Mitosis, finally, is controlled by the mitotic cyclins Clb1-4, of which Clb2 plays the most prominent role [44]. Separation of these tasks, however, is not strict, because cyclins may confer overlapping specificities to the CDK, and also show overlapping expression profiles. One mechanism for controlling the phase-specific occurrence of CDK activity functions via the inhibitor Sic1, which specifically inactivates B-type cyclins [173]. Control of cyclin abundance and additional control circuits, thus, enable the cell to form distinct kinase complexes with different functionality.

The phase-specific cyclin fluctuation in yeast - as in all eukaryotic cells - relies upon interconnected control circuits. One important aspect of these circuits is the control of gene transcription. Recently, it was shown for yeast that transcriptional activators form a fully connected cycle driving the cell cycle into the forward direction. Transcription factors are by themselves periodically expressed in such a way that activators required for one cell cycle phase contribute to control of transcription factors fulfilling tasks in the next phase [23, 240].

Ubiquitin-dependent protein degradation represents another prominent mechanism for phase-specific control of cyclin abundance. In general, the ubiquitin-proteasome pathway works

in two steps: First, target proteins are marked for degradation by covalent attachment of the small protein ubiquitin. The reactions are carried out by enzyme complexes called ubiquitin ligases. Successively assembled poly-ubiquitin chain(s) then serve as recognition signals for rapid proteolysis by the 26S proteasome [110]. From a control point of view, two types of ubiquitin ligases are most important for regulated protein destruction that is crucial to cell cycle progression. The SCF system (named after its constituting components Skp1 / Cdc53 / F-box protein) recognizes phosphorylated proteins, and mainly acts in the G1 and S phases. The anaphase promoting complex (APC), via additional factors conferring substrate specificity, is involved in the turnover of mitotic regulators [128, 142].

Evidently, the interaction between such diverse processes leads to a highly complex and interconnected regulatory network [173]. The sub-system governing mitosis, which is to be captured in close correspondence to biological reality by the mathematical model, will therefore be described in more mechanistic detail in the following section.

5.2.2 Controlling mitosis

The two main regulatory tasks to be accomplished at the end of the cell cycle are first to activate late mitotic CDK, especially Clb2-CDK to drive mitotic events. As this activity also blocks the exit of mitosis, the cell secondly has to get rid of the mitotic CDK activities for a new cell cycle round to begin. These processes are mainly regulated by transcriptional control and by selective protein degradation. An overview of the most important processes involved in the control of mitosis is given in Fig. 5.3.

In the yeast cell cycle, transcription factors form an interconnected regulatory network that, owing to the activation of transcriptional activators in one cell cycle phase by those from a preceding phase, is itself organized as a cycle [240]. The transcription factors MBF (Mbp1 / Swi4) and SBF (Swi4 / Swi6) are responsible for expression of late G1 phase genes, and, in turn, depend on (late) G1 cyclin-CDKs such as Clb5–Cdc28 for activation. In G2/M, these transcriptional activators contribute to the induction of the *CLB2* gene. More importantly, the expression of SFF as the key regulator for the *CLB2* gene cluster is induced by MBF and SBF activity [23, 240].

SFF itself is a protein complex composed of the transcriptional activator Ndd1 as its limiting component, the forkhead transcription factors Fkh1 and Fkh2 that recruit Ndd1 to its target genes, and of the protein Mcm1, which is constitutively bound to DNA [5, 145, 149, 162, 170, 197, 295]. Activation of gene expression by SFF requires post-translational modification of its components. Although the exact mechanism is not known yet, it has been shown that Ndd1 and Fkh2 are phospho-proteins, and that expression of target genes correlates with phosphorylation of the proteins [145, 197]. Since both proteins contain Cdc28 consensus sites, and are likely targets of Clb2-CDK [49, 207], this may explain for the early observation of an autocatalytic positive feedback loop for *CLB2* gene expression [7, 129]. Additional complexity, however, stems from the fact that Fkh1 and Fkh2 are transcriptional repressors as well as activators [145].

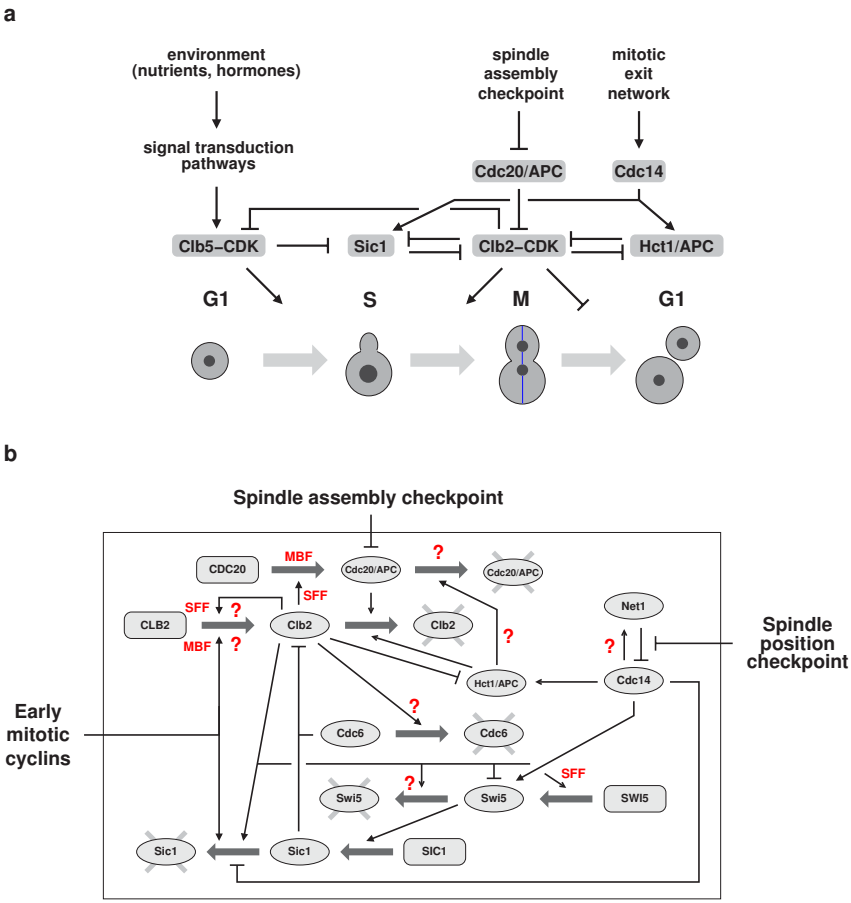

Fig. 5.3: Molecular interactions governing mitosis. a, Overview of key regulators. Positive and negative regulatory interactions are denoted by arrowheads and bars, respectively. The lower part shows changes in cell phenotype during cell cycle progression, including the localization of the genetic material (dark circles) and the spindle apparatus (vertical lines). **b,** Detailed control system. Rectangles and ellipses indicate genes and proteins, respectively. Bold arrows stand for the processes of transcription / translation and protein degradation. Transcription factors for control of the individual genes are shown in gray. Regulatory input signals from cell cycle checkpoints or from G1 control circuits are indicated accordingly. Question marks point to uncertain or hypothetical interactions. The subsystem for control of sister chromatid cohesion was omitted.

The presence of Clb2-CDK activity for promoting mitosis relies on several other factors besides the control of *CLB2* gene expression. Two proteolytic systems for Clb2 exist that are inactivated in mitosis. Earlier CDK activity, as well as Clb2-CDK inactivate one branch of the degradation machinery. Hct1 recognizes Clb2 protein and targets it for ubiquitylation by the anaphase promoting complex (APC) [230, 231]. The modified protein can subsequently be degraded by the proteasome. As Hct1 phosphorylation carried out by Clb5-CDK and Clb2-CDK abolishes the Hct1-APC interaction, the kinases inhibit the pathway [291]. The second branch of controlled proteolysis relies upon a Hct1 homologue termed Cdc20. Although the corresponding gene is expressed in the *CLB2* gene cluster, the activity of APC^{Cdc20} remains inhibited by the spindle assembly checkpoint (SAC) until anaphase [68, 159, 270].

Additionally, mitotic cyclin-dependent kinases prevent the action of two systems for their inactivation through competitive inhibition. After initiation of the process by late G1 CDK activity, they sustain the phosphorylation of the CDK inhibitor Sic1 thereby targeting it for degradation by the SCF (Skp1 / Cdc53 / F-box complex) proteasome pathway [71, 120, 232]. This functionality is also suppressed at the level of transcription, namely by phosphorylation of the transcription factor Swi5 that is contained in the *CLB2* gene cluster and activates *SIC1* gene expression [1, 141, 246, 256]. Its modification leads to export to the cytoplasm and, thereby, to inactivation [179]. Finally, the DNA replication factor Cdc6 associates with CDK complexes and presumably directly contributes to their inactivation [25, 65]. Like for the case of Sic1, however, mitotic cyclin-CDKs negatively regulate Cdc6 protein stability [53, 64, 193]. In early mitosis, *CDC6* gene expression is also blocked by the closely related transcriptional repressors Yox1 / Yhp1, which are themselves subject to cell cycle regulated transcription [198]. As a consequence, Cdc6 as well as Sic1 protein are not present in early mitosis. Through a combination of mechanisms acting at the transcriptional and the post-transcriptional level, thus, a self-sustaining state of high mitotic kinase activity establishes.

In early mitosis (metaphase), replicated chromosomes have to be attached to spindle microtubules that act as molecular motors for distribution of the genetic material to mother and daughter cell, respectively. Until this process is completed, or when cells are treated with the spindle depolymerizing agent nocodazole, the spindle assembly checkpoint delays entry into anaphase by blocking the APC^{Cdc20} proteolytic system. For this purpose, a number of proteins forms inhibitory complexes with Cdc20; the exact nature of the inhibiting signal, however, has yet to be determined [288]. Upon checkpoint inactivation, Cdc20 is responsible for abolishing sister chromatid cohesion via destruction of the anaphase inhibitor Pds1 [34, 36, 37, 159]. Concomitantly, active APC^{Cdc20} leads to proteolysis of Clb5 cyclin, and to partial degradation of Clb2 cyclin. The latter process proved to be a necessary precondition for subsequent total elimination of late mitotic kinase activity [24, 282].

The next step of Clb2 inactivation begins after the segregated chromosomes have been distributed to mother and daughter cell, which is equivalent to a correct positioning of the elongated spindle. The phosphatase Cdc14 plays a prominent role in the exit from mitosis, as it reverses

inhibitory phosphorylation caused by mitotic CDK activity [122, 268]. Until early anaphase, the competitive inhibitor Net1 retains Cdc14 in the nucleolus. This inactivation is partially relieved after inactivation of the SAC through a regulatory network termed the FEAR (Cdc fourteen early anaphase release) network [247]. However, only a signal for correct spindle position transduced by the mitotic exit network (MEN) enables its full release during telophase and early G1 phase [239,258]. Mutants carrying defects in MEN proteins arrest in late anaphase with high Clb2-CDK activity and fail to initiate cytokinesis [123]. Cell cycle progression thus depends on a further checkpoint. The MEN, in principle, is organized as a GTPase-controlled protein kinase cascade similar to signal transduction pathways in higher eukaryotes. The exact mechanism of signal generation and signal propagation remains to be determined [169]. Experimental evidence suggests that ultimately phosphorylation of Net1 and / or Cdc14 by MEN kinases induces disassembly of the Cdc14 / Net1 complex [166, 238, 271, 286], which can be reversed by Cdc14 phosphatase activity. This negative feedback loop may be partly responsible for the fact that activation of Cdc14 at the end of mitosis is only transient [239].

The effect of Cdc14 activation is at least threefold: The phosphatase is able to influence the activity of the MEN pathway positively via the kinase Cdc15 [124], but may also attenuate the signal through dephosphorylation of the regulator Bfa1 [192]. It can not be excluded that additional targets for Cdc14 exist that also serve to restrict the activity of MEN and, hence, Cdc14 phosphatase to a short window in late mitosis [85]. Once released from the nucleolus, Cdc14 removes the inhibitory phosphorylation from the APC regulator Hct1 and, as a consequence switches on proteolysis of the remaining Clb2 protein [122]. Additionally, the phosphatase is responsible for the accumulation of the CDK inhibitor Sic1. Upon de-phosphorylation of the transcription factor Swi5, the protein can enter the nucleus and induce *SIC1* gene expression. De-phosphorylation of Sic1 protein counter-acts its targeting for ubiquitin-dependent proteolysis by mitotic CDK activity, and, thus, eventually leads to stabilization of the inhibitor [268]. Moreover, in late mitosis, the protein Cdc6 is expressed, which cooperates with Sic1 in inactivation of Clb2-CDK. How the cells accomplish to alleviate transcriptional repression of the *CDC6* gene by Yox1 / Yhp1, and which mechanisms determine the subsequent stabilization of the protein, however, have to be elucidated [25,198]. Jointly, these regulatory interactions bring the cell into a G1 state characterized by low Clb2-CDK activity and high Sic1 levels.

In addition to the control scheme as already described, major gaps in the current knowledge on the regulatory network exist. Question marks in Fig. 5.3 indicate some of these areas. This concerns, in particular, the exact mechanisms for transcriptional control of the *CLB2* gene cluster. It has been shown that gene regulation in this case relies on a complex interplay between the factors Mcm1, Fkh1/2 and Ndd1, involving controlled expression, phosphorylation and presumably also degradation of the proteins. Apart from correlations such as the fact that Fkh2 phosphorylation coincides with SWI5 expression [197], sources and significance of these regulatory interactions remain unresolved. Redundancy in transcriptional regulation, for instance, owing to combinatorial control of the genes, activation by mitotic cyclin-dependent kinases,

and regulated accumulation of the transcription factors themselves seem to be important for the system's dynamics [23, 81].

Controlled protein degradation provides another area that requires additional knowledge. Conflicting conclusion were reached with respect to the proteolysis of Cdc20, and the role the APC^{Hct1} pathway plays in it [91, 117, 201, 237]. For Cdc6, different modes of proteolysis specific for different cell cycle phases, and their modulation by phase-specific CDK activities have been described. The ubiquitin-dependent pathway via SCF clearly is involved in some of these modes, but an additional role for APC-dependent pathways can not be ruled out [53, 64, 193]. It is unknown, whether degradation of the transcriptional activator Swi5 occurs constitutively, or in a regulated fashion; at least, experimental evidence suggests that APC^{Hct1} does not participate in this process [W. Seufert, personal communication]. Proteolysis of the only recently identified components of SFF, finally, has not yet been a subject of direct experimental investigation. Observations such as an onset of rapid Ndd1 degradation that coincides with the activation of APC^{Hct1} at the end of mitosis point to controlled protein degradation as a significant regulatory mechanism to be characterized [145]. Altogether, these uncertainties represent challenges for model development, but in turn mathematical modeling could provide clues on the function of the mitotic control network, if being successful.

Tab. 5.1: Genotype - phenotype relations. "Partial proteolysis" of Clb2 refers to initial protein degradation by APC^{Cdc20}, whereas "complete" removal of the protein requires APC^{Hct1} activity. According to standard yeast nomenclature, "*GAL1,10-XXX*" and "$xxx\Delta$" specify the overexpression of gene "XXX" by using the GAL1-10 promoter, and the deletion of this gene, respectively. Addition of the spindle poison nocodazole is abbreviated by "Noc".

Genotype and additional treatment	Clb2 active in mitosis	Cdc14 release	Clb2 degradation partial	Clb2 degradation complete	Clb2/CDK inactivation
wild type	+	+	+	+	+
wild type + Noc	+	–	–	–	–
men (mitotic exit network mutant)	+	–[a]	+	–	–
$hct1\Delta$	+	+	+	–	+
$sic1\Delta$	+	+	+	+	+
$hct1\Delta$ + Noc + *GAL1,10-SIC1*	+	–	–	–	+
$hct1\Delta$ + Noc + *GAL1,10-CDC6*	+	–	–	–	+

[a] In MEN-deficient cells, Cdc14 release occurs only transiently in early anaphase [247].

The existence of parallel pathways for controlling the initiation as well as the termination of late mitotic CDK activity lets one expect a robust behavior of the system. It is observed *in vivo* that many perturbations do not abolish the ability to enter and exit mitosis. For instance, deletion of either one of the three major counter-players of *CLB2* – *HCT1*, *SIC1* and *CDC6* – has little effect on the qualitative behavior. Yeast cells are still able to exit mitosis, albeit either Clb2 levels stay high in G1, or inactivation relies completely on Clb2 degradation, re-

spectively (see Table 5.1). In quantitative terms, however, these changes are detectable, as, for example, hct1Δ strains display a delay in completing mitosis and therefore grow more slowly than wild type [231]. Additionally, by manipulating mitotic checkpoint mechanisms, yeast cells can be blocked at different points in mitosis. Over-expression of appropriate genes reverses this situation again. Altogether, such controlled perturbations of the system, which correspond to standard experiments in cell cycle research, could offer the possibility to sufficiently identify the operating principles of mitotic control despite the system's robustness.

5.3 A mitosis control module

Development of mathematical models involves structural model setup, definition of behavioral characteristics (kinetics), and finally estimation of kinetic parameters based on experimental data. Starting with a brief survey of the modular modeling approach pursued herein for establishing the model for control of mitosis in budding yeast, these steps will be described in the following sections.

5.3.1 Modular modeling approach

Cellular systems composed of modules offer the possibility to develop mathematical models for each module separately and then to obtain the system model by connecting the modules. The modular approach furthermore tries to implement re-usable model entities that enable a mathematical description, which is close to the biological processes. These principles are applied at the most elementary level of biological regulation by developing and employing submodels for processes such as transcription, translation, enzymatic conversions, protein-protein-interactions, and others. These submodels and higher aggregated models are then used to build up a standardized library for the convenient modeling of cellular systems [147, 148, 248]. In brief, at the most fundamental level, a finite and disjunct set of so-called "elementary modeling objects" (Fig. 5.4) was defined. They are used to represent substance formation, degradation and storage as well as the corresponding signal transformation processes that determine, for example, the control of transcription initiation via specific DNA-protein interactions.

The organization of these modeling objects in an object-oriented class hierarchy lays the basis for computer-aided model development as described in the next section. Elementary modeling objects can subsequently be interconnected to form higher aggregated structures. A modeling object for gene expression, for instance, comprises transcription and translation. In summary, this approach enables to progressively obtain a holistic description of more complex functional units.

A prototype gene expression unit used in the mitotic control module may serve as an example for these submodels. The biochemical reaction scheme shown in Tab. 5.2 represents a simplified description for this functional unit. It comprises the binding of a transcription factor

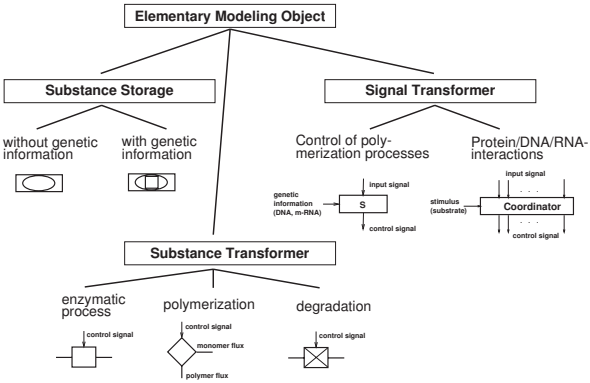

Fig. 5.4: Hierarchy of elementary modeling objects for cellular systems.

Tab. 5.2: Simplified biochemical reaction network for a single gene. RNA polymerase II, ribosomes, the proteasome pathway and a specific transcription factor j binding on the promoter of gene i are abbreviated by "RP", "RI", "PR" and "TF_j", respectively.

transcription factor binding to promoter	$[TF_j]+[GENE_{i,j}]$	$\underset{K_{XD,TF_j}}{\overset{K_{XA,TF_j}}{\rightleftharpoons}}$	$[TF_j \cdot GENE_{i,j}]$		
transcription	$[TF_j \cdot GENE_{i,j}]+[RP]$	$\underset{K_{DPol}}{\overset{K_{APol}}{\rightleftharpoons}}$	$[TF_j \cdot GENE_{i,j} \cdot RP]$	$\xrightarrow{K_{TK}}$	$[mRNA_i]+[TF_j \cdot GENE_{i,j}]+[RP]$
translation	$[mRNA_i]+[RI]$	$\underset{K_{DRib}}{\overset{K_{ARib}}{\rightleftharpoons}}$	$[mRNA_i \cdot RI]$	$\xrightarrow{K_{TL}}$	$[Protein_i]+[mRNA_i]+[RI]$
mRNA			$[mRNA_i]$	$\xrightarrow{K_{DM_i}}$	$[]$
degradation			$[mRNA_i \cdot RI]$	$\xrightarrow{K_{DM_i}}$	$[RI]$
proteolysis via the proteasome	$[Protein_i]+[PR]$	$\underset{K_{D,PR_i}}{\overset{K_{A,PR_i}}{\rightleftharpoons}}$	$[Protein_i \cdot PR]$	$\xrightarrow{K_{P,PR}}$	$[]+[PR]$

to DNA. The resulting protein-DNA complex serves as the basis for formation of the initiation complex with RNA polymerase and finally for messenger RNA (mRNA) production. Translation is described accordingly with ribosomes directly binding to mRNA. Degradation pathways for mRNA and protein (via the proteasome) complete the module.

Capturing the processes at this level of detail results in mathematical models that seem to be of unnecessary complexity. However, as one important advantage, this approach allows to integrate knowledge on well-characterized processes, for instance in the form of structural characteristic of genes, or of experimentally determined transcription and translation rates. Moreover, the number of model parameters and, thus, the parameter search space are reduced and physically meaningful. In the simplified module described above, for example, only one parameter for the DNA-transcription factor interaction and the transcription factor-RNA polymerase interaction, respectively, is used. Both features facilitate estimation of the remaining parame-

ters. Also the interplay of global and local control is considered, which proves important for a system-wide perspective [248].

To derive the mathematical equations, the entire biochemical reaction system with n molecular species X_i is decomposed into r elementary reactions $j = 1 \ldots r$ of the form

$$\alpha_{1,j} \cdot X_1 + \ldots + \alpha_{n,j} \cdot X_n \overset{k_j}{\rightharpoonup} \beta_{1,j} \cdot X_1 + \ldots + \beta_{n,j} \cdot X_n \tag{5.1}$$

Here, k_j is the kinetic constant of the reaction, whereas $\alpha_{i,j}$ and $\beta_{i,j}$ are the stoichiometric coefficients for substance X_i's involvement as educt or as product, respectively. The mathematical equations (ODEs) for the description of the reaction dynamics are derived straightforwardly from this scheme by application of mass action kinetics. In a canonical form like the one proposed in [234], the differential equations for the n_s concentrations of the components c_i ($i = 1 \ldots n_s$) can be written as:

$$\frac{dc_i}{dt} = \sum_{j=1}^{r} k_j \cdot (\beta_{i,j} - \alpha_{i,j}) \cdot \prod_{l \in S_j} c_l^{\alpha_{l,j}} \tag{5.2}$$

with S_j being the set of species actually participating in reaction j as educts, i.e. $\alpha_{l,j} > 0 \; \forall \, l \in S_j$. Here, the vector $\mathbf{c}$ corresponds to the vector of state variables $\mathbf{x}$ for a general ODE system (see equation 4.1).

Two major reasons justify the reference to the elementary chemical reactions instead of employing formal kinetics such as Michaelis-Menten rate laws. Formal kinetics essentially are approximations of networks of elementary reaction steps. However, they imply assumptions on relative velocities for the elementary reactions and / or on relative concentrations of components participating in the reactions [108]. In particular for regulatory networks, time-scale separations are not as common as in metabolic networks, and the regulators usually are present in concentrations of comparable magnitude. Formal kinetic descriptions may, thus, not be applicable, especially for a system for which parameter values are largely unknown beforehand. Model reduction in this case should be preceded by careful analysis of the detailed model. Additionally, the system of ODEs given in (5.2) is easily amendable to automatic model generation and analysis as well as to efficient numerical solution. Details on model implementation will be given in the next section after a description of the structure of the model for control of mitosis.

5.3.2 Model structure and implementation

One aim of this study was to establish a mathematical model for the control of mitosis in budding yeast, which is as close as possible to the biological mode of regulation. For this purpose, the well-established biological facts on this regulatory network as described in section 5.2.2 were included in development of the model structure. The high number of components and interactions between them, however, required an *a priori* restriction of the level of detail in which the regulatory processes were captured in order to obtain a dynamic model of manageable size. The following simplifying assumptions were employed:

(1) Focus on the core regulatory network. Since the aim of this study was to capture the core mitotic control mechanisms, signals generated by preceding cell cycle phases and by checkpoints within mitosis were modeled as discrete events at fixed time points. They include the activities of the G1 transcription factor MBF and of the early mitotic cyclin Clb5, for which initial concentrations were given, and decay of the signals was incorporated explicitly. Furthermore, licensing of Cdc20 activation by the spindle assembly checkpoint, and release of Cdc14 from the nucleolus in early anaphase as well as in late mitosis resulting from the activation of the FEAR and MEN networks were incorporated through changes in parameter values. In particular, a competitive inhibitor for Cdc20 was included that mimics the action of the spindle assembly checkpoint. The release of Cdc14 was modeled by using two kinases for early and late phosphorylation of Net1. The activities of these kinases representing the outputs of the FEAR and MEN networks, respectively, were modulated externally according to the cell cycle position.

(2) Single-compartment model. Most of the reactions involved in control of mitosis take place in the cell's nucleus. Therefore, the model was restricted to describe this compartment. However, *in vivo* translation is performed in the cytoplasm after export of the mRNAs from the nucleus. As a consequence, kinetic constants in the model do not reflect the true parameter values, but would have to be adapted according to the ratio of nuclear and cytoplasmic volume. Additionally, it has been shown that controlled protein localization of, for instance, Swi5 [179], Cdc14 [268] and potentially Hct1 [121] is important for the function of the regulatory network. In these cases, differential localization controlled by processes such as protein phosphorylation corresponds to activation or inactivation of protein function. The effects of controlled localization could, hence, be mirrored by assigning differential activities to modified and unmodified protein species, respectively. Again, protein concentrations (and kinetic parameters) would have to be scaled in order to obtain the 'true' values.

(3) Combination of regulators into single model species. Regulators with similar functionality and regulation in the cell cycle were lumped into one representative model species in order to reduce the number of components (state variables) to be tracked. This concerns the largely redundant pairs of transcriptional effectors Swi5 / Ace2 (model species 'Swi5'), Fkh1 / Fkh2 ('Fkh12'), and Yox1 / Yhp1 ('Yox1'). Based on a similar reasoning, the activity of all S-phase and early mitotic cyclins was subsumed under 'Clb5', which apparently is the most important of these cyclins with respect to the initiation of mitosis [280]. In general, the cyclin-dependent kinase Cdc28 was not modeled explicitly, since the protein is available in excess over its phase-specific activators [44]. The presence of a cyclin was, thus, assumed to translate directly into corresponding CDK activity. Finally, a coarse model was used for the description of ubiquitin-dependent proteolysis. The process in reality involves several steps of protein modification until the ubiquiti-

nated substrate is degraded by the proteasome. Here, however, this chain of reactions was incorporated into a single reaction carried out by the ubiquitin ligases APC and SCF, respectively, because they seem to catalyze the rate-limiting steps in the pathway.

(4) Omission of cooperative effects and multi-site protein modification. This point concerns cooperative transcription factor binding to DNA, for example by the forkhead transcription factor Fkh2 [111]. Additionally, multiple regulatory phosphorylation of proteins involved in cell cycle control occurs frequently. For instance, the APC regulator Hct1 [231], the nucleolar protein Net1 [238], and the CDK inhibitor Sic1 [265] are modified by cyclin-dependent kinases at several sites. Multi-site modification, instead of modification at a single, optimal site may serve to set thresholds for processes such as timely protein degradation because it determines a switch-like response to an input signal [182]. Although being of potential importance for the detailed dynamics of the system, in development of the model, these effects were not considered in order to avoid a combinatorial explosion of system states. Moreover, it can be shown that non-linearities owing to the complex interactions at these network nodes can bring about a similar dynamic behavior.

(5) Constant total amounts of selected proteins. Experimental evidence suggests that the total concentrations of several mitotic regulators do not fluctuate during the cell cycle. Controlled expression, thus, does not contribute to regulation of their activity. In particular, total amounts of Hct1 [201], SCF [83], APC [214, 290], Cdc14 and Net1 [268] could be represented by appropriate initial values. The amounts of Mcm1 and forkhead transcription factors are cell-cycle controlled, but the regulators constitutively bind to the promoters of genes in the *CLB2* cluster [5, 145]. As a consequence, Mcm1 was not included in the model, while for Fkh1 / Fkh2 only post-translational modifications that may contribute to control of gene expression [81,197] were described. Changes in highly abundant cellular components such as ribosomes and RNA polymerase should not severely affect the mitotic control system. Concentrations of these components were therefore assumed to be constant as well.

(6) Selective protein degradation. In general, presumably the basal stability of proteins and messenger RNA is not affected by interactions of the components with other species. For model development, however, this would imply that degradation reactions for the components in all the complexes they participate in would have to be captured, which would increase model size considerably. Here, these processes were included in a reduced form, namely by only considering the degradation of free, uncomplexed forms of most components. However, for example, for Sic1 it has been reported that the protein can be selectively recognized and targeted for proteolysis even when it is associated with CDKs [266]. In such cases, explicit degradation reactions for the bound components were included in the model.

Additionally, several assumptions needed to be made regarding the incompletely characterized interactions described in section 5.2.2. The most important of these interactions concern protein phosphorylation / dephosphorylation and proteolysis. The Mcm1 / Fkh1/2 / Ndd1 complex, necessary for expression of genes in the CLB2 cluster, is by itself regulated by phosphorylation. Since the effects of protein modification on complex formation and activity are only partially clarified, parameters for the efficiency of these processes depending on the protein state were included that, in principle, allow for the description of all possible combinations of activating and inhibiting effects. Since additionally the modifying enzymes have not been identified yet, but it seems likely that CDKs and Cdc14 play opposing roles in the regulation of SFF, the corresponding hypothetical reactions were introduced into the model. Moreover, for several phosphorylation reactions without known counter-parts, dephosphorylation by Cdc14 as well as constitutive dephosphorylation were assumed. Finally, the questions of how exactly Cdc6, Cdc20, Swi5 and (parts of) the SFF complex are degraded is unresolved. For these proteins, an array of possible degradation pathways, namely via SFC, APC^{Cdc20}, and APC^{Hct1} as well as constitutive degradation were incorporated into the model. Estimation of the associated efficiency and kinetic parameters based on experimental data could, thus, lead to the generation of hypotheses on the control mechanisms involved (see section 5.4.1).

An overview of the resulting model structure in terms of its modular composition according to the modeling concept is shown in Fig. 5.5. In brief, the model contains three expression units for the effectors of gene expression (upper part of the figure), and four units for the genes they control (lower part). Additional model parts not represented in the scheme serve to generate input signals, for instance, to describe the concentration of S phase cyclins. The activity of mitotic CDK constitutes the major output signal of the module. As can be seen from the figure, the model structure reflects the various feedback and feed-forward loops present in the regulatory network.

Together with the general components (RNA polymerase, ribosomes, APC and SCF) and proteins at constant level (such as Hct1 and Fkh1/2), the model comprises 18 different unmodified and uncomplexed protein species. A considerable part of the model's complexity, however, relies on complicated interactions between the cell cycle regulators that are represented by the "coordinator" (for protein-protein interactions) and "signal processor" units (for protein-DNA interactions). Owing to the high network interconnectivity, the representation of altogether 834 elementary reactions finally results in a model with 360 state variables and 242 kinetic parameters. These numbers also cover the control modules for extra- and intra-mitotic events, and additional modules for the simulation of gene overexpression experiments using the *GAL1-10* promoter. Table C.1 in the appendix gives a full account of the elementary reaction steps modeled, including the references to the experimental literature reporting the regulatory mechanisms.

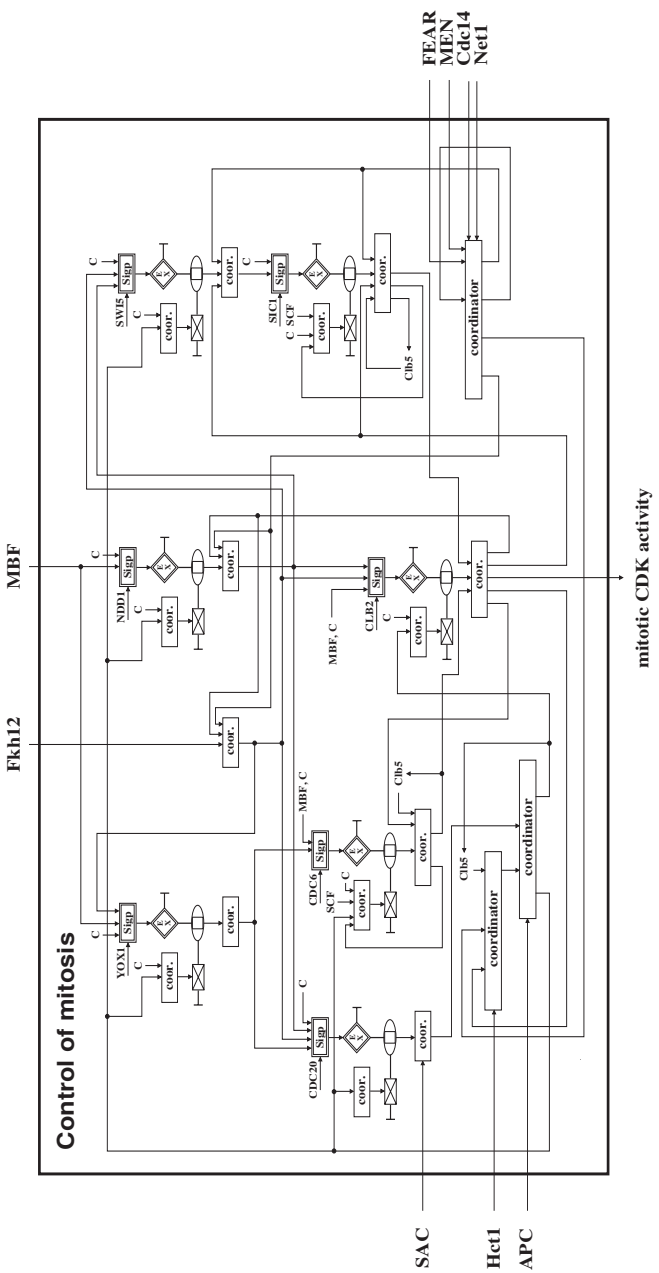

Fig. 5.5: Modular model representation for control of mitosis in budding yeast. The model structure is represented in terms of (elementary) modeling objects according to the modular modeling concept (see Fig. 5.4) [148]. Substance exchange is marked by bold lines, whereas arrowheads are used to indicate directed signal flow. Intersecting lines are unconnected unless marked by a dot. Input signals from the spindle assembly checkpoint, the FEAR network, and the mitotic exit network are denoted by "SAC", "FEAR" and "MEN", respectively; "C" indicates a constitutive signal.

The full network of reactions can be visualized in the form of an undirected graph (Fig. 5.6). Each node represents a species in the model. Whenever two species participate in the same biochemical reaction, they are connected by a link. The graph, thus, gives an overview of the model's main connectivities.

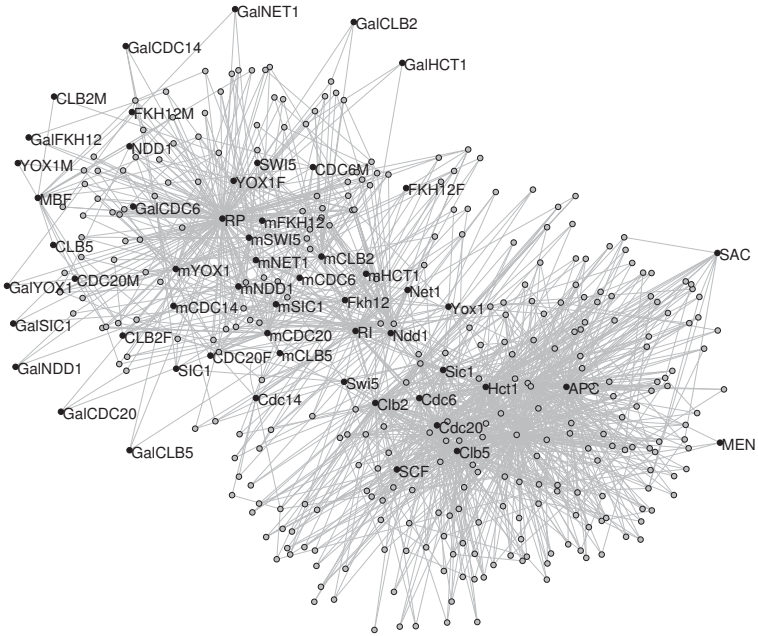

Fig. 5.6: Model structure: Connectivities. Connections between components described by the model (vertices) were introduced whenever two components participated in the same biochemical reaction, either as educts or products. Only nodes representing free, unmodified components (black circles) were labeled for clarity. Promoter sites of a gene 'XXX' were designated 'XXXF' or 'XXXM'. The gene's mRNA and protein products appear as 'mXXX' and 'Xxx', respectively. Unlabeled (gray) vertices correspond to, for instance, protein complexes and / or post-translationally modified proteins. The software package "Pajek" [14] was used for graphical representation of the network.

As can be seen in Fig. 5.6 for the energy-optimized graph, two main clusters exist. One involves predominantly transcriptional control (upper left corner), the other cluster comprises proteolytic reactions (lower right corner). The fact that input signals such as 'MEN' and 'SAC' occupy positions at the margins, concurs with them impinging on few specific reactions. Further indications can be derived from this graphical representation that correspond to the biological picture of the overall control scheme. For instance, cyclins, their inhibitors and degradation fac-

tors appear in close proximity; the phosphatase Cdc14 connects transcriptional and proteolytic control.

The model was implemented as a set of ordinary differential equations in MATLAB (Mathworks, Inc.) for numerical integration and parameter estimation. In parallel, automatic conversion of the equations into the simulation environment DIVA [89] served to verify numerical accuracy of the solutions. In particular for the implementation into MATLAB, which provides efficient numerical routines especially for matrix operations, the fact that the reaction network was composed out of elementary reaction steps alone proved advantageous. Since it is assumed that in an elementary reaction at maximum two components interact, all terms in the right hand side functionals of the ODEs are at maximum bi-linear. Therefore, a compact matrix notation for the calculation of the time derivatives of the states can be introduced as

$$\frac{d\mathbf{x}}{dt} = \mathbf{M}_1 + [\mathbf{M}_2 + \mathbf{x} \cdot \mathbf{V} \cdot \mathbf{M}_3] \cdot \mathbf{x} + \mathbf{B} \tag{5.3}$$

with the $n_s \times 1$ vectors of states $\mathbf{x}$ and constant terms $\mathbf{M}_1$, two $n_s \times n_s$ square matrices for the linear ($\mathbf{M}_2$) and a fraction of the bi-linear ($\mathbf{M}_3$) terms, and the $1 \times n_s$ identity vector $\mathbf{V}$. Those bi-linear terms for the time derivative of state i that do not depend on x_i itself, had to be captured separately by the $n_s \times 1$ vector $\mathbf{B}$, the elements of which are:

$$B_i = \sum_j M_{4_{i,j}} \cdot x_{IA_{i,j}} \cdot x_{IB_{i,j}} \tag{5.4}$$

Here, $\mathbf{M}_4$ contains the kinetic parameters for the bi-molecular reactions, and elements of the index matrices **IA** and **IB** designate the components participating in the j-th reaction. The system's stoichiometric matrix **S** and the parameter vector **p** were used to construct $\mathbf{M}_1$ to $\mathbf{M}_4$, **IA** and **IB**. In a similar way, analytically derived Jacobian matrices for the states and the partial derivatives needed for sensitivity analysis (see chapter 4.4) can be described. Altogether, this implementation then allowed for carrying out the time-consuming task of parameter estimation based on experimental data for this large model.

5.3.3 Experimental data and parameter estimation

For the particular system of budding yeast cell cycle regulation, one major challenge is to identify the model parameters. Only a very limited number of kinetic parameters such as average translation rates [82] and specific mRNA half-lives [112] have been determined experimentally. Thus, few parameters could be taken directly from literature, whereas most of the model parameters had to be estimated on the basis of experimental data. Parameter estimation then faced the problem – as encountered in a recent study by Tyson and colleagues [32] – of rare and partially incoherent quantitative data on yeast cell cycle regulators [44, 86].

Also owing to technical limitations, no single quantitative data set for all relevant regulators and conditions (mutations, treatments) in yeast cell cycle regulation exists. For this reason, experimental data had to be gathered from different studies. The risk of potentially incoherent

data associated with such an approach is illustrated in Fig. 5.7 a. Time courses of Clb2 protein concentration in cells released from G1 arrest from four different studies are compared. Pairs of two studies show very similar dynamic behavior, whereas between these pairs, large differences in the onset and duration of Clb2 presence become obvious. The different dynamics could be explained by the fact that in [282, 283] a strain was used that – in contrast to [75, 250] – contained an epitope-tagged version of Hct1 that, however, does not influence the qualitative behavior of the cell. For establishing the mitotic control model, therefore, only data determined in cells with as identical as possible genetic background were considered.

As the very similar quantitative Clb2 protein data for the untagged strains show, quantification of, for instance, Western Blots used for protein detection might be of minor importance for errors in quantitative experimental data. To investigate this possibility, Western Blots of Cdc28 protein over the cell cycle reported in [3] were analyzed by means of digital image analysis. CDK concentrations are known to be constant during the cell cycle. This is reflected by the protein quantifications for two independent experiments shown in Fig. 5.7 b. Standard deviations of relative protein concentrations of approximately 10% were calculated and none of the measurements deviates by more than 20% from the mean value. Protein quantification and other steps in experimentation such as liquid handling, thus, seem to contribute little to experimental variations. The analysis, moreover, gives an estimate of the standard measurement errors for this type of experimental investigations.

It is important to note that these considerations only apply to relative protein concentrations, whereas for realistic mathematical modeling, absolute concentrations are required. Only

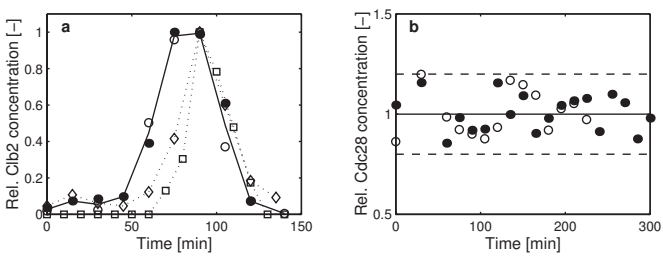

Fig. 5.7: Evaluation of experimental data quality. a, Comparison of experimentally determined concentrations of Clb2 protein in cells released from α-factor arrest a time $t = 0$ min. The following studies were considered: [75] (open circles), [250] (closed circles), [282] (squares) and [283] (diamonds). Data were normalized by their maximal values. The solid line connects the averages of the first two data sets, while the time courses for the two other data sets are visualized by dashed lines. **b,** Accuracy of protein quantification. Cdc28 protein used as a loading control for two time course analyses of cell cycle proteins [3] was quantified by digital image analysis of Western blots. Data were normalized by their mean values. Dashed lines indicate $\pm$ 20 % deviation from the average relative Cdc28 concentration (solid line).

a handful of experimental studies exist that addresses this problem (bearing as caveat the use of diploid and / or asynchronous cells) [44, 86]. Specifically investigating cell cycle regulators, the authors of [44] determined ≈ 2.400 copies of Clb2 protein per cell, which corresponds to a cellular concentration of ≈ 35 nM. The preferential nuclear localization of this protein, however, implies a higher effective concentration. Image analysis of data from [115] suggested that the nuclear concentration is at least 3-fold higher than the cytoplasmic concentration (data not shown). For model development, hence, an approximate peak Clb2 concentration of 100 nM was employed as unique reference value for all other protein concentrations. This estimate presumably constitutes a lower bound of the real abundance, however, it reflects physiological conditions, and the model can be adjusted once experiments reliably determine the cyclin concentration. For messenger RNAs, fortunately, absolute copy numbers from a genome-wide analysis [112] could be employed as reference values.

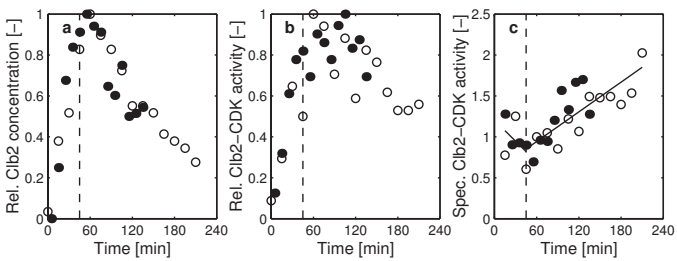

Fig. 5.8: Mitotic kinase in MEN-deficient cells. In two independent experimental studies [250] (filled circles) and [282] (open circles), cells carrying a mutation in a MEN gene (cdc15-2 mutants) were released from α-factor arrest and time courses of mitotic cyclin concentration and the corresponding CDK activity were followed until the cells arrested again in late mitosis. The dashed line indicates the estimated onset of anaphase. **a,** concentrations of Clb2 protein, normalized to the peak values (t = 0 min: start of Clb2 accumulation); **b,** normalized activity of Clb2-CDK and **c,** specific CDK activity, that is, the ratio of CDK activity and cyclin concentration; solid lines denote piecewise linear regressions for the combined data.

Another critical issue regarding quantitative experimental data concerns the relation of different system's outputs, for instance kinase concentrations and activities, even if they were determined in the same experiment. A comparison of time courses for Clb2 protein concentration and associated CDK activity in MEN-deficient cells shown in Fig. 5.8 illustrates this point. In general, because the two signals are highly correlated in unperturbed mitosis, cyclin availability is assumed to be the limiting factor for kinase activation. The reproducible, statistically significant ($r^2 = 0.65$ for linear regression in anaphase / telophase) increase in specific kinase activity (Fig. 5.8c), however, indicates that additional regulatory mechanisms, potentially slowly degraded remnants from earlier cell cycle phases, inhibit the kinase. Alternatively,

quantification of the Western blot signals may not be correct. The important consequence in the context discussed here is that, apart from late convergence to full specific activation, kinase activity data in MEN-deficient cells could not be used for parameter estimation. They do not seem to simply reflect the amount of Clb2 protein in mitosis, even though the inhibitor Sic1 is not present in this cell cycle phase.

Based on these considerations, an experimental data basis for parameter estimation was set up that also seemed promising with respect to the identification of a maximum of parameter values, using a minimum of experimental conditions. For this purpose, the wild type, for which relatively many time courses of system variables (total protein and mRNA concentrations, complex concentrations, phosphorylation states) are reported, played an important role. For dissecting the contributions of individual branches of redundant regulatory pathway, additionally, most of the perturbation experiments included in Tab. 5.1 were incorporated, although, in general, there are only few, predominantly qualitative data available for this type of experiments. The concentration of Clb2 determined in all experiments was used to check consistency of the data. A complete specification of this data is contained in Tab. C.2 in the appendix, and the experimental conditions will be described in more detail in conjunction with the simulation results in the next section.

Simulation furthermore requires definition of initial conditions and of input signals. The model is supposed to be valid between S phase, coinciding with Clb5 protein accumulation, and the next pre-START G1 phase. Initial values for mRNA concentrations were calculated from the relative data given in [149] and absolute mRNA amounts in asynchronous cell populations reported in [112]. Initial protein concentrations for species with time-varying amounts were based on [44]. For proteins with constant total concentrations, experimentally determined ratios of protein abundance were employed [W. Seufert, unpublished data]. Slightly different time delays between α-factor release and initiation of mitosis in the different experiments were accounted for by adjusting to the time course of Clb2 protein concentration. From [75], the window of $\approx$15 min duration, in which the MEN is active could be determined directly. Regarding the timing of SAC and FEAR activity, the fact was exploited that yeast cells need approximately another 15 min between onset of anaphase and complete elongation of the mitotic spindle [130, 281].

As outlined in the beginning of this section, only few values of kinetic parameters for yeast cell cycle control can be taken from the literature. Owing to potential inconsistencies in these values, and to enable an *a posteriori* check of the plausibility of the estimated parameters, however, these parameters were estimated as well. The modeling approach allowed for the integration of well–known structural parameters such as gene lengths. With additional external input parameters (e.g. for control of gene overexpression) in the model, from a total number of 242, the number of parameters to be estimated was reduced to 191. In parameter estimation, boundaries of parameter values were chosen such as to reflect the broad range of physically plausible values the kinetic parameters could attain (see Tab. C.3). For instance, constants

for (diffusion-limited) protein–protein interactions were allowed to be varied in the range of $10^{-3} \ldots 10^{2}\ \mu M^{-1} s^{-1}$ and $10^{-4} \ldots 10^{0}\ s^{-1}$ for association ($k_{ass.}$) and dissociation (k_{diss}) constants [76], respectively. Similarly, catalytic constants for enzymatic reactions ($k_{cat.}$) could lie between $10^{-3}\ s^{-1}$ and $10^{+2}\ s^{-1}$, whereby the fact that phosphatases, in general, have lower catalytic efficiencies than kinases (e.g. [122, 251, 268] vs. [18, 175]) was incorporated. In cases where reliable experimental data – for example concerning mRNA degradation [112], or general transcription and translation [82] – existed, narrower intervals could be chosen.

Finally, an evolutionary strategy based on the theories of *Rechenberg* [204] was used to estimate the model parameters (free coefficients). In brief, the algorithm mimics natural evolution in that properties of species (a set of parameter values) are subject to mutation, recombination and selection during a process where these properties are inherited from parent to children generations. By relying on the principle that only the fittest individuals (best solutions of the optimization problem) survive from generation to generation, evolutionary methods generate increasingly better solutions. Since evolutionary strategies are stochastic optimization methods, the algorithms less likely gets stuck in local optima than gradient-based (deterministic) methods. In a recent comparison of global optimization methods applied to parameter estimation in models of biochemical networks, for instance, only evolutionary strategies turned out to be capable to solve the optimization problem, and to provide rapid convergence [178].

Compared to deterministic optimization methods, however, stochastic algorithms in general require higher computation time because the fitness of many randomly generated individuals has to be assessed. Here, implementation of the algorithm started from a Pascal version of the program [206] that was transferred to MATLAB and parallelized using the MATLAB TCP / IP toolbox [available at: www.mathworks.nl/matlabcentral/fileexchange/]. A single simulation of all experiments in MATLAB requires approximately 150 s (Pentium PC, 2.4 GHz), when integration of the ODEs is carried out by the built-in Adams / Gear method for stiff systems (ODE15s routine). Solution of the model in DIVA turned out to be ≈ 4 times faster. Parameter estimation, however, required ≈ 10.000 simulations, and only by distribution of the task on up to 20 computers, parameter values could be obtained in a reasonable amount of time. Obviously, parallelization of the corresponding routine in DIVA would be the best option for large-scale parameter estimation. Furthermore, different starting guesses for the parameters were used to enhance convergence toward a globally optimal parameter set. The thus obtained reference parameter set is compiled in Tab. C.3 in the appendix. It is important to note that, except for experiment-specific conditions, this parameter set was used for all simulations described in the next section without any further adjustments.

5.4 Assessing model quality

In general, the quality of a mathematical model can, and should be assessed in several ways. A summary of approaches to the evaluation of mathematical models is depicted in Fig. 5.9.

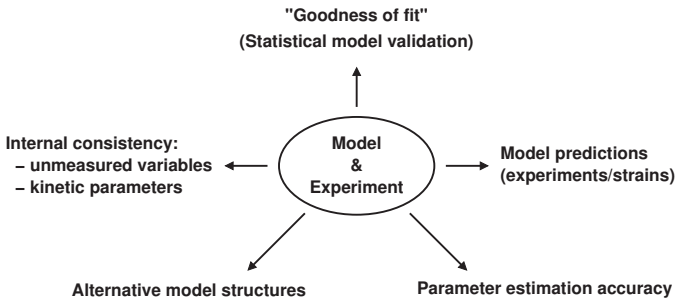

Fig. 5.9: Approaches to evaluation of model quality.

Most of these methods involve the comparison of model behavior to experimental data. This applies to judgments on the ”goodness of fit”, where the central criterion is in how far the model behavior matches the experimental data that were used in constructing the model. In a statistically rigorous sense, but relying on the same combination of experimental data and parametrized model, tests on the distribution of residuals are commonly used for model validation in control engineering [161]. Obviously, additional, independent evaluations of the model such as the prediction of the system's behavior under different (experimental) conditions are required. In practice, however, many studies constrain themselves on the first evaluation method. For a model of cell cycle regulation in yeast that was adapted to describe a large variety of mutants [32], for instance, only an *a posteriori* experimental analysis of model predictions revealed certain aspects of the model that needed to be improved [44].

Further tests include the analysis of the model's consistency in terms of the detailed behavior, but also with respect to the plausibility of the estimated values of kinetic parameters. In both cases, a comparison to independent (qualitative) experimental observations may support or question the suitability of the model. Parameter estimation accuracies as described in section 5.5.1, finally, can be employed to analyze the robustness and identifiability of a specific system. The application of these methods (in a slightly different ordering) for validation of the mitotic control module will be the subject of the following sections.

5.4.1 Descriptive qualities and consistency

The first step in assessing the model quality, its descriptive and predictive character, is to determine in how far the simulations fit the experimental data used for estimating the model parameters. Here, the focus will be on a discussion of the ”goodness of fit” in qualitative terms because residual analysis for model validation did not reveal significant deviations from normal distribution and lack of correlation of the residuals (data not shown). For the wild type yeast with undisturbed cell cycle progression after release from a block in the G1 phase, all the quantitative experimental data employed, and corresponding simulation results are shown in Fig. 5.10.

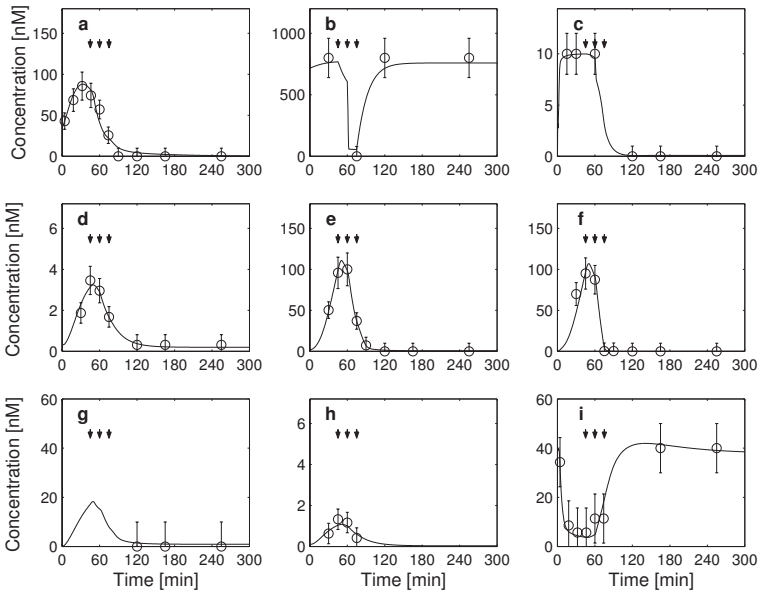

Fig. 5.10: Experiment and simulation for unperturbed cell cycle progression. Combined experimental data (symbols, see Tab. C.2 in the appendix) and simulation results (lines) for selected variables in wild type after release from α-factor arrest. Time $t = 0$ corresponds to S phase. At the time points indicated by the arrows, the spindle assembly checkpoint is inactivated with concomitant activation of the FEAR network (60 min), and MEN activity is switched on (75 min) or off (90 min), respectively. The panels show time courses for all concentrations, for which experimental data were available, namely **a,** Clb5 protein, **b,** Cdc14 / Net1 complex, **c,** phosphorylated Hct1, **d,** *CLB2* mRNA, **e,** Clb2 protein, **f,** active Clb2-CDK, **g,** Cdc20 protein, **h,** *SWI5* mRNA, and **i,** Sic1 protein.

The mitotic control model was designed such as to describe cell cycle control starting from the induction of mitotic cyclin. Initial values for all trajectories were, thus, set according to those observed in S phase, where earlier cyclins such as Clb5 are already present (Fig. 5.10a). In late S phase and early mitosis ($t \leq 60$ min), simulations and experimental data describe rapid degradation of the inhibitor Sic1 (Fig. 5.10i), inactivation of the APC^{Hct1} (Fig. 5.10c), and the induction of the co-regulated genes *CLB2* (Fig. 5.10d) and *SWI5* (Fig. 5.10h). Concomitantly, Clb2 protein concentration (Fig. 5.10e) and associated kinase activity (Fig. 5.10f) rise, which leads to entry into mitosis. Initiation of chromosome segregation ($t = 60$ min) abolishes the block of Cdc20 activity by the spindle assembly checkpoint, which was modeled as a discrete event, and an initial release of Cdc14 phosphatase from the nucleolus induced by the FEAR

network (Fig. 5.10b). The degradation of Clb5 by APC^{Cdc20} (Fig. 5.10a,g), and an onset of the repression of *CLB2* cluster genes and their protein products are consequences of these events.

Only during the time, at which the mitotic exit network is active after successful chromosome distribution (75 min $\leq t \leq$ 90 min, based on the activity profile of the MEN kinase Dbf2 [75]), however, the most important processes for exit of mitosis are induced. These include full release of Cdc14, activation of the APC^{Hct1} proteolytic pathway, *CLB2* mRNA and protein degradation, and accumulation of Sic1 protein. Consequently, the cell will be reset into a G1 state with low mitotic kinase activity and high levels of Sic1 that is stable in the further absence of G1 cell cycle control mechanisms (or, *in vivo*, in the presence of α factor leading to a block in the early G1 phase).

From comparison of experimental data and simulation results shown in Fig. 5.10, it is evident that the mitotic control module is able to capture most aspects of the cell's behavior while progressing through mitosis both qualitatively and quantitatively. Minor discrepancies exist in the dynamics of Clb5 protein concentration (panel a), and the time courses of Clb2 protein degradation and the prior onset of inactivation of Clb2-CDK (panels e,f). This may indicate shortcomings of the model, for instance, a too coarse description of processes involving multiple protein modification [182]. It has to be considered, however, that the experimental data employed in parameter estimation originated from different studies. The need to adjust the time courses, as done by normalizing concentrations and time axes for the maximum of Clb2 protein concentration, provides an uncertainty with respect to the experimental data basis.

Similar conclusions can be drawn for the conditions of perturbed cell cycle progression that were employed in the adjustment of the mathematical model to the cells' observable behavior (Fig. 5.11). There, four different experiments were considered. The first case is a strain defective in MEN activation that arrests in late mitosis (telophase) with approximately half of the peak Clb2-CDK activity (Fig. 5.11a). In a second experimental study, cells were arrested in mitosis by adding nocodazole, and then *GAL1-10 SIC1* gene expression was induced leading to a rapid exit from mitosis (Fig. 5.11b). A *HCT1* deletion mutant (hct1Δ) behaves like the wild type with respect to Clb2-CDK inactivation, but Clb2 protein can not be completely degraded (Fig. 5.11c). Finally, in this strain background, overproduction of Cdc6 protein in nocodazole-arrested yeast using the same promoter as for *SIC1* above induces a slower decline of mitotic kinase activity, while Clb2 protein levels remain unchanged (Fig. 5.11d).

In all four instances, the model could be fitted to the experimental data, with the notable exception of the dynamics of Clb2 protein and associated kinase activity in Sic1-overproducing cells. The deviation accounts for approximately 40% of the total identification functional that characterizes the match between simulation and experimental data. Presumably, this insufficiency is linked to the simplifying assumptions employed with respect to multi-site post-translational protein modifications already discussed above. In this context, it is important to note that, compared to the size of the model and the number of model parameters estimated, only comparably few experimental data were available. For the wild type, for instance, only

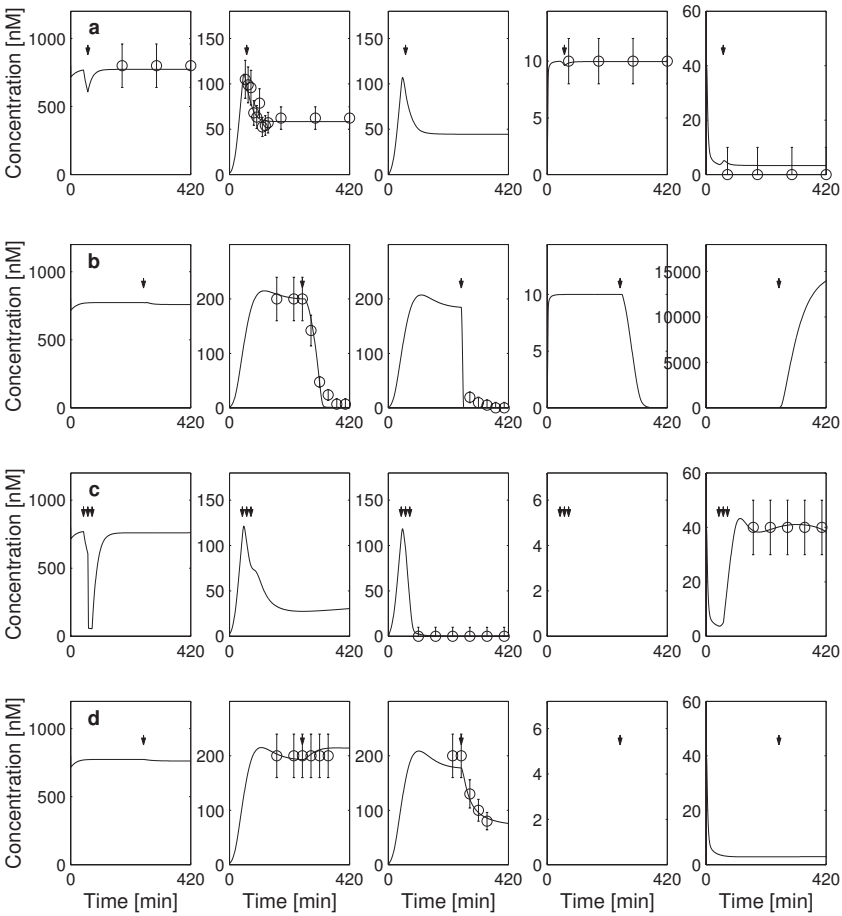

Fig. 5.11: Experiment and simulation for the disturbed system. The four mutants and / or otherwise perturbed conditions used in parameter estimation are shown in the following order (rows of panels): **a,** MEN-defective mutant, **b,** *GAL-SIC1* overexpression in nocodazole-arrested wild type cells, **c,** $hct1\Delta$ strain, and **d,** *GAL-CDC6* overexpression in nocodazole arrest of a $hct1\Delta$ mutant. All experiments start with release from α factor arrest, as for the wild type in Fig. 5.10. In cells with non-functional MEN, release of the spindle checkpoint is the only discrete event considered. In nocodazole-arrested cells, the arrow denotes the time of gene induction by addition of galactose to the culture. In each row, from left to right, the following system variables are shown: (1) Cdc14 / Net1 complex concentration, (2) total Clb2 protein concentration, (3) Clb2-CDK activity, (4) concentration of phosphorylated Hct1, and (5) total Sic1 protein, respectively. The sources of experimental data (circles) are specified in Tab. C.2.

7 out of the 16 time courses for total protein or mRNA concentrations of cell cycle regulators mirrored by the model were used in parameter estimation. This ratio was even more severe for the cases with perturbed cell cycle progression.

The overall level of coincidence between simulation results and *in vivo* behavior, thus, indicates that the structure of the mitotic control module captures the essential control mechanisms. Otherwise, as observed in the mathematical modeling of other complex regulatory networks, it would be highly unlikely that even a complex model with many degrees of freedom could display the (qualitative) behavior correctly [171, 272]. For the mitotic control module, qualitatively correct simulation results that were unsubstantiated by experimental data in parameter estimation, such as remaining Clb2 protein in the $hct1\Delta$ mutant [231], or the exit from mitosis induced by *GAL-CDC6* expression without the help of Sic1 protein accumulation [25], support this assertion. Furthermore, the difficulties with the exact dynamics of Clb2-CDK inactivation point to the importance of model structure as compared to the number of model parameters.

As noted above, experimental data suitable for model adjustment was only available for a very limited number of (aggregate) system states. In section 5.5.2, the model will be analyzed with respect to the quality of the thus identified parameters. Here, a first check of the model's consistency will be an analysis, if the model as a whole, including the unconstrained states, would show physiologically plausible behavior. Although the mitotic control module is characterized by strong internal connectivity through multiple feedback and feed-forward loops, it is conceivable that parts of the model act largely autonomously, and only certain aspects of the (potentially disintegrated) network behavior reflect the progression through mitosis as observable *in vivo*.

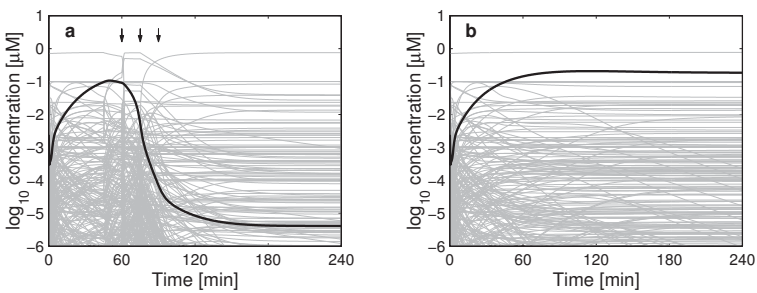

Fig. 5.12: Complete systems dynamics. Time courses of all state variables (gray lines) starting in S phase for the wild type in **a,** an undisturbed cell cycle, and **b,** with added nocodazole. In order to facilitate comparison with preceeding figures, the trajectory of mitotic CDK activity (bold line) and the timing of external signals (arrows) was included.

The complete systems dynamics is shown for two cases in Fig. 5.12, namely the wild type cell culture with or without addition of nocodazole to the medium. In reality, both cases are

characterized by the evolution towards stable steady states of low (if the G1 control is blocked) and high mitotic CDK activity, respectively. This is largely reflected by the model behavior, because most trajectories rapidly tend to such a steady state. In nocodazole-arrested cells, the decline of certain concentrations despite already constant mitotic CDK activity can be attributed to the gradual degradation of products of genes such as *CLB5* that are only induced in S phase. In the unperturbed cell cycle, vertical gray lines originating from the intersection of trajectories point to a highly concerted dynamics, which is in agreement with discrete transitions between cell cycle phases caused by the highly non-linear dynamics. Overall, thus, this survey is suggestive of a high degree of internal consistency of the mitotic control module, and additionally helps in the identification of targets for model improvement.

Furthermore, investigation of the estimated model parameters allows one to assess the plausibility of the mathematical model. Formal parameter sensitivity analysis will be at the core of section 5.5. Here, the estimated parameter values in relation to experimentally obtained qualitative and quantitative data will be of primary interest. Given that all model parameters – besides those describing structural characteristics such as mRNA lengths – were subject to the estimation, one criterion for model evaluation is, in how far estimated parameter values match with experimentally determined kinetic constants. Additionally, relative values of kinetic constants allow for qualitative comparisons, for instance, regarding the substrate preferences or relative contributions of pathways controlling gene expression. For this purpose, in complex models it is sensible to aggregate parameters such as dissociation constants K_D. Fig. 5.13 provides an overview of the estimated parameters grouped according to the type of regulatory processes they are associated with.

Parameters involved in transcriptional control are summarized in Fig 5.13a in terms of the affinities between RNA polymerase (POL), transcription factors, and promoters of cell-cycle regulated genes, respectively. Although, in the model, for these genes constitutive expression was provided as one possibility, the low affinities in the cases of *SWI5* and *CLB2* indicated a predominant role of regulated transcription. Regarding the action of the transcriptional activator MBF, estimated affinities for the cyclin genes with well-described MCB binding sites are in the order of magnitude of the experimentally determined value for the consensus cognate site [252]. A similar conclusion is reached for the forkhead transcription factors (FKH12) with respect to the control of *SWI5* expression. Additionally, relative affinities of these transcriptional regulators for promoter sequences in mitotic genes are *SWI5* > *CLB2* > *CDC20* [111]. For the first two genes, the estimated parameters reflect this ordering. Differences in the mechanism of control for the *CDC20* gene, however, are known that lead to a lower dependency on the Ndd1 transcription factor [162], and involve mitotic CDK and the proteasome as negative and positive regulators, respectively [181]. In future versions of the model, these control mechanisms should be incorporated. The interactions between Fkh1/2 and Ndd1, however, correspond to the *in vivo* situation, where phosphorylation of the latter protein is required for effective gene induction [207].

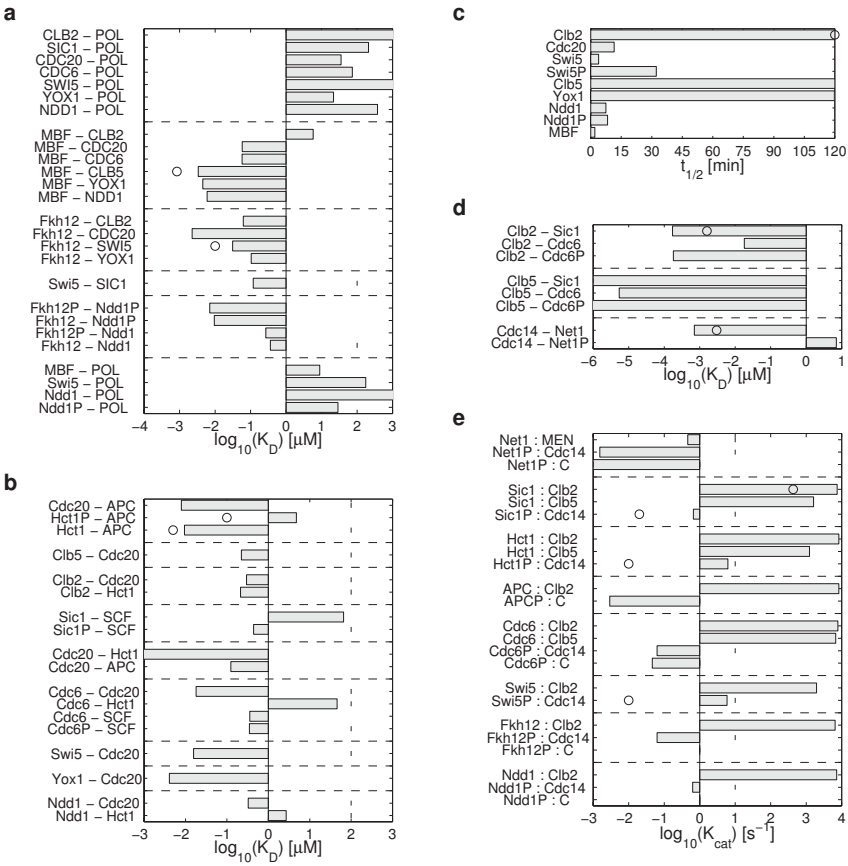

Fig. 5.13: Summary of estimated parameters. Aggregate parameter values for processes of **a,** transcriptional control, **b,** controlled proteolysis, **c,** constitutive protein degradation, **d,** competitive inhibition of CDK activity, and **e,** protein phosphorylation / dephosphorylation. The types of parameters shown are binding affinities ($K_D = k_{diss.}/k_{ass.}$), protein half lives ($t_{1/2}$), and catalytic constants for enzymatic reactions ($K_{cat.}$), respectively. In the case of enzymatic reactions, the first component denotes the substrate, the name after the colon indicates the enzyme ('C' for constitutive processes). Small vertical bars show boundaries on parameter space during estimation. Experimentally determined parameter values (circles) were included for: affinities of MBF for a generic cognate site [252], of Fkh1/2 for the *SWI5* promoter [111], and of Hct1 / Hct1P for the APC [122]; constitutive Clb2 turnover [270]; constants for Clb2–Sic1 [172] and Cdc14–Net1 complex formation [268]; phosphorylation rate of Sic1 as a prototype CDK substrate [175]; dephosphorylation rates of the Cdc14 substrates Sic1P, Swi5P [268], and Hct1P [122].

Controlled proteolysis is another regulatory mechanism of paramount importance to mitotic control. There (Fig 5.13b), analysis of parameter values first reveals the experimentally observed nature of Cdc20 and unphosphorylated Hct1 as being specific substrate-targeting factors for the APC [230]. Whereas the estimate for this affinity agrees well with experimental data for unmodified Hct1, this is not the case for its phosphorylated counter-part. The difference in SCF binding affinities of phosphorylated vs. unphosphorylated Sic1 by at least one order of magnitude corresponds to observations made in an *in vitro* reconstituted SCF system [242], and when comparing the *in vitro* ubiquitination of wild type and phosphorylation-site deficient Sic1 protein [265]. Parameter values for degradation of Cdc20 protein suggest a role of APC^{Hct1}, but not of APC^{Cdc20} in this process, which is the situation in*Xenopus* [196]. Parameters indicate that APC^{Cdc20} might be of particular importance for the complicated control of Cdc6 abundance. For the other proteins, these data indicate the improbability (for Ndd1), or possibility (for Swi5, Yox1) of regulated, ubiquitin-dependent proteolysis. Independent simulations carried out with each single of the mechanisms switched off could be used to confirm these predictions.

As an alternative to ubiquitin-dependent proteolysis, proteins may be constitutively degraded. Protein half-lives shown in Fig 5.13c denote the status of these processes in the model. Again, high stability of the cyclins, and the characterization of Cdc20 as a short-lived protein in all phases of the cell cycle match experimental observations [201]. Swi5 protein half-lives comply with the – mechanistically not yet understood – fact of rapid destruction of Swi5 upon entry of the unphosphorylated form of the protein into the nucleus in late mitosis [179]. Interestingly, Ndd1 shows a a relatively low half-life irrespective of its phosphorylation state, indicating that transcriptional control may be mainly responsible for the regulation of the protein's abundance.

Parameters related to the competitive inhibition of CDK and Cdc14 phosphatase activity, respectively, are compiled in Fig 5.13d. Estimated parameters show suitable agreement with the available data from *in vitro* assays. When comparing the inhibitory potentials of Sic1 and Cdc6, only one out of two aspects of the mitotic control module concur with experimental observations, namely a higher affinity of Sic1 than Cdc6 towards Clb5-CDK as judged by the ability of Sic1 to block the binding of Cdc6, and nearly identical binding affinities of both inhibitors for Clb2-CDK [65]. In the model, apparently, the phosphorylation status of Cdc6 matters for these interactions. This hypothesis has been discussed in, for instance, [25]. Discrepancies could result from the model's underlying assumptions, because the (barely characterized) influence of Clb5 on the G2/M inhibitory role of Cdc6 [13] was not explicitly included.

Finally, Fig 5.13e gives an overview of phosphorylation and dephosphorylation processes in terms of the maximal reaction rates. There, it is evident that the estimated parameters for Cdc14-dependent dephosphorylation as wells for Clb2-dependent phosphorylation deviate by several orders of magnitude from those measured *in vitro*. It is unlikely that the disagreement was caused by highly inaccurate protein concentrations in the model, because the relative concentrations of kinases and phosphatases were based on experimental data. Presumably, the fact that the measured activities for both classes of proteins show considerable variation with

substrates and experimental conditions (see e.g. [18, 175], or [122]) plays an important role. Additionally, analysis of parameter estimation accuracies pointed to a linear dependency of the parameters, which implies that absolute parameter values can not be estimated together. Regarding the biological implications of these parameter values, it is important to note that the known Cdc14 substrates (Sic1, Hct1 and Swi5) were correctly assigned high reaction rates. Net1 dephosphorylation by Cdc14 was only detected *in vitro* [258], and its physiological role remains unclear. Except for the Ndd1 transcription factor, Cdc14-mediated dephosphorylation does not seem to be crucial for any of the other potential substrates, for which the (hypothetical) reactions form part of the model.

Overall, the aspects of model validation discussed in this section showed a considerable ability of the mitotic control module to describe the experiments used in parameter estimation, internal consistency of the model behavior, as well as agreement of the estimated parameters with independent experimental observations. Analysis results, however, point to shortcomings of the model in minor aspects. They uncover facets of the biological system to be captured in more detail, and targets for model reduction. As discussed above, the model parameters rarely corresponded exactly to the kinetic constants measured. However, given the range of parameter values opened up in the estimation step, the match within approximately one order of magnitude seems acceptable. A judgment on whether the deviations in absolute terms are due to the robustness of the network, or result from inaccurate absolute parameter estimates has to await the quantitative parameter sensitivity analysis to be described in section 5.5.

5.4.2 Independent model predictions

Whereas so far the interpretation of model quality was based on the set of experiments used for parameter estimation, this section will discuss the decisive test-cases of true model predictions. Focusing on simulations that correspond to experiments with known outcome regarding the control system's dynamics allowed for a critical evaluation of the model's predictive power in qualitative, and – provided that experimental data was available – in quantitative terms. It is important to note that all simulations employed the set of parameters that resulted from the parameter estimation based on a small set of experiments (section 5.3.3). Only kinetic parameters or initial conditions necessary for mirroring specific strains or conditions were modified, for instance, by setting the promoter concentration of a gene to zero in order to reflect the properties of a deletion mutant.

One series of model predictions concerns the behavior of *in silico* deletion mutant strains. The protein concentration of the mitotic cyclin Clb2 and its associated kinase activity serve as key indicators for interpreting the results in terms of the physiological effects of the genetic alterations (Fig. 5.14). The behavior of the wild type (Fig. 5.14a) and of the $hct1\Delta$ mutant (Fig. 5.14e), being parts of the original experimental data basis for model development, were included for easier comparison.

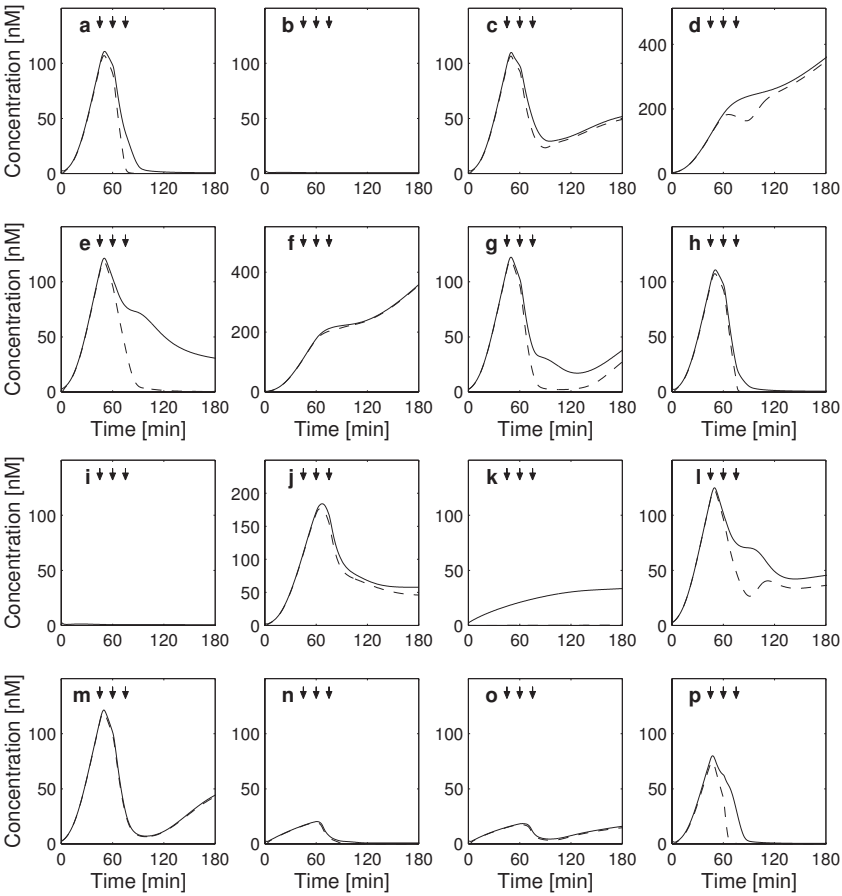

Fig. 5.14: Model predictions: Mutant phenotypes. *In silico* mutant strains were released from α-factor arrest. Discrete events at identical time points as for the wild type are denoted by the arrows as in Fig. 5.10. Lines indicate total Clb2 protein concentration (solid) and Clb2-CDK activity (dashed). Each panel refers to either **a,** wild type, or to a different mutant: **b,** $clb5\Delta$ **c,** $CLB5\Delta db$, **d,** $CLB2\Delta db$, **e,** $hct1\Delta$, **f,** $cdc20\Delta$, **g,** $sic1\Delta$, **h,** $\Delta 47CDC6$, **i,** $net1\Delta$, **j,** non-phosphorylatable APC (*APC-A*), **k,** $clb5\Delta\ hct1\Delta$, **l,** $sic1\Delta\ hct1\Delta$, **m,** $sic1\Delta\ cdc6\Delta$, **n,** $fkh1\Delta\ fkh2\Delta$, **o,** $ndd1\Delta$, and **p,** $yox1\Delta\ yhp1\Delta$, respectively. With the exceptions of the $\Delta 47CDC6$ strain (inactivation of the reactions describing Cdc6 phosphorylation and interactions with Clb2), and the *APC-A* mutant (block of its phosphorylation by Clb2-CDK), simulations were performed by setting the corresponding initial concentrations of the promoters, mRNAs and proteins to zero.

First, the effects of modifications in cyclin-encoding genes were investigated. From experiment, it is known that deletion of the $CLB5/6$ genes leads to shortening of the G2 / M phases [13], and to less efficient accumulation of Clb2 protein that completely depends on the remaining early cyclins Clb3-6. Presumably, impeded Clb2 accumulation is linked to defects in the inactivation of the APC^{Hct1}-dependent proteolytic system [283]. Keeping in mind that in the mitotic control module all early cyclins are lumped into 'Clb5', simulation results for a $clb5\Delta$ strain (Fig. 5.14b) agree with the experimentally observed inability to induce mitosis. Contrary, *in vivo* the deletion of the proteolytic recognition signal (D box) from endogenous *CLB5* has little effect on the phenotype. In particular, its ability to exit from mitosis indicates that Clb5 degradation is not an essential task of APC^{Cdc20} [280]. Similar to the experimental results, simulation of a $CLB5\Delta db$ mutant shows wild type behavior in mitosis, and inactivation of the mitotic cyclin-dependent kinase at the end of mitosis (Fig. 5.14c). Later re-accumulation of Clb2 protein in the predictions may be due to the lack of G1-specific control mechanisms in the model. A removal of the destruction boxes in the $CLB2$ gene ($CLB2\Delta db$) *in vivo* results in a block of mitotic exit with higher Clb2 protein levels than in the $hct1\Delta sic1\Delta$ double mutant [280]. For the *in silico* mutant, a corresponding behavior can be observed (Fig. 5.14d; see also panel l for the double mutant mentioned above).

Further sets of analyses of single-gene deletion mutants concerned components of the proteolytic machinery as well as competitive inhibitors. As discussed in previous sections, the inactivation of the *HCT1* gene elicits only a minor phenotype, namely a moderate delay of mitotic exit, and a continuous presence of Clb2 protein throughout the cell cycle [231,280] (Fig. 5.14e). In contrast, deletion of the gene for its counterpart in the control of APC-dependent proteolysis, *CDC20*, is lethal; strains harboring conditional alleles of *CDC20* arrest in early mitosis [270]. The simulations reflect these observations as characterized by the continuous accumulation of mitotic CDK activity over the time span considered (Fig. 5.14f), which indicates that the model correctly captures the slight differences in the two parallel pathways for proteolytic control of Clb2. Nearly wild-type control of mitosis was obtained for two strains with defects in Clb2-CDK inhibitors, encoded by the *SIC1* (Fig. 5.14g) and *CDC6* (Fig. 5.14h) genes. In the latter case, the effect of an N-terminally truncated protein that lacks the CDK interaction domain ($\Delta 47cdc6$). Both simulations provide independent confirmations of the model [25]. Deletion of the Cdc14 inhibitor Net1 ($net1\Delta$) leads to a defect in the accumulation of Clb2 protein, and strongly affects Clb2-CDK activity owing to active Hct1 and Sic1 [269], which corresponds to the (qualitative) model-based prediction (Fig. 5.14i).

Next, a mutant strain was investigated, in which the APC can not be phosphorylated ($APC-A$). Since Cdc20 preferably binds to phosphorylated APC, this set of mutations causes a considerable delay ($>$ 40 minutes) in the exit from mitosis *in vivo* [214]. Simulation results contained in Fig. 5.14j show this prolongation of the phase in which Clb2-CDK is active, but a complete inactivation of the kinase that would correspond to exit from mitosis is not predicted. The fact that in the model, APC binding of Cdc20 entirely depends on the phosphorylation,

while under the experimental conditions, residual binding to the modified APC can be observed might account for this discrepancy. It is not clear, however, whether the mitotic control module needs to be modified, or if phosphorylation sites remained in the experimental strain [214].

Another set of model predictions aimed at describing the behavior of double mutants. In contrast to the lack of Clb2 accumulation in the $clb5\Delta$ strain, simulations showed functional mitotic entry upon additional deletion of the *HCT1* gene (Fig. 5.14k). The exit from mitosis is nevertheless impaired in the double mutant. The results are supported by experimental observations which describe the cells as being able to carry out mitosis but having a reduced viability [283]. The primary role of Clb5 in the initiation of mitosis, thus, seems to be the inactivation of the proteolytic system for Clb2 [280]. Such predictions are not obvious since theoretically the low Clb2-CDK activity present in S phase could drive Clb2 protein accumulation via the positive auto-regulation of *CLB2* transcription without the initial help of S phase cyclin-dependent kinase.

An *in silico* $hct1\Delta sic1\Delta$ mutant showed a behavior similar to cells with defective mitotic exit network, namely relatively high levels of Clb2 protein and associated kinase activity after initial degradation of the protein (Fig. 5.14l). This observation is consistent with the experimental finding of a biphasic degradation of Clb2 protein owing to APC^{Cdc20}, and subsequent APC^{Hct1} action [282]. Phenotypically, synthetic lethality of the two gene deletions was detected [231, 270]. Exit from mitosis as judged by disassembly of the mitotic spindle under specific experimental conditions (Sic1-depleted cells), however, occurred albeit Clb2 protein concentration, and the associated kinase activity remained constant [280]. At large, thus model predictions and experimental results coincide, but closer investigation of this particular double mutant seems necessary.

Contradictory experimental evidence also exists in the literature concerning the combination of sic1$\Delta$with a deletion in the N-terminal domain of Cdc6 that is responsible for interactions with Clb2-CDK. Whereas in [25], the double mutant was found to be inviable under all conditions tested, the construction of viable strains in different backgrounds that had no observable defect in mitosis is reported as well [8]. This difference may result from side-effects of the method chosen for strain construction in the first study [8]. Model predictions shown in Fig. 5.14m support this interpretation. Moreover, when one compares the simulation results for wild type, the $sic1\Delta$ mutant, and the double mutant, it becomes obvious that Cdc6, but not Sic1 is responsible for the competitive inhibition of Clb2-CDK activity at the end of mitosis. Independent biochemical analyses of the system reached the same conclusion [8].

To round off the evaluation of model predictions for cells released from α-factor arrest, strains defective for transcriptional regulators were analyzed. It is noteworthy that for this class of proteins neither experimental data, nor perturbed conditions were included in the set of experiments used in parameter estimation. Inactivation of the forkhead transcription factor in living cells ($fkh1/2\Delta$) leads to cessation of the oscillations in $CLB2$ and $SWI5$ mRNA [295] and to increased basal levels of transcripts when compared to the wild type in the G1 phase of the

cell cycle [145]. Model predictions agree with these observations as judged by the concentration of Clb2 protein (Fig. 5.14n). The essential function of Ndd1 for transcriptional activation of the *CLB2* gene cluster [162], however, is not adequately captured by the model (Fig. 5.14o). Future refinements of the mitotic control module should therefore consider, for instance, the qualitative behavior of the $ndd1\Delta$ strain in the course of model development. Finally, *in vivo*, deletion of the transcriptional repressors *YOX1* and *YHP1* that are responsible for the control of *CDC20* and *CDC6* gene expression has no effect on cell cycle progression in mitosis [198]. A similar qualitative behavior is predicted by the model (Fig. 5.14o), although the simulation results clearly indicate an influence of the released transcriptional repression of *CDC6* on the dynamics of Clb2-CDK activity.

Tab. 5.3: Mitosis characteristics of *in silico* strains. Cases of monotonic increase of Clb2-CDK activity are denoted by '>', giving the values at the end of a simulation. Timing of mitotic exit (relative to wild type) was defined as the time point when decreasing Clb2-CDK activity reached a threshold of 25% of the peak activity in wild type.

Strain	max. Clb2-CDK activity [nM]	rel. timing of mitotic exit [min]
wild type	107	0
$clb5\Delta$	2	–
$CLB5\Delta db$	107	+14
$CLB2\Delta db$	> 507	–
$hct1\Delta$	119	+8
$cdc20\Delta$	> 549	–
$sic1\Delta$	120	+2
$\Delta 47CDC6$	107	+1
$net1\Delta$	2	–
APC-A	177	–
$clb5\Delta\ hct1\Delta$	31	–
$sic1\Delta\ hct1\Delta$	123	–
$sic1\Delta\ cdc6\Delta$	119	+5
$fkh1\Delta\ fkh2\Delta$	> 20	–
$ndd1\Delta$	> 18	–
$yox1\Delta\ yhp1\Delta$	75	-9

More quantitative characteristics of the *in silico* strains in terms of the peak CDK activity and the timing of the exit from mitosis are compiled in Tab. 5.3. Comparison of the maximal activities of mitotic CDK reveals that the mutants that turned out to have no phenotype in the experiment, also showed little variation in this characteristic in the simulations. While underlining the robustness of the control system, these data indicate that a more exact quantification of the kinase activity alone probably would not contribute much to a higher accuracy of model parameters. It, however, seems sensible to closer investigate this parameter in the other mu-

tants, because they show a considerable deviation from the wild type in this respect. The model is in agreement with experimental observations in that for the viable mutants, with the exception of the *APC-A* strain discussed above, only a limited variation in the timing of mitotic exit is observed. The order of magnitude of potential delays in the exit from mitosis, however, is correctly predicted by the model, although the experimental data employed in model adaptation do not provide clues on this quantitative feature. *In vivo*, for instance the $\Delta 47cdc6$ strain behaved identical to the wild type [25], whereas the cells lacking *SIC1* and *HCT1* showed slower division by up to 10 min [256], and by 10–20 min [231], respectively.

An approach that is often employed in experimental studies addressing the properties of regulators that are involved in the control of mitosis is to arrest the cells in anaphase with the help of nocodazole, and to overexpress genes of interest in the arrested cells. Experiments of this type were already used for model development, for instance, regarding the induction of *GAL1-10 SIC1* in wild type (see Fig. 5.11). To further assess the model's prediction qualities, similar *in silico* experiments were performed for cases of gene induction in wild type cells with known outcome, which could also partially be corroborated by quantitative time courses of mitotic cyclin concentration and associated kinase activity (Fig. 5.15).

Simulation results for the wild type show a steady state of high Clb2 protein concentration and mitotic CDK activity in nocodazole-treated yeast cells. This situation corresponds to an arrest owing to a blocked spindle assembly checkpoint (Fig. 5.15a). Independent model predictions were obtained for the induction of three positive regulators of mitotic exit, namely *GAL1-10 CDC14*, *GAL1-10 HCT1*, and *GAL1-10 CDC20*, respectively (Fig. 5.15b–d). As observed *in vivo*, overexpression of all three genes leads to exit of mitosis as indicated by the degradation of Clb2 protein and inactivation of the associated kinase. The quantitative dynamics of these processes show a moderate agreement between simulation results and experimental data. It is important to note that (additional) parameters for mRNA degradation and for constitutive proteolysis were set to standard values without further parameter estimation. Moreover, identical induction characteristics were assumed for all constructs based upon the *GAL1-10* promoter. Qualitatively, however, model predictions agree with the experiments in that both show a faster Clb2-CDK inactivation for *GAL1-10 CDC20* overexpression than for *GAL1-10 HCT1* (and *GAL1-10 SIC1*, see Fig. 5.15e) induction. The direct impact of Cdc20 on Clb2 proteolysis, whereas phosphorylation by Clb2-CDK functions as a counter-acting process in the case of Hct1-mediated protein degradation, may explain the distinct dynamics.

As discussed above, the importance of Cdc6 as a competitive inhibitor of mitotic CDKs currently is subject of controversies. *CDC6* overexpression in Hct1-deficient, nocodazole-treated yeast cells allows for exit from mitosis (see Fig. 5.11). This was interpreted to reveal an impact of Cdc6 on mitotic progression [25]. An experimental study that received little attention so far, however, showed that in the wild type genetic background, nocodazole-treated cells with *GAL1-10 CDC6* remain in the arrest after 3 hours of induction [64], which points to only a minor role of Cdc6 in 'normal' control of mitosis. Corresponding simulations favor the latter alternative, because although induction of *CDC6* leads to a reduction of the level of active mitotic kinase,

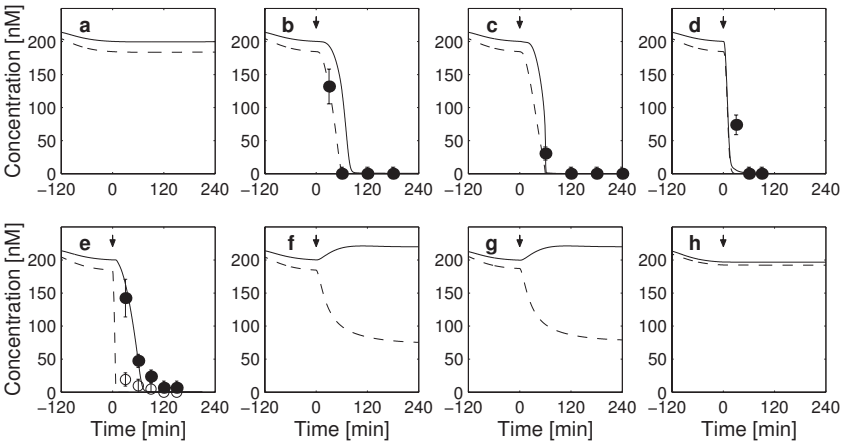

Fig. 5.15: Model predictions: Gene induction in nocodazole-arrested cells. Gene over-expression using the $GAL1-10$ promoter was simulated after a prolonged cell cycle arrest induced by nocodazole. Arrows indicate the time point of gene induction. Simulation results for total Clb2 protein concentration (solid lines) and Clb2-CDK activity (dashed lines) are shown. Experimental data from the sources specified below was included for Clb2 protein (solid circles) and mitotic CDK activity (open circles), respectively. Panels refer to **a,** wild type, and to the over-expression of different genes involved in exit from mitosis, namely **b,** *CDC14* [268][Fig. 7C, cdc15-1 strain, 3 copies of GAL1-10 CDC14], **c,** *HCT1* [231][Fig. 7C], **d,** *CDC20* [270][Fig. 2C], **e,** *SIC1* [6][Fig. 2, 5 copies of GAL1-10 SIC1], **f,** *CDC6*, **g,** *CDC6* in a $sic1\Delta$ background, and **h,** *CDC6* carrying a N-terminal deletion ($\Delta 47CDC6$)). For comparison of model predictions to experimental data, quantification by digital image analysis of western blots was employed in selected cases (panels b-d).

a steady state kinase activity is approached similar to that observed in MEN-deficient mutants, that is, of cells that prove unable to exit from mitosis (Fig. 5.15f). Moreover, *in silico* overexpression of *GAL1-10 CDC6* in nocodazole-treated yeast that lacks the *SIC1* gene shows a similar behavior. A possible indirect effect of Cdc6 on mitosis, namely by competition of this regulator with Sic1 for the SCF-dependent proteolytic pathway is discussed in the literature [65]. The model, however, provides evidence for a potential role of Cdc6 in Clb2-CDK inhibition that is independent of a 'primary' inhibition through Sic1 (Fig. 5.15g). Overexpression of a *CDC6* mutant without the N-terminal domain responsible for the interaction with Clb2 that is ineffective in suppressing mitotic CDK activity (Fig. 5.15h) further supports this conclusion.

Another experimental approach to the analysis of mitotic regulation in yeast consists in arresting the cells with the help of the spindle poison nocodazole, and after resuspension of the cells in nocodazole-free medium, to follow their recovery – or their inability to subsequently

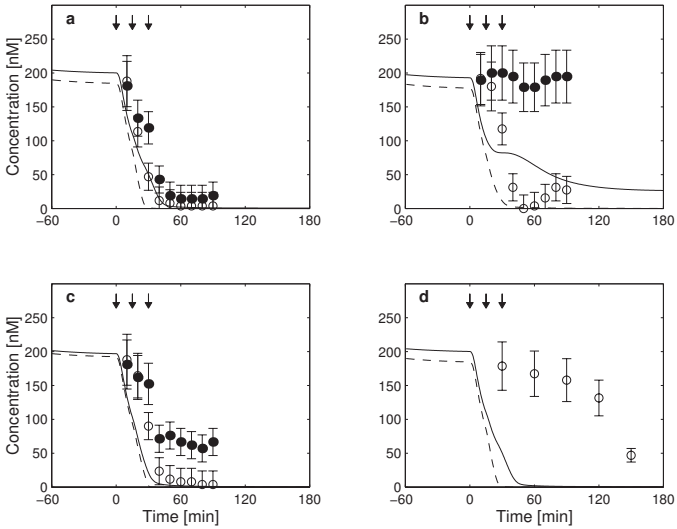

Fig. 5.16: Model predictions: Release from nocodazole arrest. In these simulations, cells were first arrested by nocodazole, and at $t = 0$, withdrawal of the spindle poison was mimicked. Here, the same symbols are used as in the preceding Fig. 5.15. The following strains were included in this analysis: **a,** wild type [26] [supplementary Fig. 2], **b,** $hct1\Delta$ [26] [supplementary Fig. 2], **c,** $\Delta 47cdc6$ [26] [supplementary Fig. 2], and **d,** *CDC28-VF* that has only $\approx 50\%$ of wild type Cdc28 kinase activity [213][Fig. 1].

complete mitosis. Arrest–release experiments had not been covered by the set of experiments employed for model adjustment, and therefore could be expected to pose greater challenges for model predictions. Dynamics of Clb2 protein content and associated kinase activity as available in the literature are compared to simulation results in Fig. 5.16.

For generating the model predictions, it was assumed that the cells immediately resume a normal cell cycle progression in terms of the timing of SAC, FEAR and MEN signals. The exact dynamics in the real system, however, have not yet been characterized. Taking this uncertainty into account, experimental data and simulation results agree reasonably well for the wild type (Fig. 5.16a). The situation is quite different for the $hct1\Delta$ mutant (Fig. 5.16b), for which in the experiment the level of Clb2 protein remained constant after the release [26], whereas in the model, degradation of the protein occurs. In this context, it is unclear, why in the experimental analysis obviously no proteolysis by the intact APC^{Cdc20} pathway was detected as in other, corresponding studies [282, 283].

Similarly, simulation results show only a slight delay in the exit of mitosis of a strain carrying a N-terminally truncated *CDC6* gene when compared to the wild type (Fig. 5.16c). In the

in vivo data, however, a certain amount of Clb2 protein remains in the modified strain, which is not predicted by the model. It therefore seems sensible to include this experimentally observed behavior into a more broadened parameter estimation in order to elucidate whether the model, in principle, could reflect these dynamics. As for the case of the $hct1\Delta$ strain analyzed by the same group, however, it could be worthwhile to critically re-investigate the strain's behavior because unanticipated side-effects of the genetic manipulations can not be excluded (see above for the discussion of the $cdc6\Delta$ strain).

In another arrest–release experiment, finally, a strain totally unrelated to the mutants considered hitherto was analyzed. A specific point mutation in the *CDC28* gene encoding for the cyclin-dependent kinase in yeast reduces the protein's activity by $\approx 50\%$ (*CDC28-VF* mutant). This leads to a strong delay in recovery from the arrest *in vivo* [213], in contrast to the simulation results. Although the qualitative behavior of the cells is captured by the model in all cases, this series of model analyses, thus, points to potential inaccuracies in the model as well as to the need for a closer experimental characterization of the strains. Both fields could warrant further studies.

Altogether, the model for mitotic control was tested in several, independent ways. These tests proved a correspondence between the model characteristics or behavior with experimental observations in many cases, pointed to and could partially clarify inconsistencies in the literature in some cases, but also indicated failures of the mitotic control module in quantitatively describing the cell cycle behavior under other conditions. Summarizing the results of the model validation performed here, it seems justified to conclude that a mathematical model of relatively high descriptive and predictive character was developed. Further, quantitative examination of the model's robustness and identifiability in order to gain insight into these structural characteristics of complex regulatory networks through the example of mitotic control in yeast will be described in the following section.

5.5 Robustness and identifiability

The analysis of robustness and identifiability of the mitotic control module will rely upon the investigation of the system's behavior when random perturbations to the parameters are applied, and on approximations of the errors in the estimated model parameters, respectively. The latter estimates have been termed 'parameter estimation accuracies'. The theoretical basis for their calculation as well as the scope of the method will be briefly described in the following section.

5.5.1 Parameter estimation accuracy

Parameter estimation accuracy refers to an estimate of the errors associated with the model parameters when these have been determined from noisy experimental (or synthetic) data. Low accuracies mean that the corresponding parameters may be varied to a larger extent - and still

describe the reference trajectories - than is possible for parameters with high estimation accuracy (low associated error). Estimation accuracies as measures for identifiability, thus, combine information on parameter sensitivities and on the errors in the data employed in parameter estimation.

The estimation of model parameters basically relies on the comparison of model behavior and the real system's behavior. For this purpose, an identification functional $\Phi(\mathbf{p})$ has to be minimized by variation of parameter values. The formulation of this functional in turn needs the error for each out of N measurements $\mathbf{e}_i$, which is the difference between measurement $\mathbf{x}^M(t_i, \mathbf{u})$ and model $\mathbf{x}(t_i, \mathbf{u}, \mathbf{p})$ at a discrete time point t_i. The differences are furthermore weighted by the inverse of the standard deviation of the measurement $\mathbf{Q}_i$. The entire optimization problem thus reads

$$\Phi(\mathbf{p}) = \sum_{i=1}^{N} \left[\mathbf{e}_i^T \cdot \mathbf{Q}_i \cdot \mathbf{e}_i\right] \quad \rightarrow \quad min$$
$$\text{with} \quad \mathbf{e}_i = \mathbf{e}_i(t_i, \mathbf{u}, \mathbf{p}) = \mathbf{x}(t_i, \mathbf{u}, \mathbf{p}) - \mathbf{x}^M(t_i, \mathbf{u}) \; . \tag{5.5}$$

Parameter estimation is supposed to lead to a set of optimal parameters $\mathbf{p}^*$. Assessing the quality of this parameter set requires knowledge of the state sensitivities, which may be obtained using the variation equation (4.4). The Fisher information matrix $\mathbf{F}(\mathbf{p}^*)$ (FIM) [66] for the given parameter values links model and experiment via the state sensitivities and the inverse of the measurement covariance matrix $\mathbf{C}(\mathbf{t}_i)^{-1}$, respectively, by

$$\mathbf{F}(\mathbf{p}^*) = \sum_{i=1}^{N} \left[\left.\frac{\partial \mathbf{x}}{\partial \mathbf{p}}\right|_{\mathbf{p}^*, t_i}^{T} \mathbf{C}^{-1}(t_i) \left.\frac{\partial \mathbf{x}}{\partial \mathbf{p}}\right|_{\mathbf{p}^*, t_i} \right] . \tag{5.6}$$

Usually for identification purposes, the diagonal elements of the covariance matrix contain the standard deviation of the measurement. They may, however, alternatively stem from the trajectories generated at the nominal parameter values by assuming fixed absolute and relative errors. This latter approach using 'synthetic' data generated from the deterministic models will be followed here for studying the mitotic control module. Alternatively, a stochastic model version could be employed for obtaining more realistic, noisy data. In future studies, it will be intriguing to compare these methods.

Under the condition that the parameter vector $\mathbf{p}^*$ is an unbiased estimator of the true system's parameters $\hat{\mathbf{p}}$, the Cramér-Rao theorem establishes a lower bound for the covariance error matrix according to

$$E\left\{(\mathbf{p}^* - \hat{\mathbf{p}})(\mathbf{p}^* - \hat{\mathbf{p}})^T\right\} \; \geq \; \mathbf{F}(\mathbf{p}^*)^{-1} \tag{5.7}$$

with $E\{\ldots\}$ being the expected value of the difference between the sets of parameters. When the inverse of the FIM (Cramér-Rao matrix) is denoted as

$$\mathbf{S}(\mathbf{p}^*) = \mathbf{F}(\mathbf{p}^*)^{-1} \tag{5.8}$$

and its elements as $s_{i,j}$, it directly follows that the lower bound for the estimation error σ_i of each model parameter i is given by

$$\sigma_i \geq \sqrt{s_{i,i}} \ . \tag{5.9}$$

In other words, the parameter estimation accuracies can readily be obtained from the main diagonal of the inverse of the FIM. It has to be noted that, strictly speaking, this derivation is based on the assumptions of an unbiased estimator as well as of additive and independent Gaussian measurement errors. For practical purposes, however, the relation yields reasonable approximations even if the first condition is violated, and the second condition holds for many real systems [66].

One problem often encountered in applications is that sub–sets of parameters can not be estimated using the given data. Additionally, combinations of parameters may exist that can not be estimated together. In these cases, the FIM becomes (close to) singular. For the treatment of this problem, an iterative 'top–down' classification scheme has been proposed to identify groups of parameters that can be estimated with a given accuracy (Fig. 5.17) [225]. Essentially, it implies a coordinate transformation in parameter space using the eigenvalues and eigenvectors of the FIM, and applying Eqns. 5.7–5.9 to the transformed system. A small eigenvalue indicates that parameter perturbations in the direction of its associated eigenvector will have little effect on model behavior. Consequently, the estimation accuracy in the direction of the eigenvector will be poor. Parameters causing small eigenvalues are iteratively eliminated from the FIM, until all remaining parameters fulfill the criterion of showing at least a given estimation accuracy. This group of parameters may be estimated together; other groups may contain parameters of similar accuracy, which, however, are linearly dependent on parameters in other groups and, hence, can not be estimated in the same run.

A more detailed description of the theoretical foundations of the Fisher information matrix is provided in [66, 225]. It should be kept in mind that eq. 5.9 can only provide a lower bound for, not an exact solution to the problem of estimation accuracy. Furthermore, the results always depend on the experimental (or synthetic) data involved. These restrictions associated with the method will be of particular importance for judgements on the effects of additional experimental data on the identifiability of the system that are to be described in the next section.

5.5.2 Systems analysis

Already the simulation studies of the mitotic control module pointed to a certain robustness of the regulatory network. Deletion of many of the regulatory genes hardly affected the ability of the network to control the initiation of mitosis, and the passage through this phase of the cell cycle. For a systematic analysis of the module's robustness, series of random perturbations were applied to the model parameters as for the two models of the circadian clock in *Drosophila* (section 4.5.3). Here, three key properties of mitotic control were assessed for the wild type as well as for two *in silico* mutant strains: the timing and magnitude of maximal Clb2-CDK activity as

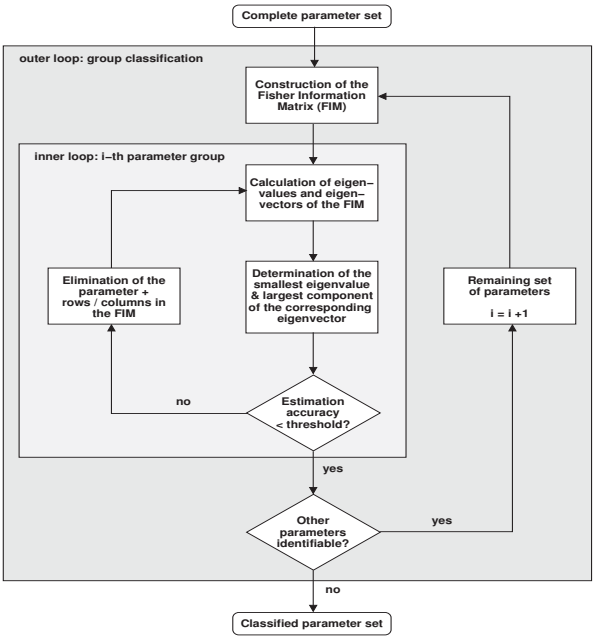

Fig. 5.17: Analysis of parameter estimation accuracies using the Fisher information matrix. The scheme illustrates the top-down classification approach proposed in [225].

indicators for the induction of mitotic processes, and the timing of mitotic exit measured by the decline of this activity below a pre-defined threshold. Again, scalar and vectorial perturbations were applied, respectively, in order to allow for statistical evaluation of the (relative) impact of variations in parameter values on the model behavior (Fig. 5.18; see legend for details of the method).

In all cases, in which only a single model parameter was varied by up to 10–fold, the wild type shows remarkably robust behavior for all three characteristics of mitotic control (Fig. 5.18a–c). In particular, deviations in the time at which mitotic entry and exit occur remain on the order of a few minutes in most simulations. Similar observations are made for changes in the maximal Clb2-CDK activity. In 1.5% of the simulations, however, perturbation of a single model parameter entrained complete failure of the control system, indicating major sources of fragility. The behavior of the $sic1\Delta$ mutant was indistinguishable from wild type, which may provide evidence for a recent proposition that, under otherwise 'normal' conditions, the regulator Sic1 mainly functions in the control of G1, and not of mitosis [8]. Slightly higher sensitivity of the $hct1\Delta$ strain – in particular regarding the exit from mitosis – is consistent with the important, yet dispensable role of that protein in the degradation of Clb2 [231, 280].

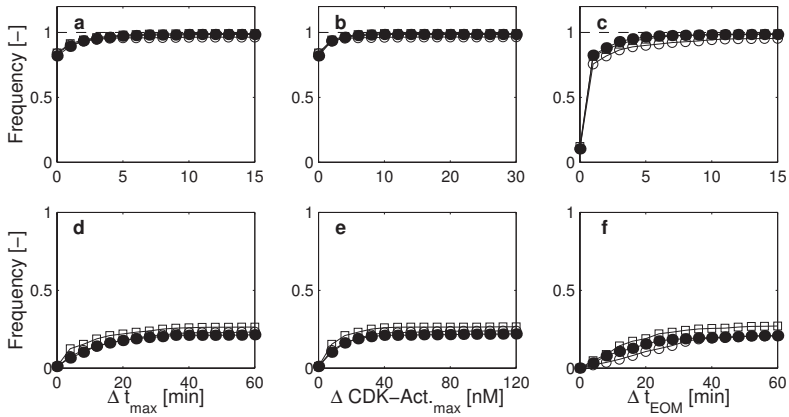

Fig. 5.18: Perturbation analysis of the mitotic control module. Characterization of the model behavior after application of normally distributed random perturbations to the reference parameter sets for wild type and mutants in the range of $0.1p^k \ldots 10p^k$ either to a single, randomly selected parameter (**a–c**), or to each of the parameters (**d–f**). In parallel, the *in silico* wild type (filled circles), the $hct1\Delta$ mutant (open circles), and the $sic1\Delta$ mutant (squares) were analyzed. In all cases, $n = 1,000$ simulations were carried out in order to determine the cumulative frequencies of deviations in the model behavior. **a,d,** Absolute differences in the timing of maximal Clb2-CDK activity of the perturbed system relative to the unperturbed system (Δt_{max}). **b,e,** Deviation of maximal Clb2-CDK activity (ΔCDK-Act.$_{max}$). **c,f,** Effect of the perturbations on the relative timing of mitotic exit (Δt_{EOM}) as defined by the time of crossing a threshold of 25% of the maximal activity in the reference wild type.

Considerably higher absolute perturbations of the system through the application of random variations in all model parameters, as would be expected, result in a high frequency of cases in which the *in silico* cells are unable to control mitotic processes. Interestingly, regarding the characteristics of mitotic control analyzed, no gradual degradation of this ability is observed. Shifts towards highly imprecise control were rarely encountered. In contrast, only a few perturbed systems operate largely similar to the parent strains, whereas in most cases, the system entirely fails. Gene deletions for *SIC1* or *HCT1*, again, do not change this behavior drastically. It is tempting to speculate that *in vivo*, catastrophic breakdown after accumulation of severe damages performs a physiological function (at the population level) by preventing these cells from replicating.

As described in detail in section 5.5.1, the parameter estimation accuracy σ quantitatively captures the sensitivity of the system's behavior towards variances in the (optimal) parameters. It can therefore be used to determine the system's identifiability on the basis of the given data, and provide an indicator for robustness against parameter perturbations. Here, the inverses of

the estimation accuracies σ^{-1} of the mitotic control module were calculated using the same experimental data as in the parameter optimization. In Fig. 5.19, bars indicate an estimation accuracy of $\sigma \leq 100\%$, whereby higher values stand for better estimates. Within the set of

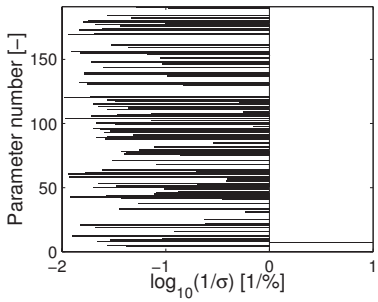

Fig. 5.19: Parameter estimation accuracies for the mitotic control module. Vertical bars show the inverse parameter estimation accuracies of all estimated model parameters, for which an accuracy below the critical value of $\sigma_{crit.} = 100\%$ was obtained via analysis of the Fisher information matrix employing all experimental data sets. The vertical line indicates 1% estimation accuracy.

parameters, the estimation accuracies vary to a large extent, but the variation is not random. Some of the parameters reach an estimation accuracy of ≤ 10 %, that is, they are highly sensitive. These parameters seem to be clustered, as the parameter numbers are ordered according to the genes and proteins included in the network. Most of the highly sensitive parameters are involved in the description of Cdc14 (parameter numbers 1–30) and of Clb2-CDK (31–90), which represent the central phosphatase and kinase activities for the control of mitosis, respectively. High sensitivity, however, is not linked to all of the interactions of these proteins, but only to specific ones, for example the biologically essential inhibition of Cdc14 by Net1. The same observation can be made for the parameters that could not be estimated within the given accuracy range. Regarding the system's robustness, these findings provide evidence for the concept of highly optimized tolerance (HOT). Robustness in biology, according to the theory, does not exclude that specific parts of the system are extremely sensitive and, thus, can lead to overall fragility [28, 29].

For the practical purpose of conducting experiments to identify a regulatory module, the parameter estimation quality gives clues on the information content of the experiments. In Fig. 5.20a, the cumulative distribution of the number of parameters with a given accuracy in terms of quantitatively describing the measurements is shown as a function of this (critical) accuracy. Parameters with an accuracy of $\sigma > 100$ % were not considered, so that this distribution does not reach the value of one for the limit of $\sigma \to \infty$.

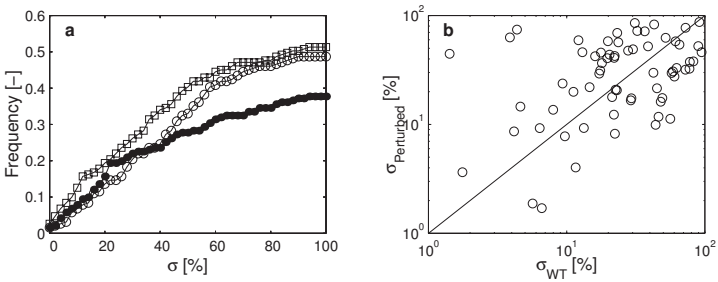

Fig. 5.20: Comparison of estimation accuracies for wild type and set of perturbed conditions. a, Cumulative distribution of parameter estimation accuracies based on the experimental data for wild type alone (filled circles), the set of perturbed conditions such as gene deletion mutants used in parameter estimation (open circles), and for the combined data (squares). **b,** Comparison of estimation accuracies for the parameters that occurred in both the analysis of the wild type (σ_{WT}), and of the set of mutants / externally influenced conditions ($\sigma_{Perturbed}$), respectively. The diagonal indicates perfect match between the two data sets.

Approximately 50% of the model parameters could be estimated within a margin of $\pm$ 90%, that is, within less than two orders of magnitude when all experimental data was taken into consideration (Fig. 5.20a). Given the size of the mathematical model (360 state variables and 191 adjustable parameters) compared to the size of the data set available (120 data points for altogether 9 different aggregate system variables), it comes as no surprise that not all parameters were identifiable. For instance, recent theoretical analysis indicates an upper limit of $2n_p + 1$ error-free measurements to be required for the exact identification of n_p parameters in smooth ODE systems of arbitrary structure [245]. For the mitotic control module, parameter estimation would have to rely on (at most) $\approx$ 400 data points. The experimental data basis used in this study, thus, carried much more information on the particular system of mitotic control in yeast than is expected from simply comparing data quantity to model complexity.

Beyond the set of identifiable parameters, two major reasons may explain the failure of parameter estimation within acceptable error bounds. The remaining parameters could require more experiments to be determined, for example, the measurement of additional states, or different perturbation conditions. The possibility of enhancing parameter identification by means of improved data quantity as well as quality will be investigated in detail later in this section. An alternative explanation is that certain parameters can generally not be estimated, because the reactions they are used to describe are insignificant for the dynamic behavior of the system. Note that the mitotic control module contains a set of hypothetical reactions based on suspected network connections, or on alternative mechanisms. Determination of parameter sensitivities could yield information on regulatory interactions that are not likely to operate *in vivo*, or on candidates for the elimination of model parts for model reduction. Although they represent

promising lines of further research, these topics reach beyond the central questions addressed herein, and therefore will not be further considered.

By variation of the set of experimental data used in determination of the Fisher information matrix, calculation of parameter estimation accuracies allows for an assessment of the information content of sub–sets of the data provided. This will necessarily be an approximation, because it can not be guaranteed that the estimated parameter values would be identical for different sets of underlying data. In a first step, the wild type, and the set of perturbed conditions were analyzed separately (Fig. 5.20a). The distribution for the perturbed conditions shows a higher absolute number of parameters that could be identified within the given error bounds, although for the wild type, the set of measured variables was considerably larger than for the latter set of experimental data (9 vs. at maximum 4 variables). A similar number of data points, however, was available in both cases. Interpretation of the data in Fig. 5.20a leads to the conclusion that the sets of parameters rendered identifiable by the two sets of experiments show considerable overlap. Further combination of the data results in higher identifiability than is achievable by either set alone. Interestingly, partially higher accuracies for the set of estimates based on perturbed operation modes of the system are observed when compared to the wild type. Closer analysis of the parameters occurring in both sets reinforces this notion (Fig. 5.20b). In approximately half of the cases, lower estimation errors were obtained for the set of perturbed conditions. For identification of the mitotic control module, thus, this analysis points to the inclusion of more mutants or otherwise 'un-normal' operation modes of the system in parameter estimation as a promising way to increase model quality and, finally, to allow for model verification.

For an increased reliance on perturbed conditions to be a viable strategy for reverse–engineering, it is of interest, to which extent a particular choice of mutants may have influenced the analysis results described above. For this purpose, parameter estimation accuracies were determined separately for each experiment. Compared to the rich data set provided for the wild type, the other experiments show a relatively high, and rather homogeneous information content (Fig. 5.21a). According to the overall number of parameters that can be determined for the given accuracies, data for the externally forced system – resulting in a behavior different from that observed in wild type – does not prove advantageous over the data for mutants showing no particular phenotype. An intuitively appealing notion that highly informative experiments have to involve a distinct phenotype is furthermore contradicted by the fact that neither for yielding the best estimate for a particular parameter (Fig. 5.21b), nor for a high degree of identifiability per data used (Fig. 5.21c), this has to be the case. Exclusive identification of some parameters on the basis of the wild type data (Fig. 5.21b), however, shows that a broader set of measured variables can be essential for parameter identification, at least in the case studied here.

These considerations directly relate to the question, which of the measured variables were most responsible for the estimation of model parameters for the mitotic control module. Similarly to the investigation of the information content of the experiments, only single variables

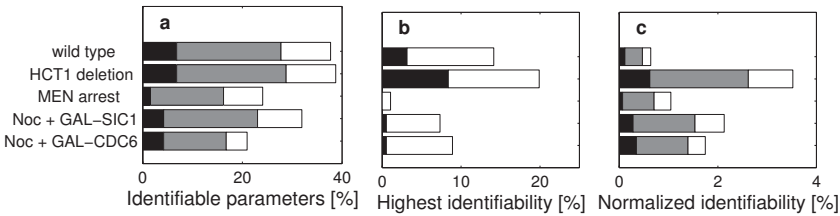

Fig. 5.21: Information content of single experiments. a, Relative number of identifiable parameters. Filled bars indicate the share of model parameters with an estimation accuracy of $\leq 10\%$ (black), $\leq 50\%$ (gray), and $\leq 100\%$ (white) based on the experiments employed in parameter estimation as denoted on the ordinate. **b,** Relative number of parameters, for which only in a specific out of all experiments available an estimation accuracy of $\sigma \leq 100\%$ (filled bars), or the best accuracy of all experiments (open bars) was calculated. **c,** Share of identifiable parameters as in **a**, but normalized by the number of measured data per experiment.

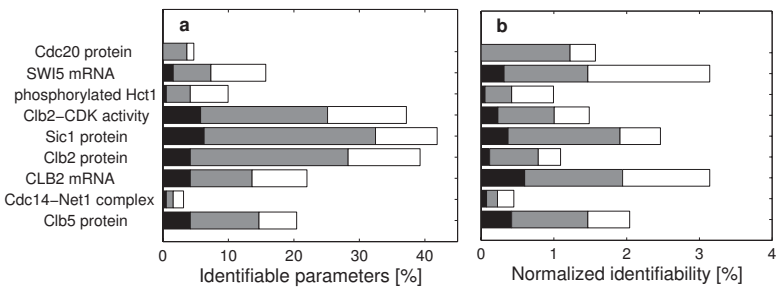

Fig. 5.22: Information content according to measured variables. Distribution of parameter estimation accuracies separated by types of experimental data provided in model adjustment (see ordinates). The color-coding scheme corresponds to Fig. 5.21. **a,** Absolute and **b,** relative (with respect to the number of measurements) shares of identifiable parameters.

such as concentrations of a particular regulator protein were used to determine the parameter estimation accuracies for the entire set of experiments. Analysis results are shown in Fig. 5.22. Here, it is important to note that the quantity as well as the quality of the data available for the different (aggregated) states of the system largely differed. For instance, whereas the concentration of the mitotic cyclin Clb2 and / or its associated kinase activity could be obtained from the experimental literature for nearly all conditions considered, only partial time courses were provided for variables such as the total concentration of the Cdc20 protein. This fact is largely reflected by the distribution of the share of identifiable parameters with respect to the experimental data types (Fig. 5.22a). The absolute numbers of parameters that can be determined using all the variables – again – indicate a considerable overlap of the information accessible through them, as for the case of the experiments. More detailed analysis reveals that this overlap primarily results in better estimates for the parameter values (data not shown). For the purpose of identification, however, this observation could imply that full identification will become increasingly difficult when adding new measured variables, but also that it could be necessary to determine every detail experimentally when relying only on a very limited set of experiments. These alternatives will be discussed later in the section.

In addition to these general considerations, it is obvious that the data on the dynamics of complex formation between the Cdc14 phosphatase and the inhibitor Net1 used in parameter estimation hardly gave any clues on the internal working principles of the system in quantitative terms. In sharp contrast, the parameters associated with these two regulators in the model belonged to those with lowest estimation errors (see Fig. 5.19). Providing more accurate time courses for this regulatory mechanism, thus, could be a suitable approach towards enhanced estimation of model parameters. Additionally, the normalized data shown in Fig. 5.22b indicate a relatively high information content of the mRNA measurements when compared to the (absolute) protein concentrations except for Sic1. Two factors may contribute to this observation, namely total mRNA concentrations being a more detailed variable in the system because of the only limited degrees of freedom of distributing the total amount of these species between different complexes (as opposed to the highly interacting proteins). Measurements of transcripts could also cover a large proportion of the parameters involved in transcriptional regulation. Additional mRNA measurements, however, do not necessarily result in better identification of the parameters for the mitotic control module (see below).

The fact that only few selected (aggregate) states of the system are described by the experimental data, and the differences in the information content of these data should result in an uneven distribution of parameter identifiability across the model. In order to investigate, which parts of the mitotic control module could best (or least) be identified based on the available data, parameters were classified by the cell cycle regulators or checkpoint mechanisms they are associated with. All kinetic parameters for reactions that involve a particular regulator's gene, mRNA or protein formed a parameter sub-set for this regulator. Obviously, the resulting parameters sub-sets are not disjointed. For interactions between regulators, or for all reactions

using complex species as educts or products, parameters were assigned to more than one class by this method. Characteristics of the distributions of parameter estimation accuracies for these parameters sets are shown in Fig. 5.23.

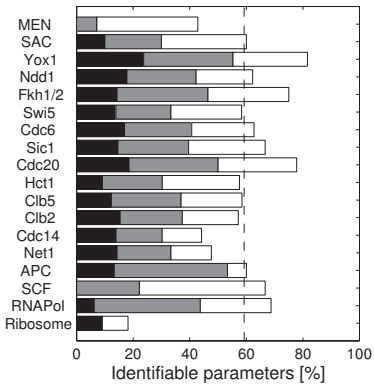

Fig. 5.23: Parameter identifiability classified by cell cycle regulators or checkpoints. Parameters that affect elementary reactions in which the cell cycle regulators or checkpoint functions participate at the gene, mRNA or protein level, were grouped together. This procedure resulted in overlapping parameter sets because, for instance, parameters describing the complex formation between two proteins belong to two sub-sets. The number of parameters with accuracies below the defined critical values is shown relative to the size of the sub-set of model parameters for each regulator or checkpoint. The dashed line indicates the average ratio of parameters with estimation accuracy $\sigma \leq 100\%$.

As expected, the shares of identifiable parameters with respect to the regulators participating in mitotic control differ considerably. Contrary to intuition, however, the degree to which a particular sub-aspect of the control system could be identified does not reflect the types of measurements provided for estimating the parameters. Transcriptional regulation (via Yox1, Ndd1, Swi5, and the forkhead transcription factors), for instance, shows higher reliability of parameter values than the regulatory mechanisms employing the mitotic cyclin Clb2 as the best represented regulator in the experimental data set. Qualitatively, it is interesting to note that highly connected nodes in the regulatory network such as Cdc14, the cyclins, and general cellular components (APC, SCF, RNA polymerase and ribosomes) are in general under–represented in the set of identifiable parameters. The predominance of hypothetical mechanisms accumulated in these parts of the model gives one explanation for this finding; by systematic model reduction, one could, thus, aim at improving parameter identification. It seems more likely, however, that a closer characterization of the detailed dynamics of the highly connected regulator may require equally detailed measurements or perturbations for the differentiation between the properties of parallel or competing regulatory mechanisms. An average identifiability of the

classified parameters that is significantly higher than for the unique set of all model parameters (see Fig. 5.20), however, is consistent with an interpretation that 'central' parameters, for example, describing maximal turnover rates of Clb2–CDK and Cdc14 may nevertheless be highly sensitive. Regarding the checkpoint mechanisms that are represented in the model at only a rudimentary level, similar observations can be made. There, moreover, it may be necessary to provide for a more elaborate representation of the control mechanisms to allow for a direct reference to experimental observations. This should preferably be achieved by connecting modules that contain detailed mathematical submodels for the signaling pathways.

The investigation of model identifiability so far relied on the experimental data basis used for model adjustment. It indicates an incomplete and fragmented capacity to validate the model with respect to the accuracy of parameter values, despite the unexpectedly high information content of the experimental data available. Already, the analysis indicated that the consideration of additional perturbed conditions of the mitotic control network may improve parameter identifiability. Conducting detailed experimental analyses of the complex network requires considerable effort and time. Therefore, it will be of importance to systematically devise strategies for efficient improvement of parameter identification.

In principle, the analysis of parameter estimation accuracies can be employed for this purpose, namely by investigating the effects of providing additional data, or data of higher quality [66]. For assessment of such effects, however, several restrictions apply. Sensitivity analyses using the Fisher information matrix require that parameter values are globally optimal with respect to the minimization of the identification functional. Changes in the experimental data basis for the calculations will tend to violate this condition. Additional experimental data or, more precisely, estimates of measurement errors employed in constructing the FIM, moreover, will have to be derived from simulations that could not be validated in every detail. The aim of the following studies, hence, will be to derive qualitative conclusions on valid strategies for experimental design in an iterative cycle of experimental and theoretical investigations [137].

An obvious strategy for gathering more detailed information on the system consists in measuring additional system properties, namely time courses of other variables than the few ones currently forming the reference data set. As a basis for judgments on different strategies for improvement of parameter estimation, it was of interest to first assess the hypothetical case that all state variables (concentrations of species) of the model were accessible experimentally. Here, simulation data were employed to mimic the additional experimental data. For each species concentration occurring in the mitotic control module, time courses were generated for all experimental conditions used for parameter estimation, yielding data and associated error estimates for all time points for which 'real' measurements existed. The effects of the assumed complete observability of the system's dynamic behavior on parameter identifiability are shown in Fig. 5.24.

Despite the fact that under these conditions, the data basis was enriched by several thousand additional *in silico* measurements, it was not possible to identify all model parameters. As dis-

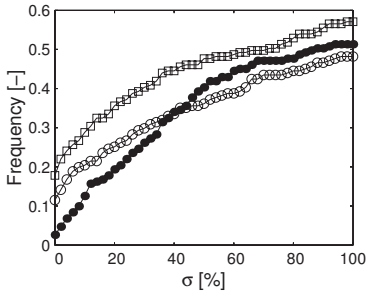

Fig. 5.24: Effect of observability of all system states on identifiability. The experimental data sets for wild type and mutants were augmented by simulation results for all state variables, using all time points provided in the original time courses. Absolute and relative measurement errors for the data generated *in silico* were assumed to be identical to those of the experimental data. These 'artificial' data sets were employed in the determination of parameter estimation accuracies for the wild type alone (open circles), or the wild type plus perturbed conditions (squares). Additionally, the distribution of estimation accuracies for the original data set (filled circles) is shown.

cussed above, dependencies of parameters as well as irrelevance of the introduced hypothetical mechanisms may render parameter values inaccessible; these intrinsic obstacles to identification will have to be dealt with by model analysis and subsequent systematic model reduction. The results obtained by means of the scenario of complete observability, however, point to perturbations of the systems as an important factor influencing the quality of parameter identification. In terms of the share of parameters that could be identified, the results for the wild type alone proved to be inferior to those obtained by using the sparse original data set for wild type and mutants. As would be expected, additional consideration of the perturbed conditions lead to an improved outcome. This complies with the earlier observation of the unexpectedly high information content of the (combined) behavior of the perturbed system. In the following, besides analyzing the effects of data quantity and quality, also the impact of including additional mutants for assessing parameter identifiability will be investigated.

From the viewpoint of experimental biology, simultaneous measurement of all system variables at the levels of genes, mRNAs, proteins and their complexes is a highly artificial scenario. The determination of total concentrations of proteins and messenger RNAs, however, could be carried out with established experimental methods. One could, for instance, make use of specifically tagged protein variants [44, 86] and of DNA micro-arrays [33, 246] for the quantification of protein and mRNA concentrations, respectively. Here, simulation data for each single total protein or mRNA concentration were employed to separately calculate parameter estimation accuracies for the original data augmented by each of the *in silico* variables. Compared to the original data set, however, including additional data on total protein or mRNA concentrations

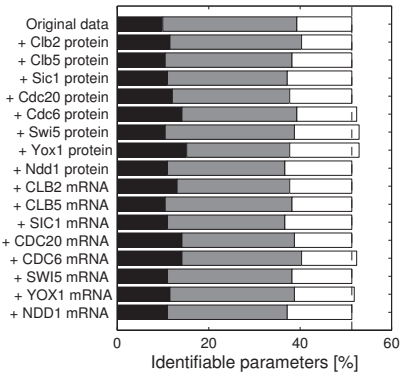

Fig. 5.25: Additionally measured total regulator concentrations and identifiability. Similar to Fig. 5.24, simulation data for each of the total concentrations of the regulators indicated was used to broaden the original data basis. For comparison, results for the original data (with the total number of identifiable parameters denoted by the dashed line) are included.

does not significantly increase the identifiability of the mitotic control system under the conditions considered (Fig. 5.25). Notably, few of the additional data lead to a better estimation of model parameters with respect to their number or accuracy. Measurements of the concentrations of the transcriptional regulator Yox1, and of the Clb2–CDK inhibitor Cdc6 would lead to the highest improvements in parameter identification, but still result in few parameters that could be estimated with a higher confidence than by using only the original data set. For the case of the mitotic control module, it can, hence, be concluded that the most evident approach to an improvement in parameter estimation – including additional measurements for the most accessible system variables – will presumably not be a viable strategy.

Instead of addressing the quantity of experimental data in order to enhance identification of the mitotic control module, one could aim at improving the data quality. Two possible ways that lead to higher accuracy of time course data were investigated, namely diminishing the measurement errors, and increasing the sampling rate. In the first case, the error estimates for the original experimental data were systematically modified. For the second case, additional data for all originally measured variables were generated at time points corresponding to measurement intervals that were varied within experimentally feasible limits.

Regarding the impact of measurement accuracy on identifiability, results from sensitivity analysis comply with the expectation that diminishing the measurement error will result in better estimates of parameter values (Fig. 5.26a). Parameter estimation accuracies, however, indicated that this influence is rather moderate. Through a four–fold reduction of the measurement error for the reference data set, the share of model parameters with a lower bound for the

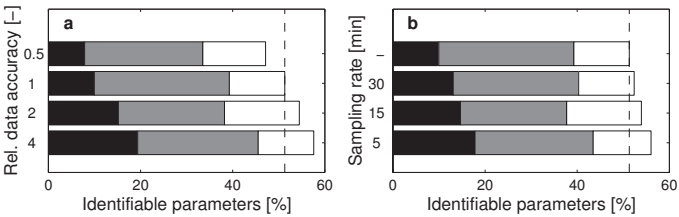

Fig. 5.26: Data quality and parameter identification. a, Variation of measurement error using the estimates of absolute and relative errors divided by the factors shown at the ordinate to change the relative data accuracy. Accordingly, entries for one correspond to the reference data. **b,** Simulation of increased sampling rate for measurements. Simulation results were employed to generate 'synthetic' data for all measured variables of the reference data set. Values on the ordinate indicate the time intervals for the sampling of additional data; '-' refers to the determination of parameter estimation accuracies based on the original experimental data alone.

estimation error of $\sigma \leq 100\%$ would remain below 60%. But this would imply, for instance, that the relative error in the determination of protein concentrations could be lowered from 20% as assumed for the original data to only 5% by employing more precise experimental analysis methods and / or increasing the number of replicates. When also taking into account the effect of lowering the measurement accuracy, it becomes evident that the efforts required for improving the identification of parameters in the mitotic control module by means of higher accuracy of data acquisition alone may outweigh the potential benefits. The analysis of the effects of higher–resolution time–course data (with otherwise unchanged data accuracy) yields qualitatively similar results (Fig. 5.26b). There, it has to be noted that decreasing the measurement intervals to 5 mins. implies an approximately ten–fold increase of the number of protein or mRNA analyses to be carried out ($\approx$ 1,200 vs. the original 120 data points). To summarize, with respect to the efforts required to obtain experimental data of higher quality, neither of the two approaches seems to be feasible to pursue the complete identification of the kinetic parameters in the yeast mitotic control, and model validation.

Given the influence of systematic perturbations in the mitotic control network on identifiability observed in several instances, finally, the effect of considering the behavior of additional mutant strains was analyzed. For this purpose, a set of mutant strains was chosen, for which model predictions were in agreement with the experimentally observed behavior, namely the $CLB5\Delta db$, $cdc20\Delta$, $sic1\Delta$, and $\Delta 47cdc6$ strains (see section 5.4.2, Fig. 5.14). In order to allow for easy reproduction of the model-based investigations in real experiments, only the total concentration of the mitotic cyclin Clb2, and its associated CDK activity were derived from simulation results by sampling in time intervals of 30 min. Altogether, 64 *in silico* measurement data were generated. Fig. 5.27 shows aggregate indicators of parameter identifiability for the cases of the single mutants, and for the combination of this data with the original data set.

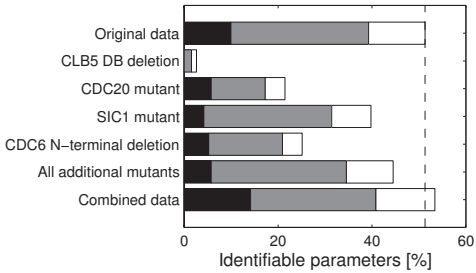

Fig. 5.27: Analysis of additional mutant strains. For the mutant strains indicated, time course data for total Clb2 protein concentration and for Clb2–CDK activity were obtained at sampling intervals of Δt =30 min. Parameter estimation accuracies were determined employing either the single *in silico* experiments, the set of the newly generated mutant data ('All additional mutants'), or its combination with the original data basis for parameter estimation ('Combined data').

When the qualities of parameter identification based on the new mutant data are considered separately, the information content of these experiments varies to a large extent. Interestingly, differences in the behavior of the strains resulting from the specific defects in the regulatory network can not be related to this outcome in an obvious manner. For instance, all mutants except for the $cdc20\Delta$ strain proceed through mitosis with nearly wild–type kinetics (see Fig. 5.14). Similar to the case of choosing appropriate additional variables to be measured, one approach could consist in a systematic, yet time–consuming analysis of all relevant mutants in order to refine the model. Preferably, however, experimental design based on sensitivity analyses as shown here would be performed. Consistent with previous results, combining the new data enables one to identify a relatively high number of parameters when compared to the original data set. Again, however, the set of parameters thus rendered identifiable largely overlaps with the one already established, because in total, an experimental data basis broadened by the additional perturbed conditions increases the share of identifiable parameters by only a few per cent.

An inherent problem for all strategies tested with respect to their ability to lead to better identification of parameters in the mitotic control module, thus, consists in the increasingly difficult accessibility of parameter values beyond a 'core' parameter set covered by all approaches. Increasing the number of measured variables, measurements of higher accuracy, as well as the consideration of the basic behavior of the system under an enlarged set of perturbed conditions brought about similar, small improvements in the accuracy of parameter estimates. For all cases, it has to be taken into account that the methods of sensitivity analysis employed here only allow for an approximate assessment of the effects that additional data would have on the system's identifiability.

Consistently, however, it was shown that perturbations applied to the mitotic control network allow for identification of model parameters at relatively high accuracy. Regarding the experimental feasibility, improvements in identification through, for instance, data acquisition for additional mutant strains can be achieved by using only a very limited amount of information on the system's behavior in terms of the measured variables and the number of data points. Systematic investigation of the already available sets of yeast single and double deletion mutants [127, 255, 279], or applying methods for externally induced perturbations of the mitotic control network will therefore likely be most efficient for model identification and validation. This does not preclude the combination with other methods for better characterization of the control system such as system–wide measurements or high sampling rates, if experimentally feasible. Systematic model analysis and model reduction where appropriate could then close the iterative cycle between experimentation and theory in order to finally obtain a validated, detailed representation of mitotic control in yeast.

5.6 Conclusions

The central motivation for a detailed model-based analysis of the mitotic control network in yeast was to examine the relation of robustness and identifiability of complex regulatory modules, using cell cycle regulation as an example system. A mathematical model for this regulatory module was developed on the basis of a modular modeling approach that aims at a close representation of the mechanisms operating in the biological system. Several simplifying assumptions nevertheless needed to be introduced in order to constrain the model's complexity. Compared to previous models [32, 248], the mitotic control module provides a higher resolution of this subsystem. For instance, parallel regulatory pathways in transcriptional control and in competitive inhibition of the mitotic cyclin–dependent kinase were included. Checkpoint mechanisms and important, recently discovered control mechanisms for *CDC20* transcriptional regulation [181] and Cdc14 release [271] will have to be considered in future versions.

Estimation of the model parameters from selected experimental data with only few assumptions on absolute concentrations was intended to narrow the usual gaps between model and experiment [105]. Model validation relied on a set of independent criteria, pointing to a high degree of descriptive quality, internal consistency, and prediction capabilities of the model. For instance, a variety of different experimentally observed behaviors of the system could be reproduced with the mitotic control module, employing a unique set of model parameters. Discrepancies between model predictions and experimental data nevertheless occurred and will provide starting points for further model improvement.

Direct perturbation studies as well as analysis of parameter estimation accuracies clearly showed robustness of the network's behavior owing, for example, to the operation of redundant pathways. There exist, however, few spots of high sensitivity in the model. The analysis therefore strongly supports the concept of highly optimized tolerance, i.e. of the co-existence

of robustness and fragility in cellular control as opposed to uniform insensitivity of the network. Parameter estimation accuracies additionally showed that the information content of the scarce quantitative data available was much higher than generally expected. For the complex model, approximately half of the 191 kinetic parameters could be estimated from time course data for few variables and experimental conditions. Analysis also proved that the combination of data from the unperturbed regulatory module in wild type with data from mutants or otherwise disturbed cells was essential for this outcome. The existence of less accessible parameters that do not occur in the largely overlapping sets of identifiable parameters for the experiments employed, however, provides a challenge.

With reservations, sensitivity analyses allow for judgments on the 'best' (combination of) experimental approaches for further identification, and subsequent experiment design [66]. Comparison of different scenarios indicated the need to apply such tools for the purpose-driven selection of experiments. For instance, if a characterization of the dynamics of all species represented in the model was experimentally feasible, system–wide measurement of the wild type's behavior alone would be useless for improved parameter identification. Sensitivity analysis highlighted the use of even rough characterizations of the system's behavior under internally or externally perturbed conditions as the most efficient strategy for reverse–engineering of the complex regulatory network. Such an approach will have to be accompanied by model analysis and model reduction. In an iterative process encompassing theory and experimentation, hence, it seems possible to develop realistic models of complex cellular control circuits based on limited quantitative data, and despite robust network behavior.

6. SUMMARY

Robustness refers to the ability of a system to maintain specific functionalities despite external or internal perturbations. It is thought to be a key property of living systems. Current approaches to the analysis of robustness in cellular networks, however, either provide high-level abstractions that are barely backed up by specific examples from biology, or involve the selective investigation of small example networks, which hardly allows for generalizations that apply to systems of realistic complexity. In particular, the relation between structural and functional properties of complex cellular networks with respect to robustness remains largely unclear. Therefore, the motivating question for this work was whether model-based analysis of representative cellular sub–systems could help to further elucidate general design principles underlying robustness in biological systems, and implications of this property for the ability to understand complex cellular networks at the system level.

For this purpose, three largely different examples of cellular metabolic and regulatory networks were analyzed, using different theoretical approaches. Structural network analysis of the central metabolism of *E. coli* relied on network decomposition via elementary flux modes. For published mathematical models of the circadian clock in *Drosophila* as an example for small genetic circuits that are able to show complex dynamic behavior, systematic analyses of parameter sensitivities were performed. Finally, mathematical modeling for a complex regulatory network involved in *S. cerevisiae* cell cycle regulation – the mitotic control system – allowed to address the influence of robustness on identifiability. For *E. coli* metabolism and yeast mitotic control, mathematical models had to be developed prior to robustness analysis. In those case, a variety of approaches for model validation was pursued in order to ensure that the models reflect the most important aspects of the systems' structures and behaviors.

All three systems investigated showed robust behavior upon internal or external disturbances with respect to their core functionalities such as sustaining bacterial growth, providing an accurate time–tracking mechanism, and switching between cell cycle phases, respectively. A recurring theme encountered in the analysis of these networks was the combination of few highly sensitive model parts with a majority of largely insensitive parts. Hence, independent observations provide strong evidence for the concept of highly optimized tolerance, stressing a highly structured character of sensitivities that results in a co-existence of robustness and fragility in cellular networks [28, 29]. For the bacterial metabolic network, these results were obtained from purely structural analysis. In the case of the circadian oscillators, a certain conservation of parametric sensitivities across operating regimes could be detected. Robustness and fragility

properties of cellular networks, hence, may largely be determined by the network structure. This can in turn allow for a more general identification of structural features of biological systems that confer robustness.

Current hypotheses on mechanisms that cause robustness in biology include redundancy of components or pathways, feedback control, as well as modular and hierarchical organization of cellular networks [45]. Structural analysis indicated that a primary cause for robustness in metabolic networks is pathway redundancy; redundant components such as iso–enzymes seem to provide degrees of freedom for cellular regulation, while not contributing significantly to the stability of steady–state operation. Systematic comparison of feedback control structures in circadian clock models revealed an advantage of more complex over simpler regulatory structures with respect to the robustness of the physiological function the oscillators are intended to provide. As for advanced engineered systems, however, increased complexity of the circadian rhythm generator may make the system more vulnerable towards unexpected disturbances.

Closer analysis of the relations between network structure, function and control substantiated the conjecture that hierarchical organization is an important design feature of biological networks affecting, among other system properties, their robustness [148, 203]. Theoretical models for the control of metabolic genes explain the available experimental data only when a hierarchy of control levels is taken into account. A combination of results from pathway analysis of the example network suggests that a hierarchy incorporating regulation at the genetic and the flux level allows for finding a trade-off between efficiency of network operation, and robustness in terms of pathway diversity. In circadian clock models, parameters linked to the general regulatory apparatus of the cell such as general transcription turned out to be the most important points of sensitivity, with this effect being more pronounced in the more complex control structure investigated. These observations suggest a hierarchical design principle of cellular regulation, namely to 'export' a specialized control circuit's points of fragility to global, well-controlled regulatory systems to enhance overall robustness as well as to integrate cellular functionality. As a drawback, if the central components are affected by perturbations, the entire system collapses. A similar, deliberate concentration of fragilities is used in technical systems such as jet fighters. There, the most sensitive electronic components are installed directly under the pilot's seat.

Robustness of biological systems can render their quantitative description difficult, in particular regarding kinetic parameters. Two opposite approaches to the identification problem in general are currently favored: experimental determination of (most) parameters separately *in vitro* [152], or large–scale perturbation studies and parameter identification based on comprehensive genomic and proteomic data [119]. For the complex mitotic control system in budding yeast, however, model–based analysis indicated an unexpectedly high information content of the scarce quantitative data available. A combination of data from the unperturbed regulatory network with data obtained from the system perturbed, for instance, by gene deletions was essential. An evaluation of strategies for further model identification – in particular regarding less

accessible parameters – favored the determination of time courses for (few) key variables in the systematically perturbed system. Additional detailed measurement of parameters may be required, but with respect to experimental feasibility and effort, this strategy could allow for an efficient model development for complex cellular networks, even when they are robust.

The general approach followed in this work was a model-based analysis of cellular sub–systems with respect to their robustness properties, underlying mechanisms, and consequences of the robustness for their system–level understanding. The systems were chosen as well–characterized representatives for classes of biological networks in order to derive more general design principles of cellular networks. The scope of analyses by few example systems necessarily is limited, but this drawback seems to be unavoidable. Sufficiently detailed models and analyses are a prerequisite to enable one to make testable and realistic predictions. Model development and / or selection, however, sought to minimize the complexity to be handled in order to investigate (aspects of) robustness in cellular networks. Applying the approaches to, for instance, genome–scale metabolic network representations [205], or to more realistic models of the circadian clock in mammals [77, 154] would be next logical steps. Analysis at multiple levels, using a combination of methods as pursued herein, may ultimately lead to a deeper understanding of complex cellular networks [22]. With this in mind, the convergence of results on design principles for achieving robustness, and the potential of efficient iterative combination of experimentation and theory seem to be encouraging.

ZUSAMMENFASSUNG

Robustheit bezieht sich auf die Fähigkeit eines Systems, spezifische Funktionen trotz externer oder interner Störungen aufrecht zu erhalten. Sie wird als eine zentrale Eigenschaft biologischer Systeme angesehen. Gegenwärtige Ansätze zur Analyse von Robustheit in zellulären Netzwerken bieten jedoch entweder Abstraktionen auf hoher Ebene, die kaum durch spezifische Beispiele aus der Biologie belegt sind, oder sie beruhen auf der beispielhaften Untersuchung kleiner Netzwerke, was kaum Generalisierungen ermöglicht, die auch auf Systeme realistischer Komplexität anwendbar sind. Insbesondere das Verhältnis von strukturellen und funktionellen Eigenschaften komplexer zellulärer Netzwerke in Bezug auf deren Robustheit ist größtenteils unverstanden. Aus diesem Grund bestand die Ausgangsfrage dieser Arbeit darin, inwiefern eine modellbasierte Analyse repräsentativer zellulärer Teilsysteme dabei helfen könnte, grundlegende Designprinzipien, die der Robustheit biologischer Systeme zugrunde liegen, weiter aufzuklären und welche Auswirkungen diese Eigenschaft auf unsere Fähigkeit hat, komplexe zelluläre Netzwerke auf der Systemebene zu verstehen.

Mit dieser Zielsetzung wurden drei stark unterschiedliche Beispiele zellulärer metabolischer und regulatorischer Netzwerke analysiert. Eine strukturelle Netzwerkanalyse des Zentralstoffwechsels von *E. coli* basierte auf der Zerlegung des Netzwerkes mit Hilfe elementarer Flussmoden. Für publizierte mathematische Modelle des circadianen Oszillators in *Drosophila* als einem Beispiel für kleine genetische Schaltkreise, die komplexes dynamisches Verhalten zeigen können, wurden systematische Analysen von Parametersensitivitäten durchgeführt. Die mathematische Modellierung eines komplexen Regulationsnetzwerkes, das in die Zellzyklusregulation von *S. cerevisiae* involviert ist – das Kontrollsystem der Mitose – erlaubte schließlich, den Einfluss der Robustheit auf die Identifizierbarkeit des Systems zu behandeln. Für den Stoffwechsel von *E. coli* und für die Mitosekontrolle in Hefe mussten zunächst mathematische Modelle als Basis für die Robustheitsanalyse entwickelt werden. In beiden Fällen wurde eine Vielfalt von Ansätzen zur Modellvalidierung verfolgt, um abzusichern, dass die Modelle die wichtigsten Aspekte von Struktur und Verhalten der Systeme abbilden.

Alle drei untersuchten Systeme zeigten bei externen oder internen Störungen ein robustes Verhalten bezüglich ihrer zentralen Funktionen wie der Aufrechterhaltung des bakteriellen Wachstums, der Bereitstellung eines präzisen Zeitgebers und der sequentiellen Steuerung von Zellzyklusphasen. Ein bei der Analyse dieser Systeme wiederkehrendes Thema war die Kombination von wenigen, hoch sensitiven Modellbestandteilen mit einer Mehrheit weitgehend insensitiver Teile. Unabhängige Beobachtungen erbrachten damit starke Indizien für das Konzept der

”hochgradig optimierten Toleranz”, das einen hoch–strukturierten Charakter von Sensitivitäten hervorhebt, die zu einer Co–Existenz von Robustheit und Fragilität in zellulären Netzwerken führt [28, 29]. Für das bakterielle Stoffwechselnetzwerk wurden diese Ergebnisse durch rein strukturelle Analysen erhalten. Im Falle der circadianen Oszillatoren konnte eine gewisse Erhaltung der relativen Parametersensitivitäten unabhängig von der Operationsweise des Systems festgestellt werden. Robustheits- und Fragilitätseigenschaften von zellulären Netzwerken können daher im wesentlichen durch die Netzwerkstruktur bestimmt sein. Damit eröffnet sich die Möglichkeit einer generelleren Identifikation von Struktureigenschaften biologischer Systeme, die Robustheit verleihen.

Gegenwärtige Hypothesen über Mechanismen, die Robustheit in der Biologie verursachen, umfassen die Redundanz von Komponenten oder Stoffwechsel- und Signalwegen, Regelung, sowie modulare und hierarchische Strukturierung zellulärer Netzwerke [45]. Strukturanalysen wiesen darauf hin, dass ein Hauptgrund für die Robustheit metabolischer Netzwerke die Redundanz von Stoffwechselwegen ist; redundante Komponenten wie Isoenzyme stellen Freiheitsgrade für die zelluläre Regulation bereit, ohne aber in signifikanter Weise zur Stabilität des Betriebs im stationären Zustand beizutragen. Ein systematischer Vergleich von Regelungsstrukturen in Modellen circadianer Zeitgeber zeigte einen Vorzug komplexerer gegenüber einfacherer Regulationsstrukturen bezüglich der Robustheit der intendierten physiologischen Funktion der Oszillatoren. Wie bei hochentwickelten technischen Systemen jedoch, wird eine erhöhte Komplexität der Generatoren für circadiane Rhythmen ihre Anfälligkeit gegenüber unvorhergesehenen Störungen verstärken.

Eine genauere Analyse der Beziehungen zwischen Netzwerkstruktur, -funktion und Regelung erhärtete die Hypothese, dass eine hierarchische Strukturierung ein wichtiges Designmerkmal biologischer Netzwerke ist, das – neben anderen Systemeigenschaften – ihre Robustheit beeinflusst [148,203]. Theoretische Modelle für die Kontrolle metabolischer Gene erklären die verfügbaren experimentellen Daten nur, wenn eine hierarchische Regelung berücksichtigt wird. Eine Kombination von Ergebnissen aus der strukturellen Analyse des Beispielnetzwerkes legt nahe, dass eine Hierarchie, die Regulation auf den Ebenen der Gene und der Stoffwechselflüsse umfasst, eine Abstimmung zwischen der effizienten Betriebsweise des Netzwerkes und der Robustheit hinsichtlich der Vielfalt von Stoffwechselwegen erlaubt. In den Modellen für circadiane Oszillatoren erwiesen sich Parameter, die mit dem generellen Regulationsapparat der Zelle verknüpft sind, als die wichtigsten Punkte für Sensitivität des Verhaltens, wobei dieser Effekt in der komplexeren der untersuchten Kontrollstrukturen ausgeprägter war. Diese Beobachtungen deuten auf ein Prinzip des hierarchischen Designs der zellulären Regulation hin, nämlich, die Fragilitäten eines speziellen Regelkreises in Richtung der globalen, gut kontrollierten Regulationssysteme zu ’exportieren’, um gleichzeitig die Robustheit des Gesamtsystems zu erhöhen und die Integration zellulärer Funktionalitäten zu ermöglichen. Der mit einer derartigen Strategie verbundene Nachteil ist, dass das gesamte System kollabiert, sobald die zentralen Komponenten durch Störungen beeinträchtig sind. Eine ähnliche, absichtliche

Konzentration von Fragilitäten wird in technischen Systemen wie Kampfflugzeugen verwendet. Dort werden die empfindlichsten elektronischen Komponenten direkt unter dem Pilotensitz installiert.

Die Robustheit biologischer Systeme kann ihre quantitative Beschreibung erschweren, insbesondere was die kinetischen Parameter betrifft. Um das generelle Identifikationsproblem zu adressieren, werden zur Zeit zwei gegensätzliche Ansätze favorisiert: die einzelne experimentelle Bestimmung aller oder der meisten kinetischen Parameter *in vitro* [152] oder großangelegte Perturbationsstudien und Parameterschätzung auf der Basis umfassender genomischer und proteomischer Daten [119]. Für das komplexe mitotische Regulationssystem der Hefe deutete die modellbasierte Analyse jedoch auf einen unerwartet hohen Informationsgehalt der wenigen verfügbaren quantitativen Daten hin. In diesem Zusammenhang erwies sich die Kombination von Daten aus dem ungestörten System mit denen aus dem, z.B. durch Gendeletionen gestörten als essentiell. Eine Bewertung möglicher Strategien für die weitergehende Modellidentifikation – insbesondere was die weniger leicht zugänglichen Parameter betrifft – favorisierte die Bestimmung von Zeitreihen weniger Schlüsselvariablen in dem systematisch gestörten System. Zusätzliche detaillierte Messungen kinetischer Parameter können sich als notwendig erweisen. Im Hinblick auf die experimentelle Machbarkeit und den damit verbundenen Aufwand kann diese Strategie eine effiziente Modellentwicklung für komplexe zelluläre Netzwerke ermöglichen, auch wenn diese robust sind.

Der generelle Ansatz, der in dieser Arbeit verfolgt wurde, bestand in der modellbasierten Analyse zellulärer Subsysteme bezüglich ihrer Robustheitseigenschaften, zugrundeliegenden Mechanismen und der Konsequenz von Robustheit für das Verständnis auf der Systemebene. Drei Systeme wurden als gut untersuchte Repräsentanten verschiedener Klassen biologischer Netzwerke ausgewählt, um generellere Designprinzipien zellulärer Netzwerke ableiten zu können. Die Aussagekraft von Analysen auf der Basis weniger Beispielsysteme ist notwendigerweise limitiert, aber dies scheint unvermeidbar, da hinreichend detaillierte mathematische Modelle und Analysen eine Grundvoraussetzung für die Generierung testbarer und realistischer Prädiktionen darstellen. Modellentwicklung und / oder -auswahl zielten jedoch darauf ab, die zu behandelnde Komplexität zu minimieren, um (Aspekte von) Robustheit in zellulären Netzwerken zu untersuchen. Die Anwendung der hier beschriebenen Methoden auf, zum Beispiel, genomweite metabolische Netzwerkrepräsentationen [205] oder auf realistischere Modelle von circadianen Oszillatoren [154] wären die nächsten logischen Schritte. Die Analyse auf unterschiedlichen Ebenen unter Verwendung einer Kombination von Methoden, wie sie hier verfolgt wurde, könnte schließlich zu einem tieferen Verständnis komplexer zellulärer Netzwerke führen [22]. Vor diesem Hintergrund scheinen die Konvergenz der erzielten Resultate zu Designprinzipien für Robustheit in zellulären Systemen, sowie das Potential einer effizienten, iterativen Kombination von Experimenten und Theorie ermutigend.

7. REFERENCES

[1] B. Aerne, A. Johnson, J. Toyn, and L. Johnston. Swi5 controls a novel wave of cyclin synthesis in late mitosis. *Mol. Biol. Cell*, 9:945–56, 1998.

[2] R. Albert, H. Jeong, and A.-L. Barabási. Error and attack tolerance of complex networks. *Nature*, 406:378–82, 2000.

[3] G. Alexandru, W. Zachariae, A. Schleiffer, and K. Nasmyth. Sister chromatid separation and chromosome re-duplication are regulated by different mechanisms in response to spindle damage. *EMBO J.*, 18(10):2707–21, 1999.

[4] U. Alon, M. Surette, N. Barkai, and S. Leibler. Robustness in bacterial chemotaxis. *Nature*, 397:168–71, 1999.

[5] H. Althoefer, A. Schleiffer, K. Wassmann, N. A, and G. Ammerer. Mcm1 is required to coordinate G_2-specific transcription in *Saccharomyces cerevisiae*. *Mol. Cell. Biol.*, 15(11):5917–28, 1995.

[6] A. Amon. Regulation of B-type cyclin proteolysis by Cdc28-associated kinases in budding yeast. *EMBO J.*, 15(10):2693–702, 1997.

[7] A. Amon, M. Tyers, B. Futcher, and K. Nasmyth. Mechanism that help the yeast cell cycle clock tick: G2 cyclins transcriptionally activate G2 cyclins and repress G1 cyclins. *Cell*, 74:993–1007, 1993.

[8] V. Archambault, C. Li, A. Tackett, R. Wäsch, B. Chait, M. Rout, and F. Cross. Genetic and biochemical evaluation of the importance of Cdc6 in regulating mitotic exit. *Mol. Biol. Cell*, 14(11):4592–604, 2003.

[9] A. Asthagiri and D. Lauffenburger. Bioengineering models of cell signaling. *Annu. Rev. Biomed. Eng.*, 2:31–53, 2000.

[10] E. Aurell, S. Brown, J. Johansen, and K. Sneppen. Stability puzzles in phage λ. *Phys. Rev. E*, 65:051914, 2002.

[11] N. Barkai and S. Leibler. Robustness in simple biochemical networks. *Nature*, 387:913–17, 1997.

[12] N. Barkai and S. Leibler. Circadian clocks limited by noise. *Nature*, 403:267–8, 2000.

[13] R. Basco, M. Segal, and S. Reed. Negative regulation of G_1 and G_2 by S-phase cyclins of *Saccharomyces cerevisiae*. *Mol. Cell. Biol.*, 15(9):5030–42, 1995.

[14] V. Batagelj and A. Mrvar. Pajek - analysis and visualization of large networks. *Lect. Notes Comput. Sc.*, 2265:477–478, 2002.

[15] A. Becskei and L. Serrano. Engineering stability in gene networks by autoregulation. *Nature*, 405:590–93, 2000.

[16] A. Becskei, B. Séraphin, and L. Serrano. Positive feedback in eukaryotic gene networks: cell differentiation by graded to binary response conversion. *EMBO J.*, 20(10):2528–35, 2001.

[17] S. Bilke and C. Peterson. Topological properties of citation and metabolic networks. *Phys. Rev. E*, 64:036106, 2001.

[18] A. Bishop, J. Ubersax, D. Petsch, D. Matheos, N. Gray, J. Blethrow, E. Shimizu, J. Tsien, P. Schultz, M. Rose, J. Wood, D. Morgan, and K. Shokat. A chemical switch for inhibitor-sensitive alleles of any protein kinase. *Nature*, 407:395–401, 2000.

[19] M. Borisuk and J. Tyson. Bifurcation analysis of a model of mitotic control in frog eggs. *J. theor. Biol.*, 195:69–85, 1998.

[20] S. Bornholdt. Modeling genetic networks and their evolution: a complex dynamical systems perspective. *Biol. Chem.*, 382:1289–99, 2001.

[21] S. Bornholdt and K. Sneppen. Robustness as an evolutionary principle. *Proc. R. Soc. Lond. B*, 267:2281–86, 2000.

[22] D. Bray. Molecular networks: the top-down view. *Science*, 301:1864–65, 2003.

[23] L. Breeden. Periodic transcription: a cycle within a cycle. *Curr. Biol.*, 13:R31–R38, 2003.

[24] M. Bäumer, G. Braus, and S. Irniger. Two different modes of cyclin Clb2 proteolysis during mitosis in *Saccharomyces cerevisiae*. *FEBS Lett.*, 468:142–48, 2000.

[25] A. Calzada, M. Sancristán, E. Sánchez, and A. Bueno. Cdc6 cooperates with Sic1 and Hct1 to inactivate mitotic cyclin-dependent kinases. *Nature*, 412:355–58, 2001.

[26] A. Calzada, M. Sánchez, E. Sánchez, and A. Bueno. The stability of the Cdc6 protein is regulated by cyclin-dependent kinase/cyclin B complexes in *Saccharomyces cerevisiae*. *J. Biol. Chem.*, 275(13):9734–41, 2000.

[27] F. Canonaco, T. Hess, S. Heri, T. Wang, T. Szyperski, and U. Sauer. Metabolic flux response to phosphoglucose isomerase knock-out in *Escherichia coli* and impact of overexpression of the soluble transhydrogenase Udha. *FEMS Microbiol. Lett.*, 204:247–54, 2001.

[28] J. Carlson and J. Doyle. Highly optimized tolerance: A mechanism for power laws in designed systems. *Phys. Rev. E*, 60(2):1412–27, 1999.

[29] J. Carlson and J. Doyle. Highly optimized tolerance: robustness and design in complex systems. *Phys. Rev. Lett.*, 84(11):2529–32, 2000.

[30] J. Carlson and J. Doyle. Complexity and robustness. *Proc. Natl. Acad. Sci. U.S.A.*, 99:2538–45, 2002.

[31] D. Chang, S. Shin, J. Rhee, and J. Pann. Acetate metabolism in a *pta* mutant of *Escherichia coli* W3110: importance of maintaining acetyl coenzyme A flux for growth and survival. *J. Bacteriol.*, 181:6656–63, 1999.

[32] K. Chen, A. Csikasz-Nagy, B. Gyorffy, J. Val, B. Novak, and J. Tyson. Kinetic analysis of a molecular model of the budding yeast cell cycle. *Mol. Biol. Cell*, 11:369–91, 2000.

[33] R. Cho, M. Campbell, E. Winzeler, L. Steinmetz, A. Conway, L. Wodicka, T. Wolfsberg, A. Gabrielian, D. Landsmann, and R. Davis. A genome-wide transcriptional analysis of the mitotic cell cycle. *Mol. Cell*, 2:65–73, 1998.

[34] R. Ciosk, W. Zachariae, C. Michaelis, A. Shevchenko, M. Mann, and K. Nasmyth. An Esp1/Pds1 complex regulates loss of sister chromatid cohesion at the metaphase to anaphase transition in yeast. *Cell*, 93:1067–76, 1998.

[35] W. Cleveland. *Visualizing data*. Murray Hill, NJ, 1993.

[36] O. Cohen-Fix, J.-M. Kirschner, and D. Koshland. Anaphase initiation in *Saccharomyces cerevisiae* is controlled by the APC-dependent degradation of the anaphase inhibitor Pds1p. *Genes Dev.*, 10:3081–93, 1996.

[37] O. Cohen-Fix and D. Koshland. Pds1p of budding yeast has dual roles: inhibition of anaphase initiation and regulation of mitotic exit. *Genes Dev.*, 13:1950–59, 1999.

[38] I. Conlon and M. Raff. Differences in the way a mammalian cell and yeast cells coordinate cell growth and cell-cycle progression. *J. Biol.*, 1:7, 2003.

[39] T. Cooper, D. Rozen, and R. Lenski. Parallel changes in gene expression after 20,000 generations of evolution in *Escherichia coli*. *Proc. Natl. Acad. Sci. U.S.A.*, 100(3):1072–77, 2003.

[40] A. Cornish-Bowden and M. Cárdenas. From genome to cellular phenotype - a role for metabolic flux analysis? *Nat. Biotechnol.*, 18:267–68, 2000.

[41] J. Courtright and U. Hennig. Malate dehydrogenase mutants in *Escherichia coli* K-12. *J. Bacteriol.*, 102:722–28, 1970.

[42] M. Covert and B. Palsson. Transcriptional regulation in constraints-based metabolic models of *Escherichia coli*. *J. Biol. Chem.*, 2002.

[43] M. Covert, C. Schilling, and B. Palsson. Regulation of gene expression in flux balance models of metabolism. *J. theor. Biol.*, 213:73–88, 2001.

[44] F. Cross, V. Archambault, M. Miller, and M. Klovstad. Testing a mathematical model of the yeast cell cycle. *Mol. Biol. Cell*, 13:52–70, 2002.

[45] M. Csete and J. Doyle. Reverse engineering of biological complexity. *Science*, 295:1664–69, 2002.

[46] L. Cunningham, M. Gruer, and J. Guest. Transcriptional regulation of the aconitase genes (*acnA* and *acnB*) of *Escherichia coli*. *Microbiology*, 143:3795–805, 1997.

[47] S. Cyran, A. Buchsbaum, K. Reddy, M.-C. Lin, N. Glossop, P. Hardin, M. Young, R. Storti, and J. Blau. *vrille*, *Pdp1* and *dClock* form a second feedback loop in the *Drosophila* circadian clock. *Cell*, 112:329–41, 2003.

[48] T. Dandekar, S. Schuster, B. Snel, M. Huynen, and P. Bork. Pathway alignment: application to the comparative analysis of glycolytic enzymes. *Biochem. J.*, 343:115–24, 1999.

[49] Z. Darieva, A. Pic-Taylor, J. Boros, A. Spanos, M. Geymonat, R. Reece, S. Sedgwick, A. Sharrocks, and B. Morgan. Cell cycle-regulated transcription through the FHA domain of Fkh2p and the coactivator Ndd1p. *Curr. Biol.*, 13:1740–45, 2003.

[50] L. Dirick, T. Böhm, and K. Nasmyth. Roles and regulations of Cln-Cdc28 kinases at the start of the cell cycle of *Saccharomyces cerevisiae*. *EMBO J.*, 14(19):4803–13, 1995.

[51] J. Doyle, B. Francis, and A. Tannenbaum. *Feedback control theory*. Macmillan Publishing Co., 1990.

[52] L. Drury, G. Perkins, and J. Diffley. The Cdc4/34/53 pathway targets Cdc6p for proteolysis in budding yeast. *EMBO J.*, 16(19):5966–76, 1997.

[53] L. Drury, G. Perkins, and J. Diffley. The cyclin-dependent kinase Cdc28p regulates distinct modes of Cdc6p proteolysis during the budding yeast cell cycle. *Curr. Biol.*, 10:231–40, 2000.

[54] G. Edelman and J. Gally. Degeneracy and complexity in biological systems. *Proc. Natl. Acad. Sci. U.S.A.*, 98(24):13763–68, 2001.

[55] D. Edelson and V. Thomas. Sensitivity analysis of oscillating reactions. 1. the period of the oregonator. *J. Phys. Chem.*, 85:1555–58, 1981.

[56] I. Edery, L. Zwiebel, M. Dembinska, and M. Rosbash. Temporal phosphorylation of the *Drosophila* period protein. *Proc. Natl. Acad. Sci. U.S.A.*, 91:2260–64, 1994.

[57] J. Edwards, R. Ibarra, and B. Palsson. *In silico* predictions of *Escherichia coli* metabolic capabilities are consistent with experimental data. *Nat. Biotechnol.*, 19:125–30, 2001.

[58] J. Edwards and B. Palsson. The *Escherichia coli* MG1655 *in silico* metabolic phenotype: its definition, characteristics and capabilities. *Proc. Natl. Acad. Sci. U.S.A.*, 97:5528–33, 2000.

[59] J. Edwards and B. Palsson. Robustness analysis of the *Escherichia coli* metabolic network. *Biotechnol. Prog.*, 16:927–39, 2000.

[60] H. El-Samad, J. Goff, and M. Khammash. Calcium homeostasis and parturient hypocalcemia: An integral feedback perspective. *J. theor. Biol.*, 214:17–29, 2002.

[61] A. Eldar, R. Dorfman, D. Weiss, H. Ashe, B.-Z. Shilo, and N. Barkai. Robustness of the BMP morphogen gradient in *Drosophila* embryonic patterning. *Nature*, 419:304–08, 2002.

[62] M. Elowitz and S. Leibler. A synthetic oscillatory network of transcriptional regulators. *Nature*, 403:335–38, 2000.

[63] M. Elowitz, A. Levine, E. Siggle, and P. Swain. Stochastic gene expression in a single cell. *Science*, 297:1183–86, 2002.

[64] S. Elsasser, Y. Chi, P. Yang, and J. Campbell. Phosphorylation controls timing of Cdc6p destruction: a biochemical analysis. *Mol. Biol. Cell*, 10:3263–77, 1999.

[65] S. Elsasser, F. Lou, B. Wang, J. Campell, and A. Jong. Interaction between yeast Cdc6 protein and B-type cyclin/Cdc28 kinases. *Mol. Biol. Cell*, 7:1723–35, 1996.

[66] A. Emery and A. Nenarokomov. Optimal experiment design. *Meas. Sci. Technol.*, 9(6):864–76, 1998.

[67] D. Endy and R. Brent. Modelling cellular behaviour. *Nature*, 409:391–95, 2001.

[68] G. Fang, H. Yu, and M. Kirschner. The checkpoint protein MAD2 and the mitotic regulator CDC20 form a ternary complex with the anaphase-promoting complex to control anaphase initiation. *Genes Dev.*, 12:1871–83, 1998.

[69] A. Feldbaum. Dual control theory I-II. *Autom. Remote Control*, 21:874–80, 1033–39, 1960.

[70] A. Feldbaum. Dual control theory III-IV. *Autom. Remote Control*, 22:1–12, 109–21, 1961.

[71] R. Feldman, C. Correll, K. Kaplan, and R. Deshaies. A complex of Cdc4p, Skp1p and Cdc53p/Cullin catalyzes ubiquitination of the phosphorylated CDK inhibitor Sic1p. *Cell*, 91:221–30, 1997.

[72] D. Fell and A. Wagner. The small world of metabolism. *Nat. Biotechnol.*, 18:1121–22, 2000.

[73] J. Ferrell. Tripping the switch fantastic: how a protein kinase cascade can convert graded inputs into switch-like outputs. *Trend Biochem. Sci.*, 21:460–66, 1996.

[74] J. Ferrell. Self-perpetuating states in signal transduction: positive feedback, double-negative feedback and bistability. *Curr. Opin. Chem. Biol.*, 6:140–48, 2002.

[75] D. Fesquet, P. Fitzpatrick, A. Johnson, K. Kramer, and K. Johnston. A Bub2p-dependent spindle checkpoint pathway regulates the Dbf2p kinase in budding yeast. *EMBO J.*, 18(9):2424–34, 1999.

[76] M. Fivash, E. Towler, and R. Fisher. BIAcore for macromolecular interaction. *Curr. Opin. Biotechnol.*, 9:97–101, 1998.

[77] D. Forger and C. Peskin. A detailed predictive model of the mammalian circadian clock. *Proc. Natl. Acad. Sci. U.S.A.*, 100:14806–11, 2003.

[78] D. Fraenkel. Glycolysis. In F. Neidhardt et al., editors, *Escherichia coli and Salmonella: Cellular and Molecular Biology*, volume 1, pages 189–198. Am. Soc. Microbiol., Washington, DC, 2nd edition, 1996.

[79] M. Freeman. Feedback control of intercellular signalling in development. *Nature*, 408:313–19, 2000.

[80] K.-U. Fröhlich and F. Madeo. Apoptosis in yeast - a monocellular organism exhibits altruistic behaviour. *FEBS Lett.*, 473:6–9, 2000.

[81] B. Futcher. Microarrays and cell cycle transcription in yeast. *Curr. Opin. Cell Biol.*, 12:710–15, 2000.

[82] B. Futcher, G. Latter, P. Monardo, C. McLaughlin, and J. Garrels. A sampling of the yeast proteome. *Mol. Cell. Biol.*, 19(11):7357–68, 1999.

[83] J.-M. Galan and M. Peter. Ubiquitin-dependent degradation of multiple F-box proteins by an autocatalytic mechanism. *Proc. Natl. Acad. Sci. U.S.A.*, 96:9124–29, 1999.

[84] T. Gardner, C. Cantor, and J. Collins. Construction of a genetic toggle switch in *Escherichia coli*. *Nature*, 403:339–42, 2000.

[85] M. Geymonat, S. Jensen, and L. Johnston. Mitotic exit: the Cdc14 double cross. *Curr. Biol.*, 12:R482–84, 2002.

[86] S. Ghaemmaghami, W.-K. Huh, K. Bower, R. Howson, A. Belle, N. Dephoure, E. O'Shea, and J. Weissman. Global analysis of protein expression in yeast. *Nature*, 425:737–41, 2003.

[87] E. Gilles. Control - key to better understanding of biological systems. *Automatisierungstechnik*, 50(1):7–17, 2002.

[88] A. Gilman and A. Arkin. Genetic "code": representations and dynamical models of genetic components and networks. *Annu. Rev. Genomics Hum. Genet.*, 3:341–69, 2002.

[89] M. Ginkel, A. Kremling, T. Nutsch, R. Rehner, and E. Gilles. Modular modeling of cellular systems with ProMoT/Diva. *Bioinformatics*, 19:1169–76, 2003.

[90] M. Girvan and M. Newman. Community structure in social and biological networks. *Proc. Natl. Acad. Sci. U.S.A.*, 99(12):7821–26, 2002.

[91] P.-Y. Goh, H. Lim, and U. Surana. Cdc20 contains a destruction-box but, unlike Clb2, its proteolysis is not acutely dependent on the activity of the anaphase-promoting complex. *Eur. J. Biochem.*, 267:434–49, 2000.

[92] A. Goldbeter. A model for circadian oscillations in the *Drosophila* period protein PER. *Proc. R. Soc. London Ser. B*, 261:319–324, 1995.

[93] A. Goldbeter. *Biochemical oscillations and circadian rhythms: the molecular basis of periodic and chaotic behaviour*. Cambridge Univ. Press, 1996.

[94] A. Goldbeter. Computational approaches to cellular rhythms. *Nature*, 420:238–45, 2002.

[95] D. Gonze, J. Halloy, and A. Goldbeter. Robustness of circadian rhythms with respect to molecular noise. *Proc. Natl. Acad. Sci. USA*, 99(2):673–678, 2002.

[96] B. Goodwin. Oscillatory behavior in enzymatic control processes. *Adv. Enzyme Regul.*, 3:425–38, 1965.

[97] N. Grandin, A. de Almeida, and M. Charbonneau. The Cdc14 phosphatase is functionally associated with the Dbf2 protein kinase in *Saccharomyces cerevisiae*. *Mol. Gen. Genet.*, 258:104–16, 1998.

[98] B. Grima, A. Lamouroux, E. Chélot, C. Papin, B. Limbourg-Bouchon, and F. Rouyer. The F-box protein Slimb controls the levels of clock proteins Period and Timeless. *Nature*, 420:178–82, 2002.

[99] Y. Gu, L. Steinmetz, X. Gu, C. Scharfe, R. Davis, and W.-H. Li. Role of duplicate genes in genetic robustness against null mutations. *Nature*, 421:63–66, 2003.

[100] R. Guimerà, A. Arenas, and A. Díaz-Guilera. Communication and optimal hierarchical networks. *Physica A*, 299:247–52, 2001.

[101] S. Harmer, S. Panda, and S. Kay. Molecular bases of circadian rhythms. *Annu. Rev. Cell Dev. Biol.*, 17:215–53, 2001.

[102] J. Hartman, B. Garvik, and L. Hartwell. Principles of the buffering of genetic variation. *Science*, 291:1001–04, 2001.

[103] L. Hartwell, J. Hopfield, S. Leibler, and A. Murray. From molecular to modular cell biology. *Nature*, 402 (Supp.):C47–C52, 1999.

[104] M. Hastings. Circadian clockwork: two loops are better than one. *Nat. Rev. Neurosci.*, 1:143–46, 2000.

[105] J. Hasty, D. McMillen, and J. Collins. Computational studies of gene regulatory networks: *in numero* molecular biology. *Nat. Rev. Genet.*, 2:268–79, 2001.

[106] J. Hasty, D. McMillen, and J. Collins. Engineered genetic circuits. *Nature*, 420:224–30, 2002.

[107] R. Heinrich, B. Neel, and T. Rapoport. Mathematical models of protein kinase signal transduction. *Molec. Cell*, 9:957–70, 2002.

[108] R. Heinrich and S. Schuster. *The regulation of cellular systems*. Chapman & Hall, New York, 1996.

[109] J. Helton and F. Davis. Sampling-based methods. In A. Saltelli, K. Chan, and E. Scott, editors, *Sensitivity analysis*, chapter 6, pages 101–53. John Wiley & Sons, Ltd., Chichester, UK, 2000.

[110] A. Hershko. Roles of ubiquitin-mediated proteolysis in cell cycle control. *Curr. Opin. Cell Biol.*, 9:788–99, 1997.

[111] P. Hollenhorst, G. Pietz, and C. Fox. Mechanisms controlling differential promoter-occupancy by the yeast forkhead proteins Fkh1p and Fkh2p: implications for regulating the cell cycle and differentiation. *Genes Dev.*, 15:2445–56, 2001.

[112] F. Holstege, E. Jennings, J. Wyrick, T. Lee, C. Hengartner, M. Green, T. Golub, E. Lander, and R. Young. Dissecting the regulatory circuitry of a eukaryotic genome. *Cell*, 95:717–28, 1998.

[113] N. Holter, A. Maritan, M. Cieplak, N. Feodoroff, and J. Banavar. Dynamic modeling of gene expression data. *Proc. Natl. Acad. Sci. U.S.A.*, 98:1693–98, 2001.

[114] N. Holter, M. Mitra, M. Cieplak, J. Banavar, and N. Fedoroff. Fundamental patterns underlying gene expression profiles: Simplicity from complexity. *Proc. Natl. Acad. Sci. U.S.A.*, 97(15):8409–14, 2000.

[115] J. Hood, W. Hwang, and P. Silver. The *Saccharmoyces cerevisiae* cyclin Clb2p is targeted to multiple subcellular locations by *cis*- and *trans*-acting determinants. *J. Cell Sci.*, 114:589–97, 2001.

[116] C.-Y. Huang and J. Ferrell. Ultrasensitivity in the mitogen-activated protein kinase cascade. *Proc. Natl. Acad. Sci. U.S.A.*, 93:10078–83, 1996.

[117] J. Huang, I. Park, E. Ellingson, L. Littlepage, and D. Pellman. Activity of the APC^{Cdh1} form of the anaphase-promoting complex persits until S phase and prevents the premature expression of Cdc20p. *J. Cell Biol.*, 154(1):85–94, 2001.

[118] L. Hwang, L. Lau, D. Smith, C. Mistrot, K. Hardwick, E. Hwang, A. Amon, and A. Murray. Budding yeast Cdc20: a target of the spindle checkpoint. *Science*, 279:1041–45, 1998.

[119] T. Ideker, V. Thorsson, J. Ranish, R. Christmas, J. Buhler, J. Eng, R. Bumgarner, D. Goodlett, R. Aebersold, and L. Hood. Integrated genomic and proteomic analysis of a systematically perturbed metabolic network. *Science*, 292:929–34, 2001.

[120] S. Irniger and K. Nasmyth. The anaphase-promoting complex is required in G_1 arrested yeast cells to inhibit B-type cyclin accumulation and to prevent uncontrolled entry into S-phase. *J. Cell Sci.*, 110(13):1523–31, 1997.

[121] M. Jaquenoud, F. van Drogen, and M. Peter. Cell cycle-dependent nuclear export of Cdh1p may contribute to the inactivation of APC/C(Cdh1). *EMBO J.*, 21:6515–26, 2002.

[122] S. Jaspersen, J. Charles, and D. Morgan. Inhibitory phosphorylation of the APC regulator Hct1 is controlled by the kinase Cdc28 and the phosphatase Cdc14. *Curr. Biol.*, 9:227–36, 1999.

[123] S. Jaspersen, J. Charles, R. Tinker-Kuhlberg, and D. Morgan. A late mitotic regulatory network controlling cyclin destruction in *Saccharomyces cerevisiae*. *Mol. Biol. Cell*, 9:2803–17, 1998.

[124] S. Jaspersen and D. Morgan. Cdc14 activates Cdc15 to promote mitotic exit in budding yeast. *Curr. Biol.*, 10:615–18, 2000.

[125] E. Jen. Stable or robust? What's the difference? *Sante Fe Institute working papers*, 2001. (RS-2001-024, available at http://discuss.santafe.edu/robustness/).

[126] H. Jeong, B. Tombor, R. Albert, Z. Oltvai, and A.-L. Barabási. The large-scale organization of metabolic networks. *Nature*, 407:651–54, 2000.

[127] P. Jorgensen, B. Nelson, M. Robinson, Y. Chen, B. Andrews, and C. Boone. High-resolution genetic mapping with ordered arrays of *Saccharomyces cerevisiae* deletion mutants. *Genetics*, 162:1091–99, 2002.

[128] P. Jorgensen and M. Tyers. Altered states: programmed proteolysis and the budding yeast cell cycle. *Curr. Opin. Microbiol.*, 2:610–17, 1999.

[129] P. Jorgensen and M. Tyers. The fork'ed path to mitosis. *Genome Biol.*, 1(3):1022.1–1022.4, 2000.

[130] J. Kahana, B. Schnapp, and P. Silver. Kinetics of spindle pole body separation in budding yeast. *Proc. Natl. Acad. Sci. U.S.A.*, 92:9707–11, 1995.

[131] B. Kholodenko, J. Hoek, H. Westerhoff, and G. Brown. Quantification of information transfer via cellular signal transduction pathways. *FEBS Letters*, 414:430–434, 1997.

[132] B. Kholodenko, A. Kiyatkin, F. Bruggeman, E. Sontag, H. Westerhoff, and J. Hoek. Untangling the wires: a strategy to trace functional interactions in signaling and gene networks. *Proc. Natl. Acad. Sci. U.S.A.*, 99(20):12841–46, 2002.

[133] M. Kirschner. Intracellular proteolysis. *Trends Cell Biol.*, 24(12):M42–M45, 1999.

[134] M. Kirschner and J. Gerhart. Evolvability. *Proc. Natl. Acad. Sci. U.S.A.*, 95:8420–27, 1998.

[135] T. Kitami and J. Nadeau. Biochemical networking contributes more to genetic buffering in human and mouse metabolic pathways than does gene duplication. *Nat. Genetics*, 32:191–94, 2002.

[136] H. Kitano. Computational systems biology. *Nature*, 420:206–10, 2002.

[137] H. Kitano. Systems biology: a brief overview. *Science*, 295:1662–64, 2002.

[138] S. Klamt and J. Stelling. Combinatorial complexity of pathway analysis in metabolic networks. *Mol. Biol. Rep.*, 29:233–36, 2002.

[139] S. Klamt and J. Stelling. Two approaches for pathway analysis in metabolic networks? *Trends Biotechnol.*, 21(2):64–69, 2003.

[140] S. Klamt, J. Stelling, M. Ginkel, and E. Gilles. *FluxAnalyzer*: Exploring structure, pathways, and flux distributions in metabolic networks on interactive flux maps. *Bioinformatics*, 19(2):261–69, 2003.

[141] D. Knapp, L. Bhoite, D. Stillman, and K. Nasmyth. The transcription factor Swi5 regulates expression of the cyclin kinase inhibitor p40^{SIC1}. *Mol. Cell. Biol.*, 16(10):5701–07, 1996.

[142] D. Koepp, J. Harper, and S. Elledge. How the cyclin became a cyclin: regulated proteolysis in the cell cycle. *Cell*, 97:431–34, 1999.

[143] M. Kohn, A. Tohmaz, K. Giroux, G. Blumenthal, M. Feezor, and D. Millington. Robustness of MetaNet graph models: Predicting control of urea production in humans. *Biosys.*, 65:61–78, 2002.

[144] D. Kompala, D. Ramkrishna, N. Jansen, and G. Tsao. Investigation of bacterial growth on mixed substrates: experimental evaluation of cybernetic models. *Biotechnol. Bioeng.*, 28:1044–55, 1986.

[145] M. Koranda, A. Schleiffer, L. Endler, and G. Ammerer. Forkhead-like transcription factors recruit Ndd1 to the chromatin of G2/M-specific promoters. *Nature*, 406:94–98, 2000.

[146] D. Krakauer and J. Plotkin. Redundancy, antiredundancy, and the robustness of genomes. *Proc. Natl. Acad. Sci. U.S.A.*, 99(3):1405–09, 2002.

[147] A. Kremling and E. Gilles. The organization of metabolic reaction networks: II. Signal processing in hierarchical structured functional units. *Metabolic Eng.*, 3(2):138–50, 2001.

[148] A. Kremling, K. Jahreis, J. Lengeler, and E. Gilles. The organization of metabolic reaction networks: A signal-oriented approach to cellular models. *Metabolic Eng.*, 2(3):190–200, 2000.

[149] R. Kumar, D. Reynolds, A. Shevchenko, A. Shevchenko, S. Goldstone, and S. Dalton. Forkhead transcription factors, Fkh1p and Fkh2p, collaborate with Mcm1p to control transcription required for M-phase. *Curr. Biol.*, 10:896–906, 2000.

[150] M. Laub, H. McAdams, T. Feldblyum, C. Fraser, and L. Shapiro. Global analysis of the genetic network controlling a bacterial cell cycle. *Science*, 290:2144–48, 2000.

[151] D. Lauffenburger. Cell signaling pathways as control modules: Complexity for simplicity? *Proc. Natl. Acad. Sci. U.S.A.*, 97(10):5031–33, 2000.

[152] E. Lee, A. Salic, R. Kruger, R. Heinrich, and M. Kirschner. The roles of APC and axin derived from experimental and theoretical analysis of the Wnt pathway. *PLoS Biol.*, 1:E10, 2003.

[153] T. Lee, N. Rinaldi, D. Odom, Z. Bar-Joseph, G. Gerber, N. Hannett, C. Harbison, C. Thompson, I. Simon, J. Zeitlinger, E. Jennings, H. Murray, D. Gordon, B. Ren, J. Wyrick, J. Tagne, T. Volkert, E. Fraenkel, D. Clifford, and R. Young. Transcriptional regulatory networks in *Saccharomyces cerevisiae*. *Science*, 298:799–804, 2002.

[154] J. Leloup and A. Goldbeter. Toward a detailed computational model for the mammalian circadian clock. *Proc. Natl. Acad. Sci. U.S.A.*, 100:7051–56, 2003.

[155] J.-C. Leloup and A. Goldbeter. A model for circadian rhythms in *Drosophila* incorporating the formation of a complex between the PER and TIM proteins. *J. Biol. Rhythms*, 13(1):70–87, 1998.

[156] J.-C. Leloup and A. Goldbeter. Chaos and birhythmicity in a model for circadian oscillations of the PER and TIM proteins in *Drosophila*. *J. Theor. Biol.*, 198:445–459, 1999.

[157] M. Lema, D. Golombek, and J. Echave. Delay model of the circadian pacemaker. *J. Theor. Biol.*, 204:565–73, 2000.

[158] A. Levchenko and P. Iglesias. Models of eukaryotic gradient sensing: Application to chemotaxis of amoebae and neutrophils. *Biophys. J.*, 82:50–63, 2002.

[159] H. Lim, P.-Y. Goh, and U. Surana. Cdc20 is essential for the cyclosome-mediated proteolysis of both Pds1 and Clb2 during M phase in budding yeast. *Curr. Biol.*, 8:231–34, 1998.

[160] J. Little, D. Shepley, and D. Wert. Robustness of a gene regulatory circuit. *EMBO J.*, 18(15):4299–307, 1999.

[161] L. Ljung. Model validation and model error modeling. In B. Wittenmark and A. Rantzer, editors, *The Åström Symposium on Control*, pages 15 –42, Lund, Sweden, Aug 1999. Studentlitteratur.

[162] C. Loy, D. Lydall, and U. Surana. NDD1, a high-dosage suppressor of cdc28-1N, is essential for expression of a subset of late-S-phase-specific genes in *Saccharomyces cerevisiae*. *Mol. Cell. Biol.*, 19(5):3312–27, 1999.

[163] D. Lydall, G. Ammerer, and K. Nasmyth. A new role for MCM1 in yeast: cell cycle regulation of SWI5 transcription. *Genes Dev.*, 5:2405–19, 1991.

[164] A. Lyngstaadas, G. Sprenger, and E. Boye. Impaired growth of an *Escherichia coli rpe* mutant lacking ribulose-5-phosphate epimerase activity. *Biochim. Biophys. Acta*, 1381:319–30, 1998.

[165] L. Ma and P. Iglesias. Quantifying robustness of biochemical network models. *BMC Bioinformatics*, 3:38, 2002.

[166] A. Mah, J. Jang, and R. Deshaies. Protein kinase Cdc15 activates the Dbf2-Mob1 kinase complex. *Proc. Natl. Acad. Sci. U.S.A.*, 98(13):7325–30, 2001.

[167] S. Martinek, S. Inonog, A. Manoukian, and M. Young. Role for the segment polarity gene shaggy/GSK-3 in the *Drosophila* circadian clock. *Cell*, 105:769–779, 2001.

[168] S. Maslov and K. Sneppen. Specificity and stability in topology of protein networks. *Science*, 296:910–13, 2002.

[169] D. McCollum and K. Gould. Timing is everything: regulation of mitotic exit and cytokinesis by the MEN and SIN. *Trends Cell Biol.*, 11(2):89–95, 2001.

[170] C. McInerny, J. Partridge, G. Mikesell, D. Creemer, and L. Breeden. A novel Mcm1-dependent element in the SWI4, CLN3, CDC6, and CDC47 promoters activates M/G_1-specific transcription. *Genes Dev.*, 11:1277–88, 1997.

[171] E. Meir, G. von Dassow, E. Munro, and G. Odell. Robustness, flexibility, and the role of lateral inhibition in the neurogenic network. *Curr. Biol.*, 12:778–86, 2002.

[172] M. Mendenhall. An inhibitor for p34^{CDC28} protein kinase activity from *Saccharomyces cerevisiae*. *Science*, 259:216–19, 1993.

[173] M. Mendenhall and A. Hodge. Regulation of Cdc28 cyclin-dependent protein kinase activity during the cell cycle of the yeast *Saccharomyces cerevisiae*. *Microbiol. Mol. Biol. Rev.*, 62(4):1191–1243, 1998.

[174] M. Mesarovic, D. Macko, and Y. Takahara. *Theory of hierarchical, multilevel, systems*. Academic Press, New York and London, 1970.

[175] M. Miller and F. Cross. Distinct subcellular localization patterns contribute to functional specificity of the Cln2 and Cln3 cyclins of *Saccharomyces cerevisiae*. *Mol. Cell. Biol.*, 20(2):542–55, 2000.

[176] M. Miller and F. Cross. Cyclin specificity: how many wheels do you need on a unicycle? *J. Cell Sci.*, 114:1811–20, 2001.

[177] R. Milo, S. Shen-Orr, S. Itzkovitz, N. Kashtan, D. Chklovskii, and U. Alon. Network motifs: simple building blocks of complex networks. *Science*, 298:824–27, 2002.

[178] C. Moles, P. Mendes, and J. Banga. Parameter estimation in biochemical pathways: A comparison of global optimization methods. *Genome Res.*, 13:2467–74, 2003.

[179] T. Moll, G. Tebb, U. Surana, H. Robitsch, and K. Nasmyth. The role of phosphorylation and the CDC28 protein kinase in cell cycle-regulated nuclear import of the *S. cerevisiae* transcription factor SWI5. *Cell*, 66:743–58, 1991.

[180] M. Morohashi, A. Winn, M. Borisuk, H. Bolouri, J. Doyle, and H. Kitano. Robustness as a measure of plausibility in models of biochemical networks. *J. theor. Biol.*, 216:19–30, 2002.

[181] M. Morris, P. Kaiser, S. Rudyak, C. Baskerville, M. Watson, and S. Reed. Cks1-dependent proteasome recruitment and activation of *CDC20* transcription in budding yeast. *Nature*, 423:1009–13, 2003.

[182] P. Nash, X. Tang, S. Orlicky, Q. Chen, F. Gertlers, M. Mendenhall, F. Sicheri, T. Pawson, and M. Tyers. Multisite phosphorylation of a CDK inhibitor sets a threshold for the onset of DNA replication. *Nature*, 414:514–21, 2001.

[183] F. Neidhardt, J. Ingraham, and M. Schaechter. *Physiology of the bacterial cell: A molecular approach*. Sinauer Associates, Sunderland, Massachusetts, 1990.

[184] M. Newman, M. Girvan, and J. Farmer. Optimal design, robustness and risk aversion. *Phys. Rev. Lett.*, 89(2):28301, 2002.

[185] M. Oh and J. Liao. DNA microarray detection of metabolic responses to protein overproduction in *Escherichia coli*. *Metab. Eng.*, 2:201–09, 2000.

[186] M. Oh, L. Rohlin, K. Kao, and J. Liao. Global expression profiling of acetate grown *Escherichia coli*. *J. Biol. Chem.*, 277:13175–83, 2002.

[187] M.-K. Oh and J. Liao. Gene expression profiling by DNA microarrays and metabolic fluxes in *Escherichia coli*. *Biotechnol. Prog.*, 16:278–86, 2000.

[188] Z. Oltvai and A.-L. Barabási. Life's complexity pyramid. *Science*, 298:763–64, 2002.

[189] S. Panda, J. Hogenesch, and S. Kay. Circadian rhythms from flies to human. *Nature*, 417:329–35, 2002.

[190] J. Papin, N. Price, J. Edwards, and B. Palsson. The genome-scale metabolic extreme pathway structure in *Haemophilus influenzae* shows significant network redundancy. *J. theor. Biol.*, 215:67–82, 2002.

[191] J. Paulsson, O. Berg, and M. Ehrenberg. Stochastic focusing: fluctuation-enhanced sensitivity of intracellular regulation. *Proc. Natl. Acad. Sci. U.S.A.*, 97(13):7148–53, 2000.

[192] G. Pereira, C. Manson, J. Grindlay, and E. Schiebel. Regulation of the Bfa1p-Bub2 complex at the spindle pole bodies by the cell cycle phosphatase Cdc14p. *J. Cell Biol.*, 157:367–79, 2002.

[193] G. Perkins, L. Drury, and J. Diffley. Separate SCF^{CDC4} recognition elements target Cdc6 for proteolysis in S phase and mitosis. *EMBO J.*, 20(17):4836–45, 2001.

[194] B. Petersen, C. Wagener, F. Marinoni, E. Kramer, M. Melixetian, E. Denchi, C. Gieffers, C. Matteucci, J.-M. Peters, and K. Helin. Cell cycle and cell growth- regulated proteolysis of mammalian CDC6 is dependent on APC-CDH1. *Genes Dev.*, 14:2330–43, 2000.

[195] T. Pfeiffer, S. Schuster, and S. Bonhoeffer. Cooperation and competition in the evolution of ATP-producing pathways. *Science*, 292:504–07, 2001.

[196] C. Pfleger and M. Kirschner. The KEN box: an APC recognition signal distinct from the D box targeted by Cdh1. *Genes Dev.*, 14:655–65, 2000.

[197] A. Pic, F.-L. Lim, S. Ross, E. Veal, A. Johnson, M. Sutlan, A. West, L. Johnston, A. Sharrocks, and B. Morgan. The forkhead protein Fkh2 is a component of the yeast cell cycle transcription factor SFF. *EMBO J.*, 19(14):3750–61, 2000.

[198] T. Pramila, S. Miles, D. GuhaThakurta, D. Jemiolo, and L. Breeden. Conserved homeodomain proteins interact with MADS box protein Mcm1 to restrict ECB-dependent transcription to the M/G1 phase of the cell cycle. *Genes Dev.*, 16:3034–3045, 2002.

[199] J. Price, J. Blau, A. Rothenfluh, M. Abodeely, B. Kloss, and M. Young. double-time is a novel *Drosophila* clock gene that regulates PERIOD protein accumulation. *Cell*, 94:83–95, 1998.

[200] N. Price, J. Papin, and B. Palsson. Determination of redundancy and systems properties of the metabolic network of *Helicobacter pylori* using genome-scale extreme pathway analysis. *Genome Res.*, 12:760–69, 2002.

[201] S. Prinz, E. Hwang, R. Visintin, and A. Amon. The regulation of Cdc20 proteolysis reveals a role for the APC components Cdc23 and Cdc27 during S phase and early mitosis. *Curr. Biol.*, 8:750–60, 1998.

[202] C. Rao, D. Wolf, and A. Arkin. Control, exploitation and tolerance of intracellular noise. *Nature*, 420:231–37, 2002.

[203] E. Ravasz, A. Somera, D. Mongru, Z. Oltvai, and A.-L. Barabási. Hierarchical organization of modularity in metabolic networks. *Science*, 297:1551–55, 2002.

[204] I. Rechenberg. The evolution strategy – a mathematical model of Darwinian evolution. In E. Frehland, editor, *Synergistics – From microscopic to macroscopic order*, pages 122–32. Springer, Berlin-Heidelberg, 1984.

[205] J. Reed, T. Vo, C. Schilling, and B. Palsson. An expanded genome-scale model of *Escherichia* coli K-12 (iJR904 GSM/GPR). *Genome Biol.*, 4:R54, 2003.

[206] A. Rettinger. Parameteroptimierung mittels Evolutionsstrategien. Studienarbeit, Universität Stuttgart, 1995.

[207] D. Reynolds, B. Shi, C. McLean, F. Katsis, B. Kemp, and S. Dalton. Recruitment of Thr-319 phosphorylated Ndd1p to the FHA domain of Fkh2p requires Clb kinase activity: a mechanism for CLB cluster gene activation. *Genes Dev.*, 17:1789–802, 2003.

[208] A. Rives and T. Galitski. Modular organization of cellular networks. *Proc. Natl. Acad. Sci. U.S.A.*, 100(3):1128–33, 2003.

[209] C. Robert, J. Carlson, and J. Doyle. Highly optimized tolerance in epidemic models incorporating local optimization and regrowth. *Phys. Rev. E*, 63:056122, 2001.

[210] R. Rockafellar. *Convex Analysis*. University Press, Princeton, 1970.

[211] J. Rohwer and F. Botha. Analysis of sucrose accumulation in sugar cane culm on the basis of *in vitro* kinetic data. *Biochem. J.*, 358:437–45, 2001.

[212] J. Rohwer, S. Schuster, and H. Westerhoff. How to recognize monofunctional units in a metabolic system. *J. theor. Biol.*, 179:213–28, 1996.

[213] A. Rudner, K. Hardwick, and A. Murray. Cdc28 activates exit from mitosis in budding yeast. *J. Cell Biol.*, 149(7):1361–76, 2000.

[214] A. Rudner and A. Murray. Phosphorylation by Cdc28 activates the Cdc20-dependent activity of the anaphase-promoting complex. *J. Cell Biol.*, 149(7):1377–90, 2000.

[215] N. Sabnis, H. Yang, and T. Romeo. Pleiotropic regulation of central carbohydrate metabolism in *Escherichia coli* via the gene *crsA*. *J. Biol. Chem.*, 270:29096–104, 1995.

[216] A. Sachs and S. Buratowski. Common themes in translational and transcriptional regulation. *Trends Biochem. Sci.*, 22:189–92, 1997.

[217] A. Saltelli. What is sensitivity analysis? In A. Saltelli, K. Chan, and E. Scott, editors, *Sensitivity analysis*, chapter 1, pages 3–13. John Wiley & Sons, Ltd., Chichester, UK, 2000.

[218] M. Savageau. Parameter sensitivity as a criterion for evaluating and comparing the performance of biochemical systems. *Nature*, 229:542–44, 1971.

[219] M. Savageau. The behavior of intact biochemical control systems. *Curr. Topics Cellular Regulation*, 6:63–130, 1972.

[220] M. Savageau. Comparison of classical and autogenous systems of regulation in inducible operons. *Nature*, 252:546–49, 1974.

[221] T. Scheper, D. Klinkenberg, C. Pennartz, and J. van Pelt. A mathematical model for the intracellular rhythm generator. *J. Neurosci.*, 19:40–47, 1999.

[222] C. Schilling, J. Edwards, D. Letscher, and B. Palsson. Combining pathway analysis with flux balance analysis for the comprehensive study of metabolic systems. *Biotechnol. Bioeng.*, 71:286–306, 2000/2001.

[223] C. Schilling, D. Letscher, and B. Palsson. Theory for the systemic definition of metabolic pathways and their use in interpreting metabolic function from a pathway-oriented perspective. *J. theor. Biol.*, 203:229–48, 2000.

[224] C. Schilling and B. Palsson. The underlying pathway structure of biochemical reaction networks. *Proc. Natl. Acad. Sci. U.S.A.*, 95:4193–98, 1998.

[225] R. Schneider, C. Posten, and A. Munack. Application of linear balance equations in an on-line observation system for fermentation processes. In *Proc. IFAC Modeling and Control of Biotechnical Processes*, pages 319–22, Colorado, USA, 1992.

[226] S. Schuster, T. Dandekar, and D. Fell. Detection of elementary flux modes in biochemical networks: a promising tool for pathway analysis and metabolic engineering. *Trends Biotechnol.*, 17:53–60, 1999.

[227] S. Schuster, D. Fell, and T. Dandekar. A general definition of metabolic pathways useful for systematic organization and analysis of complex metabolic networks. *Nat. Biotechnol.*, 18:326–32, 2000.

[228] S. Schuster and C. Hilgetag. On elementary flux modes in biochemical reaction systems at steady state. *J. Biol. Syst.*, 2:165–82, 1994.

[229] S. Schuster, B. Kholodenko, and H. Westerhoff. Cellular information transfer regarded from a stoichiometry and control analysis perspective. *Biosystems*, 55(1-3):73–81, 2000.

[230] M. Schwab, M. Neutzner, D. Möcker, and W. Seufert. Yeast Hct1 recognizes the mitotic cyclin Clb2 and other substrates of the ubiquitin ligase APC. *EMBO J.*, 20(18):5165–75, 2001.

[231] M. Schwab, A. Schulze-Lutum, and W. Seufert. Yeast Hct1 is a regulator of Clb2 cyclin proteolysis. *Cell*, 90(4):683–93, 1997.

[232] E. Schwob, T. Böhm, M. Mendenhall, and K. Nasmyth. The B-type cyclin kinase inhibitor $p40^{SIC1}$ controls the G1 to S transition in *S. cerevisiae*. *Cell*, 79:233–44, 1994.

[233] A. Sengupta, M. Djordjevic, and B. Shraiman. Specificity and robustness in transcription control networks. *Proc. Natl. Acad. Sci. U.S.A.*, 99(4):2072–77, 2002.

[234] B. Shapiro, A. Levchenko, and E. Mjolsness. Automatic model generation for signal transduction with applications to MAP-kinase pathways. In *Proc. 1st Intl. Conf. Systems Biol.*, pages 64–74, Tokyo, 2000.

[235] S. Shen-Orr, R. Milo, S. Mangan, and U. Alon. Network motifs in the transcriptional regulation network of *Escherichia coli*. *Nat. Genet.*, 31(1):64–68, 2002.

[236] M. Shirayama, A. Tóth, M. Gálová, and K. Nasmyth. APC^{Cdc20} promotes exit from mitosis by destroying the anaphase inhibitor Pds1 and cyclin Clb5. *Nature*, 402:203–207, 1999.

[237] M. Shirayama, W. Zachariae, R. Ciosk, and K. Nasmyth. The Polo-like kinase Cdc5p and the WD-repeat protein Cdc20p/fizzy are regulators and substrates of the anaphase promoting complex in *Saccharomyces cerevisiae*. *EMBO J.*, 17(5):1336–49, 1998.

[238] W. Shou, R. Azzam, S. Chen, M. Huddleston, C. Baskerville, H. Charbonneau, R. Annan, and R. Deshaies. Cdc5 influences phosphorylation of Net1 and disassembly of the RENT complex. *BMC Mol. Biol.*, 3(1):3, 2002.

[239] W. Shou, J. Seol, A. Shevchenko, C. Baskerville, D. Moazed, Z. Chen, J. Jang, A. Shevchenko, H. Charbonneau, and R. Deshaies. Exit from mitosis is triggered by Tem1-dependent release of the protein phosphatase Cdc14 from the nucleolar RENT complex. *Cell*, 97:233–44, 1999.

[240] I. Simon, J. Barnett, N. Hannett, C. Harbison, N. Rinaldi, T. Volkert, J. Wyrick, J. Zeitlinger, D. Gifford, T. Jaakkola, and R. Young. Serial regulation of transcriptional regulators in the yeast cell cycle. *Cell*, 106:697–708, 2001.

[241] M. Singer, W. Walter, B. Cali, B. Rouviere, H. Liebke, R. Gourse, and C. Gross. Physiological effects of the fructose-1,6-diphosphate aldolase ts8 mutation on stable RNA synthesis in *Escherichia coli*. *J. Bacteriol.*, 173:6249–57, 1991.

[242] D. Skowyra, K. Craig, M. Tyers, S. Elledge, and J. Harper. F-box proteins are receptors that recruit phosphorylated substrates to the SCF ubiquitin-ligase complex. *Cell*, 91:209–19, 1997.

[243] P. Smolen, D. Baxter, and J. Byrne. Modeling circadian oscillations with interlocking positive and negative feedback loops. *J. Neurosc.*, 21:6644–56, 2001.

[244] P. Smolen, D. Baxter, and J. Byrne. A reduced model clarifies the role of feedback loops and time delays in the *Drosophila* circadian oscillator. *Biophys. J.*, 83:2349–59, 2002.

[245] E. Sontag. For differential equations with r parameters, 2r+1 experiments are enough for identification. *J. Nonlinear Sci.*, 12:553–83, 2002.

[246] P. Spellman, G. Sherlock, M. Zhang, V. Iyer, K. Anders, M. Eisen, P. Brown, D. Botstein, and B. Futcher. Comprehensive identification of cell-cycle regulated genes of the yeast *Saccharomyces cerevisiae* by microarray hybridization. *Mol. Biol. Cell*, 9:3273–97, 1998.

[247] F. Stegmeier, R. Visintin, and A. Amon. Separase, polo kinase, the kinetochore protein Slk19, and Spo12 function in a network that controls Cdc14 localization during early anaphase. *Cell*, 108:207–220, 2002.

[248] J. Stelling, A. Kremling, M. Ginkel, K. Bettenbrock, and E. Gilles. Towards a Virtual Biological Laboratory. In H. Kitano, editor, *Foundations of Systems Biology*, pages 189–212. MIT Press, Cambridge, MA, 2001.

[249] S. Strogatz. Exploring complex networks. *Nature*, 410:268–76, 2001.

[250] U. Surana, A. Amon, C. Dowzer, J. McGrew, B. Byers, and K. Nasmyth. Destruction of the CDC28/CLB mitotic kinase is not required for the metaphase to anaphase transition in budding yeast. *EMBO J.*, 12(5):1969–78, 1993.

[251] G. Taylor, Y. Liu, C. Baskerville, and H. Charbonneau. The activity of Cdc14p, an oligomeric dual specificity protein phosphatase from *Saccharomyces cerevisiae*, is required for cell cycle progression. *J. Biol. Chem.*, 272(38):24054–63, 1997.

[252] I. Taylor, P. McIntosh, P. Pala, M. Treiber, S. Howell, A. Lane, and S. Smerdon. Characterization of the DNA-binding domains from the yeast cell-cycle transcription factors Mbp1 and Swi4. *Biochemistry*, 39:3943–54, 2000.

[253] B. ter Kuile and H. Westerhoff. Transcriptome meets metabolome: hierarchical and metabolic regulation of the glycolytic pathway. *FEBS Lett.*, 500:169–71, 2001.

[254] M. Thattai and A. van Oudenaarden. Intrinsic noise in gene regulatory networks. *Proc. Natl. Acad. Sci. U.S.A.*, 98(15):8614–19, 2001.

[255] A. Tong, M. Evangelista, A. Parsons, H. Xu, G. Bader, N. Pagé, M. Robinson, S. Rhagibizadeh, C. Hogue, H. Bussey, B. Andrews, M. Tyers, and C. Boone. Systematic genetic analysis with ordered arrays of yeast deletion mutants. *Science*, 294:2364–68, 2001.

[256] J. Toyn, A. Johnson, J. Conovan, W. Toone, and L. Johnston. The Swi5 transcription factor of *Saccharomyces cerevisiae* has a role in exit from mitosis through induction of the cdk-inhibitor Sic1 in telophase. *Genetics*, 145(1):85–96, 1997.

[257] J. Toyn and L. Johnston. The Dbf2 and Dbf20 protein kinases of budding yeast are activated after the metaphase to anaphase cell cycle transition. *EMBO J.*, 13(5):1103–13, 1994.

[258] E. Traverso, C. Baskerville, H. Liu, W. Shou, P. James, R. Deshaies, and H. Charbonneau. Characterization of the Net1 cell-cycle dependent regulator of the Cdc14 phosphatase from budding yeast. *J. Biol. Chem.*, 276(24):21924–31, 2001.

[259] T. Turányi and H. Rabitz. Local methods. In A. Saltelli, K. Chan, and E. Scott, editors, *Sensitivity analysis*, chapter 5, pages 81–100. John Wiley & Sons, Ltd., Chichester, UK, 2000.

[260] J. Tyson, C. Hong, D. Thron, and B. Novak. A simple model of circadian rhythms based on dimerization and proteolysis of PER and TIM. *Biophys. J.*, 77:2411–17, 1999.

[261] H. Ueda, M. Hagiwara, and H. Kitano. Robust oscillations within the interlocked feedback model of *Drosophila* circadian rhythm. *J. theor. Biol.*, 210:401–06, 2001.

[262] A. van der Gugten and H. Westerhoff. Internal regulation of a modular system: the different faces of internal control. *BioSystems*, 44:79–106, 1997.

[263] M. van der Rest, C. Frank, and D. Molebaar. Functions of the membrane-associated and cytoplasmic malate dehydrogenases in the citric acid cycle of *Escherichia coli*. *J. Bacteriol.*, 182:6892–99, 2000.

[264] A. Varma and B. Palsson. Metabolic flux balancing: basic concepts, scientific and practical use. *Biotechnol. Bioeng.*, 12:994–98, 1993.

[265] R. Verma, R. Annan, M. Huddleston, S. Carr, G. Reynard, and R. Deshaies. Phosphorylation of Sic1p by G_1 Cdk required for its degradation and entry into S phase. *Science*, 278(5337):455–60, 1997.

[266] R. Verma, H. McDonald, J. Yates, and R. Deshaies. Selective degradation of ubiquitinated Sic1 by purified 26S proteasome yields active S phase Cyclin-Cdk. *Molec. Cell.*, 8:439–48, 2001.

[267] J. Vilar, H. Kueh, N. Barkai, and S. Leibler. Mechanisms of noise-resistance in genetic oscillators. *Proc. Natl. Acad. Sci. U.S.A.*, 99(9):5988–92, 2002.

[268] R. Visintin, K. Craig, E. Hwang, S. Prinz, M. Tyers, and A. Amon. The phosphatase Cdc14 triggers mitotic exit by reversal of Cdk-dependent phosphorylation. *Mol. Cell*, 2:709–18, 1998.

[269] R. Visintin, E. Hwang, and A. Amon. Cfi1 prevents premature exit form mitosis by anchoring Cdc14 phosphatase in the nucleolus. *Nature*, 398:818–23, 1999.

[270] R. Visintin, S. Prinz, and A. Amon. CDC20 and CDH1: A family of substrate-specific activators of APC-dependent proteolysis. *Science*, 278(5337):460–63, 1997.

[271] R. Visintin, F. Stegmeier, and A. Amon. The role of the polo kinase Cdc5 in controlling Cdc14 localization. *Mol. Biol. Cell*, 14:4486–96, 2003.

[272] G. von Dassow, E. Meir, E. Munro, and G. Odell. The segment polarity network is a robust developmental module. *Nature*, 406:188–92, 2000.

[273] A. Wagner. Robustness against mutations in genetic networks of yeast. *Nat. Genetics*, 24:355–61, 2000.

[274] X. Wang and G. Chen. Pinning control of scale-free dynamical networks. *Physica A*, 310:521–31, 2002.

[275] G. Weng, U. Bhalla, and R. Iyengar. Complexity in biological signaling systems. *Science*, 284:92–96, 1999.

[276] J. Willems. Models for dynamics. *Dynamics Reported*, 2:171–269, 1989.

[277] J. Willems. Paradigms and puzzles in the theory of dynamical systems. *IEEE Transac. Automat. Control*, 36(3):259–94, 1991.

[278] J. Williams and A. Sehgal. Molecular components of the circadian system in *Drosophila*. *Annu. Rev. Physiol.*, 63:129–55, 2001.

[279] E. Winzeler, D. Shoemaker, A. Astromoff, H. Liang, K. Anderson, B. Andre, R. Bangham, R. Benito, J. Boeke, H. Bussey, A. Chu, C. Connelly, K. Davis, F. Dietrich, S. Dow, M. E. Bakkoury, F. Foury, S. Friend, E. Gentalen, G. Giaever, J. Hegemann, T. Jones, M. Laub, H. Liao, R. Davis, and *et al.* Functional characterization of the *S. cerevisiae* genome by gene deletion and parallel analysis. *Science*, 285:901–06, 1999.

[280] R. Wäsch and F. Cross. APC-dependent proteolysis of the mitotic cyclin Clb2 is essential for mitotic exit. *Nature*, 418:556–62, 2002.

[281] E. Yeh, R. Skibbens, J. Cheng, E. Salmon, and K. Bloom. Spindle dynamics and cell cycle regulation of dynein in the budding yeast *Saccharomyces cerevisiae*. *J. Cell Biol.*, 130(3):687–700, 1995.

[282] F. Yeong, H. Lim, C. Padmashree, and U. Surana. Exit from mitosis in budding yeast: biphasic inactivation of the Cdc28-Clb2 mitotic kinase and the role of Cdc20. *Mol. Cell*, 5:501–11, 2000.

[283] F. Yeong, J. Lim, Y. Wang, and U. Surana. Early expressed Clb proteins allow accumulation of mitotic cyclin by inactivating proteolytic machinery during S phase. *Mol. Cell. Biol.*, 21(15):5071–81, 2001.

[284] T.-M. Yi, Y. Huang, M. Simon, and J. Doyle. Robust perfect adaptation in bacterial chemotaxis through integral feedback control. *Proc. Natl. Acad. Sci. U.S.A.*, 97(9):4649–53, 2000.

[285] S. Yoshida, K. Asakawa, and A. Toh-e. Mitotic exit network controls the localization of Cdc14 to the spindle pole body in *Saccharomyces cerevisiae*. *Curr. Biol.*, 12(11):944–50, 2002.

[286] S. Yoshida and A. Toh-e. Budding yeast Cdc5 phosphorylates Net1 and assists Cdc14 release from the nucleolus. *Biochem. Biophys. Res. Commun.*, 294(3):687–91, 2002.

[287] M. Young and S. Kay. Time zones: a comparative genetics of circadian clocks. *Nat. Rev. Genet.*, 2:702–15, 2001.

[288] H. Yu. Regulation of APC-Cdc20 by the spindle checkpoint. *Curr. Opin. Cell Biol.*, 14:706–14, 2002.

[289] M. Yuste-Rojas and F. Cross. Mutations in *CDC14* result in high sensitivity to cyclin gene dosage in *Saccharomyces cerevisiae*. *Mol. Gen. Genet.*, 263:60–72, 2000.

[290] W. Zachariae and K. Nasmyth. Whose end is destruction: cell division and the anaphase-promoting complex. *Genes Dev.*, 13:2039–58, 1999.

[291] W. Zachariae, M. Schwab, K. Nasmyth, and W. Seufert. Control of cyclin ubiquination by CDK-regulated binding of Hct1 to the anaphase promoting complex. *Science*, 282:1721–24, 1998.

[292] D. Zak, F. Doyle, D. Vlachos, and J. Schwaber. Stochastic kinetic analysis of transcriptional feedback models for circadian rhythms. In *Proc. 40th IEEE Conference on Decision and Control*, pages 849–54, 2001.

[293] K. Zhou, J. Doyle, and K. Glover. *Robust and optimal control*. Prentice-Hall, Englewood Cliffs, N.J., 1996.

[294] T. Zhou, J. Carlson, and J. Doyle. Mutation, specialization, and hypersensitivity in highly optimized tolerance. *Proc. Natl. Acad. Sci. U.S.A.*, 99:2049–54, 2002.

[295] G. Zhu, P. Spellman, T. Volpe, P. Brown, D. Botstein, T. Davis, and B. Futcher. Two yeast forkhead genes regulate the cell cycle and pseudohyphal growth. *Nature*, 406:90–94, 2000.

A. *E. COLI*: STOICHIOMETRIC MODEL AND EXPERIMENTAL DATA

Tab. A.1: Network structure for *E. coli* central metabolism. Oxidized reduction equivalents (NAD, NADP) and ADP were ommitted for simplicity.

Identifier	Stoichiometry / reversibility	Gene	Enzyme / reaction description
Substrate uptake:			
Glc_PTS_up	PEP → G6P + Pyr	ptsG	PTS system, glucose-specific IIBC component
Glc_ATP_up	ATP → G6P	glk	glucokinase
Succ_up	→ Succ		Succinate uptake
Glyc_up	→ Glyc		Glycerol uptake
O2_up	→ O2		Oxygen uptake
N_up	→ N		Nitrogen (ammonia) uptake
S_up	4 ATP + 4 NADPH → S		Sulfur (SO4) uptake
Ac_up	→ Ac		Acetate uptake
Central carbon metabolism:			
G6P::F6P	G6P ↔ F6P	pgi	glucosephosphate isomerase
F16P::F6P	F16P → F6P	fbp	fructose-bisphosphatase
F6P::F16P	F6P + ATP → F16P	pfkA	6-phosphofructokinase I
F16P::T3P	F16P ↔ DHAP + G3P	fba	fructose-bisphosphate aldolase, class II
DHAP::G3P	DHAP ↔ G3P	tpiA	triosephosphate isomerase
G3P::DPG	G3P ↔ DPG + NADH	gapA	glyceraldehyde-3-phosphate dehydrogenase A
DPG::3PG	DPG ↔ 3PG + ATP	pgk	phosphoglycerate kinase
3PG::2PG	3PG ↔ 2PG	gpmA	phosphoglyceromutase 1
2PG::PEP	2PG ↔ PEP	eno	Enolase
PEP::PYR	PEP → Pyr + ATP	pykAF	pyruvate kinase I / II
Pyr::PEP	Pyr + 2 ATP → PEP	ppsA	phosphoenolpyruvate synthase
PYR::AcCoA	Pyr → AcCoA + NADH + CO2	aceEF	pyruvate dehydrogenase
AcCoA::Cit	AcCoA + OxA → Cit	gltA	citrate synthase
Cit::Icit	Cit ↔ ICit	acnB	aconitate hydrase B
ICit::alKG	ICit ↔ alKG + NADPH + CO2	icdA	isocitrate dehydrogenase, specific for NADP+

Identifier	Stoichiometry / reversibility	Gene	Enzyme / reaction description
alKG::SuccCoA	alKG → SuccCoA + NADH + CO2	sucAB	2-oxoglutarate dehydrogenase
SuccCoA::Succ	SuccCoA ↔ Succ + ATP	sucCD	succinyl-CoA synthetase
Succ::Fum	Succ → Fum + QuiH2	sdhC	succinate dehydrogenase, cytochrome b556
Fum::Succ	Fum + QuiH2 → Succ	frdA	fumarate reductase, anaerobic
Fum::Mal	Fum ↔ Mal	fumA	fumarase A ; aerobic isozyme
Mal::OxA	Mal ↔ OxA + NADH	mdh	malate dehydrogenase
ICit::Glyox	ICit → Succ + Glyox	aceA	isocitrate lyase
Glyox::Mal	AcCoA + Glyox → Mal	glcB	malate synthase G
G6P::PGlac	G6P ↔ PGlac + NADPH	zwf	glucose-6-phosphate dehydrogenase
AcCoA::Adh	AcCoA + NADH ↔ Adh	adhE	CoA-linked acetaldehyde dehydrogenase
Adh::Eth	Adh + NADH ↔ Eth	adhE	CoA-linked acetaldehyde dehydrogenase
PGluc::Rl5P	PGluc → Rl5P + NADPH + CO2	gnd	Gluconate-6-phosphate dehydrogenase, decarboxylating
Rl5P::X5P	Rl5P ↔ X5P	rpe	D-ribulose-5-phosphate 3-epimerase
Rl5P::R5P	Rl5P ↔ R5P	rpiA	ribosephosphate isomerase, constitutive
Transket1	R5P + X5P ↔ G3P + S7P	tktAB	transketolase 1 / 2 isozyme
Transaldo	G3P + S7P ↔ F6P + E4P	talB	transaldolase B
Transket2	E4P + X5P ↔ F6P + G3P	tktAB	transketolase 1 / 2 isozyme
OxA::PEP	OxA + ATP → PEP + CO2	pckA	phosphoenolpyruvate carboxykinase
PEP::OxA	PEP + CO2 → OxA	ppc	phosphoenolpyruvate carboxylase
AcCoA::AcP	AcCoA ↔ AcP	pta	Phosphotransacetylase
AcP::Ac	AcP ↔ ATP + Ac	ackA	acetate kinase
Pyr::Form	Pyr → AcCoA + Form	pflB	formate acetyltransferase 1
Pyr::Lac	Pyr + NADH ↔ Lac	ldhA	fermentative D-lactate dehydrogenase, NAD-dependent
Glyc::Glyc3P	ATP + Glyc → Glyc3P	glpK	glycerol kinase
Mal::Pyr	Mal → Pyr + NADH + CO2	sfcA	NAD-linked malate dehydrogenase (malic enzyme)
Glyc3P::DHAP	Glyc3P → DHAP + QuiH2	glpD	sn-glycerol-3-phosphate dehydrogenase (aerobic)
DHAP::Glyc3P	DHAP + NADH → Glyc3P	gpsA	glycerol-3-phosphate dehydrogenase (NAD+)

Identifier	Stoichiometry / reversibility	Gene	Enzyme / reaction description
Pyr::Ac	Pyr → QuiH2 + CO2 + Ac	poxB	pyruvate oxidase
Ac::AcCoA	2 ATP + Ac → AcCoA	acs	acetyl-CoA synthetase
Energy and reduction equivalents:			
NADHDehydro	NADH ↔ QuiH2 + 2 H_ex	nuo	NADH dehydrogenase I
Oxidase	QuiH2 + 0.5 O2 → 2 H_ex	cyd	cytochrome d terminal oxidase
TransHydro	NADH + H_ex ↔ NADPH	pntA	pyridine nucleotide transhydrogenase, alpha subunit
ATPSynth	3 H_ex ↔ ATP	atp	membrane-bound ATP synthase
ATPdrain	ATP →		Surplus ATP production
Monomer and precursor synthesis:			
Chor_Synth	2 PEP + E4P + ATP + NADPH → Chor		Chorismate synthesis
PRPP_Synth	R5P + 2 ATP → PRPP		5-Phosphoribosyl-1-pyrophosphate synthesis
MTHF_Synth	ATP + NADPH ↔ MTHF		5-10-Methylen-tetrahydrofolate synthesis
Ala_Synth	Pyr + Glu → alKG + Ala		Alanine synthesis
Val_Synth	2 Pyr + NADPH + Glu → alKG + CO2 + Val		Valine synthesis
Leu_Synth	2 Pyr + AcCoA + NADPH + Glu → alKG + NADH + 2 CO2 + Leu		Leucine synthesis
Asn_Synth	2 ATP + N + Asp → Asn	asnA	asparagine synthetase A
Asp_synth	OxA + Glu → alKG + Asp	aspC	aspartate aminotransferase
Asp::Fum	Asp → Fum + N	aspA	aspartate ammonia-lyase (aspartase)
Asp::AspSAld	ATP + NADPH + Asp → AspSAld		Aspartatesemialdehyde synthesis
AspSAld::HSer	NADPH + AspSAld → HSer		Homoserine synthesis
Lys_Synth	di_am_pim → CO2 + Lys		Lysine synthesis
Met_Synth	SuccCoA + MTHF + HSer + Cys → Pyr + Succ + N + Met		Methionine synthesis
Thr_Synth	ATP + HSer → Thr		Threonine synthesis
Ile_Synth	Pyr + NADPH + Glu + Thr → alKG + CO2 + N + Ile		Isoleucine synthesis
His_Synth	ATP + PRPP + Gln → alKG + 2 NADH + His		Histidine synthesis
Glu_synth	alKG + NADPH + N → Glu	gdhA	NADP-specific glutamate dehydrogenase
Gln_Synth	ATP + N + Glu → Gln	glnA	Glutamine synthetase
Pro_Synth	ATP + 2 NADPH + Glu → Pro		Proline synthesis

Identifier	Stoichiometry / reversibility	Gene	Enzyme / reaction description
Arg_Synth	AcCoA + 4 ATP + NADPH + CO2 + N + Asp + 2 Glu → alKG + Fum + Ac + Arg		Arginine synthesis
Trp_Synth	Chor + PRPP + Gln + Ser → G3P + Pyr + CO2 + Glu + Trp		Tryptophan synthesis
Tyr_Synth	Chor + Glu → alKG + NADH + CO2 + Tyr		Tyrosine synthesis
Phe_Synth	Chor + Glu → alKG + CO2 + Phe		Phenylalanine synthesis
Ser_Synth	3PG + Glu → alKG + NADH + Ser		Serine synthesis
Gly_Synth	Ser → MTHF + Gly		Glycine synthesis
Cys_Synth	AcCoA + S + Ser → Ac + Cys		Cysteine synthesis
rATP_Synth	5 ATP + CO2 + PRPP + 2 MTHF + 2 Asp + Gly + 2 Gln → 2 Fum + NADPH + 2 Glu + rATP		Synthesis of ATP for RNA
rGTP_Synth	6 ATP + CO2 + PRPP + 2 MTHF + Asp + Gly + 3 Gln → 2 Fum + NADH + NADPH + 3 Glu + rGTP		Synthesis of GTP for RNA
rCTP_Synth	ATP + Gln + rUTP → Glu + rCTP		Synthesis of CTP for RNA
rUTP_Synth	4 ATP + N + PRPP + Asp → NADH + rUTP		Synthesis of UTP for RNA
dATP_Synth	NADPH + rATP → dATP		Synthesis of ATP for DNA
dGTP_Synth	NADPH + rGTP → dGTP		Synthesis of GTP for DNA
dCTP_Synth	NADPH + rCTP → dCTP		Synthesis of CTP for DNA
dTTP_Synth	2 NADPH + MTHF + rUTP → dTTP		Synthesis of TTP for DNA
mit_FS_Synth	8.24 AcCoA + 7.24 ATP + 13.91 NADPH → mit_FS		Average fatty acid synthesis
UDPGlc_Synth	G6P + ATP → UDPGlc		UDP-glucose synthesis
CDPEth_Synth	3PG + 3 ATP + NADPH + N → NADH + CDPEth		CDP-ethanolamine synthesis
OH_myr_ac_Synth	7 AcCoA + 6 ATP + 11 NADPH → OH_myr_ac		Hydroxy-myristoic-acid synthesis
C14_0_FS_Synth	7 AcCoA + 6 ATP + 12 NADPH → C14_0_FS		Synthesis of C(14:0) fatty acid
CMP_KDO_Synth	PEP + R5P + 2 ATP → CMP_KDO		CMP-2-keto-3-deoxy octonic acid synthesis
NDPHep_Synth	1.5 G6P + ATP → 4 NADPH + NDPHep		NDP-heptose synthesis
TDPGlcs_Synth	F6P + 2 ATP + N → TDPGlcs		TDP-glucosamine synthesis

Identifier	Stoichiometry / reversibility	Gene	Enzyme / reaction description
UDP_NAG_Synth	F6P + AcCoA + ATP + Gln → Glu + UDP_NAG		UDP-N-acetylglucosamine synthesis
UDP_NAM_Synth	PEP + NADPH + UDP_NAG → UDP_NAM		UDP-N-acetylmuramine synthesis
di_am_pim_Synth	Pyr + SuccCoA + NADPH + Asp-SAld + Glu → alKG + Succ + di_am_pim		Diaminopimelate synthesis
ADPGlc_Synth	G6P + ATP → ADPGlc		Glycogen monomer synthesis
Polymer synthesis (mmol metabolite / g polymer), stoichiometry according to [264]:			
Prot_Synth	39.9455 ATP + 0.88727 Ala + 0.15818 Cys + 0.41636 Asp + 0.45455 Glu + 0.32 Phe + 1.0582 Gly + 0.16364 His + 0.50182 Ile + 0.59273 Lys + 0.77818 Leu + 0.26546 Met + 0.41636 Asn + 0.38182 Pro + 0.45455 Gln + 0.51091 Arg + 0.37273 Ser + 0.43818 Thr + 0.73091 Val + 0.09818 Trp + 0.23818 Tyr → Prot		Protein synthesis
RNA_Synth	1.2488 ATP + 0.80488 rATP + 0.99024 rGTP + 0.61436 rCTP + 0.66341 rUTP → RNA		RNA synthesis
DNA_Synth	4.4129 ATP + 0.7968 dATP + 0.8194 dGTP + 0.8194 dCTP + 0.7968 dTTP → DNA		DNA synthesis
Lip_Synth	1.4176 Glyc3P + 2.8352 ATP + 1.4176 Ser + 2.8352 mit_FS → Lip		Lipid synthesis
LPS_Synth	0.46176 UDPGlc + 0.69118 CDPEth + 0.69118 OH_myr_ac + 0.69118 C14_0_FS + 0.69118 CMP_KDO + 0.69118 NDPHep + 0.46176 TDPGlcs → LPS		Lipopolysaccharide synthesis
PepGly_Synth	5.52 ATP + 2.208 Ala + 1.104 Glu + 1.104 UDP_NAG + 1.104 UDP_NAM + 1.104 di_am_pim → PepGly		Peptidoglycan synthesis
Glyc_Synth	6.16 ADPGlc → Glyc		Glycogen synthesis

Identifier	Stoichiometry / reversibility	Gene	Enzyme / reaction description
Biomass production (g polymer / g biomass), stoichiometry for scenario 1, Tab. 3.1:			
Mue	0.64 Prot + 0.185 RNA + 0.03 DNA + 0.1 Lip + 0.015 LPS + 0.015 PepGly + 0.015 Glyc → Biomass		Biomass production
By-product excretion:			
CO2_ex	CO2 ↔		Carbon dioxide exchange
Lac_ex	Lac →		Lactate excretion
Eth_ex	Eth →	AdhE	CoA-linked acetaldehyde dehydrogenase
Ac_ex	Ac →		Acetate excretion
Form_ex	Form →	FdhF	formate dehydrogenase

Tab. A.2: Abbreviations for metabolites and cellular compounds.

Abbreviation	Compound	Abbreviation	Compound
G6P	Glucose-6-phosphate	PRPP	5-Phosphoribosyl-1-pyrophosphate
F6P	Fructose-6-phosphate	MTHF	5-10-Methylen-tetrahydrofolate
F16P	Fructose-1,6-bisphosphate	AspSAld	Aspartate-4-semialdehyde
DHAP	Dihydroxyacetone-phosphate	HSer	Homoserine
Glyc3P	Glycerol-3-phosphate	Ala	Alanine
G3P	Glyceraldehyde-3-phosphate	Cys	Cysteine
DPG	Diphosphoglycerate	Asp	Aspartate
3PG	3-Phosphoglycerate	Glu	Glutamate
2PG	2-Phosphoglycerate	Phe	Phenylalanine
PEP	Phosphoenolpyruvate	Gly	Glycine
Pyr	Pyruvate	His	Histidine
AcCoA	AcetylCoA	Ile	Isoleucine
Cit	Citrate	Lys	Lysine
ICit	Iso-Citrate	Leu	Leucine
alKG	alpha-Ketoglutarate	Met	Methionine
SuccCoA	Succinyl-CoA	Asn	Asparagine
Succ	Succinate	Pro	Proline
Fum	Fumarate	Gln	Glutamine
Mal	Malate	Arg	Arginine
OxA	Oxaloacetate	Ser	Serine
Glyox	Glyoxylate	Thr	Threonine
R5P	Ribose-5-phosphate	Val	Valine
Rl5P	Ribulose-5-phosphate	Trp	Tryptophan
E4P	Erythrose-4-phosphate	Tyr	Tyrosine

Abbreviation	Compound	Abbreviation	Compound
X5P	Xylulose-5-phosphate	rATP	ATP for RNA synthesis
S7P	Sedoheptulose-7-phosphate	rGTP	GTP for RNA synthesis
Glucn	Gluconate	rCTP	CTP for RNA synthesis
KetoPGluc	2-Keto-3-desoxy-6-phosphogluconate	rUTP	UTP for RNA synthesis
ATP	Adenosinetriphosphate	dATP	ATP for DNA synthesis
NADH	NADH	dGTP	GTP for DNA synthesis
NADPH	NADPH	dCTP	CTP for DNA synthesis
QuiH2	Ubiquinone, reduced	dTTP	TTP for DNA synthesis
H_ex	extraplasmic protons	mit_FS	Average fatty acid
O2	Oxygen	UDPGlc	UDP-glucose
CO2	Carbon dioxide	CDPEth	CDP-ethanolamine
N	Ammonia	OH_myr_ac	Hydroxy-myristoic-acid
S	Sulfur (SO4)	C14_0_FS	C(14:0) fatty acid
Glyc	Glycerol	CMP_KDO	CMP-2-keto-3-deoxy octonic acid
AcP	Acetyl-phosphate	NDPHep	NDP-heptose
Ac	Acetate	TDPGlcs	TDP-glucosamine
Form	Formate	UDP_NAG	UDP-N-acetylglucosamine
Lac	Lactate	UDP_NAM	UDP-N-acetylmuramic acid
Adh	Acetaldehyde	di_am_pim	Diaminopimelate
Eth	Ethanol	ADPGlc	Glycogen monomer
Chor	Chorismate		

Tab. A.3: Mutant phenotypes and experimentally determined gene expression ratios. Mutant phenotype data was based on a list compiled previously [58]; additional entries were made for deletions of the following genes: pta [31]. pte [164], pps, scfA and mdh [263]. Experimentally determined transcript ratios for growth on acetate vs. growth on glucose were taken from published microarray data [186] . For growth on glycerol vs. growth on glucose [187], an estimate of the average standard deviation for the measurement obtained in a companion study [185] was used to calculate 95% confidence intervals assuming normal distribution of the errors.

Gene	Mutant phenotype: growth on				Transcript ratios	
	Glc	Gly	Suc	Ac	Ac / Glc	Gly / Glc
ptsG	+				0.21 - 0.44	0.15 - 0.45
glk	+				0.74 - 1.6	-
pgi	+	+	+		0.57 - 1.4	0.75 - 1.05
fbp	+	–	–	–	2.5 - 4.3	0.75 - 1.05
pfkA	–				0.45 - 0.78	0.65 - 0.95
fba	–				0.4 - 0.62	0.85 - 1.15

Gene	Mutant phenotype: growth on				Transcript ratios	
	Glc	Gly	Suc	Ac	Ac / Glc	Gly / Glc
tpiA	–	–	–	–	0.65 - 1.4	0.75 - 1.05
gapA	–	–	–	–	0.3 - 0.69	1.05 - 1.35
pgk	–	–	–	–	0.46 - 0.77	1.05 - 1.35
gpmA					0.84 - 4	0.75 - 1.05
eno	–	–	–	–	0.34 - 0.86	0.65 - 0.95
pykAF	+				0.59 - 1.06	2.05 - 2.35
ppsA	+	+	+	+	8.6 - 21	0.75 - 1.05
aceEF					0.27 - 0.64	0.55 - 0.85
gltA	–			–	3.5 - 6.8	3.35 - 3.65
acnB	–			–	3.6 - 13.1	1.75 - 2.05
icdA	–			–	1.3 - 2.5	1.05 - 1.35
sucAB	+		–	–	1.2 - 3.2	3.55 - 3.85
sucCD					1.8 - 4.7	-
sdhC	+		–	–	1.2 - 2.5	1.25 - 1.55
frdA	+		+	+	0.77 - 2.2	0.85 - 1.15
fumA					2.2 - 5.7	2.45 - 2.75
mdh	+	+	+	–	2.4 - 6.2	1.75 - 2.05
aceA	+		+	–	17.4 - 32.8	1.35 - 1.65
glcB	+	+	+	–	9.33 - 31.6	-
zwf	+	+	+		0.41 - 0.77	1.05 - 1.35
adhE					0.09 - 0.26	1.35 - 1.65
adhE					0.09 - 0.26	1.35 - 1.65
gnd	+				0.43 - 0.84	0.85 - 1.15
rpe	+	+	+	+	0.78 - 1.4	0.95 - 1.25
rpiA	–	–	–	–	0.71 - 1.8	1.05 - 1.35
tktAB					0.88 - 2	0.95 - 1.25
talB					0.69 - 1.3	0.85 - 1.15
tktAB					0.88 - 2	0.95 - 1.25
pckA					4.9 - 14.4	2.85 - 3.15
ppc	o	–	+		0.17 - 0.45	0.75 - 1.05
pta	+	+	+	+	0.45 - 0.96	0.65 - 0.95
ackA				+	0.38 - 0.71	0.25 - 0.55
pflB					1.38 - 2.24	1.35 - 1.65
ldhA					0.76 - 1.2	0.95 - 1.25
glpK					1.41 - 3.39	-
sfcA	+	+	o	+	1.2 - 2.4	-
glpD					1.32 - 2.34	-
gpsA					0.91 - 1.29	-
poxB					0.98 - 4.27	-
acs				+	7.8 - 11.6	-

Gene	Mutant phenotype: growth on				Transcript ratios	
	Glc	Gly	Suc	Ac	Ac / Glc	Gly / Glc
nuo	+	+			0.58 - 1.45	-
cyd	+				0.78 - 1.60	-
pntA	+	+	+		0.28 - 0.69	1.05 - 1.35
atp	+		o	–	0.89 - 1.5	-
asnA					0.54 - 1.05	3.45 - 3.75
aspC					1 - 2	0.85 - 1.15
aspA					1.66 - 3.98	1.95 - 2.25
gdhA					0.76 - 1.78	-
glnA					0.34 - 0.56	-
AdhE					0.09 - 0.26	1.35 - 1.65
FdhF					0.62 - 1.2	1.05 - 1.35

B. *DROSOPHILA*: CIRCADIAN CLOCK MODELS

Tab. B.1: Differential equations for the single-feedback model.

$$
\begin{aligned}
\frac{dM}{dt} &= v_s \frac{K_I^n}{K_I^n + P_n^n} - v_m \frac{M}{K_m + M} \\
\frac{dP_0}{dt} &= k_s M - V_1 \frac{P_0}{K_1 + P_0} + V_2 \frac{P_1}{K_2 + P_1} \\
\frac{dP_1}{dt} &= V_1 \frac{P_0}{K_1 + P_0} - V_2 \frac{P_1}{K_2 + P_1} - V_3 \frac{P_1}{K_3 + P_1} + V_4 \frac{P_2}{K_4 + P_2} \\
\frac{dP_2}{dt} &= V_3 \frac{P_1}{K_3 + P_1} - V_4 \frac{P_2}{K_4 + P_2} - k_1 P_2 + k_2 P_n - v_d \frac{P_2}{K_d + P_2} \\
\frac{dP_n}{dt} &= k_1 P_2 - k_2 P_n
\end{aligned}
$$

Tab. B.2: Reference parameter sets, single-feedback model.

Nr.	Name	Goldbeter [92]	Gonze *et al.* [95]
1	v_s	0.76 $\mu M/h$	0.50 nM/h
2	v_m	0.65 $\mu M/h$	0.30 nM/h
3	k_s	0.38 h^{-1}	2.00 h^{-1}
4	v_d	0.76 $\mu M/h$	1.50 nM/h
5	k_1	1.90 h^{-1}	2.00 h^{-1}
6	k_2	1.30 h^{-1}	1.00 h^{-1}
7	K_I	1.00 μM	2.00 nM
8	K_m	0.50 μM	0.20 nM
9	K_d	0.20 μM	0.10 nM
10	K_1	2.00 μM	1.50 nM
11	K_2	2.00 μM	2.00 nM
12	K_3	2.00 μM	1.50 nM
13	K_4	2.00 μM	2.00 nM
14	V_1	3.20 $\mu M/h$	6.00 nM/h
15	V_2	1.58 $\mu M/h$	3.00 nM/h
16	V_3	5.00 $\mu M/h$	6.00 nM/h
17	V_4	2.50 $\mu M/h$	3.00 nM/h
18	n	4	4

Tab. B.3: Differential equations for the dual-feedback model.

$$
\begin{aligned}
\frac{dM_P}{dt} &= v_{sP}\frac{K_{IP}^n}{K_{IP}^n + C_N^n} - v_{mP}\frac{M_P}{K_{mP} + M_P} - k_d M_P \\
\frac{dP_0}{dt} &= k_{sP}M_P - V_{1P}\frac{P_0}{K_{1P} + P_0} + V_{2P}\frac{P_1}{K_{2P} + P_1} - k_d P_0 \\
\frac{dP_1}{dt} &= V_{1P}\frac{P_0}{K_{1P} + P_0} - V_{2P}\frac{P_1}{K_{2P} + P_1} - V_{3P}\frac{P_1}{K_{3P} + P_1} + V_{4P}\frac{P_2}{K_{4P} + P_2} - k_d P_1 \\
\frac{dP_2}{dt} &= V_{3P}\frac{P_1}{K_{3P} + P_1} - V_{4P}\frac{P_2}{K_{4P} + P_2} - k_3 P_2 T_2 + k_4 C - v_{dP}\frac{P_2}{K_{dP} + P_2} - k_d P_2 \\
\frac{dM_T}{dt} &= v_{sT}\frac{K_{IT}^n}{K_{IT}^n + C_N^n} - v_{mT}\frac{M_T}{K_{mT} + M_T} - k_d M_T \\
\frac{dT_0}{dt} &= k_{sT}M_T - V_{1T}\frac{T_0}{K_{1T} + T_0} + V_{2T}\frac{T_1}{K_{2T} + T_1} - k_d T_0 \\
\frac{dT_1}{dt} &= V_{1T}\frac{T_0}{K_{1T} + T_0} - V_{2T}\frac{T_1}{K_{2T} + T_1} - V_{3T}\frac{T_1}{K_{3T} + T_1} + V_{4T}\frac{T_2}{K_{4T} + T_2} - k_d T_1 \\
\frac{dT_2}{dt} &= V_{3T}\frac{T_1}{K_{3T} + T_1} - V_{4T}\frac{T_2}{K_{4T} + T_2} - k_3 P_2 T_2 + k_4 C - v_{dT}\frac{T_2}{K_{dT} + T_2} - k_d T_2 \\
\frac{dC}{dt} &= k_3 P_2 T_2 - k_4 C - k_1 C + k_2 C_N - k_{dC} C \\
\frac{dC_N}{dt} &= k_1 C - k_2 C_N - k_{dN} C_N
\end{aligned}
$$

C. *SACCHAROMYCES CEREVISIAE*: MITOTIC CONTROL MODULE

Tab. C.1: Model structure of the mitotic control module (see following pages). The table lists all elementary reaction steps used in deriving the mathematical model. Submodules that contains gene expression units for the regulators, and the reactions they catalyze (if applicable) serve to structure the compilation of biochemical reactions. The order of these submodules does not have functional implications, but simply reflects the fact that the mitosis control module is embedded into a larger model for the whole cell cycle.

Each row of the table specifies the meaning of and references for a specific composite biochemical reaction such as complex formation, or an enzyme-catalyzed protein modification. Model parts, for which no reference to the literature is given either comprise constitutive processes, or were introduced as hypothetical mechanisms. Arrows in the reaction schemes indicate elementary reaction steps, their directionality, and the associated kinetic parameters.

The following nomenclature for the components was employed: '$[X]$' represents a single component X, '$[X \cdot Y]$' the complex of two species X and Y. According to conventions for budding yeast, genes are given in uppercase letters ('XXX'). A promoter Z of gene XXX is written as 'XXX_Z'. Lowercase for all but the first letters distinguishes proteins ('Xxx') from their genes; the corresponding messenger RNAs are designated '$mXXX$'.

. For most of the model parameters, a naming scheme was used that refers to the submodule i, in which the parameter occurs. Accordingly, 'K_{iAj}' and 'K_{iDj}' are association and dissociation constants for the j-the reaction in submodule i. Parameters 'E_{iPj}' describe the corresponding catalytic efficiencies. Affinities between transcription factors S and promoters of gene T follow the nomenclature '$K_{XA/DST}$'. Furthermore, all structural parameters that represent, for example, transcript length start with 'L', whereas the first letter of relative factors modulating basal reaction rates is always an 'F'.

(2) Cdc14:					
De-phosphorylation of Net1 [239]	$[Net1P] + [Cdc14 \cdot Cdc14]$	$\underset{K_{2D5}}{\overset{K_{2A5}}{\rightleftharpoons}}$	$[Net1P \cdot Cdc14 \cdot Cdc14]$	$\xrightarrow{F_{ACDC14NET1} \cdot K_{PCDC14}}$	$[Net1] + [Cdc14 \cdot Cdc14]$
Sequestration by Net1 [239, 269]	$[Cdc14] + [Net1]$	$\underset{K_{2D6}}{\overset{K_{2A6}}{\rightleftharpoons}}$	$[Cdc14 \cdot Net1]$		
”	$[Cdc14] + [Net1P]$	$\underset{K_{DNet1PCdc14} \cdot K_{2D6}}{\overset{K_{2A6}}{\rightleftharpoons}}$	$[Cdc14 \cdot Net1P]$		
Dimerisation [97, 251]	$[Cdc14] + [Cdc14]$	$\underset{K_{2D8}}{\overset{K_{2A8}}{\rightleftharpoons}}$	$[Cdc14 \cdot Cdc14]$		
De-phosphorylation of Hct1 [122, 291]	$[Hct1P] + [Cdc14 \cdot Cdc14]$	$\underset{K_{2D10}}{\overset{K_{2A10}}{\rightleftharpoons}}$	$[Hct1P \cdot Cdc14 \cdot Cdc14]$	$\xrightarrow{E_{2P10} \cdot K_{PCDC14}}$	$[Hct1] + [Cdc14 \cdot Cdc14]$
De-phosphorylation of Swi5 [268]	$[Swi5P] + [Cdc14 \cdot Cdc14]$	$\underset{K_{2D11}}{\overset{K_{2A11}}{\rightleftharpoons}}$	$[Swi5P \cdot Cdc14 \cdot Cdc14]$	$\xrightarrow{E_{2P11} \cdot K_{PCDC14}}$	$[Swi5] + [Cdc14 \cdot Cdc14]$
De-phosphorylation of Sic1 [268]	$[Sic1P] + [Cdc14 \cdot Cdc14]$	$\underset{K_{2D12}}{\overset{K_{2A12}}{\rightleftharpoons}}$	$[Sic1P \cdot Cdc14 \cdot Cdc14]$	$\xrightarrow{E_{2P12} \cdot K_{PCDC14}}$	$[Sic1] + [Cdc14 \cdot Cdc14]$
”	$[Clb2 \cdot Sic1P] + [Cdc14 \cdot Cdc14]$	$\underset{K_{2D12}}{\overset{K_{2A12}}{\rightleftharpoons}}$	$[Clb2 \cdot Sic1P \cdot Cdc14 \cdot Cdc14]$	$\xrightarrow{E_{2P12} \cdot K_{PCDC14}}$	$[Clb2 \cdot Sic1] + [Cdc14 \cdot Cdc14]$
”	$[Clb5 \cdot Sic1P] + [Cdc14 \cdot Cdc14]$	$\underset{K_{2D12}}{\overset{K_{2A12}}{\rightleftharpoons}}$	$[Clb5 \cdot Sic1P \cdot Cdc14 \cdot Cdc14]$	$\xrightarrow{E_{2P12} \cdot K_{PCDC14}}$	$[Clb5 \cdot Sic1] + [Cdc14 \cdot Cdc14]$
De-phosphorylation of MEN [247, 257, 285]	$[MENP] + [Cdc14 \cdot Cdc14]$	$\underset{K_{2D13}}{\overset{K_{2A13}}{\rightleftharpoons}}$	$[MENP \cdot Cdc14 \cdot Cdc14]$	$\xrightarrow{E_{2P13} \cdot K_{PCDC14}}$	$[MEN] + [Cdc14 \cdot Cdc14]$
De-phosphorylation of Cdc6 [289]	$[Cdc6P] + [Cdc14 \cdot Cdc14]$	$\underset{K_{2D16}}{\overset{K_{2A16}}{\rightleftharpoons}}$	$[Cdc6P \cdot Cdc14 \cdot Cdc14]$	$\xrightarrow{E_{2P16} \cdot K_{PCDC14}}$	$[Cdc6] + [Cdc14 \cdot Cdc14]$
”	$[Clb2 \cdot Cdc6P] + [Cdc14 \cdot Cdc14]$	$\underset{K_{2D16}}{\overset{K_{2A16}}{\rightleftharpoons}}$	$[Clb2 \cdot Cdc6P \cdot Cdc14 \cdot Cdc14]$	$\xrightarrow{E_{2P16} \cdot K_{PCDC14}}$	$[Clb2 \cdot Cdc6] + [Cdc14 \cdot Cdc14]$
”	$[Clb5 \cdot Cdc6P] + [Cdc14 \cdot Cdc14]$	$\underset{K_{2D16}}{\overset{K_{2A16}}{\rightleftharpoons}}$	$[Clb5 \cdot Cdc6P \cdot Cdc14 \cdot Cdc14]$	$\xrightarrow{E_{2P16} \cdot K_{PCDC14}}$	$[Clb5 \cdot Cdc6] + [Cdc14 \cdot Cdc14]$
De-phosphorylation of Fkh12	$[Fkh12P] + [Cdc14 \cdot Cdc14]$	$\underset{K_{2D17}}{\overset{K_{2A17}}{\rightleftharpoons}}$	$[Fkh12P \cdot Cdc14 \cdot Cdc14]$	$\xrightarrow{E_{2P17} \cdot K_{PCDC14}}$	$[Fkh12] + [Cdc14 \cdot Cdc14]$
De-phosphorylation of Ndd1	$[Ndd1P] + [Cdc14 \cdot Cdc14]$	$\underset{K_{2D18}}{\overset{K_{2A18}}{\rightleftharpoons}}$	$[Ndd1P \cdot Cdc14 \cdot Cdc14]$	$\xrightarrow{E_{2P18} \cdot K_{PCDC14}}$	$[Ndd1] + [Cdc14 \cdot Cdc14]$
(3) Clb2:					
Complex formation with Sic1, Clb2-CDK inactivation [232]	$[Clb2] + [Sic1]$	$\underset{K_{3D1}}{\overset{K_{3A1}}{\rightleftharpoons}}$	$[Clb2 \cdot Sic1]$		
”	$[Clb2] + [Sic1P]$	$\underset{K_{3D1}}{\overset{K_{3A1}}{\rightleftharpoons}}$	$[Clb2 \cdot Sic1P]$		

Phosphorylation / targeting for proteolysis of Sic1 [120, 266]	$[Sic1]+[Clb2]$	$\underset{K_{3D2}}{\overset{K_{3A2}}{\rightleftharpoons}}$	$[Sic1 \cdot Clb2]$	$\xrightarrow{E_{3P2} \cdot F_{ACIb} \cdot K_{PCDC28}}$	$[Sic1P]+[Clb2]$
”	$[Clb2 \cdot Sic1]+[Clb2]$	$\underset{K_{3D2}}{\overset{K_{3A2}}{\rightleftharpoons}}$	$[Clb2 \cdot Sic1 \cdot Clb2]$	$\xrightarrow{E_{3P2} \cdot F_{ACIb} \cdot K_{PCDC28}}$	$[Clb2 \cdot Sic1P]+[Clb2]$
”	$[Clb5 \cdot Sic1]+[Clb2]$	$\underset{K_{3D2}}{\overset{K_{3A2}}{\rightleftharpoons}}$	$[Clb5 \cdot Sic1 \cdot Clb2]$	$\xrightarrow{E_{3P2} \cdot F_{ACIb} \cdot K_{PCDC28}}$	$[Clb5 \cdot Sic1P]+[Clb2]$
Phosphorylation / inactivation of Hct1 [231]	$[Hct1]+[Clb2]$	$\underset{K_{3D3}}{\overset{K_{3A3}}{\rightleftharpoons}}$	$[Hct1 \cdot Clb2]$	$\xrightarrow{E_{3P3} \cdot F_{ACIb} \cdot K_{PCDC28}}$	$[Hct1P]+[Clb2]$
Gene expression via Mcm1 / Fkh12 / Ndd1 [5,240]	$[Fkh12P]+[CLB2_F]$	$\underset{K_{XFkh12Clb2} \cdot K_{XDFkh12}}{\overset{K_{XAFkh12}}{\rightleftharpoons}}$	$[Fkh12P \cdot CLB2_F]$		
	$[Fkh12]+[CLB2_F]$	$\underset{K_{XFkh12Clb2} \cdot K_{XDFkh12}}{\overset{K_{XAFkh12}}{\rightleftharpoons}}$	$[Fkh12 \cdot CLB2_F]$		
	$[Fkh12 \cdot CLB2_F]+[Ndd1]$	$\underset{K_{DFkh12Ndd1}}{\overset{K_{AFkh12Ndd1}}{\rightleftharpoons}}$	$[Fkh12 \cdot Ndd1 \cdot CLB2_F]$		
	$[Fkh12P \cdot CLB2_F]+[Ndd1]$	$\underset{K_{DFkh12Ndd1}}{\overset{F_{AFPN} \cdot K_{AFkh12Ndd1}}{\rightleftharpoons}}$	$[Fkh12P \cdot Ndd1 \cdot CLB2_F]$		
	$[Fkh12 \cdot CLB2_F]+[Ndd1P]$	$\underset{K_{DFkh12Ndd1}}{\overset{F_{AFNP} \cdot K_{AFkh12Ndd1}}{\rightleftharpoons}}$	$[Fkh12 \cdot Ndd1P \cdot CLB2_F]$		
	$[Fkh12P \cdot CLB2_F]+[Ndd1P]$	$\underset{K_{DFkh12Ndd1}}{\overset{F_{AFPN} \cdot F_{AFNP} \cdot K_{AFkh12Ndd1}}{\rightleftharpoons}}$	$[Fkh12P \cdot Ndd1P \cdot CLB2_F]$		
	$[Fkh12 \cdot Ndd1 \cdot CLB2_F]+[RP]$	$\underset{K_{DPol}}{\overset{F_{ATFNdd1} \cdot F_{APolNdd1} \cdot K_{APol}}{\rightleftharpoons}}$	$[Fkh12 \cdot Ndd1 \cdot CLB2_F \cdot RP]$	$\xrightarrow{L_{TKCLB2} \cdot K_{TK}}$	$[mCLB2]+[Fkh12 \cdot Ndd1 \cdot CLB2_F]+[RP]$
	$[Fkh12 \cdot Ndd1P \cdot CLB2_F]+[RP]$	$\underset{K_{DPol}}{\overset{F_{APolNdd1} \cdot K_{APol}}{\rightleftharpoons}}$	$[Fkh12 \cdot Ndd1P \cdot CLB2_F \cdot RP]$	$\xrightarrow{L_{TKCLB2} \cdot K_{TK}}$	$[mCLB2]+[Fkh12 \cdot Ndd1P \cdot CLB2_F]+[RP]$
	$[Fkh12P \cdot Ndd1 \cdot CLB2_F]+[RP]$	$\underset{K_{DPol}}{\overset{F_{ATFNdd1} \cdot F_{APolNdd1} \cdot K_{APol}}{\rightleftharpoons}}$	$[Fkh12P \cdot Ndd1 \cdot CLB2_F \cdot RP]$	$\xrightarrow{L_{TKCLB2} \cdot K_{TK}}$	$[mCLB2]+[Fkh12P \cdot Ndd1 \cdot CLB2_F]+[RP]$
	$[Fkh12P \cdot Ndd1P \cdot CLB2_F]+[RP]$	$\underset{K_{DPol}}{\overset{F_{APolNdd1} \cdot K_{APol}}{\rightleftharpoons}}$	$[Fkh12P \cdot Ndd1P \cdot CLB2_F \cdot RP]$	$\xrightarrow{L_{TKCLB2} \cdot K_{TK}}$	$[mCLB2]+[Fkh12P \cdot Ndd1P \cdot CLB2_F]+[RP]$
Translation / mRNA degradation	$[mCLB2]+[RI]$	$\underset{K_{DRib}}{\overset{K_{ARib}}{\rightleftharpoons}}$	$[mCLB2 \cdot RI]$	$\xrightarrow{L_{TLCLB2} \cdot K_{TL}}$	$[Clb2]+[mCLB2]+[RI]$
			$[mCLB2]$	$\xrightarrow{K_{DMClb2}}$	$[]$
			$[mCLB2 \cdot RI]$	$\xrightarrow{K_{DMClb2}}$	$[RI]$
Gene expression via MBF [240]	$[MBF]+[CLB2_M]$	$\underset{K_{XMBFClb2} \cdot K_{XDMBF}}{\overset{K_{XAMBF}}{\rightleftharpoons}}$	$[MBF \cdot CLB2_M]$		
	$[MBF \cdot CLB2_M]+[RP]$	$\underset{K_{DPol}}{\overset{F_{APolMBF} \cdot K_{APol}}{\rightleftharpoons}}$	$[MBF \cdot CLB2_M \cdot RP]$	$\xrightarrow{L_{TKCLB2} \cdot K_{TK}}$	$[mCLB2]+[MBF \cdot CLB2_M]+[RP]$
Basal expression	$[CLB2_F]+[RP]$	$\underset{K_{DPol}}{\overset{F_{BXClb2} \cdot K_{APol}}{\rightleftharpoons}}$	$[CLB2_F \cdot RP]$	$\xrightarrow{L_{TKCLB2} \cdot K_{TK}}$	$[mCLB2]+[CLB2_F]+[RP]$

Proteolysis via Hct1 / APC [231]	$[Clb2] + [Hct1]$	$\underset{k_{3D4}}{\overset{K_{3A4}}{\rightleftharpoons}}$	$[Clb2 \cdot Hct1]$		
”	$[Clb2] + [Hct1P]$	$\underset{k_{3D4}}{\overset{K_{3A4}}{\rightleftharpoons}}$	$[Clb2 \cdot Hct1P]$		
”	$[Clb2 \cdot Sic1] + [Hct1]$	$\underset{k_{3D4}}{\overset{K_{3A4}}{\rightleftharpoons}}$	$[Clb2 \cdot Sic1 \cdot Hct1]$		
”	$[Clb2 \cdot Sic1P] + [Hct1]$	$\underset{k_{3D4}}{\overset{K_{3A4}}{\rightleftharpoons}}$	$[Clb2 \cdot Sic1P \cdot Hct1]$		
”	$[Clb2 \cdot Sic1] + [Hct1P]$	$\underset{k_{3D4}}{\overset{K_{3A4}}{\rightleftharpoons}}$	$[Clb2 \cdot Sic1 \cdot Hct1P]$		
”	$[Clb2 \cdot Sic1P] + [Hct1P]$	$\underset{k_{3D4}}{\overset{K_{3A4}}{\rightleftharpoons}}$	$[Clb2 \cdot Sic1P \cdot Hct1P]$		
”	$[Clb2 \cdot Cdc6] + [Hct1]$	$\underset{k_{3D4}}{\overset{K_{3A4}}{\rightleftharpoons}}$	$[Clb2 \cdot Cdc6 \cdot Hct1]$		
”	$[Clb2 \cdot Cdc6P] + [Hct1]$	$\underset{k_{3D4}}{\overset{K_{3A4}}{\rightleftharpoons}}$	$[Clb2 \cdot Cdc6P \cdot Hct1]$		
”	$[Clb2 \cdot Cdc6] + [Hct1P]$	$\underset{k_{3D4}}{\overset{K_{3A4}}{\rightleftharpoons}}$	$[Clb2 \cdot Cdc6 \cdot Hct1P]$		
”	$[Clb2 \cdot Cdc6P] + [Hct1P]$	$\underset{k_{3D4}}{\overset{K_{3A4}}{\rightleftharpoons}}$	$[Clb2 \cdot Cdc6P \cdot Hct1P]$		
Proteolysis via Cdc20 / APC [24, 282]	$[Clb2] + [Cdc20]$	$\underset{k_{3D5}}{\overset{K_{3A5}}{\rightleftharpoons}}$	$[Clb2 \cdot Cdc20]$		
”	$[Clb2 \cdot Sic1] + [Cdc20]$	$\underset{k_{3D5}}{\overset{K_{3A5}}{\rightleftharpoons}}$	$[Clb2 \cdot Sic1 \cdot Cdc20]$		
”	$[Clb2 \cdot Sic1P] + [Cdc20]$	$\underset{k_{3D5}}{\overset{K_{3A5}}{\rightleftharpoons}}$	$[Clb2 \cdot Sic1P \cdot Cdc20]$		
”	$[Clb2 \cdot Cdc6] + [Cdc20]$	$\underset{k_{3D5}}{\overset{K_{3A5}}{\rightleftharpoons}}$	$[Clb2 \cdot Cdc6 \cdot Cdc20]$		
”	$[Clb2 \cdot Cdc6P] + [Cdc20]$	$\underset{k_{3D5}}{\overset{K_{3A5}}{\rightleftharpoons}}$	$[Clb2 \cdot Cdc6P \cdot Cdc20]$		
Phosphorylation / inactivation of Swi5 [179]	$[Swi5] + [Clb2]$	$\underset{k_{3D9}}{\overset{K_{3A9}}{\rightleftharpoons}}$	$[Swi5 \cdot Clb2]$	$\xrightarrow{E_{3P9} \cdot F_{ACIb} \cdot K_{PCDC28}}$	$[Swi5P] + [Clb2]$
Phosphorylation / activation of APC [213,214]	$[APC] + [Clb2]$	$\underset{k_{3D10}}{\overset{K_{3A10}}{\rightleftharpoons}}$	$[APC \cdot Clb2]$	$\xrightarrow{E_{3P10} \cdot F_{ACIb} \cdot K_{PCDC28}}$	$[APCP] + [Clb2]$
Phosphorylation of MEN [247]	$[MEN] + [Clb2]$	$\underset{k_{3D13}}{\overset{K_{3A13}}{\rightleftharpoons}}$	$[MEN \cdot Clb2]$	$\xrightarrow{E_{3P13} \cdot F_{ACIb} \cdot K_{PCDC28}}$	$[MENP] + [Clb2]$
Constitutive proteolysis			$[Clb2]$	$\xrightarrow{K_{3P14}}$	$[]$
”			$[Clb2 \cdot Sic1]$	$\xrightarrow{K_{3P14}}$	$[Sic1]$
”			$[Clb2 \cdot Sic1P]$	$\xrightarrow{K_{3P14}}$	$[Sic1P]$
”			$[Clb2 \cdot Cdc6]$	$\xrightarrow{K_{3P14}}$	$[Cdc6]$

”			$[Clb2 \cdot Cdc6P]$	$\xrightarrow{K_{3P14}}$	$[Cdc6P]$
Complex formation with Cdc6 [65]	$[Clb2] + [Cdc6]$	$\underset{K_{3D15}}{\overset{K_{3A15}}{\rightleftharpoons}}$	$[Clb2 \cdot Cdc6]$		
”	$[Clb2] + [Cdc6P]$	$\underset{K_{3D15}}{\overset{F_{CPCdc6} \cdot K_{3A15}}{\rightleftharpoons}}$	$[Clb2 \cdot Cdc6P]$		
Phosphorylation of Cdc6 [53, 193]	$[Cdc6] + [Clb2]$	$\underset{K_{3D16}}{\overset{F_{PFCdc6} \cdot K_{3A16}}{\rightleftharpoons}}$	$[Cdc6 \cdot Clb2]$	$\xrightarrow{E_{3P16} \cdot F_{AClb} \cdot K_{PCDC28}}$	$[Cdc6P] + [Clb2]$
”	$[Clb2 \cdot Cdc6] + [Clb2]$	$\underset{K_{3D16}}{\overset{K_{3A16}}{\rightleftharpoons}}$	$[Clb2 \cdot Cdc6 \cdot Clb2]$	$\xrightarrow{E_{3P16} \cdot F_{AClb} \cdot K_{PCDC28}}$	$[Clb2 \cdot Cdc6P] + [Clb2]$
”	$[Clb5 \cdot Cdc6] + [Clb2]$	$\underset{K_{3D16}}{\overset{K_{3A16}}{\rightleftharpoons}}$	$[Clb5 \cdot Cdc6 \cdot Clb2]$	$\xrightarrow{E_{3P16} \cdot F_{AClb} \cdot K_{PCDC28}}$	$[Clb5 \cdot Cdc6P] + [Clb2]$
Phosphorylation of Fkh1/2	$[Fkh12] + [Clb2]$	$\underset{K_{3D17}}{\overset{K_{3A17}}{\rightleftharpoons}}$	$[Fkh12 \cdot Clb2]$	$\xrightarrow{E_{3P17} \cdot F_{AClb} \cdot K_{PCDC28}}$	$[Fkh12P] + [Clb2]$
Phosphorylation of Ndd1 [207]	$[Ndd1] + [Clb2]$	$\underset{K_{3D18}}{\overset{K_{3A18}}{\rightleftharpoons}}$	$[Ndd1 \cdot Clb2]$	$\xrightarrow{E_{3P18} \cdot F_{AClb} \cdot K_{PCDC28}}$	$[Ndd1P] + [Clb2]$
(4) Sic1:					
Gene expression via Swi5 [141, 256]	$[Swi5] + [SIC1]$	$\underset{K_{XDSwi5}}{\overset{K_{XASwi5}}{\rightleftharpoons}}$	$[Swi5 \cdot SIC1]$		
	$[Swi5 \cdot SIC1] + [RP]$	$\underset{K_{DPol}}{\overset{F_{APolSwi5} \cdot K_{APol}}{\rightleftharpoons}}$	$[Swi5 \cdot SIC1 \cdot RP]$	$\xrightarrow{L_{TKSIC1} \cdot K_{TK}}$	$[mSIC1] + [Swi5 \cdot SIC1] + [RP]$
Basal gene expression [141]	$[SIC1] + [RP]$	$\underset{K_{DPol}}{\overset{F_{BXSic1} \cdot F_{APolSwi5} \cdot K_{APol}}{\rightleftharpoons}}$	$[SIC1 \cdot RP]$	$\xrightarrow{L_{TKSIC1} \cdot K_{TK}}$	$[mSIC1] + [SIC1] + [RP]$
	$[mSIC1] + [RI]$	$\underset{K_{DRib}}{\overset{K_{ARib}}{\rightleftharpoons}}$	$[mSIC1 \cdot RI]$	$\xrightarrow{L_{TLSIC1} \cdot K_{TL}}$	$[Sic1] + [mSIC1] + [RI]$
			$[mSIC1]$	$\xrightarrow{K_{DMSic}}$	$[]$
			$[mSIC1 \cdot RI]$	$\xrightarrow{K_{DMSic}}$	$[RI]$
Proteolysis via SCF [71, 266]	$[Sic1P] + [SCF]$	$\underset{K_{4D1}}{\overset{K_{4A1}}{\rightleftharpoons}}$	$[Sic1P \cdot SCF]$	$\xrightarrow{F_{PRSCFSic1} \cdot K_{PSCF}}$	$[] + [SCF]$
”	$[Clb2 \cdot Sic1P] + [SCF]$	$\underset{K_{4D1}}{\overset{F_{DCSic1} \cdot K_{4A1}}{\rightleftharpoons}}$	$[Clb2 \cdot Sic1P \cdot SCF]$	$\xrightarrow{F_{PRSCFSic1} \cdot K_{PSCF}}$	$[Clb2] + [SCF]$
”	$[Clb5 \cdot Sic1P] + [SCF]$	$\underset{K_{4D1}}{\overset{F_{DCSic1} \cdot K_{4A1}}{\rightleftharpoons}}$	$[Clb5 \cdot Sic1P \cdot SCF]$	$\xrightarrow{F_{PRSCFSic1} \cdot K_{PSCF}}$	$[Clb5] + [SCF]$
”	$[Sic1] + [SCF]$	$\underset{K_{4D1}}{\overset{F_{DSic1} \cdot K_{4A1}}{\rightleftharpoons}}$	$[Sic1 \cdot SCF]$	$\xrightarrow{F_{PRSCFSic1} \cdot K_{PSCF}}$	$[] + [SCF]$
”	$[Clb2 \cdot Sic1] + [SCF]$	$\underset{K_{4D1}}{\overset{F_{DSic1} \cdot F_{DCSic1} \cdot K_{4A1}}{\rightleftharpoons}}$	$[Clb2 \cdot Sic1 \cdot SCF]$	$\xrightarrow{F_{PRSCFSic1} \cdot K_{PSCF}}$	$[Clb2] + [SCF]$
”	$[Clb5 \cdot Sic1] + [SCF]$	$\underset{K_{4D1}}{\overset{F_{DSic1} \cdot F_{DCSic1} \cdot K_{4A1}}{\rightleftharpoons}}$	$[Clb5 \cdot Sic1 \cdot SCF]$	$\xrightarrow{F_{PRSCFSic1} \cdot K_{PSCF}}$	$[Clb5] + [SCF]$

(5) Hct1:

Proteolysis of Clb2 [231]	$[Clb2 \cdot Hct1] + [APC]$	$\underset{k_{5D2}}{\overset{K_{5A2}}{\rightleftharpoons}}$	$[Clb2 \cdot Hct1 \cdot APC]$	$\xrightarrow{F_{PRAPCClb2} \cdot K_{PAPC}}$	$[Hct1] + [APC]$
”	$[Clb2 \cdot Hct1] + [APCP]$	$\underset{k_{5D2}}{\overset{K_{5A2}}{\rightleftharpoons}}$	$[Clb2 \cdot Hct1 \cdot APCP]$	$\xrightarrow{F_{PRAPCClb2} \cdot K_{PAPC}}$	$[Hct1] + [APCP]$
”	$[Clb2 \cdot Hct1P] + [APC]$	$\underset{k_{5D2}}{\overset{F_{AHct1APC} \cdot K_{5A2}}{\rightleftharpoons}}$	$[Clb2 \cdot Hct1P \cdot APC]$	$\xrightarrow{F_{PRAPCClb2} \cdot K_{PAPC}}$	$[Hct1P] + [APC]$
”	$[Clb2 \cdot Hct1P] + [APCP]$	$\underset{k_{5D2}}{\overset{F_{AHct1APC} \cdot K_{5A2}}{\rightleftharpoons}}$	$[Clb2 \cdot Hct1P \cdot APCP]$	$\xrightarrow{F_{PRAPCClb2} \cdot K_{PAPC}}$	$[Hct1P] + [APCP]$
”	$[Clb2 \cdot Sic1 \cdot Hct1] + [APC]$	$\underset{k_{5D2}}{\overset{K_{5A2}}{\rightleftharpoons}}$	$[Clb2 \cdot Sic1 \cdot Hct1 \cdot APC]$	$\xrightarrow{F_{PRAPCClb2} \cdot K_{PAPC}}$	$[Hct1] + [Sic1] + [APC]$
”	$[Clb2 \cdot Sic1 \cdot Hct1] + [APCP]$	$\underset{k_{5D2}}{\overset{K_{5A2}}{\rightleftharpoons}}$	$[Clb2 \cdot Sic1 \cdot Hct1 \cdot APCP]$	$\xrightarrow{F_{PRAPCClb2} \cdot K_{PAPC}}$	$[Hct1] + [Sic1] + [APCP]$
”	$[Clb2 \cdot Sic1 \cdot Hct1P] + [APC]$	$\underset{k_{5D2}}{\overset{F_{AHct1APC} \cdot K_{5A2}}{\rightleftharpoons}}$	$[Clb2 \cdot Sic1 \cdot Hct1P \cdot APC]$	$\xrightarrow{F_{PRAPCClb2} \cdot K_{PAPC}}$	$[Hct1P] + [Sic1] + [APC]$
”	$[Clb2 \cdot Sic1 \cdot Hct1P] + [APCP]$	$\underset{k_{5D2}}{\overset{F_{AHct1APC} \cdot K_{5A2}}{\rightleftharpoons}}$	$[Clb2 \cdot Sic1 \cdot Hct1P \cdot APCP]$	$\xrightarrow{F_{PRAPCClb2} \cdot K_{PAPC}}$	$[Hct1P] + [Sic1] + [APCP]$
”	$[Clb2 \cdot Sic1P \cdot Hct1] + [APC]$	$\underset{k_{5D2}}{\overset{K_{5A2}}{\rightleftharpoons}}$	$[Clb2 \cdot Sic1P \cdot Hct1 \cdot APC]$	$\xrightarrow{F_{PRAPCClb2} \cdot K_{PAPC}}$	$[Hct1] + [Sic1P] + [APC]$
”	$[Clb2 \cdot Sic1P \cdot Hct1] + [APCP]$	$\underset{k_{5D2}}{\overset{K_{5A2}}{\rightleftharpoons}}$	$[Clb2 \cdot Sic1P \cdot Hct1 \cdot APCP]$	$\xrightarrow{F_{PRAPCClb2} \cdot K_{PAPC}}$	$[Hct1] + [Sic1P] + [APCP]$
”	$[Clb2 \cdot Sic1P \cdot Hct1P] + [APC]$	$\underset{k_{5D2}}{\overset{F_{AHct1APC} \cdot K_{5A2}}{\rightleftharpoons}}$	$[Clb2 \cdot Sic1P \cdot Hct1P \cdot APC]$	$\xrightarrow{F_{PRAPCClb2} \cdot K_{PAPC}}$	$[Hct1P] + [Sic1P] + [APC]$
”	$[Clb2 \cdot Sic1P \cdot Hct1P] + [APCP]$	$\underset{k_{5D2}}{\overset{F_{AHct1APC} \cdot K_{5A2}}{\rightleftharpoons}}$	$[Clb2 \cdot Sic1P \cdot Hct1P \cdot APCP]$	$\xrightarrow{F_{PRAPCClb2} \cdot K_{PAPC}}$	$[Hct1P] + [Sic1P] + [APCP]$
”	$[Clb2 \cdot Cdc6 \cdot Hct1] + [APC]$	$\underset{k_{5D2}}{\overset{K_{5A2}}{\rightleftharpoons}}$	$[Clb2 \cdot Cdc6 \cdot Hct1 \cdot APC]$	$\xrightarrow{F_{PRAPCClb2} \cdot K_{PAPC}}$	$[Hct1] + [Cdc6] + [APC]$
”	$[Clb2 \cdot Cdc6 \cdot Hct1] + [APCP]$	$\underset{k_{5D2}}{\overset{K_{5A2}}{\rightleftharpoons}}$	$[Clb2 \cdot Cdc6 \cdot Hct1 \cdot APCP]$	$\xrightarrow{F_{PRAPCClb2} \cdot K_{PAPC}}$	$[Hct1] + [Cdc6] + [APCP]$
”	$[Clb2 \cdot Cdc6 \cdot Hct1P] + [APC]$	$\underset{k_{5D2}}{\overset{F_{AHct1APC} \cdot K_{5A2}}{\rightleftharpoons}}$	$[Clb2 \cdot Cdc6 \cdot Hct1P \cdot APC]$	$\xrightarrow{F_{PRAPCClb2} \cdot K_{PAPC}}$	$[Hct1P] + [Cdc6] + [APC]$
”	$[Clb2 \cdot Cdc6 \cdot Hct1P] + [APCP]$	$\underset{k_{5D2}}{\overset{F_{AHct1APC} \cdot K_{5A2}}{\rightleftharpoons}}$	$[Clb2 \cdot Cdc6 \cdot Hct1P \cdot APCP]$	$\xrightarrow{F_{PRAPCClb2} \cdot K_{PAPC}}$	$[Hct1P] + [Cdc6] + [APCP]$
”	$[Clb2 \cdot Cdc6P \cdot Hct1] + [APC]$	$\underset{k_{5D2}}{\overset{K_{5A2}}{\rightleftharpoons}}$	$[Clb2 \cdot Cdc6P \cdot Hct1 \cdot APC]$	$\xrightarrow{F_{PRAPCClb2} \cdot K_{PAPC}}$	$[Hct1] + [Cdc6P] + [APC]$
”	$[Clb2 \cdot Cdc6P \cdot Hct1] + [APCP]$	$\underset{k_{5D2}}{\overset{K_{5A2}}{\rightleftharpoons}}$	$[Clb2 \cdot Cdc6P \cdot Hct1 \cdot APCP]$	$\xrightarrow{F_{PRAPCClb2} \cdot K_{PAPC}}$	$[Hct1] + [Cdc6P] + [APCP]$
”	$[Clb2 \cdot Cdc6P \cdot Hct1P] + [APC]$	$\underset{k_{5D2}}{\overset{F_{AHct1APC} \cdot K_{5A2}}{\rightleftharpoons}}$	$[Clb2 \cdot Cdc6P \cdot Hct1P \cdot APC]$	$\xrightarrow{F_{PRAPCClb2} \cdot K_{PAPC}}$	$[Hct1P] + [Cdc6P] + [APC]$

”	$[Clb2 \cdot Cdc6P \cdot Hct1P] + [APCP]$	$\xrightleftharpoons[k_{5D2}]{F_{AHct1APC} \cdot K_{5A2}}$	$[Clb2 \cdot Cdc6P \cdot Hct1P \cdot APCP]$	$\xrightarrow{F_{PRAPCClb2} \cdot K_{PAPC}}$	$[Hct1P] + [Cdc6P] + [APCP]$
Proteolysis of Ndd1	$[Ndd1 \cdot Hct1] + [APC]$	$\xrightleftharpoons[k_{5D2}]{K_{5A2}}$	$[Ndd1 \cdot Hct1 \cdot APC]$	$\xrightarrow{F_{PRAPCNdd1} \cdot K_{PAPC}}$	$[Hct1] + [APC]$
”	$[Ndd1 \cdot Hct1] + [APCP]$	$\xrightleftharpoons[k_{5D2}]{K_{5A2}}$	$[Ndd1 \cdot Hct1 \cdot APCP]$	$\xrightarrow{F_{PRAPCNdd1} \cdot K_{PAPC}}$	$[Hct1] + [APCP]$
”	$[Ndd1P \cdot Hct1] + [APC]$	$\xrightleftharpoons[k_{5D2}]{K_{5A2}}$	$[Ndd1P \cdot Hct1 \cdot APC]$	$\xrightarrow{F_{PRAPCNdd1} \cdot K_{PAPC}}$	$[Hct1] + [APC]$
”	$[Ndd1P \cdot Hct1] + [APCP]$	$\xrightleftharpoons[k_{5D2}]{K_{5A2}}$	$[Ndd1P \cdot Hct1 \cdot APCP]$	$\xrightarrow{F_{PRAPCNdd1} \cdot K_{PAPC}}$	$[Hct1] + [APCP]$
”	$[Ndd1 \cdot Hct1P] + [APC]$	$\xrightleftharpoons[k_{5D2}]{F_{AHct1APC} \cdot K_{5A2}}$	$[Ndd1 \cdot Hct1P \cdot APC]$	$\xrightarrow{F_{PRAPCNdd1} \cdot K_{PAPC}}$	$[Hct1P] + [APC]$
”	$[Ndd1 \cdot Hct1P] + [APCP]$	$\xrightleftharpoons[k_{5D2}]{F_{AHct1APC} \cdot K_{5A2}}$	$[Ndd1 \cdot Hct1P \cdot APCP]$	$\xrightarrow{F_{PRAPCNdd1} \cdot K_{PAPC}}$	$[Hct1P] + [APCP]$
”	$[Ndd1P \cdot Hct1P] + [APC]$	$\xrightleftharpoons[k_{5D2}]{F_{AHct1APC} \cdot K_{5A2}}$	$[Ndd1P \cdot Hct1P \cdot APC]$	$\xrightarrow{F_{PRAPCNdd1} \cdot K_{PAPC}}$	$[Hct1P] + [APC]$
”	$[Ndd1P \cdot Hct1P] + [APCP]$	$\xrightleftharpoons[k_{5D2}]{F_{AHct1APC} \cdot K_{5A2}}$	$[Ndd1P \cdot Hct1P \cdot APCP]$	$\xrightarrow{F_{PRAPCNdd1} \cdot K_{PAPC}}$	$[Hct1P] + [APCP]$
Proteolysis of Yox1	$[Yox1 \cdot Hct1] + [APC]$	$\xrightleftharpoons[k_{5D2}]{K_{5A2}}$	$[Yox1 \cdot Hct1 \cdot APC]$	$\xrightarrow{F_{PRAPCYox1} \cdot K_{PAPC}}$	$[Hct1] + [APC]$
”	$[Yox1 \cdot Hct1] + [APCP]$	$\xrightleftharpoons[k_{5D2}]{K_{5A2}}$	$[Yox1 \cdot Hct1 \cdot APCP]$	$\xrightarrow{F_{PRAPCYox1} \cdot K_{PAPC}}$	$[Hct1] + [APCP]$
”	$[Yox1 \cdot Hct1P] + [APC]$	$\xrightleftharpoons[k_{5D2}]{F_{AHct1APC} \cdot K_{5A2}}$	$[Yox1 \cdot Hct1P \cdot APC]$	$\xrightarrow{F_{PRAPCYox1} \cdot K_{PAPC}}$	$[Hct1P] + [APC]$
”	$[Yox1 \cdot Hct1P] + [APCP]$	$\xrightleftharpoons[k_{5D2}]{F_{AHct1APC} \cdot K_{5A2}}$	$[Yox1 \cdot Hct1P \cdot APCP]$	$\xrightarrow{F_{PRAPCYox1} \cdot K_{PAPC}}$	$[Hct1P] + [APCP]$
Proteolysis of Cdc20	$[Cdc20 \cdot Hct1] + [APC]$	$\xrightleftharpoons[k_{5D2}]{K_{5A2}}$	$[Cdc20 \cdot Hct1 \cdot APC]$	$\xrightarrow{F_{PRAPCCdc20} \cdot K_{PAPC}}$	$[Hct1] + [APC]$
”	$[Cdc20 \cdot Hct1] + [APCP]$	$\xrightleftharpoons[k_{5D2}]{K_{5A2}}$	$[Cdc20 \cdot Hct1 \cdot APCP]$	$\xrightarrow{F_{PRAPCCdc20} \cdot K_{PAPC}}$	$[Hct1] + [APCP]$
”	$[Cdc20 \cdot Hct1P] + [APC]$	$\xrightleftharpoons[k_{5D2}]{F_{AHct1APC} \cdot K_{5A2}}$	$[Cdc20 \cdot Hct1P \cdot APC]$	$\xrightarrow{F_{PRAPCCdc20} \cdot K_{PAPC}}$	$[Hct1P] + [APC]$
”	$[Cdc20 \cdot Hct1P] + [APCP]$	$\xrightleftharpoons[k_{5D2}]{F_{AHct1APC} \cdot K_{5A2}}$	$[Cdc20 \cdot Hct1P \cdot APCP]$	$\xrightarrow{F_{PRAPCCdc20} \cdot K_{PAPC}}$	$[Hct1P] + [APCP]$
”	$[Cdc20 \cdot SAC \cdot Hct1] + [APC]$	$\xrightleftharpoons[k_{5D2}]{K_{5A2}}$	$[Cdc20 \cdot SAC \cdot Hct1 \cdot APC]$	$\xrightarrow{F_{PRAPCCdc20} \cdot K_{PAPC}}$	$[Hct1] + [SAC] + [APC]$
”	$[Cdc20 \cdot SAC \cdot Hct1] + [APCP]$	$\xrightleftharpoons[k_{5D2}]{K_{5A2}}$	$[Cdc20 \cdot SAC \cdot Hct1 \cdot APCP]$	$\xrightarrow{F_{PRAPCCdc20} \cdot K_{PAPC}}$	$[Hct1] + [SAC] + [APCP]$
”	$[Cdc20 \cdot SAC \cdot Hct1P] + [APC]$	$\xrightleftharpoons[k_{5D2}]{F_{AHct1APC} \cdot K_{5A2}}$	$[Cdc20 \cdot SAC \cdot Hct1P \cdot APC]$	$\xrightarrow{F_{PRAPCCdc20} \cdot K_{PAPC}}$	$[Hct1P] + [SAC] + [APC]$
”	$[Cdc20 \cdot SAC \cdot Hct1P] + [APCP]$	$\xrightleftharpoons[k_{5D2}]{F_{AHct1APC} \cdot K_{5A2}}$	$[Cdc20 \cdot SAC \cdot Hct1P \cdot APCP]$	$\xrightarrow{F_{PRAPCCdc20} \cdot K_{PAPC}}$	$[Hct1P] + [SAC] + [APCP]$

Proteolysis of Cdc6	$[Cdc6 \cdot Hct1] + [APC]$	$\underset{k_{5D2}}{\overset{K_{5A2}}{\rightleftharpoons}}$	$[Cdc6 \cdot Hct1 \cdot APC]$	$\xrightarrow{F_{PRAPCCdc6} \cdot K_{PAPC}}$	$[Hct1] + [APC]$
”	$[Cdc6 \cdot Hct1] + [APCP]$	$\underset{k_{5D2}}{\overset{K_{5A2}}{\rightleftharpoons}}$	$[Cdc6 \cdot Hct1 \cdot APCP]$	$\xrightarrow{F_{PRAPCCdc6} \cdot K_{PAPC}}$	$[Hct1] + [APCP]$
”	$[Cdc6 \cdot Hct1P] + [APC]$	$\underset{k_{5D2}}{\overset{F_{AHct1APC} \cdot K_{5A2}}{\rightleftharpoons}}$	$[Cdc6 \cdot Hct1P \cdot APC]$	$\xrightarrow{F_{PRAPCCdc6} \cdot K_{PAPC}}$	$[Hct1P] + [APC]$
”	$[Cdc6 \cdot Hct1P] + [APCP]$	$\underset{k_{5D2}}{\overset{F_{AHct1APC} \cdot K_{5A2}}{\rightleftharpoons}}$	$[Cdc6 \cdot Hct1P \cdot APCP]$	$\xrightarrow{F_{PRAPCCdc6} \cdot K_{PAPC}}$	$[Hct1P] + [APCP]$
”	$[Cdc6P \cdot Hct1] + [APC]$	$\underset{k_{5D2}}{\overset{K_{5A2}}{\rightleftharpoons}}$	$[Cdc6P \cdot Hct1 \cdot APC]$	$\xrightarrow{F_{PRAPCCdc6} \cdot K_{PAPC}}$	$[Hct1] + [APC]$
”	$[Cdc6P \cdot Hct1] + [APCP]$	$\underset{k_{5D2}}{\overset{K_{5A2}}{\rightleftharpoons}}$	$[Cdc6P \cdot Hct1 \cdot APCP]$	$\xrightarrow{F_{PRAPCCdc6} \cdot K_{PAPC}}$	$[Hct1] + [APCP]$
”	$[Cdc6P \cdot Hct1P] + [APC]$	$\underset{k_{5D2}}{\overset{F_{AHct1APC} \cdot K_{5A2}}{\rightleftharpoons}}$	$[Cdc6P \cdot Hct1P \cdot APC]$	$\xrightarrow{F_{PRAPCCdc6} \cdot K_{PAPC}}$	$[Hct1P] + [APC]$
”	$[Cdc6P \cdot Hct1P] + [APCP]$	$\underset{k_{5D2}}{\overset{F_{AHct1APC} \cdot K_{5A2}}{\rightleftharpoons}}$	$[Cdc6P \cdot Hct1P \cdot APCP]$	$\xrightarrow{F_{PRAPCCdc6} \cdot K_{PAPC}}$	$[Hct1P] + [APCP]$
”	$[Cdc6 \cdot Clb2 \cdot Hct1] + [APC]$	$\underset{k_{5D2}}{\overset{K_{5A2}}{\rightleftharpoons}}$	$[Cdc6 \cdot Clb2 \cdot Hct1 \cdot APC]$	$\xrightarrow{F_{PRAPCCdc6} \cdot K_{PAPC}}$	$[Hct1] + [Clb2] + [APC]$
”	$[Cdc6 \cdot Clb2 \cdot Hct1] + [APCP]$	$\underset{k_{5D2}}{\overset{K_{5A2}}{\rightleftharpoons}}$	$[Cdc6 \cdot Clb2 \cdot Hct1 \cdot APCP]$	$\xrightarrow{F_{PRAPCCdc6} \cdot K_{PAPC}}$	$[Hct1] + [Clb2] + [APCP]$
”	$[Cdc6 \cdot Clb2 \cdot Hct1P] + [APC]$	$\underset{k_{5D2}}{\overset{F_{AHct1APC} \cdot K_{5A2}}{\rightleftharpoons}}$	$[Cdc6 \cdot Clb2 \cdot Hct1P \cdot APC]$	$\xrightarrow{F_{PRAPCCdc6} \cdot K_{PAPC}}$	$[Hct1P] + [Clb2] + [APC]$
”	$[Cdc6 \cdot Clb2 \cdot Hct1P] + [APCP]$	$\underset{k_{5D2}}{\overset{F_{AHct1APC} \cdot K_{5A2}}{\rightleftharpoons}}$	$[Cdc6 \cdot Clb2 \cdot Hct1P \cdot APCP]$	$\xrightarrow{F_{PRAPCCdc6} \cdot K_{PAPC}}$	$[Hct1P] + [Clb2] + [APCP]$
”	$[Cdc6P \cdot Clb2 \cdot Hct1] + [APC]$	$\underset{k_{5D2}}{\overset{K_{5A2}}{\rightleftharpoons}}$	$[Cdc6P \cdot Clb2 \cdot Hct1 \cdot APC]$	$\xrightarrow{F_{PRAPCCdc6} \cdot K_{PAPC}}$	$[Hct1] + [Clb2] + [APC]$
”	$[Cdc6P \cdot Clb2 \cdot Hct1] + [APCP]$	$\underset{k_{5D2}}{\overset{K_{5A2}}{\rightleftharpoons}}$	$[Cdc6P \cdot Clb2 \cdot Hct1 \cdot APCP]$	$\xrightarrow{F_{PRAPCCdc6} \cdot K_{PAPC}}$	$[Hct1] + [Clb2] + [APCP]$
”	$[Cdc6P \cdot Clb2 \cdot Hct1P] + [APC]$	$\underset{k_{5D2}}{\overset{F_{AHct1APC} \cdot K_{5A2}}{\rightleftharpoons}}$	$[Cdc6P \cdot Clb2 \cdot Hct1P \cdot APC]$	$\xrightarrow{F_{PRAPCCdc6} \cdot K_{PAPC}}$	$[Hct1P] + [Clb2] + [APC]$
”	$[Cdc6P \cdot Clb2 \cdot Hct1P] + [APCP]$	$\underset{k_{5D2}}{\overset{F_{AHct1APC} \cdot K_{5A2}}{\rightleftharpoons}}$	$[Cdc6P \cdot Clb2 \cdot Hct1P \cdot APCP]$	$\xrightarrow{F_{PRAPCCdc6} \cdot K_{PAPC}}$	$[Hct1P] + [Clb2] + [APCP]$
”	$[Cdc6 \cdot Clb5 \cdot Hct1] + [APC]$	$\underset{k_{5D2}}{\overset{K_{5A2}}{\rightleftharpoons}}$	$[Cdc6 \cdot Clb5 \cdot Hct1 \cdot APC]$	$\xrightarrow{F_{PRAPCCdc6} \cdot K_{PAPC}}$	$[Hct1] + [Clb5] + [APC]$
”	$[Cdc6 \cdot Clb5 \cdot Hct1] + [APCP]$	$\underset{k_{5D2}}{\overset{K_{5A2}}{\rightleftharpoons}}$	$[Cdc6 \cdot Clb5 \cdot Hct1 \cdot APCP]$	$\xrightarrow{F_{PRAPCCdc6} \cdot K_{PAPC}}$	$[Hct1] + [Clb5] + [APCP]$
”	$[Cdc6 \cdot Clb5 \cdot Hct1P] + [APC]$	$\underset{k_{5D2}}{\overset{F_{AHct1APC} \cdot K_{5A2}}{\rightleftharpoons}}$	$[Cdc6 \cdot Clb5 \cdot Hct1P \cdot APC]$	$\xrightarrow{F_{PRAPCCdc6} \cdot K_{PAPC}}$	$[Hct1P] + [Clb5] + [APC]$
”	$[Cdc6 \cdot Clb5 \cdot Hct1P] + [APCP]$	$\underset{k_{5D2}}{\overset{F_{AHct1APC} \cdot K_{5A2}}{\rightleftharpoons}}$	$[Cdc6 \cdot Clb5 \cdot Hct1P \cdot APCP]$	$\xrightarrow{F_{PRAPCCdc6} \cdot K_{PAPC}}$	$[Hct1P] + [Clb5] + [APCP]$

”	$[Cdc6P \cdot Clb5 \cdot Hct1] + [APC]$	$\underset{K_{5D2}}{\overset{K_{5A2}}{\rightleftharpoons}}$	$[Cdc6P \cdot Clb5 \cdot Hct1 \cdot APC]$	$\xrightarrow{F_{PRAPCCdc6} \cdot K_{PAPC}}$	$[Hct1] + [Clb5] + [APC]$
”	$[Cdc6P \cdot Clb5 \cdot Hct1] + [APCP]$	$\underset{K_{5D2}}{\overset{K_{5A2}}{\rightleftharpoons}}$	$[Cdc6P \cdot Clb5 \cdot Hct1 \cdot APCP]$	$\xrightarrow{F_{PRAPCCdc6} \cdot K_{PAPC}}$	$[Hct1] + [Clb5] + [APCP]$
”	$[Cdc6P \cdot Clb5 \cdot Hct1P] + [APC]$	$\underset{K_{5D2}}{\overset{F_{AHct1APC} \cdot K_{5A2}}{\rightleftharpoons}}$	$[Cdc6P \cdot Clb5 \cdot Hct1P \cdot APC]$	$\xrightarrow{F_{PRAPCCdc6} \cdot K_{PAPC}}$	$[Hct1P] + [Clb5] + [APC]$
”	$[Cdc6P \cdot Clb5 \cdot Hct1P] + [APCP]$	$\underset{K_{5D2}}{\overset{F_{AHct1APC} \cdot K_{5A2}}{\rightleftharpoons}}$	$[Cdc6P \cdot Clb5 \cdot Hct1P \cdot APCP]$	$\xrightarrow{F_{PRAPCCdc6} \cdot K_{PAPC}}$	$[Hct1P] + [Clb5] + [APCP]$
(6) Cdc20:					
Inhibition via nocodazole (spindle assembly checkpoint) [118]	$[Cdc20] + [SAC]$	$\underset{K_{6D1}}{\overset{K_{6A1}}{\rightleftharpoons}}$	$[Cdc20 \cdot SAC]$		
Gene expression via Mcm1 / Fkh12 / Ndd1 [240,246]	$[Fkh12P] + [CDC20_F]$	$\underset{F_{XFkh12Cdc20} \cdot K_{XDFkh12}}{\overset{K_{XAFkh12}}{\rightleftharpoons}}$	$[Fkh12P \cdot CDC20_F]$		
	$[Fkh12] + [CDC20_F]$	$\underset{F_{XFkh12Cdc20} \cdot K_{XDFkh12}}{\overset{K_{XAFkh12}}{\rightleftharpoons}}$	$[Fkh12 \cdot CDC20_F]$		
	$[Fkh12 \cdot CDC20_F] + [Ndd1]$	$\underset{K_{DFkh12Ndd1}}{\overset{K_{AFkh12Ndd1}}{\rightleftharpoons}}$	$[Fkh12 \cdot Ndd1 \cdot CDC20_F]$		
	$[Fkh12P \cdot CDC20_F] + [Ndd1]$	$\underset{K_{DFkh12Ndd1}}{\overset{F_{AFPN} \cdot K_{AFkh12Ndd1}}{\rightleftharpoons}}$	$[Fkh12P \cdot Ndd1 \cdot CDC20_F]$		
	$[Fkh12 \cdot CDC20_F] + [Ndd1P]$	$\underset{K_{DFkh12Ndd1}}{\overset{F_{AFNP} \cdot K_{AFkh12Ndd1}}{\rightleftharpoons}}$	$[Fkh12 \cdot Ndd1P \cdot CDC20_F]$		
	$[Fkh12P \cdot CDC20_F] + [Ndd1P]$	$\underset{K_{DFkh12Ndd1}}{\overset{F_{AFPN} \cdot F_{AFNP} \cdot K_{AFkh12Ndd1}}{\rightleftharpoons}}$	$[Fkh12P \cdot Ndd1P \cdot CDC20_F]$		
	$[Fkh12 \cdot Ndd1 \cdot CDC20_F] + [RP]$	$\underset{K_{DPol}}{\overset{F_{ATFNdd1} \cdot F_{APolNdd1} \cdot K_{APol}}{\rightleftharpoons}}$	$[Fkh12 \cdot Ndd1 \cdot CDC20_F \cdot RP]$	$\xrightarrow{L_{TKCDC20} \cdot K_{TK}}$	$[mCDC20] + [Fkh12 \cdot Ndd1 \cdot CDC20_F] + [RP]$
	$[Fkh12 \cdot Ndd1P \cdot CDC20_F] + [RP]$	$\underset{K_{DPol}}{\overset{F_{APolNdd1} \cdot K_{APol}}{\rightleftharpoons}}$	$[Fkh12 \cdot Ndd1P \cdot CDC20_F \cdot RP]$	$\xrightarrow{L_{TKCDC20} \cdot K_{TK}}$	$[mCDC20] + [Fkh12 \cdot Ndd1P \cdot CDC20_F] + [RP]$
	$[Fkh12P \cdot Ndd1 \cdot CDC20_F] + [RP]$	$\underset{K_{DPol}}{\overset{F_{ATFNdd1} \cdot F_{APolNdd1} \cdot K_{APol}}{\rightleftharpoons}}$	$[Fkh12P \cdot Ndd1 \cdot CDC20_F \cdot RP]$	$\xrightarrow{L_{TKCDC20} \cdot K_{TK}}$	$[mCDC20] + [Fkh12P \cdot Ndd1 \cdot CDC20_F] + [RP]$
	$[Fkh12P \cdot Ndd1P \cdot CDC20_F] + [RP]$	$\underset{K_{DPol}}{\overset{F_{APolNdd1} \cdot K_{APol}}{\rightleftharpoons}}$	$[Fkh12P \cdot Ndd1P \cdot CDC20_F \cdot RP]$	$\xrightarrow{L_{TKCDC20} \cdot K_{TK}}$	$[mCDC20] + [Fkh12P \cdot Ndd1P \cdot CDC20_F] + [RP]$
	$[mCDC20] + [RI]$	$\underset{K_{DRib}}{\overset{K_{ARib}}{\rightleftharpoons}}$	$[mCDC20 \cdot RI]$	$\xrightarrow{L_{TLCDC20} \cdot K_{TL}}$	$[Cdc20] + [mCDC20] + [RI]$
			$[mCDC20]$	$\xrightarrow{K_{DMCdc20}}$	$[]$
			$[mCDC20 \cdot RI]$	$\xrightarrow{K_{DMCdc20}}$	$[RI]$

Gene expression via MBF [240]	$[MBF]+[CDC20_M]$	$\xrightleftharpoons[F_{XMBFCdc20}\cdot K_{XDMBF}]{K_{XAMBF}}$	$[MBF\cdot CDC20_M]$		
	$[MBF\cdot CDC20_M]+[RP]$	$\xrightleftharpoons[K_{DPol}]{F_{APolMBF}\cdot K_{APol}}$	$[MBF\cdot CDC20_M\cdot RP]$	$\xrightarrow{L_{TKCDC20}\cdot K_{TK}}$	$[mCDC20]+[MBF\cdot CDC20_M]+[RP]$
Basal expression	$[CDC20_F]+[RP]$	$\xrightleftharpoons[K_{DPol}]{F_{BXCdc20}\cdot K_{APol}}$	$[CDC20_F\cdot RP]$	$\xrightarrow{L_{TKCDC20}\cdot K_{TK}}$	$[mCDC20]+[CDC20_F]+[RP]$
Repression of gene expression via Yox1 [198]	$[Yox1]+[CDC20_F]$	$\xrightleftharpoons[F_{XICdc20}\cdot K_{XDYox1}]{K_{XAYox1}}$	$[Yox1\cdot CDC20_F]$		
APC-dependent proteolysis of Cdc20 [201,237]	$[Cdc20]+[APCP]$	$\xrightleftharpoons[K_{6D3}]{F_{DCdc20APC}\cdot K_{6A3}}$	$[Cdc20\cdot APCP]$	$\xrightarrow{K_{PAPC}}$	$[]+[APCP]$
APC-independent proteolysis of Cdc20 [91]			$[Cdc20]$	$\xrightarrow{K_{6P2}}$	$[]$
”			$[Cdc20\cdot SAC]$	$\xrightarrow{F_{DCdc20SAC}\cdot K_{6P2}}$	$[SAC]$
Proteolysis of Clb5 [236]	$[Clb5\cdot Cdc20]+[APCP]$	$\xrightleftharpoons[K_{6D2}]{K_{6A2}}$	$[Clb5\cdot Cdc20\cdot APCP]$	$\xrightarrow{F_{PRAPCClb5}\cdot K_{PAPC}}$	$[Cdc20]+[APCP]$
”	$[Clb5\cdot Sic1\cdot Cdc20]+[APCP]$	$\xrightleftharpoons[K_{6D2}]{K_{6A2}}$	$[Clb5\cdot Sic1\cdot Cdc20\cdot APCP]$	$\xrightarrow{F_{PRAPCClb5}\cdot K_{PAPC}}$	$[Cdc20]+[Sic1]+[APCP]$
”	$[Clb5\cdot Sic1P\cdot Cdc20]+[APCP]$	$\xrightleftharpoons[K_{6D2}]{K_{6A2}}$	$[Clb5\cdot Sic1P\cdot Cdc20\cdot APCP]$	$\xrightarrow{F_{PRAPCClb5}\cdot K_{PAPC}}$	$[Cdc20]+[Sic1P]+[APCP]$
”	$[Clb5\cdot Cdc6\cdot Cdc20]+[APCP]$	$\xrightleftharpoons[K_{6D2}]{K_{6A2}}$	$[Clb5\cdot Cdc6\cdot Cdc20\cdot APCP]$	$\xrightarrow{F_{PRAPCClb5}\cdot K_{PAPC}}$	$[Cdc20]+[Cdc6]+[APCP]$
”	$[Clb5\cdot Cdc6P\cdot Cdc20]+[APCP]$	$\xrightleftharpoons[K_{6D2}]{K_{6A2}}$	$[Clb5\cdot Cdc6P\cdot Cdc20\cdot APCP]$	$\xrightarrow{F_{PRAPCClb5}\cdot K_{PAPC}}$	$[Cdc20]+[Cdc6P]+[APCP]$
Proteolysis of Clb2 [159,282]	$[Clb2\cdot Cdc20]+[APCP]$	$\xrightleftharpoons[K_{6D2}]{K_{6A2}}$	$[Clb2\cdot Cdc20\cdot APCP]$	$\xrightarrow{F_{PRAPCClb2}\cdot K_{PAPC}}$	$[Cdc20]+[APCP]$
”	$[Clb2\cdot Sic1\cdot Cdc20]+[APCP]$	$\xrightleftharpoons[K_{6D2}]{K_{6A2}}$	$[Clb2\cdot Sic1\cdot Cdc20\cdot APCP]$	$\xrightarrow{F_{PRAPCClb2}\cdot K_{PAPC}}$	$[Cdc20]+[Sic1]+[APCP]$
”	$[Clb2\cdot Sic1P\cdot Cdc20]+[APCP]$	$\xrightleftharpoons[K_{6D2}]{K_{6A2}}$	$[Clb2\cdot Sic1P\cdot Cdc20\cdot APCP]$	$\xrightarrow{F_{PRAPCClb2}\cdot K_{PAPC}}$	$[Cdc20]+[Sic1P]+[APCP]$
”	$[Clb2\cdot Cdc6\cdot Cdc20]+[APCP]$	$\xrightleftharpoons[K_{6D2}]{K_{6A2}}$	$[Clb2\cdot Cdc6\cdot Cdc20\cdot APCP]$	$\xrightarrow{F_{PRAPCClb2}\cdot K_{PAPC}}$	$[Cdc20]+[Cdc6]+[APCP]$
”	$[Clb2\cdot Cdc6P\cdot Cdc20]+[APCP]$	$\xrightleftharpoons[K_{6D2}]{K_{6A2}}$	$[Clb2\cdot Cdc6P\cdot Cdc20\cdot APCP]$	$\xrightarrow{F_{PRAPCClb2}\cdot K_{PAPC}}$	$[Cdc20]+[Cdc6P]+[APCP]$
Proteolysis of Yox1	$[Yox1\cdot Cdc20]+[APCP]$	$\xrightleftharpoons[K_{6D2}]{K_{6A2}}$	$[Yox1\cdot Cdc20\cdot APCP]$	$\xrightarrow{F_{PRAPCYox1}\cdot K_{PAPC}}$	$[Cdc20]+[APCP]$
Proteolysis of Cdc6	$[Cdc6\cdot Cdc20]+[APCP]$	$\xrightleftharpoons[K_{6D2}]{K_{6A2}}$	$[Cdc6\cdot Cdc20\cdot APCP]$	$\xrightarrow{F_{PRAPCCdc6}\cdot K_{PAPC}}$	$[Cdc20]+[APCP]$
”	$[Cdc6P\cdot Cdc20]+[APCP]$	$\xrightleftharpoons[K_{6D2}]{K_{6A2}}$	$[Cdc6P\cdot Cdc20\cdot APCP]$	$\xrightarrow{F_{PRAPCCdc6}\cdot K_{PAPC}}$	$[Cdc20]+[APCP]$

”	$[Cdc6 \cdot Clb2 \cdot Cdc20] + [APCP]$	$\underset{k_{6D2}}{\overset{K_{6A2}}{\rightleftharpoons}}$	$[Cdc6 \cdot Clb2 \cdot Cdc20 \cdot APCP]$	$\xrightarrow{F_{PRAPCCdc6} \cdot K_{PAPC}}$	$[Cdc20] + [Clb2] + [APCP]$
”	$[Cdc6P \cdot Clb2 \cdot Cdc20] + [APCP]$	$\underset{k_{6D2}}{\overset{K_{6A2}}{\rightleftharpoons}}$	$[Cdc6P \cdot Clb2 \cdot Cdc20 \cdot APCP]$	$\xrightarrow{F_{PRAPCCdc6} \cdot K_{PAPC}}$	$[Cdc20] + [Clb2] + [APCP]$
”	$[Cdc6 \cdot Clb5 \cdot Cdc20] + [APCP]$	$\underset{k_{6D2}}{\overset{K_{6A2}}{\rightleftharpoons}}$	$[Cdc6 \cdot Clb5 \cdot Cdc20 \cdot APCP]$	$\xrightarrow{F_{PRAPCCdc6} \cdot K_{PAPC}}$	$[Cdc20] + [Clb5] + [APCP]$
”	$[Cdc6P \cdot Clb5 \cdot Cdc20] + [APCP]$	$\underset{k_{6D2}}{\overset{K_{6A2}}{\rightleftharpoons}}$	$[Cdc6P \cdot Clb5 \cdot Cdc20 \cdot APCP]$	$\xrightarrow{F_{PRAPCCdc6} \cdot K_{PAPC}}$	$[Cdc20] + [Clb5] + [APCP]$
Proteolysis via Hct1 / APC [117]	$[Cdc20] + [Hct1]$	$\underset{k_{6D4}}{\overset{K_{6A4}}{\rightleftharpoons}}$	$[Cdc20 \cdot Hct1]$		
”	$[Cdc20] + [Hct1P]$	$\underset{k_{6D4}}{\overset{K_{6A4}}{\rightleftharpoons}}$	$[Cdc20 \cdot Hct1P]$		
”	$[Cdc20 \cdot SAC] + [Hct1]$	$\underset{k_{6D4}}{\overset{F_{DCdc20SAC} \cdot K_{6A4}}{\rightleftharpoons}}$	$[Cdc20 \cdot SAC \cdot Hct1]$		
”	$[Cdc20 \cdot SAC] + [Hct1P]$	$\underset{k_{6D4}}{\overset{F_{DCdc20SAC} \cdot K_{6A4}}{\rightleftharpoons}}$	$[Cdc20 \cdot SAC \cdot Hct1P]$		
Proteolysis of Swi5	$[Swi5 \cdot Cdc20] + [APCP]$	$\underset{k_{6D2}}{\overset{K_{6A2}}{\rightleftharpoons}}$	$[Swi5 \cdot Cdc20 \cdot APCP]$	$\xrightarrow{F_{PRAPCSwi5} \cdot K_{PAPC}}$	$[Cdc20] + [APCP]$
”	$[Swi5P \cdot Cdc20] + [APCP]$	$\underset{k_{6D2}}{\overset{K_{6A2}}{\rightleftharpoons}}$	$[Swi5P \cdot Cdc20 \cdot APCP]$	$\xrightarrow{F_{PRAPCSwi5} \cdot K_{PAPC}}$	$[Cdc20] + [APCP]$
Proteolysis of Ndd1	$[Ndd1 \cdot Cdc20] + [APCP]$	$\underset{k_{6D2}}{\overset{K_{6A2}}{\rightleftharpoons}}$	$[Ndd1 \cdot Cdc20 \cdot APCP]$	$\xrightarrow{F_{PRAPCNdd1} \cdot K_{PAPC}}$	$[Cdc20] + [APCP]$
”	$[Ndd1P \cdot Cdc20] + [APCP]$	$\underset{k_{6D2}}{\overset{K_{6A2}}{\rightleftharpoons}}$	$[Ndd1P \cdot Cdc20 \cdot APCP]$	$\xrightarrow{F_{PRAPCNdd1} \cdot K_{PAPC}}$	$[Cdc20] + [APCP]$
(7) Mitotic exit network (MEN):					
Phosphorylation of Net1 (mitotic exit network activity) [238, 285, 286]	$[Net1] + [MENP]$	$\underset{k_{7D1}}{\overset{K_{7A1}}{\rightleftharpoons}}$	$[Net1 \cdot MENP]$	$\xrightarrow{F_{PMENP} \cdot K_{7P1}}$	$[Net1P] + [MENP]$
”	$[Cdc14 \cdot Net1] + [MENP]$	$\underset{k_{7D1}}{\overset{K_{7A1}}{\rightleftharpoons}}$	$[Cdc14 \cdot Net1 \cdot MENP]$	$\xrightarrow{F_{PMENP} \cdot K_{7P1}}$	$[Cdc14 \cdot Net1P] + [MENP]$
”	$[Net1] + [MEN]$	$\underset{k_{7D1}}{\overset{K_{7A1}}{\rightleftharpoons}}$	$[Net1 \cdot MEN]$	$\xrightarrow{K_{7P1}}$	$[Net1P] + [MEN]$
”	$[Cdc14 \cdot Net1] + [MEN]$	$\underset{k_{7D1}}{\overset{K_{7A1}}{\rightleftharpoons}}$	$[Cdc14 \cdot Net1 \cdot MEN]$	$\xrightarrow{K_{7P1}}$	$[Cdc14 \cdot Net1P] + [MEN]$
(8) Cdc14 early anaphase release network (FEAR):					
Phosphorylation of Net1 [238,286]	$[Net1] + [FEAR]$	$\underset{k_{8D1}}{\overset{K_{8A1}}{\rightleftharpoons}}$	$[Net1 \cdot FEAR]$	$\xrightarrow{K_{8P1}}$	$[Net1P] + [FEAR]$

”	$[Cdc14 \cdot Net1] + [FEAR]$	$\underset{k_{8D1}}{\overset{K_{8A1}}{\rightleftharpoons}}$	$[Cdc14 \cdot Net1 \cdot FEAR]$	$\xrightarrow{K_{8P1}}$	$[Cdc14 \cdot Net1P] + [FEAR]$
(11) Cdc6:					
Gene expression via MBF [240]	$[MBF] + [CDC6_M]$	$\underset{k_{XMBFCdc6} \cdot k_{XDMBF}}{\overset{K_{XAMBF}}{\rightleftharpoons}}$	$[MBF \cdot CDC6_M]$		
	$[MBF \cdot CDC6_M] + [RP]$	$\underset{k_{DPol}}{\overset{F_{APolMBF} \cdot K_{APol}}{\rightleftharpoons}}$	$[MBF \cdot CDC6_M \cdot RP]$	$\xrightarrow{L_{TKCDC6} \cdot K_{TK}}$	$[mCDC6] + [MBF \cdot CDC6_M] + [RP]$
	$[mCDC6] + [RI]$	$\underset{k_{DRib}}{\overset{K_{ARib}}{\rightleftharpoons}}$	$[mCDC6 \cdot RI]$	$\xrightarrow{L_{TLCDC6} \cdot K_{TL}}$	$[Cdc6] + [mCDC6] + [RI]$
			$[mCDC6]$	$\xrightarrow{K_{DMCdc6}}$	$[]$
			$[mCDC6 \cdot RI]$	$\xrightarrow{K_{DMCdc6}}$	$[RI]$
Basal expression	$[CDC6_M] + [RP]$	$\underset{k_{DPol}}{\overset{F_{BXCdc6} \cdot K_{APol}}{\rightleftharpoons}}$	$[CDC6_M \cdot RP]$	$\xrightarrow{L_{TKCDC6} \cdot K_{TK}}$	$[mCDC6] + [CDC6_M] + [RP]$
Inhibition of gene expression by Yox1 [198]	$[Yox1] + [CDC6_M]$	$\underset{k_{XICdc6} \cdot k_{XDYox1}}{\overset{K_{XAYox1}}{\rightleftharpoons}}$	$[Yox1 \cdot CDC6_M]$		
Proteolysis via SCF [52, 64, 193]	$[Cdc6P] + [SCF]$	$\underset{k_{11D1}}{\overset{K_{11A1}}{\rightleftharpoons}}$	$[Cdc6P \cdot SCF]$	$\xrightarrow{F_{PRSCFCdc6} \cdot K_{PSCF}}$	$[] + [SCF]$
”	$[Clb2 \cdot Cdc6P] + [SCF]$	$\underset{k_{11D1}}{\overset{F_{DCCdc6} \cdot K_{11A1}}{\rightleftharpoons}}$	$[Clb2 \cdot Cdc6P \cdot SCF]$	$\xrightarrow{F_{PRSCFCdc6} \cdot K_{PSCF}}$	$[Clb2] + [SCF]$
”	$[Clb5 \cdot Cdc6P] + [SCF]$	$\underset{k_{11D1}}{\overset{F_{DCCdc6} \cdot K_{11A1}}{\rightleftharpoons}}$	$[Clb5 \cdot Cdc6P \cdot SCF]$	$\xrightarrow{F_{PRSCFCdc6} \cdot K_{PSCF}}$	$[Clb5] + [SCF]$
”	$[Cdc6] + [SCF]$	$\underset{k_{11D1}}{\overset{F_{DCdc6} \cdot K_{11A1}}{\rightleftharpoons}}$	$[Cdc6 \cdot SCF]$	$\xrightarrow{F_{PRSCFCdc6} \cdot K_{PSCF}}$	$[] + [SCF]$
”	$[Clb2 \cdot Cdc6] + [SCF]$	$\underset{k_{11D1}}{\overset{F_{DCdc6} \cdot F_{DCCdc6} \cdot K_{11A1}}{\rightleftharpoons}}$	$[Clb2 \cdot Cdc6 \cdot SCF]$	$\xrightarrow{F_{PRSCFCdc6} \cdot K_{PSCF}}$	$[Clb2] + [SCF]$
”	$[Clb5 \cdot Cdc6] + [SCF]$	$\underset{k_{11D1}}{\overset{F_{DCdc6} \cdot F_{DCCdc6} \cdot K_{11A1}}{\rightleftharpoons}}$	$[Clb5 \cdot Cdc6 \cdot SCF]$	$\xrightarrow{F_{PRSCFCdc6} \cdot K_{PSCF}}$	$[Clb5] + [SCF]$
Proteolysis via Hct1 / APC [194]	$[Cdc6] + [Hct1]$	$\underset{k_{11D2}}{\overset{K_{11A2}}{\rightleftharpoons}}$	$[Cdc6 \cdot Hct1]$		
”	$[Cdc6] + [Hct1P]$	$\underset{k_{11D2}}{\overset{K_{11A2}}{\rightleftharpoons}}$	$[Cdc6 \cdot Hct1P]$		
”	$[Cdc6P] + [Hct1]$	$\underset{k_{11D2}}{\overset{K_{11A2}}{\rightleftharpoons}}$	$[Cdc6P \cdot Hct1]$		
”	$[Cdc6P] + [Hct1P]$	$\underset{k_{11D2}}{\overset{K_{11A2}}{\rightleftharpoons}}$	$[Cdc6P \cdot Hct1P]$		
”	$[Clb2 \cdot Cdc6] + [Hct1]$	$\underset{k_{11D2}}{\overset{K_{11A2}}{\rightleftharpoons}}$	$[Cdc6 \cdot Clb2 \cdot Hct1]$		
”	$[Clb2 \cdot Cdc6P] + [Hct1]$	$\underset{k_{11D2}}{\overset{K_{11A2}}{\rightleftharpoons}}$	$[Cdc6P \cdot Clb2 \cdot Hct1]$		
”	$[Clb2 \cdot Cdc6] + [Hct1P]$	$\underset{k_{11D2}}{\overset{K_{11A2}}{\rightleftharpoons}}$	$[Cdc6 \cdot Clb2 \cdot Hct1P]$		

”	$[Clb2 \cdot Cdc6P] + [Hct1P]$	$\underset{k_{11D2}}{\overset{K_{11A2}}{\rightleftharpoons}}$	$[Cdc6P \cdot Clb2 \cdot Hct1P]$		
”	$[Clb5 \cdot Cdc6] + [Hct1]$	$\underset{k_{11D2}}{\overset{K_{11A2}}{\rightleftharpoons}}$	$[Cdc6 \cdot Clb5 \cdot Hct1]$		
”	$[Clb5 \cdot Cdc6P] + [Hct1]$	$\underset{k_{11D2}}{\overset{K_{11A2}}{\rightleftharpoons}}$	$[Cdc6P \cdot Clb5 \cdot Hct1]$		
”	$[Clb5 \cdot Cdc6] + [Hct1P]$	$\underset{k_{11D2}}{\overset{K_{11A2}}{\rightleftharpoons}}$	$[Cdc6 \cdot Clb5 \cdot Hct1P]$		
”	$[Clb5 \cdot Cdc6P] + [Hct1P]$	$\underset{k_{11D2}}{\overset{K_{11A2}}{\rightleftharpoons}}$	$[Cdc6P \cdot Clb5 \cdot Hct1P]$		
Proteolysis via Cdc20	$[Cdc6] + [Cdc20]$	$\underset{k_{11D3}}{\overset{K_{11A3}}{\rightleftharpoons}}$	$[Cdc6 \cdot Cdc20]$		
”	$[Cdc6P] + [Cdc20]$	$\underset{k_{11D3}}{\overset{K_{11A3}}{\rightleftharpoons}}$	$[Cdc6P \cdot Cdc20]$		
”	$[Clb2 \cdot Cdc6] + [Cdc20]$	$\underset{k_{11D3}}{\overset{K_{11A3}}{\rightleftharpoons}}$	$[Cdc6 \cdot Clb2 \cdot Cdc20]$		
”	$[Clb2 \cdot Cdc6P] + [Cdc20]$	$\underset{k_{11D3}}{\overset{K_{11A3}}{\rightleftharpoons}}$	$[Cdc6P \cdot Clb2 \cdot Cdc20]$		
”	$[Clb5 \cdot Cdc6] + [Cdc20]$	$\underset{k_{11D3}}{\overset{K_{11A3}}{\rightleftharpoons}}$	$[Cdc6 \cdot Clb5 \cdot Cdc20]$		
”	$[Clb5 \cdot Cdc6P] + [Cdc20]$	$\underset{k_{11D3}}{\overset{K_{11A3}}{\rightleftharpoons}}$	$[Cdc6P \cdot Clb5 \cdot Cdc20]$		
(12) Swi5:					
Gene expression via Mcm1 / Fkh12 / Ndd1 [163,240]	$[Fkh12P] + [SWI5]$	$\underset{k_{XFkh12Swi5} \cdot k_{XDFkh12}}{\overset{K_{XAFkh12}}{\rightleftharpoons}}$	$[Fkh12P \cdot SWI5]$		
	$[Fkh12] + [SWI5]$	$\underset{k_{XFkh12Swi5} \cdot k_{XDFkh12}}{\overset{K_{XAFkh12}}{\rightleftharpoons}}$	$[Fkh12 \cdot SWI5]$		
	$[Fkh12 \cdot SWI5] + [Ndd1]$	$\underset{k_{DFkh12Ndd1}}{\overset{K_{AFkh12Ndd1}}{\rightleftharpoons}}$	$[Fkh12 \cdot Ndd1 \cdot SWI5]$		
	$[Fkh12P \cdot SWI5] + [Ndd1]$	$\underset{k_{DFkh12Ndd1}}{\overset{F_{AFPN} \cdot K_{AFkh12Ndd1}}{\rightleftharpoons}}$	$[Fkh12P \cdot Ndd1 \cdot SWI5]$		
	$[Fkh12 \cdot SWI5] + [Ndd1P]$	$\underset{k_{DFkh12Ndd1}}{\overset{F_{AFNP} \cdot K_{AFkh12Ndd1}}{\rightleftharpoons}}$	$[Fkh12 \cdot Ndd1P \cdot SWI5]$		
	$[Fkh12P \cdot SWI5] + [Ndd1P]$	$\underset{k_{DFkh12Ndd1}}{\overset{F_{AFPN} \cdot F_{AFNP} \cdot K_{AFkh12Ndd1}}{\rightleftharpoons}}$	$[Fkh12P \cdot Ndd1P \cdot SWI5]$		
	$[Fkh12 \cdot Ndd1 \cdot SWI5] + [RP]$	$\underset{k_{DPol}}{\overset{F_{ATFNdd1} \cdot F_{APolNdd1} \cdot K_{APol}}{\rightleftharpoons}}$	$[Fkh12 \cdot Ndd1 \cdot SWI5 \cdot RP]$	$\xrightarrow{L_{TKSWI5} \cdot K_{TK}}$	$[mSWI5] + [Fkh12 \cdot Ndd1 \cdot SWI5] + [RP]$
	$[Fkh12 \cdot Ndd1P \cdot SWI5] + [RP]$	$\underset{k_{DPol}}{\overset{F_{APolNdd1} \cdot K_{APol}}{\rightleftharpoons}}$	$[Fkh12 \cdot Ndd1P \cdot SWI5 \cdot RP]$	$\xrightarrow{L_{TKSWI5} \cdot K_{TK}}$	$[mSWI5] + [Fkh12 \cdot Ndd1P \cdot SWI5] + [RP]$
	$[Fkh12P \cdot Ndd1 \cdot SWI5] + [RP]$	$\underset{k_{DPol}}{\overset{F_{ATFNdd1} \cdot F_{APolNdd1} \cdot K_{APol}}{\rightleftharpoons}}$	$[Fkh12P \cdot Ndd1 \cdot SWI5 \cdot RP]$	$\xrightarrow{L_{TKSWI5} \cdot K_{TK}}$	$[mSWI5] + [Fkh12P \cdot Ndd1 \cdot SWI5] + [RP]$

	$[Fkh12P \cdot Ndd1P \cdot SWI5] + [RP]$	$\xrightleftharpoons[K_{DPol}]{F_{APolNdd1} \cdot K_{APol}}$	$[Fkh12P \cdot Ndd1P \cdot SWI5 \cdot RP]$	$\xrightarrow{L_{TKSWI5} \cdot K_{TK}}$	$[mSWI5] + [Fkh12P \cdot Ndd1P \cdot SWI5] + [RP]$
Translation / mRNA degradation	$[mSWI5] + [RI]$	$\xrightleftharpoons[K_{DRib}]{K_{ARib}}$	$[mSWI5 \cdot RI]$	$\xrightarrow{L_{TLSWI5} \cdot K_{TL}}$	$[Swi5] + [mSWI5] + [RI]$
			$[mSWI5]$	$\xrightarrow{K_{DMSwi5}}$	$[]$
			$[mSWI5 \cdot RI]$	$\xrightarrow{K_{DMSwi5}}$	$[RI]$
Basal expression	$[SWI5] + [RP]$	$\xrightleftharpoons[K_{DPol}]{F_{BXSwi5} \cdot K_{APol}}$	$[SWI5 \cdot RP]$	$\xrightarrow{L_{TKSWI5} \cdot K_{TK}}$	$[mSWI5] + [SWI5] + [RP]$
Constitutive proteolysis [179]			$[Swi5]$	$\xrightarrow{K_{12P}}$	$[]$
”			$[Swi5P]$	$\xrightarrow{F_{DSwi5} \cdot K_{12P}}$	$[]$
Proteolysis via Cdc20	$[Swi5] + [Cdc20]$	$\xrightleftharpoons[K_{12D3}]{K_{12A3}}$	$[Swi5 \cdot Cdc20]$		
”	$[Swi5P] + [Cdc20]$	$\xrightleftharpoons[K_{12D3}]{F_{DSwi5} \cdot K_{12A3}}$	$[Swi5P \cdot Cdc20]$		
(13) Clb5:					
Complex formation with Sic1, Clb5-CDK inactivation [71,232]	$[Clb5] + [Sic1]$	$\xrightleftharpoons[K_{13D1}]{K_{13A1}}$	$[Clb5 \cdot Sic1]$		
”	$[Clb5] + [Sic1P]$	$\xrightleftharpoons[K_{13D1}]{K_{13A1}}$	$[Clb5 \cdot Sic1P]$		
Phosphorylation of Sic1 [71]	$[Sic1] + [Clb5]$	$\xrightleftharpoons[K_{13D2}]{K_{13A2}}$	$[Sic1 \cdot Clb5]$	$\xrightarrow{E_{13P2} \cdot F_{AClb} \cdot K_{PCDC28}}$	$[Sic1P] + [Clb5]$
”	$[Clb5 \cdot Sic1] + [Clb5]$	$\xrightleftharpoons[K_{13D2}]{K_{13A2}}$	$[Clb5 \cdot Sic1 \cdot Clb5]$	$\xrightarrow{E_{13P2} \cdot F_{AClb} \cdot K_{PCDC28}}$	$[Clb5 \cdot Sic1P] + [Clb5]$
”	$[Clb2 \cdot Sic1] + [Clb5]$	$\xrightleftharpoons[K_{13D2}]{K_{13A2}}$	$[Clb2 \cdot Sic1 \cdot Clb5]$	$\xrightarrow{E_{13P2} \cdot F_{AClb} \cdot K_{PCDC28}}$	$[Clb2 \cdot Sic1P] + [Clb5]$
Phosphorylation of Hct1 [283,291]	$[Hct1] + [Clb5]$	$\xrightleftharpoons[K_{13D3}]{K_{13A3}}$	$[Hct1 \cdot Clb5]$	$\xrightarrow{E_{13P3} \cdot F_{AClb} \cdot K_{PCDC28}}$	$[Hct1P] + [Clb5]$
Proteolysis via Cdc20 [120,236]	$[Clb5] + [Cdc20]$	$\xrightleftharpoons[K_{13D4}]{K_{13A4}}$	$[Clb5 \cdot Cdc20]$		
”	$[Clb5 \cdot Sic1] + [Cdc20]$	$\xrightleftharpoons[K_{13D4}]{K_{13A4}}$	$[Clb5 \cdot Sic1 \cdot Cdc20]$		
”	$[Clb5 \cdot Sic1P] + [Cdc20]$	$\xrightleftharpoons[K_{13D4}]{K_{13A4}}$	$[Clb5 \cdot Sic1P \cdot Cdc20]$		
”	$[Clb5 \cdot Cdc6] + [Cdc20]$	$\xrightleftharpoons[K_{13D4}]{K_{13A4}}$	$[Clb5 \cdot Cdc6 \cdot Cdc20]$		
”	$[Clb5 \cdot Cdc6P] + [Cdc20]$	$\xrightleftharpoons[K_{13D4}]{K_{13A4}}$	$[Clb5 \cdot Cdc6P \cdot Cdc20]$		
Gene expression via MBF [50]	$[MBF] + [CLB5]$	$\xrightarrow[K_{XMBFClb5} \cdot K_{XDMBF}]{K_{XAMBF}}$	$[MBF \cdot CLB5]$		

	$[MBF \cdot CLB5] + [RP]$	$\underset{K_{DPol}}{\overset{F_{APolMBF} \cdot K_{APol}}{\rightleftharpoons}}$	$[MBF \cdot CLB5 \cdot RP]$	$\xrightarrow{L_{TKCLB5} \cdot K_{TK}}$	$[mCLB5] + [MBF \cdot CLB5] + [RP]$
	$[mCLB5] + [RI]$	$\underset{K_{DRib}}{\overset{K_{ARib}}{\rightleftharpoons}}$	$[mCLB5 \cdot RI]$	$\xrightarrow{L_{TLCLB5} \cdot K_{TL}}$	$[Clb5] + [mCLB5] + [RI]$
			$[mCLB5]$	$\xrightarrow{K_{DMClb5}}$	$[]$
			$[mCLB5 \cdot RI]$	$\xrightarrow{K_{DMClb5}}$	$[RI]$
Phosphorylation of Swi5 [179]	$[Swi5] + [Clb5]$	$\underset{K_{13D10}}{\overset{K_{13A10}}{\rightleftharpoons}}$	$[Swi5 \cdot Clb5]$	$\xrightarrow{E_{13P10} \cdot F_{ACIb} \cdot K_{PCDC28}}$	$[Swi5P] + [Clb5]$
Constitutive proteolysis			$[Clb5]$	$\xrightarrow{K_{13P1}}$	$[]$
”			$[Clb5 \cdot Sic1]$	$\xrightarrow{K_{13P1}}$	$[Sic1]$
”			$[Clb5 \cdot Sic1P]$	$\xrightarrow{K_{13P1}}$	$[Sic1P]$
”			$[Clb5 \cdot Cdc6]$	$\xrightarrow{K_{13P1}}$	$[Cdc6]$
”			$[Clb5 \cdot Cdc6P]$	$\xrightarrow{K_{13P1}}$	$[Cdc6P]$
Complex formation with Cdc6 [65]	$[Clb5] + [Cdc6]$	$\underset{K_{13D12}}{\overset{K_{13A12}}{\rightleftharpoons}}$	$[Clb5 \cdot Cdc6]$		
”	$[Clb5] + [Cdc6P]$	$\underset{K_{13D12}}{\overset{F_{CPCdc6} \cdot K_{13A12}}{\rightleftharpoons}}$	$[Clb5 \cdot Cdc6P]$		
Phosphorylation of Cdc6 [64]	$[Cdc6] + [Clb5]$	$\underset{K_{13D13}}{\overset{F_{PFCdc6} \cdot K_{13A13}}{\rightleftharpoons}}$	$[Cdc6 \cdot Clb5]$	$\xrightarrow{E_{13P13} \cdot F_{ACIb} \cdot K_{PCDC28}}$	$[Cdc6P] + [Clb5]$
”	$[Clb5 \cdot Cdc6] + [Clb5]$	$\underset{K_{13D13}}{\overset{K_{13A13}}{\rightleftharpoons}}$	$[Clb5 \cdot Cdc6 \cdot Clb5]$	$\xrightarrow{E_{13P13} \cdot F_{ACIb} \cdot K_{PCDC28}}$	$[Clb5 \cdot Cdc6P] + [Clb5]$
”	$[Clb2 \cdot Cdc6] + [Clb5]$	$\underset{K_{13D13}}{\overset{K_{13A13}}{\rightleftharpoons}}$	$[Clb2 \cdot Cdc6 \cdot Clb5]$	$\xrightarrow{E_{13P13} \cdot F_{ACIb} \cdot K_{PCDC28}}$	$[Clb2 \cdot Cdc6P] + [Clb5]$
(17) Unspecific phosphorylation / dephosphorylation /degradation:					
De-phosphorylation of APC			$[APCP]$	$\xrightarrow{K_{17P6}}$	$[APC]$
De-phosphorylation of Net1			$[Net1P]$	$\xrightarrow{K_{17P}}$	$[Net1]$
De-phosphorylation of Cdc6			$[Cdc6P]$	$\xrightarrow{K_{17P10}}$	$[Cdc6]$
De-phosphorylation of MEN			$[MENP]$	$\xrightarrow{K_{17P1}}$	$[MEN]$
Degradation of MBF, constitutive			$[MBF]$	$\xrightarrow{K_{17P13}}$	$[]$

De-phosphorylation of Fkh12			$[Fkh12P]$	$\xrightarrow{K_{17P14}}$	$[Fkh12]$
De-phosphorylation of Ndd1			$[Ndd1P]$	$\xrightarrow{K_{17P15}}$	$[Ndd1]$
(27) Yox1/Yhp1:					
Gene expression via MBF [240]	$[MBF]+[YOX1_M]$	$\underset{K_{XMBFYox1}\cdot K_{XDMBF}}{\overset{K_{XAMBF}}{\rightleftharpoons}}$	$[MBF\cdot YOX1_M]$		
	$[MBF\cdot YOX1_M]+[RP]$	$\underset{K_{DPol}}{\overset{F_{APolMBF}\cdot K_{APol}}{\rightleftharpoons}}$	$[MBF\cdot YOX1_M\cdot RP]$	$\xrightarrow{L_{TKYOX1}\cdot K_{TK}}$	$[mYOX1]+[MBF\cdot YOX1_M]+[RP]$
”	$[mYOX1]+[RI]$	$\underset{K_{DRib}}{\overset{K_{ARib}}{\rightleftharpoons}}$	$[mYOX1\cdot RI]$	$\xrightarrow{L_{TLYOX1}\cdot K_{TL}}$	$[Yox1]+[mYOX1]+[RI]$
”			$[mYOX1]$	$\xrightarrow{K_{DMYox1}}$	$[]$
”			$[mYOX1\cdot RI]$	$\xrightarrow{K_{DMYox1}}$	$[RI]$
Gene expression via Mcm1 / Fkh12 / Ndd1 [198,246]	$[Fkh12P]+[YOX1_F]$	$\underset{K_{XFkh12Yox1}\cdot K_{XDFkh12}}{\overset{K_{XAFkh12}}{\rightleftharpoons}}$	$[Fkh12P\cdot YOX1_F]$		
	$[Fkh12]+[YOX1_F]$	$\underset{K_{XFkh12Yox1}\cdot K_{XDFkh12}}{\overset{K_{XAFkh12}}{\rightleftharpoons}}$	$[Fkh12\cdot YOX1_F]$		
	$[Fkh12\cdot YOX1_F]+[Ndd1]$	$\underset{K_{DFkh12Ndd1}}{\overset{K_{AFkh12Ndd1}}{\rightleftharpoons}}$	$[Fkh12\cdot Ndd1\cdot YOX1_F]$		
	$[Fkh12P\cdot YOX1_F]+[Ndd1]$	$\underset{K_{DFkh12Ndd1}}{\overset{F_{AFPN}\cdot K_{AFkh12Ndd1}}{\rightleftharpoons}}$	$[Fkh12P\cdot Ndd1\cdot YOX1_F]$		
	$[Fkh12\cdot YOX1_F]+[Ndd1P]$	$\underset{K_{DFkh12Ndd1}}{\overset{F_{AFNP}\cdot K_{AFkh12Ndd1}}{\rightleftharpoons}}$	$[Fkh12\cdot Ndd1P\cdot YOX1_F]$		
	$[Fkh12P\cdot YOX1_F]+[Ndd1P]$	$\underset{K_{DFkh12Ndd1}}{\overset{F_{AFPN}\cdot F_{AFNP}\cdot K_{AFkh12Ndd1}}{\rightleftharpoons}}$	$[Fkh12P\cdot Ndd1P\cdot YOX1_F]$		
	$[Fkh12\cdot Ndd1\cdot YOX1_F]+[RP]$	$\underset{K_{DPol}}{\overset{F_{ATFNdd1}\cdot F_{APolNdd1}\cdot K_{APol}}{\rightleftharpoons}}$	$[Fkh12\cdot Ndd1\cdot YOX1_F\cdot RP]$	$\xrightarrow{L_{TKYOX1}\cdot K_{TK}}$	$[mYOX1]+[Fkh12\cdot Ndd1\cdot YOX1_F]+[RP]$
	$[Fkh12\cdot Ndd1P\cdot YOX1_F]+[RP]$	$\underset{K_{DPol}}{\overset{F_{APolNdd1}\cdot K_{APol}}{\rightleftharpoons}}$	$[Fkh12\cdot Ndd1P\cdot YOX1_F\cdot RP]$	$\xrightarrow{L_{TKYOX1}\cdot K_{TK}}$	$[mYOX1]+[Fkh12\cdot Ndd1P\cdot YOX1_F]+[RP]$
	$[Fkh12P\cdot Ndd1\cdot YOX1_F]+[RP]$	$\underset{K_{DPol}}{\overset{F_{ATFNdd1}\cdot F_{APolNdd1}\cdot K_{APol}}{\rightleftharpoons}}$	$[Fkh12P\cdot Ndd1\cdot YOX1_F\cdot RP]$	$\xrightarrow{L_{TKYOX1}\cdot K_{TK}}$	$[mYOX1]+[Fkh12P\cdot Ndd1\cdot YOX1_F]+[RP]$
	$[Fkh12P\cdot Ndd1P\cdot YOX1_F]+[RP]$	$\underset{K_{DPol}}{\overset{F_{APolNdd1}\cdot K_{APol}}{\rightleftharpoons}}$	$[Fkh12P\cdot Ndd1P\cdot YOX1_F\cdot RP]$	$\xrightarrow{L_{TKYOX1}\cdot K_{TK}}$	$[mYOX1]+[Fkh12P\cdot Ndd1P\cdot YOX1_F]+[RP]$
Basal expression	$[YOX1_F]+[RP]$	$\underset{K_{DPol}}{\overset{F_{BXYox1}\cdot K_{APol}}{\rightleftharpoons}}$	$[YOX1_F\cdot RP]$	$\xrightarrow{L_{TKYOX1}\cdot K_{TK}}$	$[mYOX1]+[YOX1_F]+[RP]$
Constitutive proteolysis			$[Yox1]$	$\xrightarrow{K_{27P1}}$	$[]$

Proteolysis via Hct1 / APC	$[Yox1]+[Hct1]$	$\underset{K_{27D2}}{\overset{K_{27A2}}{\rightleftharpoons}}$	$[Yox1 \cdot Hct1]$		
”	$[Yox1]+[Hct1P]$	$\underset{K_{27D2}}{\overset{K_{27A2}}{\rightleftharpoons}}$	$[Yox1 \cdot Hct1P]$		
Proteolysis via Cdc20	$[Yox1]+[Cdc20]$	$\underset{K_{27D3}}{\overset{K_{27A3}}{\rightleftharpoons}}$	$[Yox1 \cdot Cdc20]$		
(28) Ndd1:					
Gene expression via MBF [240]	$[MBF]+[NDD1_M]$	$\xrightarrow{K_{XAMBF}}$ $K_{XMBFNdd1} \cdot K_{XDMBF}$	$[MBF \cdot NDD1_M]$		
	$[MBF \cdot NDD1_M]+[RP]$	$\underset{K_{DPol}}{\overset{F_{APolMBF} \cdot K_{APol}}{\rightleftharpoons}}$	$[MBF \cdot NDD1_M \cdot RP]$	$\xrightarrow{L_{TKNDD1} \cdot K_{TK}}$	$[mNDD1]+[MBF \cdot NDD1_M]+[RP]$
	$[mNDD1]+[RI]$	$\underset{K_{DRib}}{\overset{K_{ARib}}{\rightleftharpoons}}$	$[mNDD1 \cdot RI]$	$\xrightarrow{L_{TLNDD1} \cdot K_{TL}}$	$[Ndd1]+[mNDD1]+[RI]$
			$[mNDD1]$	$\xrightarrow{K_{DMNdd1}}$	$[]$
			$[mNDD1 \cdot RI]$	$\xrightarrow{K_{DMNdd1}}$	$[RI]$
Gene expression via Mcm1 / Fkh12 / Ndd1	$[Fkh12P]+[NDD1_F]$	$\xrightarrow{K_{XAFkh12}}$ $K_{XFkh12Ndd1} \cdot K_{XDFkh12}$	$[Fkh12P \cdot NDD1_F]$		
	$[Fkh12]+[NDD1_F]$	$\xrightarrow{K_{XAFkh12}}$ $K_{XFkh12Ndd1} \cdot K_{XDFkh12}$	$[Fkh12 \cdot NDD1_F]$		
	$[Fkh12 \cdot NDD1_F]+[Ndd1]$	$\underset{K_{DFkh12Ndd1}}{\overset{K_{AFkh12Ndd1}}{\rightleftharpoons}}$	$[Fkh12 \cdot Ndd1 \cdot NDD1_F]$		
	$[Fkh12P \cdot NDD1_F]+[Ndd1]$	$\underset{K_{DFkh12Ndd1}}{\overset{F_{AFPN} \cdot K_{AFkh12Ndd1}}{\rightleftharpoons}}$	$[Fkh12P \cdot Ndd1 \cdot NDD1_F]$		
	$[Fkh12 \cdot NDD1_F]+[Ndd1P]$	$\underset{K_{DFkh12Ndd1}}{\overset{F_{AFNP} \cdot K_{AFkh12Ndd1}}{\rightleftharpoons}}$	$[Fkh12 \cdot Ndd1P \cdot NDD1_F]$		
	$[Fkh12P \cdot NDD1_F]+[Ndd1P]$	$\underset{K_{DFkh12Ndd1}}{\overset{F_{AFPN} \cdot F_{AFNP} \cdot K_{AFkh12Ndd1}}{\rightleftharpoons}}$	$[Fkh12P \cdot Ndd1P \cdot NDD1_F]$		
	$[Fkh12 \cdot Ndd1 \cdot NDD1_F]+[RP]$	$\underset{K_{DPol}}{\overset{F_{ATFNdd1} \cdot F_{APolNdd1} \cdot K_{APol}}{\rightleftharpoons}}$	$[Fkh12 \cdot Ndd1 \cdot NDD1_F \cdot RP]$	$\xrightarrow{L_{TKNDD1} \cdot K_{TK}}$	$[mNDD1]+[Fkh12 \cdot Ndd1 \cdot NDD1_F]+[RP]$
	$[Fkh12 \cdot Ndd1P \cdot NDD1_F]+[RP]$	$\underset{K_{DPol}}{\overset{F_{APolNdd1} \cdot K_{APol}}{\rightleftharpoons}}$	$[Fkh12 \cdot Ndd1P \cdot NDD1_F \cdot RP]$	$\xrightarrow{L_{TKNDD1} \cdot K_{TK}}$	$[mNDD1]+[Fkh12 \cdot Ndd1P \cdot NDD1_F]+[RP]$
	$[Fkh12P \cdot Ndd1 \cdot NDD1_F]+[RP]$	$\underset{K_{DPol}}{\overset{F_{ATFNdd1} \cdot F_{APolNdd1} \cdot K_{APol}}{\rightleftharpoons}}$	$[Fkh12P \cdot Ndd1 \cdot NDD1_F \cdot RP]$	$\xrightarrow{L_{TKNDD1} \cdot K_{TK}}$	$[mNDD1]+[Fkh12P \cdot Ndd1 \cdot NDD1_F]+[RP]$
	$[Fkh12P \cdot Ndd1P \cdot NDD1_F]+[RP]$	$\underset{K_{DPol}}{\overset{F_{APolNdd1} \cdot K_{APol}}{\rightleftharpoons}}$	$[Fkh12P \cdot Ndd1P \cdot NDD1_F \cdot RP]$	$\xrightarrow{L_{TKNDD1} \cdot K_{TK}}$	$[mNDD1]+[Fkh12P \cdot Ndd1P \cdot NDD1_F]+[RP]$
Basal expression	$[NDD1_F]+[RP]$	$\underset{K_{DPol}}{\overset{F_{BXNdd1} \cdot K_{APol}}{\rightleftharpoons}}$	$[NDD1_F \cdot RP]$	$\xrightarrow{L_{TKNDD1} \cdot K_{TK}}$	$[mNDD1]+[NDD1_F]+[RP]$

Constitutive proteolysis			$[Ndd1]$	$\xrightarrow{F_{DNdd1} \cdot K_{28P1}}$	$[]$
”			$[Ndd1P]$	$\xrightarrow{K_{28P}}$	$[]$
Proteolysis via Hct1 / APC	$[Ndd1] + [Hct1]$	$\underset{K_{28D2}}{\overset{K_{28A2}}{\rightleftharpoons}}$	$[Ndd1 \cdot Hct1]$		
”	$[Ndd1] + [Hct1P]$	$\underset{K_{28D2}}{\overset{K_{28A2}}{\rightleftharpoons}}$	$[Ndd1 \cdot Hct1P]$		
”	$[Ndd1P] + [Hct1]$	$\underset{K_{28D2}}{\overset{K_{28A2}}{\rightleftharpoons}}$	$[Ndd1P \cdot Hct1]$		
”	$[Ndd1P] + [Hct1P]$	$\underset{K_{28D2}}{\overset{K_{28A2}}{\rightleftharpoons}}$	$[Ndd1P \cdot Hct1P]$		
Proteolysis via Cdc20 / APC	$[Ndd1] + [Cdc20]$	$\underset{K_{28D3}}{\overset{K_{28A3}}{\rightleftharpoons}}$	$[Ndd1 \cdot Cdc20]$		
”	$[Ndd1P] + [Cdc20]$	$\underset{K_{28D3}}{\overset{K_{28A3}}{\rightleftharpoons}}$	$[Ndd1P \cdot Cdc20]$		
Protein overexpression using the *GAL1-10* promoter:					
GAL Overexpression Sic1	$[GalSIC1] + [RP]$	$\underset{F_{OVXSic1} \cdot K_{DTKGal}}{\overset{F_{OVXSic1} \cdot K_{ATKGal}}{\rightleftharpoons}}$	$[GalSIC1 \cdot RP]$	$\xrightarrow{L_{TKSIC1} \cdot K_{TK}}$	$[mSIC1] + [GalSIC1] + [RP]$
GAL Overexpression Cdc6	$[GalCDC6] + [RP]$	$\underset{F_{OVXCdc6} \cdot K_{DTKGal}}{\overset{F_{OVXCdc6} \cdot K_{ATKGal}}{\rightleftharpoons}}$	$[GalCDC6 \cdot RP]$	$\xrightarrow{L_{TKCDC6} \cdot K_{TK}}$	$[mCDC6]+[GalCDC6]+[RP]$
GAL Overexpression Clb5	$[GalCLB5] + [RP]$	$\underset{F_{OVXClb5} \cdot K_{DTKGal}}{\overset{F_{OVXClb5} \cdot K_{ATKGal}}{\rightleftharpoons}}$	$[GalCLB5 \cdot RP]$	$\xrightarrow{L_{TKCLB5} \cdot K_{TK}}$	$[mCLB5] + [GalCLB5] + [RP]$
GAL Overexpression Clb2	$[GalCLB2] + [RP]$	$\underset{F_{OVXClb2} \cdot K_{DTKGal}}{\overset{F_{OVXClb2} \cdot K_{ATKGal}}{\rightleftharpoons}}$	$[GalCLB2 \cdot RP]$	$\xrightarrow{L_{TKCLB2} \cdot K_{TK}}$	$[mCLB2] + [GalCLB2] + [RP]$
GAL Overexpression Cdc20	$[GalCDC20] + [RP]$	$\underset{F_{OVXCdc20} \cdot K_{DTKGal}}{\overset{F_{OVXCdc20} \cdot K_{ATKGal}}{\rightleftharpoons}}$	$[GalCDC20 \cdot RP]$	$\xrightarrow{L_{TKCDC20} \cdot K_{TK}}$	$[mCDC20] + [GalCDC20] + [RP]$
GAL Overexpression Yox1	$[GalYOX1] + [RP]$	$\underset{F_{OVXYox1} \cdot K_{DTKGal}}{\overset{F_{OVXYox1} \cdot K_{ATKGal}}{\rightleftharpoons}}$	$[GalYOX1 \cdot RP]$	$\xrightarrow{L_{TKYOX1} \cdot K_{TK}}$	$[mYOX1]+[GalYOX1]+[RP]$
GAL Overexpression Ndd1	$[GalNDD1] + [RP]$	$\underset{K_{DTKGal}}{\overset{F_{OVXNdd1} \cdot K_{ATKGal}}{\rightleftharpoons}}$	$[GalNDD1 \cdot RP]$	$\xrightarrow{L_{TKNDD1} \cdot K_{TK}}$	$[mNDD1] + [GalNDD1] + [RP]$
GAL Overexpression Fkh1/2	$[GalFKH12] + [RP]$	$\underset{K_{DTKGal}}{\overset{F_{OVXFkh12} \cdot K_{ATKGal}}{\rightleftharpoons}}$	$[GalFKH12 \cdot RP]$	$\xrightarrow{L_{TKFkh12} \cdot K_{TK}}$	$[mFKH12] + [GalFKH12] + [RP]$
GAL Overexpression Hct1	$[GalHCT1] + [RP]$	$\underset{K_{DTKGal}}{\overset{F_{OVXHct1} \cdot K_{ATKGal}}{\rightleftharpoons}}$	$[GalHCT1 \cdot RP]$	$\xrightarrow{L_{TKHCT1} \cdot K_{TK}}$	$[mHCT1]+[GalHCT1]+[RP]$
Translation / mRNA degradation	$[mHCT1] + [RI]$	$\underset{K_{DRib}}{\overset{K_{ARib}}{\rightleftharpoons}}$	$[mHCT1 \cdot RI]$	$\xrightarrow{L_{TLHCT1} \cdot K_{TL}}$	$[Hct1] + [mHCT1] + [RI]$
”			$[mHCT1]$	$\xrightarrow{K_{DMHct}}$	$[]$

”			$[mHCT1 \cdot RI]$	$\xrightarrow{K_{DMHct1}}$	$[RI]$
Proteolysis			$[Hct1]$	$\xrightarrow{F_{OVXHct1} \cdot K_{DOVXP}}$	$[]$
”			$[Hct1P]$	$\xrightarrow{F_{OVXHct1} \cdot K_{DOVXP}}$	$[]$
GAL Overexpression Cdc14	$[GalCDC14] + [RP]$	$\underset{K_{DTKGal}}{\overset{F_{OVXCdc14} \cdot K_{ATKGal}}{\rightleftharpoons}}$	$[GalCDC14 \cdot RP]$	$\xrightarrow{L_{TKCdc14} \cdot K_{TK}}$	$[mCDC14] + [GalCDC14] + [RP]$
Translation / mRNA degradation	$[mCDC14] + [RI]$	$\underset{K_{DRib}}{\overset{K_{ARib}}{\rightleftharpoons}}$	$[mCDC14 \cdot RI]$	$\xrightarrow{L_{TLCDC14} \cdot K_{TL}}$	$[Cdc14] + [mCDC14] + [RI]$
”			$[mCDC14]$	$\xrightarrow{K_{DMCdc14}}$	$[]$
”			$[mCDC14 \cdot RI]$	$\xrightarrow{K_{DMCdc14}}$	$[RI]$
Proteolysis			$[Cdc14]$	$\xrightarrow{F_{OVXCdc14} \cdot K_{DOVXP}}$	$[]$
GAL Overexpression Net1	$[GalNET1] + [RP]$	$\underset{K_{DTKGal}}{\overset{F_{OVXNet1} \cdot K_{ATKGal}}{\rightleftharpoons}}$	$[GalNET1 \cdot RP]$	$\xrightarrow{L_{TKNET1} \cdot K_{TK}}$	$[mNET1] + [GalNET1] + [RP]$
Translation / mRNA degradation	$[mNET1] + [RI]$	$\underset{K_{DRib}}{\overset{K_{ARib}}{\rightleftharpoons}}$	$[mNET1 \cdot RI]$	$\xrightarrow{L_{TLNET1} \cdot K_{TL}}$	$[Net1] + [mNET1] + [RI]$
”			$[mNET1]$	$\xrightarrow{K_{DMNet1}}$	$[]$
”			$[mNET1 \cdot RI]$	$\xrightarrow{K_{DMNet1}}$	$[RI]$
Proteolysis			$[Net1]$	$\xrightarrow{F_{OVXNet1} \cdot K_{DOVXP}}$	$[]$

System size:	**State variables:**	**360**
	Elementary reactions:	**834**
	Parameters:	**242**

Tab. C.2: Experimental data employed in parameter estimation. Unless indicated otherwise, α-factor block-and-release experiments were used, in which cells were synchronized through chemically induced arrest in the G1 phase, and then enabled to resume cell cycle progression. Total concentrations refer to the sum of all species of a protein or mRNA. The activity of Clb2-CDK was approximated by the concentration of free Clb2 plus all concentrations of protein complexes, in which Clb2 participated and was not inhibited by either Sic1 or Cdc6.

Genotype and additional treatment	total *CLB2* mRNA	total Clb2 protein	Clb2-CDK activity	Cdc14/Net1 complex	Hct1 phosphorylation	total Sic1 protein	total Clb5 protein	total Cdc20 protein	total *SWI5* mRNA
wild type	[149] Fig. 7	[75] Fig. 1	[75] Fig. 1 + low activity in G1	complete release in telophase [247] Fig. 1A	high in M, low in G1 [117, 231]	≈ 40% of peak Clb2 conc. in G1 [44]	[44], Fig. 7	undetectable protein in G1 [201]	[197], Fig. 10
mitotic exit network mutant: *cdc15-2*	–	[250] Fig. 2	–	no release in telophase [247] Fig. 1B	high in arrest [291] Fig. 3	undetectable protein [232]	–	–	–
$hct1\Delta$	–	–	no activity in G1 [44] Fig. 6	–	–	≈ wild type levels in G1 [44] Fig. 6	–	–	–
wild type + Noc + $5xGAL1,10-SIC1$	–	≈ 200% of peak Clb2 conc. in arrest [3, 25, 44] + [6] Fig. 2	constant specific activity [3] + [6] Fig. 2	–	–	–	–	–	–
$hct1\Delta$ + Noc + $GAL1,10-CDC6$	–	[25] Fig. 1	[25] Fig. 1	–	–	–	–	–	–

Tab. C.3: Reference parameter values for the module "control of mitosis". Apart from the parameters names, a brief description and the reference parameter values, in the last two columns, the upper and lower bounds on admissible parameter space that were used in parameter estimation are provided, respectively. Missing entries in both of these columns mean that the parameter was not estimated. A lower bound of zero leads to an undefined entry for the $\log_{10}$-scaled boundaries.

Name	Description	Parameter value		Log_{10} range	
K_{2A5}	$k_{ass.}$ dephosph. of Net1 by Cdc14	$1.13 \cdot 10^{-2}$	$\mu M^{-1}s^{-1}$	-2.00	$+1.00$
K_{2D5}	$k_{diss.}$ dephosph. of Net1 by Cdc14	$1.00 \cdot 10^{0}$	s^{-1}	-4.00	$+0.00$
$F_{ACDC14NET1}$	Relative dephosph. of Net1 by Cdc14	$2.45 \cdot 10^{-3}$		$--$	$+1.00$
K_{PCDC14}	$k_{cat.}$ Cdc14	$6.27 \cdot 10^{-1}$	s^{-1}	-2.00	$+0.00$
K_{2A6}	$k_{ass.}$ complex formation Cdc14–Net1	$4.01 \cdot 10^{0}$	$\mu M^{-1}s^{-1}$	-2.00	$+2.00$
K_{2D6}	$k_{diss.}$ complex formation Cdc14–Net1	$2.83 \cdot 10^{-3}$	s^{-1}	-4.00	$+0.00$
$F_{DNET1PCDC14}$	Relative affinity of Cdc14 for Net1P	$1.00 \cdot 10^{4}$		$+0.00$	$+4.00$
K_{2A8}	$k_{ass.}$ dimerization of Cdc14	$9.08 \cdot 10^{-2}$	$\mu M^{-1}s^{-1}$	-2.00	$+2.00$
K_{2D8}	$k_{diss.}$ dimerization of Cdc14	$2.79 \cdot 10^{-1}$	s^{-1}	-4.00	$+0.00$
K_{2A10}	$k_{ass.}$ dephosph. of Hct1 by Cdc14	$4.77 \cdot 10^{1}$	$\mu M^{-1}s^{-1}$	-2.00	$+2.00$
K_{2D10}	$k_{diss.}$ dephosph. of Hct1 by Cdc14	$8.69 \cdot 10^{-1}$	s^{-1}	-4.00	$+0.00$
E_{2P10}	Efficiency dephosph. of Hct1 by Cdc14	$9.95 \cdot 10^{0}$		-1.00	$+1.00$
K_{2A11}	$k_{ass.}$ dephosph. of Swi5 by Cdc14	$5.30 \cdot 10^{0}$	$\mu M^{-1}s^{-1}$	-2.00	$+2.00$
K_{2D11}	$k_{diss.}$ dephosph. of Swi5 by Cdc14	$3.28 \cdot 10^{-2}$	s^{-1}	-4.00	$+0.00$
E_{2P11}	Efficiency dephosph. of Swi5 by Cdc14	$9.43 \cdot 10^{0}$		-1.00	$+1.00$
K_{2A12}	$k_{ass.}$ dephosph. of Sic1 by Cdc14	$4.43 \cdot 10^{1}$	$\mu M^{-1}s^{-1}$	-2.00	$+2.00$
K_{2D12}	$k_{diss.}$ dephosph. of Sic1 by Cdc14	$8.14 \cdot 10^{-4}$	s^{-1}	-4.00	$+0.00$
E_{2P12}	Efficiency dephosph. of Sic1 by Cdc14	$1.06 \cdot 10^{0}$		-1.00	$+1.00$
K_{2A13}	$k_{ass.}$ dephosph. of MEN by Cdc14	$3.48 \cdot 10^{1}$	$\mu M^{-1}s^{-1}$	-2.00	$+2.00$
K_{2D13}	$k_{diss.}$ dephosph. of MEN by Cdc14	$8.64 \cdot 10^{-1}$	s^{-1}	-4.00	$+0.00$
E_{2P13}	Efficiency dephosph. of MEN by Cdc14	$9.72 \cdot 10^{0}$		-1.00	$+1.00$
K_{2A16}	$k_{ass.}$ dephosph. of Cdc6 by Cdc14	$9.97 \cdot 10^{1}$	$\mu M^{-1}s^{-1}$	-2.00	$+2.00$
K_{2D16}	$k_{diss.}$ dephosph. of Cdc6 by Cdc14	$4.42 \cdot 10^{-3}$	s^{-1}	-4.00	$+0.00$
E_{2P16}	Efficiency dephosph. of Cdc6 by Cdc14	$1.00 \cdot 10^{-1}$		-1.00	$+1.00$
K_{2A17}	$k_{ass.}$ dephosph. of Fkh12 by Cdc14	$1.00 \cdot 10^{2}$	$\mu M^{-1}s^{-1}$	-2.00	$+2.00$
K_{2D17}	$k_{diss.}$ dephosph. of Fkh12 by Cdc14	$1.42 \cdot 10^{-1}$	s^{-1}	-4.00	$+0.00$
E_{2P17}	Efficiency dephosph. of Fkh12 by Cdc14	$1.01 \cdot 10^{-1}$		-1.00	$+1.00$
K_{2A18}	$k_{ass.}$ dephosph. of Ndd1 by Cdc14	$1.02 \cdot 10^{0}$	$\mu M^{-1}s^{-1}$	-2.00	$+2.00$
K_{2D18}	$k_{diss.}$ dephosph. of Ndd1 by Cdc14	$8.38 \cdot 10^{-1}$	s^{-1}	-4.00	$+0.00$
E_{2P18}	Efficiency dephosph. of Ndd1 by Cdc14	$1.01 \cdot 10^{0}$		-1.00	$+1.00$
K_{3A1}	$k_{ass.}$ complex formation Clb2–Sic1	$9.96 \cdot 10^{1}$	$\mu M^{-1}s^{-1}$	-2.00	$+2.00$
K_{3D1}	$k_{diss.}$ complex formation Clb2–Sic1	$1.70 \cdot 10^{-2}$	s^{-1}	-4.00	$+0.00$
K_{3A2}	$k_{ass.}$ phosphorylation of Sic1 by Clb2	$1.42 \cdot 10^{0}$	$\mu M^{-1}s^{-1}$	-2.00	$+2.00$
K_{3D2}	$k_{diss.}$ phosphorylation of Sic1 by Clb2	$9.50 \cdot 10^{-1}$	s^{-1}	-4.00	$+0.00$
E_{3P2}	Efficiency phosph. of Sic1 by Clb2	$8.95 \cdot 10^{0}$		-1.00	$+1.00$
F_{ACLB}	Relative $k_{cat.}$ Clb - Cdc28	$9.97 \cdot 10^{0}$		-1.00	$+1.00$
K_{PCDC28}	$k_{cat.}$ Cdc28	$8.36 \cdot 10^{1}$	s^{-1}	-2.00	$+2.00$
K_{3A3}	$k_{ass.}$ phosphorylation of Hct1 by Clb2	$4.69 \cdot 10^{1}$	$\mu M^{-1}s^{-1}$	-2.00	$+2.00$
K_{3D3}	$k_{diss.}$ phosphorylation of Hct1 by Clb2	$1.61 \cdot 10^{-2}$	s^{-1}	-4.00	$+0.00$
E_{3P3}	Efficiency phosph. of Hct1 by Clb2	$9.99 \cdot 10^{0}$		-1.00	$+1.00$
$K_{XAFKH12}$	$k_{ass.}$ Fkh12–DNA	$9.11 \cdot 10^{1}$	$\mu M^{-1}s^{-1}$	-2.00	$+2.00$
$F_{XFKH12CLB2}$	Relative affinity Fkh12 for CLB2 promoter	$5.97 \cdot 10^{0}$		-1.00	$+1.00$
$K_{XDFKH12}$	$k_{diss.}$ Fkh12–DNA	$9.52 \cdot 10^{-1}$	s^{-1}	-4.00	$+0.00$
$K_{AFKH12NDD1}$	$k_{ass.}$ complex formation Fkh12–Ndd1	$2.53 \cdot 10^{0}$	$k_{ass.}$	-2.00	$+2.00$
$K_{DFKH12NDD1}$	$k_{diss.}$ complex formation Fkh12–Ndd1	$9.17 \cdot 10^{-1}$	s^{-1}	-4.00	$+0.00$
F_{AFPN}	Relative aff. Fkh12 / Fkh12P for Ndd1	$1.34 \cdot 10^{0}$		-2.00	$+2.00$
F_{AFNP}	Relative aff. Ndd1 / Ndd1P for Fkh12	$3.80 \cdot 10^{1}$		-2.00	$+2.00$

Name	Description	Parameter value		Log_{10} range	
$F_{ATFNDD1}$	Relative transcriptional act. Ndd1 / Ndd1P	$1.00 \cdot 10^{-2}$		-2.00	$+0.00$
$F_{APOLNDD1}$	Relative association Ndd1–RNA pol.	$7.29 \cdot 10^{-1}$		-2.00	$+2.00$
K_{APOL}	$k_{ass.}$ RNA pol.–transcriptional activators	$4.75 \cdot 10^{-2}$	$\mu M^{-1}s^{-1}$	-2.00	$+2.00$
K_{DPOL}	$k_{diss.}$ RNA pol.–transcriptional activators	$1.00 \cdot 10^{0}$	s^{-1}	-4.00	$+0.00$
L_{TKCLB2}	Transcript length mCLB2	$6.79 \cdot 10^{-4}$		–	–
K_{TK}	$k_{cat.}$ general transcription	$1.86 \cdot 10^{1}$	s^{-1}	$+1.26$	$+1.56$
K_{ARIB}	$k_{ass.}$ association ribosomes–mRNA	$1.00 \cdot 10^{2}$	$\mu M^{-1}s^{-1}$	-2.00	$+2.00$
K_{DRIB}	$k_{diss.}$ association ribosomes–mRNA	$9.98 \cdot 10^{-1}$	s^{-1}	-4.00	$+0.00$
L_{TLCLB2}	Protein length Clb2	$2.04 \cdot 10^{-3}$		–	–
K_{TL}	$k_{cat.}$ general translation	$1.29 \cdot 10^{1}$	s^{-1}	$+0.70$	$+1.30$
K_{DMCLB2}	mRNA degradation rate CLB2	$8.08 \cdot 10^{-4}$	s^{-1}	-3.10	-3.01
K_{XAMBF}	$k_{ass.}$ MBF–DNA	$6.05 \cdot 10^{1}$	$\mu M^{-1}s^{-1}$	-3.00	$+2.00$
$F_{XMBFCLB2}$	Relative affinity MBF for CLB2 promoter	$1.00 \cdot 10^{3}$		–	–
K_{XDMBF}	$k_{diss.}$ MBF–DNA	$3.51 \cdot 10^{-1}$	s^{-1}	-4.00	$+0.00$
$F_{APOLMBFP}$	Relative association MBF–RNA pol.	$2.38 \cdot 10^{0}$		-2.00	$+2.00$
F_{BXCLB2}	Relative constitutive expression CLB2	$1.17 \cdot 10^{-2}$		-2.00	$+0.00$
K_{3A4}	$k_{ass.}$ complex formation Clb2–Hct1	$4.06 \cdot 10^{0}$	$\mu M^{-1}s^{-1}$	-2.00	$+2.00$
K_{3D4}	$k_{diss.}$ complex formation Clb2–Hct1	$8.65 \cdot 10^{-1}$	s^{-1}	-4.00	$+0.00$
K_{3A5}	$k_{ass.}$ complex formation Clb2–Cdc20	$3.34 \cdot 10^{0}$	$\mu M^{-1}s^{-1}$	-2.00	$+2.00$
K_{3D5}	$k_{diss.}$ complex formation Clb2–Cdc20	$9.93 \cdot 10^{-1}$	s^{-1}	-4.00	$+0.00$
K_{3A9}	$k_{ass.}$ phosphorylation of Swi5 by Clb2	$3.96 \cdot 10^{0}$	$\mu M^{-1}s^{-1}$	-2.00	$+2.00$
K_{3D9}	$k_{diss.}$ phosphorylation of Swi5 by Clb2	$9.44 \cdot 10^{-1}$	s^{-1}	-4.00	$+0.00$
E_{3P9}	Efficiency phosph. of Swi5 by Clb2	$2.35 \cdot 10^{0}$		-1.00	$+1.00$
K_{3A10}	$k_{ass.}$ phosphorylation of APC by Clb2	$9.99 \cdot 10^{1}$	$\mu M^{-1}s^{-1}$	-2.00	$+2.00$
K_{3D10}	$k_{diss.}$ phosphorylation of APC by Clb2	$7.59 \cdot 10^{-1}$	s^{-1}	-4.00	$+0.00$
E_{3P10}	Efficiency phosph. of APC by Clb2	$1.00 \cdot 10^{1}$		-1.00	$+1.00$
K_{3A13}	$k_{ass.}$ phosphorylation of MEN by Clb2	$3.22 \cdot 10^{0}$	$\mu M^{-1}s^{-1}$	-2.00	$+2.00$
K_{3D13}	$k_{diss.}$ phosphorylation of MEN by Clb2	$1.22 \cdot 10^{-1}$	s^{-1}	-4.00	$+0.00$
E_{3P13}	Efficiency phosph. of MEN by Clb2	$2.36 \cdot 10^{0}$		-1.00	$+1.00$
K_{3P14}	$k_{cat.}$ constitutive degradation of Clb2	$9.63 \cdot 10^{-5}$	s^{-1}	-4.02	-2.24
K_{3A15}	$k_{ass.}$ complex formation Clb2–Cdc6	$9.98 \cdot 10^{1}$	$\mu M^{-1}s^{-1}$	-2.00	$+2.00$
K_{3D15}	$k_{diss.}$ complex formation Clb2–Cdc6	$9.36 \cdot 10^{-1}$	s^{-1}	-4.00	$+0.00$
F_{CPCDC6}	Relative association Clb2–Cdc6P / Cdc6	$9.90 \cdot 10^{1}$		-2.00	$+2.00$
F_{PFCDC6}	Relative phosph. free / complexed Cdc6	$9.95 \cdot 10^{1}$		-2.00	$+2.00$
K_{3A16}	$k_{ass.}$ phosphorylation of Cdc6 by Clb2	$5.47 \cdot 10^{1}$	$\mu M^{-1}s^{-1}$	-2.00	$+2.00$
K_{3D16}	$k_{diss.}$ phosphorylation of Cdc6 by Clb2	$9.83 \cdot 10^{-1}$	s^{-1}	-4.00	$+0.00$
E_{3P16}	Efficiency phosph. of Cdc6 by Clb2	$9.37 \cdot 10^{0}$		-1.00	$+1.00$
K_{3A17}	$k_{ass.}$ phosphorylation of Fkh12 by Clb2	$9.93 \cdot 10^{1}$	$\mu M^{-1}s^{-1}$	-2.00	$+2.00$
K_{3D17}	$k_{diss.}$ phosphorylation of Fkh12 by Clb2	$7.42 \cdot 10^{-1}$	s^{-1}	-4.00	$+0.00$
E_{3P17}	Efficiency phosph. of Fkh12 by Clb2	$7.80 \cdot 10^{0}$		-1.00	$+1.00$
K_{3A18}	$k_{ass.}$ phosphorylation of Ndd1 by Clb2	$9.65 \cdot 10^{1}$	$\mu M^{-1}s^{-1}$	-2.00	$+2.00$
K_{3D18}	$k_{diss.}$ phosphorylation of Ndd1 by Clb2	$8.53 \cdot 10^{-1}$	s^{-1}	-4.00	$+0.00$
E_{3P18}	Efficiency phosph. of Ndd1 by Clb2	$8.64 \cdot 10^{0}$		-1.00	$+1.00$
K_{XASWI5}	$k_{ass.}$ Swi5–DNA	$7.76 \cdot 10^{0}$	$\mu M^{-1}s^{-1}$	-2.00	$+2.00$
K_{XDSWI5}	$k_{diss.}$ Swi5–DNA	$9.23 \cdot 10^{-1}$	s^{-1}	-4.00	$+0.00$
$F_{APOLSWI5}$	Relative association Swi5–RNA pol.	$1.20 \cdot 10^{-1}$		-2.00	$+2.00$
L_{TKSIC1}	Transcript length mSIC1	$1.17 \cdot 10^{-3}$		–	–
F_{BXSIC1}	Relative constitutive expression SIC1	$1.00 \cdot 10^{-1}$		-1.00	$+0.00$
L_{TLSIC1}	Protein length Sic1	$3.52 \cdot 10^{-3}$		–	–
K_{DMSIC1}	mRNA degradation rate SIC1	$6.75 \cdot 10^{-4}$	s^{-1}	-3.21	-3.13
K_{4A1}	$k_{ass.}$ degradation of Sic1P by SCF	$2.11 \cdot 10^{0}$	$\mu M^{-1}s^{-1}$	-2.00	$+2.00$
K_{4D1}	$k_{diss.}$ degradation of Sic1P by SCF	$9.30 \cdot 10^{-1}$	s^{-1}	-4.00	$+0.00$
$F_{PRSCFSIC1}$	Relative degradation of Sic1 by SCF	$1.00 \cdot 10^{0}$		–	–
K_{PSCF}	$k_{cat.}$ SCF	$4.21 \cdot 10^{-1}$	s^{-1}	-3.00	$+0.00$

Name	Description	Parameter value		Log_{10} range	
F_{DCSIC1}	Relative degradation complexed / free Sic1	$9.18 \cdot 10^{-2}$		-2.00	$+2.00$
F_{DSIC1}	Relative degradation Sic1 / Sic1P	$6.71 \cdot 10^{-3}$		-3.00	$+0.00$
K_{5A2}	$k_{ass.}$ complex formation Hct1–APC	$9.12 \cdot 10^{1}$	$\mu M^{-1}s^{-1}$	-2.00	$+2.00$
K_{5D2}	$k_{diss.}$ complex formation Hct1–APC	$8.59 \cdot 10^{-1}$	s^{-1}	-4.00	$+0.00$
$F_{PRAPCCLB2}$	Relative degradation of Clb2 by APC	$1.00 \cdot 10^{0}$		–	–
K_{PAPC}	$k_{cat.}$ APC	$5.60 \cdot 10^{-2}$	s^{-1}	-3.00	$+0.00$
$F_{AHCT1APC}$	Relative affinity Hct1P / Hct1 – APC	$1.99 \cdot 10^{-3}$		-3.00	-1.00
$F_{PRAPCNDD1}$	Relative degradation of Ndd1 by APC	$1.00 \cdot 10^{0}$		–	–
$F_{PRAPCYOX1}$	Relative degradation of Yox1 by APC	$1.00 \cdot 10^{0}$		–	–
$F_{PRAPCCDC20}$	Relative degradation of Cdc20 by APC	$1.00 \cdot 10^{0}$		–	–
$F_{PRAPCCDC6}$	Relative degradation of Cdc6 by APC	$1.00 \cdot 10^{0}$		–	–
K_{6A1}	$k_{ass.}$ complex formation Cdc20–SAC	$1.48 \cdot 10^{0}$	$\mu M^{-1}s^{-1}$	-2.00	$+2.00$
K_{6D1}	$k_{diss.}$ complex formation Cdc20–SAC	$1.00 \cdot 10^{-4}$	s^{-1}	-4.00	$+0.00$
$F_{XFKH12CDC20}$	Relative aff. Fkh12 for CDC20 promoter	$2.16 \cdot 10^{-1}$		-1.00	$+1.00$
$L_{TKCDC20}$	Transcript length mCDC20	$5.46 \cdot 10^{-4}$		–	–
$L_{TLCDC20}$	Protein length Cdc20	$1.64 \cdot 10^{-3}$		–	–
$K_{DMCDC20}$	mRNA degradation rate CDC20	$7.29 \cdot 10^{-4}$	s^{-1}	-3.19	-3.10
$F_{XMBFCDC20}$	Relative affinity MBF for CDC20 promoter	$1.00 \cdot 10^{1}$		-1.00	$+1.00$
$F_{BXCDC20}$	Relative constitutive expression CDC20	$5.95 \cdot 10^{-1}$		-2.00	$+0.00$
K_{XAYOX1}	$k_{ass.}$ Yox1–DNA	$7.32 \cdot 10^{1}$	$\mu M^{-1}s^{-1}$	-2.00	$+2.00$
$F_{XICDC20}$	Relative affinity Yox1 for CDC20 promoter	$4.29 \cdot 10^{1}$		-2.00	$+2.00$
K_{XDYOX1}	$k_{diss.}$ Yox1–DNA	$3.73 \cdot 10^{-3}$	s^{-1}	-4.00	$+0.00$
$F_{DCDC20APC}$	Relative degradation of Cdc20 via APC	$6.46 \cdot 10^{-1}$		$--$	$+0.00$
K_{6A3}	$k_{ass.}$ degradation of Cdc20 by APCP	$4.74 \cdot 10^{0}$	$\mu M^{-1}s^{-1}$	-2.00	$+2.00$
K_{6D3}	$k_{diss.}$ degradation of Cdc20 by APCP	$3.81 \cdot 10^{-1}$	s^{-1}	-4.00	$+0.00$
K_{6P2}	$k_{cat.}$ constitutive degradation of Cdc20	$1.00 \cdot 10^{-3}$	s^{-1}	-4.02	-2.24
$F_{DCDC20NOC}$	Relative degradation inhibited / free Cdc20	$9.21 \cdot 10^{-1}$		-3.00	$+1.00$
K_{6A2}	$k_{ass.}$ complex formation Cdc20–APCP	$7.27 \cdot 10^{1}$	$\mu M^{-1}s^{-1}$	-2.00	$+2.00$
K_{6D2}	$k_{diss.}$ complex formation Cdc20–APCP	$5.76 \cdot 10^{-1}$	s^{-1}	-4.00	$+0.00$
$F_{PRAPCCLB5}$	Relative degradation of Clb5 by APC	$1.00 \cdot 10^{0}$		–	–
K_{6A4}	$k_{ass.}$ complex formation Cdc20–Hct1	$3.61 \cdot 10^{0}$	$\mu M^{-1}s^{-1}$	$--$	$+1.00$
K_{6D4}	$k_{diss.}$ complex formation Cdc20–Hct1	$6.76 \cdot 10^{-4}$	s^{-1}	-4.00	$+0.00$
$F_{PRAPCSWI5}$	Relative degradation of Swi5 by APC	$1.00 \cdot 10^{0}$		–	–
K_{7A1}	$k_{ass.}$ phosphorylation of Net1 by MENP	$3.00 \cdot 10^{1}$	$\mu M^{-1}s^{-1}$	-2.00	$+2.00$
K_{7D1}	$k_{diss.}$ phosphorylation of Net1 by MENP	$7.48 \cdot 10^{-1}$	s^{-1}	-4.00	$+0.00$
F_{PDBF2P}	Relative kinase activity MENP / MEN	$1.04 \cdot 10^{-2}$		-2.00	$+0.00$
K_{7P1}	$k_{cat.}$ phosphorylation of Net1 by MENP	$4.59 \cdot 10^{-1}$	s^{-1}	-3.00	$+1.00$
K_{8A1}	$k_{ass.}$ phosphorylation of Net1 by FEAR	$2.30 \cdot 10^{0}$	$\mu M^{-1}s^{-1}$	-2.00	$+2.00$
K_{8D1}	$k_{diss.}$ phosphorylation of Net1 by FEAR	$2.43 \cdot 10^{-1}$	s^{-1}	-4.00	$+0.00$
K_{8P1}	$k_{cat.}$ phosphorylation of Net1 by FEAR	$1.46 \cdot 10^{-2}$	s^{-1}	-3.00	$+1.00$
$F_{XMBFCDC6}$	Relative affinity MBF for CDC6 promoter	$9.96 \cdot 10^{0}$		-1.00	$+1.00$
L_{TKCDC6}	Transcript length mCDC6	$6.50 \cdot 10^{-4}$		–	–
L_{TLCDC6}	Protein length Cdc6	$1.95 \cdot 10^{-3}$		–	–
K_{DMCDC6}	mRNA degradation rate CDC6	$4.92 \cdot 10^{-4}$	s^{-1}	-3.34	-3.16
F_{BXCDC6}	Relative constitutive expression CDC6	$2.87 \cdot 10^{-1}$		-2.00	$+0.00$
F_{XICDC6}	Relative affinity Yox1 for CDC6 promoter	$8.91 \cdot 10^{1}$		-2.00	$+2.00$
K_{11A1}	$k_{ass.}$ degradation of Cdc6P by SCF	$2.86 \cdot 10^{0}$	$\mu M^{-1}s^{-1}$	-2.00	$+2.00$
K_{11D1}	$k_{diss.}$ degradation of Cdc6P by SCF	$9.98 \cdot 10^{-1}$	s^{-1}	-4.00	$+0.00$
$F_{PRSCFCDC6}$	Relative degradation of Cdc6 by SCF	$1.00 \cdot 10^{0}$		–	–
F_{DCCDC6}	Relative degradation complexed / free Cdc6	$6.01 \cdot 10^{-3}$		-3.00	$+0.00$
F_{DCDC6}	Relative degradation Cdc6 / Cdc6P	$9.81 \cdot 10^{-1}$		$--$	$+0.00$
K_{11A2}	$k_{ass.}$ complex formation Cdc6–Hct1	$1.68 \cdot 10^{-2}$	$\mu M^{-1}s^{-1}$	-2.00	$+2.00$
K_{11D2}	$k_{diss.}$ complex formation Cdc6–Hct1	$7.70 \cdot 10^{-1}$	s^{-1}	-4.00	$+0.00$
K_{11A3}	$k_{ass.}$ complex formation Cdc6–Cdc20	$2.58 \cdot 10^{1}$	$\mu M^{-1}s^{-1}$	-2.00	$+2.00$

Name	Description	Parameter value		Log_{10} range	
K_{11D3}	$k_{diss.}$ complex formation Cdc6–Cdc20	$4.65 \cdot 10^{-1}$	s^{-1}	-4.00	$+0.00$
$F_{XFKH12SWI5}$	Relative affinity Fkh12 for SWI5 promoter	$3.00 \cdot 10^{0}$		-1.00	$+1.00$
L_{TKSWI5}	Transcript length mSWI5	$4.70 \cdot 10^{-4}$		–	–
L_{TLSWI5}	Protein length Swi5	$1.41 \cdot 10^{-3}$		–	–
K_{DMSWI5}	mRNA degradation rate SWI5	$7.47 \cdot 10^{-4}$	s^{-1}	-3.21	-3.13
F_{BXSWI5}	Relative constitutive expression SWI5	$1.00 \cdot 10^{-2}$		-2.00	$+0.00$
K_{12P1}	$k_{cat.}$ constitutive degradation of Swi5	$2.96 \cdot 10^{-3}$	s^{-1}	-4.02	-2.24
F_{DSWI5}	Relative degradation Swi5P / Swi5	$1.21 \cdot 10^{-1}$		-2.00	$+0.00$
K_{12A3}	$k_{ass.}$ complex formation Swi5–Cdc20	$9.98 \cdot 10^{0}$	$\mu M^{-1}s^{-1}$	-2.00	$+1.00$
K_{12D3}	$k_{diss.}$ complex formation Swi5–Cdc20	$1.57 \cdot 10^{-1}$	s^{-1}	-4.00	$+0.00$
K_{13A1}	$k_{ass.}$ complex formation Clb5–Sic1	$1.00 \cdot 10^{2}$	$\mu M^{-1}s^{-1}$	-2.00	$+2.00$
K_{13D1}	$k_{diss.}$ complex formation Clb5–Sic1	$1.00 \cdot 10^{-4}$	s^{-1}	-4.00	$+0.00$
K_{13A2}	$k_{ass.}$ phosphorylation of Sic1 by Clb5	$2.03 \cdot 10^{1}$	$\mu M^{-1}s^{-1}$	-2.00	$+2.00$
K_{13D2}	$k_{diss.}$ phosphorylation of Sic1 by Clb5	$1.00 \cdot 10^{0}$	s^{-1}	-4.00	$+0.00$
E_{13P2}	Efficiency phosph. of Sic1 by Clb5	$1.93 \cdot 10^{0}$		-1.00	$+1.00$
K_{13A3}	$k_{ass.}$ phosphorylation of Hct1 by Clb5	$1.00 \cdot 10^{2}$	$\mu M^{-1}s^{-1}$	-2.00	$+2.00$
K_{13D3}	$k_{diss.}$ phosphorylation of Hct1 by Clb5	$4.90 \cdot 10^{-1}$	s^{-1}	-4.00	$+0.00$
E_{13P3}	Efficiency phosph. of Hct1 by Clb5	$1.49 \cdot 10^{0}$		-1.00	$+1.00$
K_{13A4}	$k_{ass.}$ complex formation Clb5–Cdc20	$4.47 \cdot 10^{0}$	$\mu M^{-1}s^{-1}$	-2.00	$+2.00$
K_{13D4}	$k_{diss.}$ complex formation Clb5–Cdc20	$9.99 \cdot 10^{-1}$	s^{-1}	-4.00	$+0.00$
$F_{XMBFCLB5}$	Relative affinity MBF for CLB5 promoter	$5.77 \cdot 10^{-1}$		-1.00	$+1.00$
L_{TKCLB5}	Transcript length mCLB5	$7.66 \cdot 10^{-4}$		–	–
L_{TLCLB5}	Protein length Clb5	$2.30 \cdot 10^{-3}$		–	–
K_{DMCLB5}	mRNA degradation rate CLB5	$1.16 \cdot 10^{-3}$	s^{-1}	-2.94	-2.85
K_{13A10}	$k_{ass.}$ phosphorylation of Swi5 by Clb5	$0.00 \cdot 10^{0}$	$\mu M^{-1}s^{-1}$	–	–
K_{13D10}	$k_{diss.}$ phosphorylation of Swi5 by Clb5	$0.00 \cdot 10^{0}$	s^{-1}	–	–
E_{13P10}	Efficiency phosph. of Swi5 by Clb5	$0.00 \cdot 10^{0}$		–	–
K_{13P11}	$k_{cat.}$ constitutive degradation of Clb5	$9.63 \cdot 10^{-5}$	s^{-1}	-4.02	-2.24
K_{13A12}	$k_{ass.}$ complex formation Clb5–Cdc6	$2.28 \cdot 10^{1}$	$\mu M^{-1}s^{-1}$	-2.00	$+2.00$
K_{13D12}	$k_{diss.}$ complex formation Clb5–Cdc6	$1.23 \cdot 10^{-4}$	s^{-1}	-4.00	$+0.00$
K_{13A13}	$k_{ass.}$ phosphorylation of Cdc6 by Clb5	$8.86 \cdot 10^{1}$	$\mu M^{-1}s^{-1}$	-2.00	$+2.00$
K_{13D13}	$k_{diss.}$ phosphorylation of Cdc6 by Clb5	$8.80 \cdot 10^{-2}$	s^{-1}	-4.00	$+0.00$
E_{13P13}	Efficiency phosph. of Cdc6 by Clb5	$8.11 \cdot 10^{0}$		-1.00	$+1.00$
K_{17P6}	$k_{cat.}$ constitutive dephosph. of APC	$2.93 \cdot 10^{-3}$	s^{-1}	-3.00	$+0.00$
K_{17P}	$k_{cat.}$ constitutive dephosph. of Net1	$1.00 \cdot 10^{-3}$	s^{-1}	-3.00	$+0.00$
K_{17P10}	$k_{cat.}$ constitutive dephosph. of Cdc6	$4.63 \cdot 10^{-2}$	s^{-1}	-3.00	$+0.00$
K_{17P11}	$k_{cat.}$ constitutive dephosph. of MEN	$1.01 \cdot 10^{-3}$	s^{-1}	-3.00	$+0.00$
K_{17P13}	$k_{cat.}$ constitutive degradation of MBFP	$5.76 \cdot 10^{-3}$	s^{-1}	-4.02	-2.24
K_{17P14}	$k_{cat.}$ constitutive dephosph. of Fkh12	$1.00 \cdot 10^{0}$	s^{-1}	-3.00	$+0.00$
K_{17P15}	$k_{cat.}$ constitutive dephosph. of Ndd1	$9.91 \cdot 10^{-1}$	s^{-1}	-3.00	$+0.00$
$F_{XMBFYOX1}$	Relative affinity MBF for YOX1 promoter	$7.80 \cdot 10^{-1}$		-1.00	$+1.00$
L_{TKYOX1}	Transcript length mYOX1	$8.66 \cdot 10^{-4}$		–	–
L_{TLYOX1}	Protein length Yox1	$2.60 \cdot 10^{-3}$		–	–
K_{DMYOX1}	mRNA degradation rate YOX1	$6.60 \cdot 10^{-4}$	s^{-1}	-3.18	-3.00
$F_{XFKH12YOX1}$	Relative affinity Fkh12 for YOX1 promoter	$9.99 \cdot 10^{0}$		-1.00	$+1.00$
F_{BXYOX1}	Relative constitutive expression YOX1	$9.71 \cdot 10^{-1}$		-2.00	$+0.00$
K_{27P1}	$k_{cat.}$ constitutive degradation of Yox1	$9.65 \cdot 10^{-5}$	s^{-1}	-4.02	-2.24
K_{27A2}	$k_{ass.}$ complex formation Yox1–Hct1	$4.33 \cdot 10^{1}$	$\mu M^{-1}s^{-1}$	$--$	$+2.00$
K_{27D2}	$k_{diss.}$ complex formation Yox1–Hct1	$9.48 \cdot 10^{-1}$	s^{-1}	$--$	$+0.00$
K_{27A3}	$k_{ass.}$ complex formation Yox1–Cdc20	$1.00 \cdot 10^{2}$	$\mu M^{-1}s^{-1}$	$--$	$+2.00$
K_{27D3}	$k_{diss.}$ complex formation Yox1–Cdc20	$4.08 \cdot 10^{-1}$	s^{-1}	-4.00	$+0.00$
$F_{XMBFNDD1}$	Relative affinity MBF for NDD1 promoter	$1.03 \cdot 10^{0}$		-1.00	$+1.00$
L_{TKNDD1}	Transcript length mNDD1	$6.02 \cdot 10^{-4}$		–	–
L_{TLNDD1}	Protein length Ndd1	$1.81 \cdot 10^{-3}$		–	–

Name	Description	Parameter value		Log_{10} range	
K_{DMNDD1}	mRNA degradation rate NDD1	$1.07 \cdot 10^{-3}$	s^{-1}	-3.15	-2.97
$F_{XFKH12NDD1}$	Relative affinity Fkh12 for NDD1 promoter	$9.99 \cdot 10^{0}$		-3.00	$+1.00$
F_{BXNDD1}	Relative constitutive expression NDD1	$5.61 \cdot 10^{-2}$		-2.00	$+0.00$
F_{DNDD1}	Relative degradation Ndd1P / Ndd1	$9.01 \cdot 10^{-1}$		-3.00	$+0.00$
K_{28P1}	$k_{cat.}$ constitutive degradation of Ndd1	$1.55 \cdot 10^{-3}$	s^{-1}	-4.02	-2.24
K_{28A2}	$k_{ass.}$ complex formation Ndd1–Hct1	$2.52 \cdot 10^{-1}$	$\mu M^{-1}s^{-1}$	-2.00	$+2.00$
K_{28D2}	$k_{diss.}$ complex formation Ndd1–Hct1	$6.78 \cdot 10^{-1}$	s^{-1}	-4.00	$+0.00$
K_{28A3}	$k_{ass.}$ complex formation Ndd1–Cdc20	$1.60 \cdot 10^{-1}$	$\mu M^{-1}s^{-1}$	-2.00	$+2.00$
K_{28D3}	$k_{diss.}$ complex formation Ndd1–Cdc20	$5.20 \cdot 10^{-2}$	s^{-1}	-4.00	$+0.00$
$F_{OVXSIC1}$	Relative over-expression SIC1	$0.00 \cdot 10^{0}$		–	–
K_{ATKGAL}	$k_{ass.}$ RNA polymerase–GAL1-10 promoter	$1.59 \cdot 10^{1}$	$\mu M^{-1}s^{-1}$	-2.00	$+2.00$
K_{DTKGAL}	$k_{diss.}$ RNA pol.–GAL1-10 promoter	$4.57 \cdot 10^{1}$	s^{-1}	-2.00	$+2.00$
$F_{OVXCDC6}$	Relative over-expression CDC6	$0.00 \cdot 10^{0}$		–	–
$F_{OVXCLB5}$	Relative over-expression CLB5	$0.00 \cdot 10^{0}$		–	–
$F_{OVXCLB2}$	Relative over-expression CLB2	$0.00 \cdot 10^{0}$		–	–
$F_{OVXCDC20}$	Relative over-expression CDC20	$0.00 \cdot 10^{0}$		–	–
$F_{OVXYOX1}$	Relative over-expression YOX1	$0.00 \cdot 10^{0}$		–	–
$F_{OVXNDD1}$	Relative over-expression NDD1	$0.00 \cdot 10^{0}$		–	–
$F_{OVXFKH12}$	Relative over-expression FKH12	$0.00 \cdot 10^{0}$		–	–
$L_{TKFKH12}$	Transcript length mFKH12	$4.95 \cdot 10^{-4}$		–	–
$F_{OVXHCT1}$	Relative over-expression HCT1	$0.00 \cdot 10^{0}$		–	–
L_{TKHCT1}	Transcript length mHCT1	$5.89 \cdot 10^{-4}$		–	–
L_{TLHCT1}	Protein length Hct1	$1.77 \cdot 10^{-3}$		–	–
K_{DMHCT1}	mRNA degradation rate HCT1	$5.47 \cdot 10^{-4}$	s^{-1}	–	–
K_{DOVXP}	$k_{cat.}$ degradation overexpressed protein	$1.20 \cdot 10^{-4}$	s^{-1}	–	–
$F_{OVXCDC14}$	Relative over-expression CDC14	$0.00 \cdot 10^{0}$		–	–
$L_{TKCDC14}$	Transcript length mCDC14	$6.05 \cdot 10^{-4}$		–	–
$L_{TLCDC14}$	Protein length Cdc14	$1.81 \cdot 10^{-3}$		–	–
$K_{DMCDC14}$	mRNA degradation rate CDC14	$1.05 \cdot 10^{-3}$	s^{-1}	–	–
$F_{OVXNET1}$	Relative over-expression NET1	$0.00 \cdot 10^{0}$		–	–
L_{TKNET1}	Transcript length mNET1	$2.80 \cdot 10^{-4}$		–	–
L_{TLNET1}	Protein length Net1	$8.41 \cdot 10^{-4}$		–	–
K_{DMNET1}	mRNA degradation rate NET1	$7.70 \cdot 10^{-4}$	s^{-1}	–	–